DESIGNING INJECTABLE POLY(OLIGO ETHYLENE GLYCOL METHACRYLATE)-BASED HYDROGELS FOR DRUG DELIVERY AND TISSUE ENGINEERING APPLICATIONS

DESIGNING INJECTABLE POLY(OLIGO ETHYLENE GLYCOL METHACRYLATE)-BASED HYDROGELS FOR DRUG DELIVERY AND TISSUE ENGINEERING APPLICATIONS

By EMILIA PARON, B.Sc

A Thesis Submitted to the School of Graduate Studies in Partial Fulfillment of the Requirements for the Degree Ph.D of Chemical Engineering

TITLE: Designing Injectable Poly(oligo ethylene glycol methacrylate)-based Hydrogels for Drug Delivery and Tissue Engineering Applications

AUTHOR: Emilia Paron, B.Sc (University of Waterloo)

SUPERVISOR: Dr. Todd R. Hoare

NUMBER OF PAGES: 271

Lay Abstract

Injectable hydrogels are 3D water swollen gel networks formed by simple mixing of water-soluble polymers. Such hydrogels have the potential to mimic or stimulate native tissue functions and thus hold enormous promise in treating organ failures resulting from injuries, aging and disease. Injectable hydrogels can also act as vehicles for various therapeutics including drugs or cells, and they can be administered minimally invasively. They can be formed from a variety of materials of natural and synthetic origins and through rapid physical or chemical crosslinking mechanisms. This thesis presents the development of degradable, thermoresponsive and injectable hydrogels using poly(oligo ethylene glycol methacrylate) (POEGMA). We demonstrate that by modifying the chemistry of POEGMA as well as how it is combined with other materials (e.g. charged functional groups or natural polymers like dextran) can significantly change the swelling, degradation, mechanical, protein interaction, cell interaction, and *in* vivo tissue response properties of the hydrogels, allowing them to be customized for various applications in drug delivery, cell delivery, or tissue engineering to improve efficacy relative to current materials.

Abstract

Injectable hydrogels are 3D water swollen polymeric networks formed through *in situ* gelling mechanisms. The minimally invasive nature of their delivery into the body, coupled with their highly tunable chemical properties, offer broad promise in mimicking or stimulating native tissue functions, essential to effectively treat organ failures resulting from injuries, aging and disease. Alternately, injectable hydrogels can act as depot-based drug delivery vehicles for various therapeutics including drugs or cells that can be injected directly at a desired site of action for long-term efficacy. While such hydrogels can be formed from a variety of materials (both natural and synthetic) and through a variety of *in situ* crosslinking mechanisms (both physical and covalent), combining the chemical flexibility of synthetic polymers with reversible covalent gelation in which gel degradation can be better programmed according to its environment offers an attractive combination of properties to rationally engineer *in situ* gelling hydrogels for a variety of applications.

This thesis presents the development of degradable, thermoresponsive and injectable hydrogels based on poly(oligo ethylene glycol methacrylate) (POEGMA), using the rapid covalent crosslinking of hydrazide and aldehyde functionalized POEGMA precursors to form a hydrazone bond capable of undergoing hydrolytic degredation at physiological pH/temperature. First, a new method to make synthetic and degradable hydrogels based on POEGMA is presented, demonstrating that POEGMA *in situ*-gelling systems can offer the advantageous biological interactions of current state-of-the-art poly (ethylene glycol) (PEG) hydrogels while also offering superior flexibility to control gel properties. The thesis then proceeds to show the facile modulation of POEGMA hydrogel volume phase transition temperatures (VPTT) through varying the length of the ethylene oxide side chains of the OEGMA monomers used during copolymerization. A thermoresponsive gel (similar to the conventional poly(N-isopropylacrylamide) networks) can be achieved while maintaining the excellent stealth like properties *in vitro* and *in vivo* of PEG hydrogels. By mixing POEGMA precursor polymers with different phase transition temperatures together, hydrogels with additive properties and the potential for the rational formation of internal microdomains are generated, domains that can be leveraged to control the kinetics of protein release. Next, the

microscopic and macroscopic effects of incorporating the charged moieties *N,N*-dimethylaminoethyl methacrylate (DMAEMA) and acrylic acid (AA) into the POEGMA backbone are explored. We identify both the potential for secondary network formation that enhances gel mechanics as well as the potential to modulate cell responses with the hydrogels as a function of charge type and density, including the application of these charged hydrogels as injectable delivery vehicles for human retinal epithelial cells. Finally, mixed natural-synthetic hydrogels were reported by the incorporation of natural polymer dextran (DEX) into the POEGMA hydrogel platform. We show the resulting hydrogels offer the benefits of both POEGMA (low non-specific adsorption, thermoresponsivity) and dextran (cell interactions and enzymatic degradability), facilitating the generation of hydrogels with desirable *in vivo* properties. Based on the demonstrated capacity throughout this thesis to rationally change the properties of *in situ*-gelling hydrogels (often independent of other properties), this research has significant implications for the improvement of hydrogel materials for drug delivery and tissue engineering.

Acknowledgements

I would like to start off by saying that this work would not have been possible to complete without the support and guidance of a number of very important people over many years. I will start off by thanking my supervisor Prof. Todd Hoare. Dr. Hoare has been not only an inspiring mentor to me, but an incredible and devoted leader to his students and a brilliant, innovative scientist. I started off my graduate degree feeling like a 'fish out of water', coming from a biomedical science degree and working before returning to school to start my engineering degree. Dr. Hoare gave me the opportunity to discover a completely different world, that I never could have imaged myself loving so much. In every aspect of my studies here at McMaster, I have felt fully supported and encouraged by Dr. Hoare to freely conduct my own research and collaborate with many wonderful researchers at McMaster. I couldn't have asked for a better supervisor, and I look forward to continuing to learn from and collaborate with Dr. Todd Hoare in the future. I am so grateful and proud to have been his student.

I would secondly like to thank Dr. Niels Smeets. Dr. Niels Smeets, has been in short, an excellent mentor and friend. Beginning the journey of POEGMA hydrogel discovery with him has led me to learn things about polymer science and myself that I never thought possible. Niels' guidance and collaboration in the lab has been invaluable. It has been an incredibly rewarding adventure working with him.

I would also like to thank my committee members Dr. Jose Moran-Mirabal and Dr. Heather Sheardown. They have provided such helpful comments and guidance throughout my graduate degree. They have been an integral part to the success of this thesis, and this thesis would not have been possible without them.

I would also like to thank the NSERC CREATE Integrated Design of Extracellular Matrices (IDEM) Network for not only funding, but the incredible opportunity to collaborate with excellent researchers at McMaster University in Chemistry, Health Science and Physics.

Over the past 6 years of my graduate degree, I have had the privilege to work with amazing members of the Hoare Lab past and present. Many of these members have become my close friends and in addition to getting to work together on many projects, they have continually supported me as a friend and scientist. I would like to especially thank Sabrina

Hodgson, Stephanie Kedzior, Madeline Simpson, Ivan Urosev, Helen Dorrington, Eva Mueller, Fei Xu, Max Yavitt, Lukas Sadowski, Daryl Sivakumaran, Mathew Patenaude and Trevor Gilbert for excellent conservations over coffee and providing me with such an enriched graduate experience.

Finally, but most importantly, I would like to thank my husband Todd Paron for making me feel like I can achieve anything. Thank you for supporting me unconditionally over these past six years of completing this degree and in every facet of our lives together. I could never have imagined doing this without you. I love you.

Table of Contents

List of Figures

Chapter 1: Injectable Hydrogels Based on Poly(ethylene glycol) and Derivatives as Functional Biomaterials

Figure S5.4: Degree of ionization measured using potentiometric titration with 0.1M NaOH at 22˚C of $PO_{100}H_{30}C_{20}$ (red) and $PO_{100}A_{30}D_{20}$ (green) precursor polymers.

Figure S5.5: (B) Scattering intensities with fits using Porod model (in 10 mM D_2O PBS, 22˚C): **(A)** PO_{100} **(B)** PO_{100}-$_{100/0}$ **(C)** PO_{100}-$_{100/100}$ **(D)** PO_{100}-$_{0/100}$ **(E)** $PO_{100\text{-}50/50}$ **(F)** PO_{100}-$_{75/25}$ and **(G)** PO_{100}-$_{25/75}$.

Chapter 6: Injectable and Degradable Poly(Oligoethylene glycol methacrylate) Hydrogels With Tunable Charge Densities: Adhesive Peptide-Free Cell Scaffolds

Scheme 6.1. Synthesis of charged POEGMA precursors.

Figure 6.1. Swelling kinetics of POEGMA hydrogels in 10 mM (A) citrate buffer pH 3, (B) phosphate buffer pH 7.4 and (C) carbonate buffer pH 10 at 37°C.

Figure 6.2. Swelling kinetics of POEGMA hydrogels in pH 3, 7.4 or 10 buffers as a function of temperature.

Figure 6.3. Degradation profiles of POEGMA hydrogels in 0.1mM HCl solution at 37°C.

Figure 6.4. Average elastic storage moduli (*G'*) of the fully swollen mixed precursor POEGMA hydrogels in 10 mM PBS at 37°C.

Figure 6.5. Resazurin cell viability assay of POEGMA precursor polymers after 24 hours incubation with 3T3 mouse fibroblasts at 37°C.

Figure 6.6. Protein adsorption to charged POEGMA hydrogels in 10 mM PBS at 37°C: (A) bovine serum albumin; (B) lysozyme.

Figure 6.7. Adhesion of mouse 3T3 fibroblasts to charged POEGMA hydrogels following 48 hours of incubation: (A) PO_{10} (neutral); (B) PO_{10}-cat (cationic); (C) PO_{10}-amp (amphoteric); (D) PO_{10}-an (anionic) (E) tissue culture polystyrene control. Scale bar = 100 µm.

Figure 6.8. Histological sections of stained subcutaneous tissue samples following injection of PO_{10} (A,E), PO_{10}-cat (B,F), PO-$_{amp}$ (C,G) and PO-$_{an}$ (D,H) hydrogels following acute (A-D) and chronic (E-H) time points. Arrows indicate the presence of leukocytes. All hydrogels are still present at chronic time points. Scale bars = 100 µm.

Figure 6.9. 3D encapsulation of ARPE-19 cells imaged using confocal microscopy (200 µm z-stack) after 3 days and 15 days in neutral and charged POEGMA hydrogels.

Figure S7.1 Cloud point temperature measurements of PO_5H_{30}-$PO_{20}H_{30}$ prior to hydrazide functionalization as measured in HCl/KCl buffer at pH = 2 (ensuring protonation of the -COOH groups).
Figure S7.2 Cloud point temperature measurements of PO_5H_{30}-$PO_{20}H_{30}$ after to hydrazide functionalization as measured in PBS buffer at pH = 7.4.

Figure S7.3. Reversibility of the thermal phase transition of POEGMA-DEXA hydrogels in PBS.

List of Tables

List of Terminology, Symbols and Abbreviations

^{1}H-NMR	Proton nuclear magnetic resonance
3T3	NIH mouse fibroblast line
Å	Angstrom
AA	Acrylic Acid
ADH	Adipic acid dihydrazide
AIBME	2,2-azobisisobutyric acid dimethyl ester
ARPE-19	Human retinal epithelial cells
BSA	Bovine serum albumin
$CDCl_3$	Deuterated chloroform
CuAAC	Copper (I)-catalyzed alkyne-azide click
Đ	Dispersity
D_2O	Deuterated Water
Da	Dalton
DEX	Dextran
DMAEMA	Dimethyl amino ethyl methacrylate
DMEM	Dulbecco's Modified Eagle Medium
EDC	1-Ethyl-3(3-dimethylaminopropyl)carbodiimide
FBS	Fetal bovine serum
FITC	Fluorescein isothiocyanate
G'	Shear storage modulus
G"	Shear loss modulus
GPC	Gel permeation chromatography
H&E	Hemotoxylin and eosin histological stain
HCl	Hydrochloric acid
LCST	Lower critical solution temperature
MEHQ	Methyl ether hydroquinone
$M(EO)_2MA$	Diethylene glycol methacrylate

Mn	Number average molecular weight
Mc	Molecular weight between cross-links
MTT	3-(4,5-dimethylthiazol-2-yl)-2,5-diphenyltetrazolium
MWCO	Molecular weight cut-off
N_A	Avogadro's number (6.022×10^{23})
NaCl	Sodium chloride
NaOH	Sodium hydroxide
PBS	Phosphate buffered saline
PEG	Poly(ethylene glycol)
PEO	Poly(ethylene oxide)
PNIPAM	Poly(N-isopropylacrylamide)
POEGMA	Poly(oligo ethylene glycol methacrylate)
PS	Penicillin streptomycin
Q_m	Mass-based swelling ratio
Q_v	Volumetric swell ratio
SANS	Small angle neutron scattering
TGA	Thioglycolic acid
VPTT	Volume phase transition temperature

Declaration of Academic Achievement:

The majority of the work described in this thesis was conceived, conducted, interpreted and written by the author of this thesis, with the following exceptions:

Chapter 1: The manuscript used for Chapter 1 was written by myself, but largely edited by Dr. Niels Smeets.

Chapter 2: The manuscript used for Chapter 2 was conceptualized and co-written by myself and Dr. Niels Smeets equally. We are co-first authors on this work. Dr. Niels Smeets contributed largely to the synthesis and characterization of the POEGMA polymers in addition to the co-conceptualization of design of experiments for the project. My contributions to this work include material design and characterization, and all biological experiments except the *in vivo* injections, which were done by Dr. Mathew Patenaude.

Chapter 3: The manuscript used for Chapter 3 was again conceptualized and co-written by myself and Dr. Niels Smeets equally. We are co-first authors on this work. Dr. Niels Smeets contributed largely to the characterization of the POEGMA polymers in addition to the co-conceptualization of design of experiments for the project . My contributions to this work include material design and characterization, and all biological experiments except the *in vivo* injections which were done by Dr. Mathew Patenaude.

Chapter 4: The manuscript used for Chapter 4 was written by myself and edited by Dr. Niels Smeets. My contributions to this work, including material design and characterization, were aided by student Helen Dorrington.

Chapter 5: Chapter 5 experiments were conducted by myself with the help of a co-op student Owen Barrigar, who is a co-author of the work. Richard Alsop AND Maikel C. Rheinstädter helped with the overall interpretation of the small angle neutron scattering (SANS) data.

Chapter 6: Chapter 6 experiments were conducted by myself with the help of a student Owen Barrigar, who is a co-author of the work. The 2D and 3D ARPE-19 cell experiments were aided by Megan Dodd and the *in vivo* injections were done by Maryam Badv. The histological scoring of slides prepared at McMaster was performed by Emily Siebers and Dr. Michael Lawlor at the University of Wisconsin-Madison.

Chapter 7: Chapter 7 experiments were performed primarily by myself, while Dr. Niels Smeets contributed significantly to the characterization of the hydrazide functionalized POEGMA polymers. *In vivo* injections were done and interpreted by Dr. Mathew Patenaude.

Chapter 1: Injectable Hydrogels Based on Poly(ethylene glycol) and Derivatives as Functional Biomaterials

Preface:

This chapter has been adapted from the original publication of a review of injectable and non-injectable poly(ethylene glycol) based systems, as well as an outline of the design criteria for injectable, *in situ*-gelling hydrogels. Examples of recent progress in the preparation of injectable poly(ethylene glycol) (PEG) and PEG-analogue poly(oligo ethylene glycol methacrylate) (POEGMA) hydrogels published since this review are also included to give a current summary of the state-of-the-art in this area. An addendum is included at the end with a statement of the objectives of the thesis and a summary of how the following experimental chapters address the overall objectives.

Emilia Bakaic, Niels M.B. Smeets, and Todd Hoare*

Department of Chemical Engineering, McMaster University, 1280 Main St. W, Hamilton, Ontario, Canada L8S 4L7

Bakaic, E.; Smeets, N.M.B.; Hoare, T. "Injectable Hydrogels Based on Poly(Ethylene Glycol) and Derivatives as Functional Biomaterials". *RSC Advances*, **2015**, *5*, 35469 – 35486.

1. Introduction

Hydrogels are water-swollen polymeric networks capable of absorbing large quantities of water and biological fluids while maintaining a distinct three-dimensional structure.[1] The high water content of hydrogels, combined with the structural similarity of hydrogels to natural extracellular matrix (ECM),[2] makes hydrogels attractive synthetic materials for biomedical devices including drug release depots,[3,4,5] cell delivery scaffolds,[6,7,8] functional tissues,[9,10,11] or wound dressings.[12] The cross-linked, three-dimensional structure, while key to the ultimate applications of hydrogels, also severely limits the ability of hydrogels to be delivered inside the body by minimally invasive routes (i.e. non-surgical procedures such as injections). As a result, significant focus has shifted to the design of "injectable" or "*in-situ* gelling" hydrogels that form after injection *in vivo*.[13,14,15] The hydrogel precursor solution can be introduced in a minimally invasive manner directly to the area of interest, significantly reducing patient discomfort, risk of infection, recovery time, and treatment cost. Once injected, hydrogel formation occurs through either physical cross-linking, typically exploiting the physiological conditions in the target tissue, or by chemical cross-linking, exploiting click and/or dynamic covalent bond chemistry.[16–18] For many applications, the use of chemical cross-linking is preferred to improve the mechanical properties of the soft material, preserve the integrity of the hydrogel over an externally-programmed period of time (based on the type and density of cross-links present), and enhance the chemical flexibility of hydrogel in terms of its ability to be easily functionalized with physical or biological cues that improve its function and/or compatibility with the surrounding tissue.[19]

Herein, the relevant design criteria for injectable hydrogels will be briefly outlined and illustrated by reviewing a number of examples from the current state-of-the-art in injectable PEG hydrogels.

1.2. Design Criteria for Covalently Cross-linked Injectable Hydrogels

The clinical lifetime of an injectable hydrogel can be divided into three separate stages: (*i*) pre-gelation (precursor polymers in solution), (*ii*) therapeutic window (after injection and gelation) and (*iii*) degradation (hydrogel degradation products). Rational design of injectable hydrogels thus requires careful consideration of the synthetic and biological aspects of the precursor polymers, resulting hydrogel, as well as the hydrogel degradation products. The key design criteria will be discussed accordingly, as schematically depicted in Scheme 1.[20,21,22]

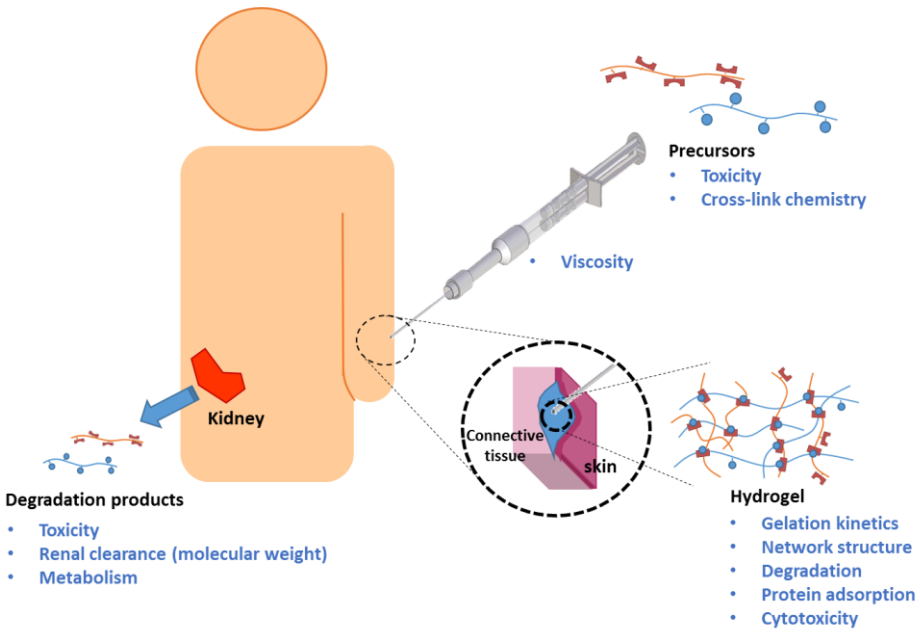

Scheme 1. Schematic representation of the various design criteria for injectable hydrogels

1.2.1 Precursor Polymers: Hydrogel precursor polymers can be based on naturally occurring polymers (e.g. collagen,[23] fibrin,[24,25] hyaluronic acid,[26] alginate,[27,28] agarose,[27] or dextran[29,30]) or synthetic polymers (e.g. poly(*N*-isopropylacrylamide) (PNIPAAm),[31,32] polyacrylamide (PAAm),[33] poly(hydroxyethyl methacrylate) (PHEMA),[34] poly(vinylpyrrolidone) (PVP),[35] poly(ethylene glycol) (PEG)[4,36,37] or other water-soluble polymers[38–40]). Although most natural polymers can be directly cross-linked by small bifunctional molecules such as epichlorohydrin or glyoxal,[38] a large variety of chemistries has been developed to functionalize these polymers with cross-linkable functional groups and thus avoid the need for often toxic small molecule cross-linkers.[41] Synthetic polymers can be functionalized directly through the use of functional comonomers and/or via post-polymerization modification. Regardless of the chemical nature of the precursor, the precursor polymer needs to be

stable, non-cytotoxic, and not elicit a significant inflammatory response from the patient's immune system upon injection. This latter point is especially challenging in the context of covalently cross-linked injectable hydrogels since chemically-driven gelation requires that the hydrogel precursors are functionalized with reactive functional groups that are not necessarily bioorthogonal[42] (e.g. amine, aldehyde, or thiol groups that are also present in, or cross-reactive with, polypeptides including enzymes, membrane proteins, etc.) However, it must be emphasized that the toxicity of functional polymeric precursors is typically low compared to low molecular weight chemicals with the same functionalities. For example, low molecular weight vinylsulfones (used in Michael-type addition cross-linking with thiols) demonstrate significant toxicity, but polymer-bound vinyl sulfones cannot enter cells and thus do not undergo toxic reactions with glutathione and DNA.[43] Similarly, the use of low molecular weight glutaraldehyde for gelation has been reported to induce toxicity,[44] but Hoffmann and co-workers noted no apparent cytotoxic effects associated with chitosan-glutaraldehyde hydrogels cultivated with ATDC5 and chrondrocytes up to 14 days.[45] In our experience, both natural (oxidized dextran or carboxymethyl cellulose) as well as synthetic aldehyde-functionalized precursors do not show any significant toxicity either *in vitro* (via an MTT assay on 3T3 mouse fibroblasts at concentrations up to 2000 μg/mL) [46, 47]or *in vivo* (via subcutaneous injection in BALB/c mice).[48]

The precursor polymers are likely to be stored for a considerable amount of time prior to clinical use and thus need to demonstrate high stability in aqueous solution. Furthermore, as administration occurs through a needle, the precursor solutions need to be of sufficiently low viscosity, or at least possess sufficient shear-thinning properties, to allow for easy injection. For routine applications, the maximum needle size for injections is 25G;[49] however, many ophthalmic or cosmetic applications require as small as a 33G needle sizes. This requirement makes both molecular weight control and polymer architecture very important in the design of a scaffold.

1.2.2 Hydrogels: For successful *in vivo* application, gelation (i.e. cross-linking of the precursor polymers) must occur at physiologically relevant conditions (i.e. $5.5 \leq pH \leq 7.5$ and $T = 37 \pm 2ºC$) relatively quickly (i.e. seconds to minutes) following injection. The emergence of click chemistries has introduced a variety of cross-linking approaches that are advantageous to the design of injectable hydrogels,[42] most notably copper-catalyzed alkyne azide reactions (CuAAC),[50] strain promoted azide-

alkyne click cycloaddtions (SPACC),[18,51] thiol-Michael additions,[43,52,53] Diels-Alder cycloaddition,[54,55] disulfide formation,[26,56,52,57] , oxime chemistry,[58,59] and Schiff base[37] formation. While not all of these cross-link chemistries are strictly bioorthogonal, *in vitro* and *in vivo* toxicity of such chemistries can be minimized by controlling gelation kinetics, as fast gelation kinetics reduce the amount of time that the non-bioorthogonal functional groups are exposed to native tissue prior to consumption via cross-linking. Gelation kinetics can be controlled by varying precursor polymer concentration, the number of reactive groups per chain, and/or the molecular weight of the precursor polymers.[60–63] Relatively fast gelation kinetics are typically beneficial in an injectable system to minimize the diffusion of precursors from the site of injection, which may cause adverse effects in neighboring tissues and/or prevent hydrogel formation entirely if the dilution is too significant. However, it is important minimize the formation of structural and mechanical defects in the hydrogel network, which directly influences the diffusivity of therapeutics, nutrients, oxygen and (toxic) waste products. Controlling the cross-link density of hydrogels allows for the design of injectable hydrogels that mimic a broad range of tissue mechanics ranging from soft brain tissue (0.2-1 kPa) to relatively stiff cartilage or pre-calcified bone tissue (20-60 kPa).[64] However, in most *in situ* gelling systems, cross-link density and gelation kinetics are inextricably linked (as both are governed by the degree of precursor polymer functionalization), representing a challenge in rational hydrogel design of highly cross-linked gels that can still be delivered by injection or weaker gels that need to be gelled quickly.

Aside from certain applications (e.g. dermal fillers),[65] injectable hydrogels must be either biodegradable[66,20,67,68]or bio-erodible[69,] to avoid surgical removal after its therapeutic lifetime has expired. In tissue engineering applications, controlled degradation is even more important as a functional aspect of the hydrogel that provides temporal cues to regulate cell proliferation and migration within the hydrogel matrix.[70] Whereas injectable hydrogels based on natural polymers are intrinsically degradable as a result of enzymatic activity *in vivo*, the degradation of synthetic precursor hydrogels must be programmed into the hydrogel design by using reversible chemistries that both cross-link the hydrogel and provide a hydrolyzable or oxidative link that facilitates degradation over time. The majority of biorthogonal cross-link chemistries listed earlier are reversible and therefore perfectly suited for the synthesis of injectable hydrogels.

Similar to the precursor polymers, the hydrogel itself must not elicit an inflammatory response once formed *in vivo*.[32] The ability of the hydrogel to "mask" itself from the host's immune system by

repelling protein adsorption is crucial to its success both short and long term. Protein adsorption is generally recognized as the first step of an inflammatory cascade that recruits inflammatory macrophages to the site of injury, initiates the formation of granulation tissue and (eventually, at least for slow or non-degrading materials) creates a fibrotic capsule around the material.[71,72] This "walling-off" is particularly problematic for hydrogels designed for drug release or tissue regeneration applications as it inhibits the effective diffusion of drugs, nutrients, and/or waste products between the hydrogel and surrounding tissue.[72,] Although hydrogels are less prone to protein adsorption relative to most biomaterials due to their hydrophilic and highly hydrated nature, the choice of polymeric components in the hydrogel is crucial to further reduce protein adsorption. PEG is still considered the gold-standard polymer to minimize protein adsorption, with PEG derivatives (e.g. poly(oligoethylene glycol (meth(acrylate)),[73,74,75] natural polymers,[76] polyoxazolines,[77] and zwitterionic polymers[78,79,80] also demonstrating favorable and, in some cases, superior protein repellency properties.

1.2.3 Degradation Products: Hydrogel degradation can occur via direct degradation of the polymer backbone and/or degradation of the cross-links between the individual polymer chains. Degradation of the polymer backbone may proceed via an oxidative,[56] hydrolytic,[81,46,48] and/or enzymatic mechanism.[82,83] The rate of degradation depends on the chemical structure of the polymer and the cross-link density, which govern both the thermodynamics of the bond stability as well as the kinetics of diffusion of the bond-breaking stimulus (e.g. water, enzymes, etc.) to the degradation site. Most biopolymers degrade via one or more of these mechanisms, resulting in non-toxic degradation products that can be metabolized by the body. Examples of synthetic polymers that contain either hydrolytically or enzymatically cleavable fragments in the polymer backbone have been reported[84] but require elaborate synthesis. Degradation of the cross-links[80,85] is therefore the commonly used clearance mechanism for synthetic hydrogels. Consequently, the degradation products of the hydrogel are structurally similar or in some cases identical to the original precursor polymers. Since the carbon-carbon backbone synthetic precursors cannot be metabolized by the body, the molecular weight of such precursor polymers needs to be carefully controlled to prevent bioaccumulation and ensure renal clearance following degradation. Typically, a molecular weight cut-off of 20×10^3 - 60×10^3 g/mol has been reported as the kidney clearance limit.[86]

Recent progress in the design of self-immolative polymers which degrade systematically following an external stimulus to remove a capping agent should also be noted as a potentially promising strategy for driving hydrogel degradation.[87,88] By controlling the stability of the capping material, programmed or even on-demand timed degradation may be achievable using this type of strategy. While current chemistries for the design of self-immolative polymers are not directly amenable to *in situ* gelation and some concerns persist regarding the ultimate toxicity of the degradation products resulting from many of these proposed mechanisms,[2] this strategy may be increasingly important moving forward as the chemistry of self-immolative polymers continues to develop.

1.3. Current state-of-the art of injectable poly(ethylene glycol)-based hydrogels

Polyethylene glycol (PEG) is a synthetic polymer that has found wide-spread application in the design of biomaterials due to its demonstrated non-cytotoxic, non-immunogenic and protein repellent properties that effectively mask it from the host's immune system.[89] Hydroxyl-terminated di- and multifunctional PEG polymers can readily be functionalized with a variety of desired functional groups (e.g. aminoxy,[90] azide,[91,92,51] thiol,[43] vinyl sulfone,[93] or maleimide,[54]) and cross-linked into PEG hydrogels using a step-growth polymerization approach,[4,94,95] resulting in highly organized PEG hydrogel networks.[96] These PEG hydrogels have been demonstrated to provide excellent synthetic matrices for the controlled release of therapeutics[4,30] as well as tissue engineering applications, particularly when coupled with functional biomacromolecules such as the cell adhesive peptide RGD to enable PEG to effectively support cell growth.[97,98,39,99] The following discussion will highlight specific cross-linking chemistries that have been reported to generate injectable PEG-based hydrogels.

1.3.1 Azide-Alyne Cycloadditions: The cycloaddition of an azide with a terminal alkyne has received considerable interest for the design of hydrogels due the high selectivity and bioorthogonality of this cross-linking chemistry. The copper(I)-catalyzed alkyne-azide (CuAAC) click reaction[100] is of particular interest as it proceeds under physiological conditions. Ossipov and co-workers[17] reported the first azide-alkyne cross-linked hydrogel for a poly(vinyl alcohol) (PVA) system. A number of PEG-based azide-alkyne cross-linked hydrogels have since been reported. For example, Adzima and co-workers[101] reported a PEG hydrogel based on 4-arm PEG azide and a bifunctional PEG alkyne. This

group demonstrated temporal and spatial control over the CuAAC click reaction by using standard photolithographic techniques to photochemically reduce Cu(II) to Cu(I). This technique offers the ability to selectively pattern hydrogels to e.g. promote cell adhesion and could drastically reduce the amount of Cu(I) required for the synthesis of functional and well-defined PEG hydrogels. The reduction of the Cu(I) concentration is particularly relevant as the associated cytotoxicity of copper ions and reactive oxygen species generated by copper ions *in vivo* may pose a limitation towards clinical application.[16] Alternately, PEG-based hydrogels have been prepared based on mixtures of PEG with other functional entities.[101,102,103] For example, Tan and co-workers[103] developed a PEG hydrogel based on PEG-alkyne and an azido-functionalized α-cyclodextrin (αCD) that can cross-link through azide-alkyne chemistry as well as the formation of PEG-αCD inclusion complexes, providing cooperative control over both cross-link density and degradation mechanism/time (Figure 1.1).[104]

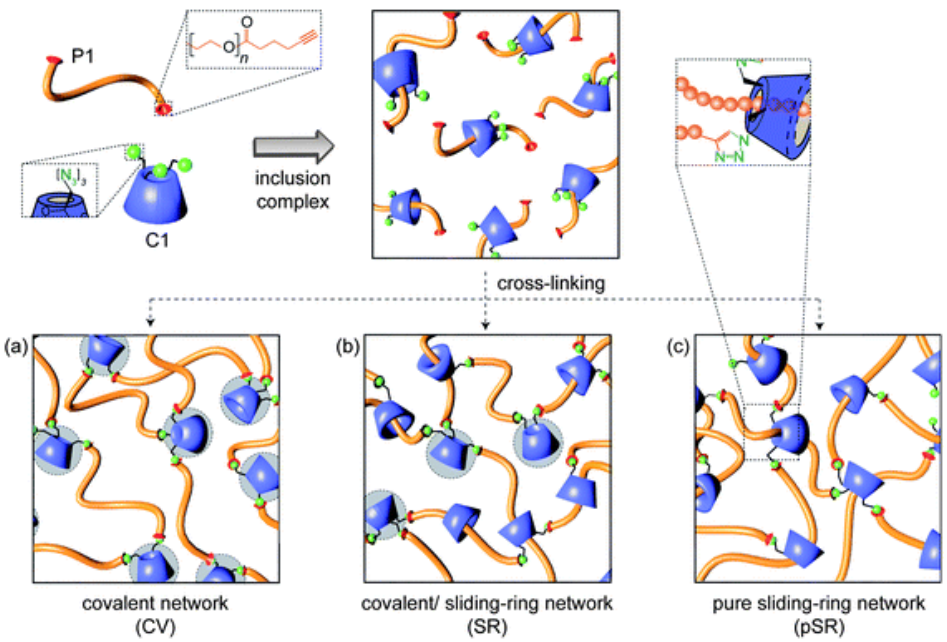

Figure 1.1. Schematic representation of the formation of α-cyclodextrin (αCD)-polyethylene glycol(PEG) hydrogels through the formation of alkyne-azide chemistry (CV), inclusion complexes (pSR) and a combination of both (SR). Reproduced from reference 103 with permission from RSC Publishing.

Strain-promoted alkyne-azide cycloaddition (SPAAC)[96] has been reported as a promising alternative to CuAAC, as cross-linking can occur under physiological conditions in the absence of Cu(I). Examples of SPAAC cross-linked PEG hydrogels have been reported by Anseth's group,[92,16] which demonstrated cross-linking of a 4-arm PEG tetraazide and a bis(cyclooctyne)-peptide. Zheng

and co-workers[105] reported an injectable PEG hydrogel based on 4-dibenzocyclooctynol (DIBO) functionalized difunctional PEG and a 3-arm glycerol exytholate triazide. These hydrogels formed within 5 minutes with a modulus of ~0.8 kPa and were capable of sustaining hMSC cell viability for 24 hours *in vitro*. Furthermore, the polymer precursors did not exhibit significant cytotoxicity at relevant concentrations for hydrogel preparation.[105] More recently, Hodgson et al., described the development of a series of PEG hydrogels synthesized using strain-promoted alkyne-azide cycloaddition (SPAAC) between PEG chains terminated with either aza-dibenzocyclooctynes or azide functionalities (Figure 1.2). The mechanical, rheological properties, gelation kinetics, and degradation kinetics could all be controlled based on the molecular weight of the precursor polymers, which were non-cytotoxic to 3T3 mouse fibroblasts at varying precursor concentrations.[51]

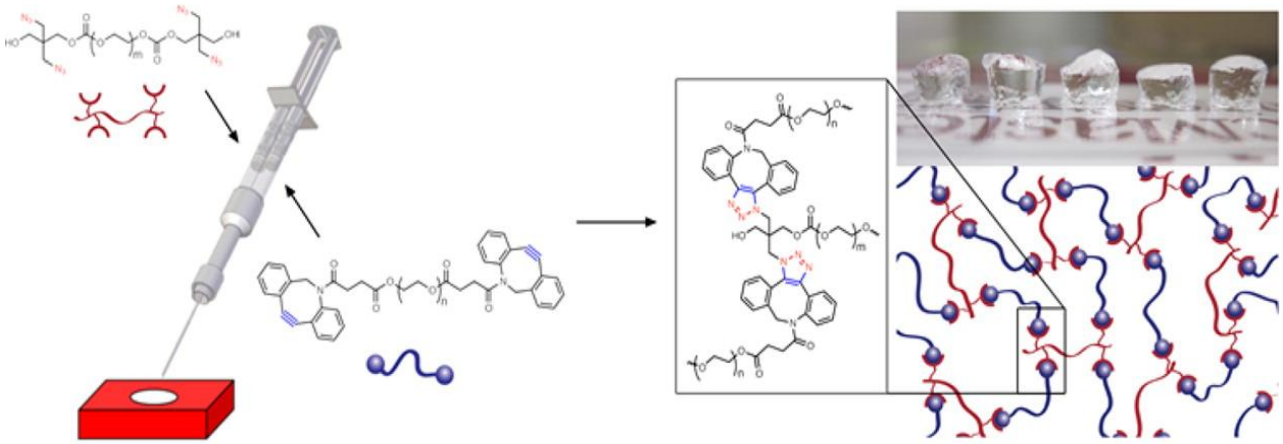

Figure 1.2. Graphical representation of hydrogel formation between $PEG_n(DIBAC)_2$ (blue polymer) and $PEG10k(N_3)_m$ (red polymer) using a double barrel syringe (left). The photograph (top right) shows actual hydrogel disks produced, with a visual representation of an idealized hydrogel network formed between the strained alkyne (blue) and azide (red) polymers shown below.

The high specificity, fast cross-linking kinetics, and excellent bioorthogonality will drive continuing interest in SPAAC, although the currently cumbersome synthesis of the cyclooctynes does at least now limit the broad applicability of this chemistry.

1.3.2 Michael Additions: The 1,4-addition of a nucleophile to the β position of an α,β-unsaturated carbonyl compound such as an aldehyde or ketone, commonly referred to as a Michael- type addition, is a widely investigated approach for injectable hydrogel preparation.[106] This cross-linking chemistry occurs spontaneously under physiological conditions, especially when thiols are used as the nucleophiles, and the formed thioether bonds are relatively weak and can be reversible. Different α,β-unsaturated electrophiles have been used in conjunction with thiols for the preparation of injectable hydrogels.[107] Although acrylates are the most commonly used electrophiles for Michael additions, maleimides[54, 108, 109]and vinyl sulfones[93] offer higher rates of cross-linking and have attracted more recent attention for this purpose. García and co-workers[39] demonstrated the advantages of these alternative electrophiles in preparing functional PEG hydrogels by cross-linking a thiol-containing adhesive peptide (GRGDSPC) with 4-arm PEG containing acrylate (PEG-4-AC), vinyl sulfone (PEG-4-VS), or maleimide (PEG-4-MAL) functional groups. In the presence of 4 mM triethanolamine (TEA), gelation kinetics depended considerably on the choice of Michael acceptor, ranging from 1-5 min for PEG-4-MAL, 30-60 min for PEG-4-VS, and 60 min for PEG-4-AC. Furthermore, the maleimide-based hydrogels required two orders of magnitude less TEA to gel, a significant attribute considering the known cytotoxic effects of TEA on endothelial cells, cells in the ovarian follicles, and pancreatic islet cells.[110] These hydrogels can also readily be functionalized using a dithiol protease-cleavable RGD peptide to create an *in vivo* degradable network that promoted the spreading of encapsulated C2C12 murine myoblasts.[111] Successful use of this hydrogel formulation was demonstrated *in vivo* via injection onto the pericardium of an excised rat heart (Figure 1.3).

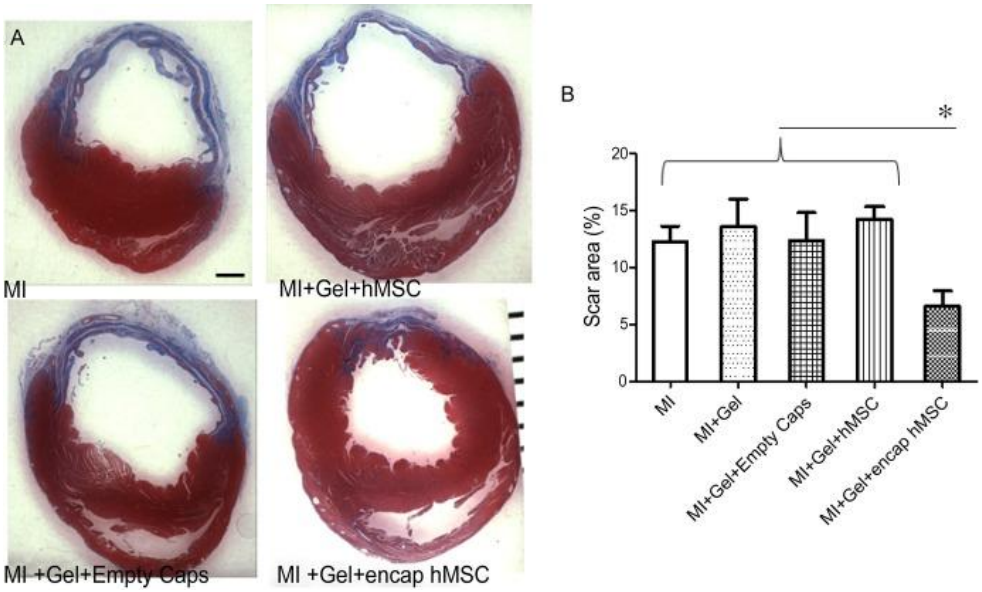

Figure 1.3. Treatment of hearts using human mesenchymal stem cells (hMSC) encapsulated in a 4-arm PEG maleimide- GRGDSPC dithiol injectable hydrogel showed reduced myocardial scarring after 28 days. A) Representative sections of infarcted hearts stained with Masson's Trichrome and treated with encapsulated hMSCs or control gels. Blue indicates fibrotic scar. ×15, scale bar=1 mm. B) Animals treated with encapsulated hMSCs showed reduced scar area (7±1%; n = 6) at 28 days compared to control treated hearts (MI: 12±1%, n = 8; MI+Gel: 14±2%, n = 7; MI+Gel+hMSC: 14±1%, n = 7; MI+Gel+Empty Caps: 12±2%, n = 5). Data represent mean±SEM. *P<0.05. MI indicates myocardial infarction. Reproduced from reference 111 with permission from the American Heart Association.

Michael addition cross-linked hydrogels have also been reported in the context of drug delivery applications, with Yu et al. cross-linking tetramaleimide and tetrathiol PEG to form transparent PEG hydrogels that quickly gelled under physiological conditions for the ocular delivery of Avastin®.[112] *In vitro* cytotoxicity indicated that the developed PEG hydrogel had no apparent cytotoxicity on L-929 fibroblast cells after 7 days of incubation; the cytotoxicity of the precursors was not determined despite concerns regarding the potential cross-reactivity and oxidation of thiols *in vivo* which persists as a potential limitation of thiol Michael additions. Prolonged Avastin® release was shown *in vitro* from these hydrogels for a period up to 14 days.[112]

1.3.3 Disulfide Formation: Disulfide bonds, formed via the oxidation of two thiol groups, play an essential structural and chemical role in protein folding and assembly. Thiols are protonated and unreactive in their reduced states (such as in the cytoplasm), but form S–S bonds in the presence of an oxidizing environment such as in the endoplasmic reticulum and extracellular space. Disulfide cross-linking is of significant interest for the design of injectable hydrogels as thiol-functionalized

precursors readily cross-link in the presence of oxidizing agents such as oxygen[113] but then degrade in the presence of reducing agents such as glutathione. Alternately, disulfide rearrangements (commonly found in nature for the formation of disulfide bonds in proteins) can be exploited for the formation of hydrogels and/or to promote hydrogel degradation. PEG-based disulfide cross-linked injectable hydrogels have been reported by Choh and co-workers,[113] prepared by coextruding pyridyl disulfide functionalized hyaluronic acid (HA-PD) with a PEG dithiol. Mixing of these precursors at physiological conditions results in macroscopic gelation within 4-5 minutes. Fibroblasts, endothelial cells (HUVECs), and adult stem cells (pMSCs) were successfully encapsulated *in vitro* and shown to proliferate over several days, even in the presence of unreacted thiols and the low-molecular-weight pyridine-2-thione cross-linking by-product. More recently, Kar et al. investigated whether the incorporation of disulfide moieties onto the backbone of PEG-based hydrogels could create injectable gels with degradation profiles that could be controlled by the cells encapsulated within them. The resulting hydrogels demonstrated tunable degradation kinetics ranging from hours to months, as facilitated by molecules secreted from human induced pluripotent stem cells (hiPSCs) and human mesenchymal stem cells (hMSCs) such as glutathione. After *in vivo* administration, hMSCs were more abundant in the host tissue compared to cells that were transplanted without the PEGDA gel after 48 and 72 hrs.[114]

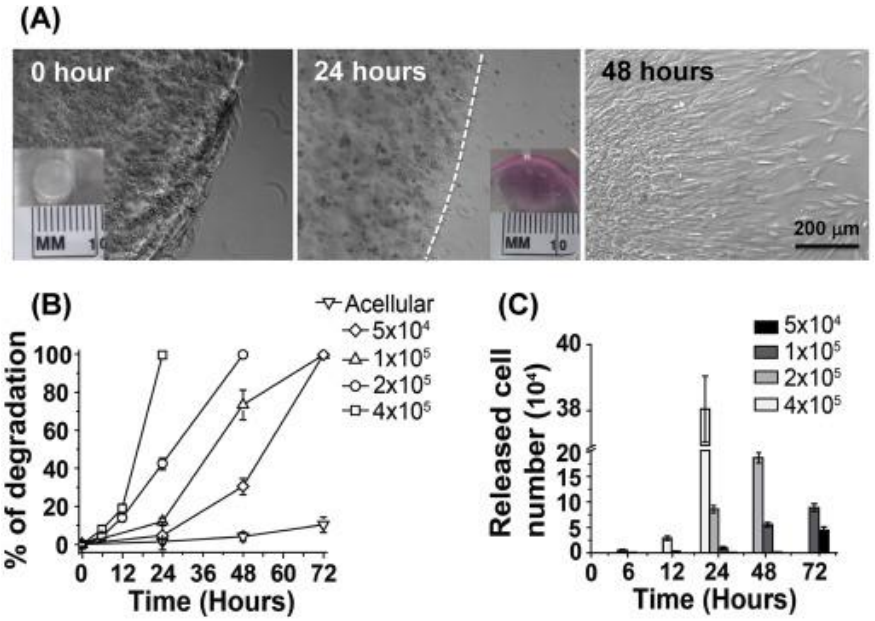

Figure 1.4. Cell-mediated degradation of dPEGDA hydrogels. (A) Bright-field images of the release of hMSCs from a 10-wt% cell-laden dPEGDA hydrogel, containing 2×10^5hMSCs, as a function of time (0–48 h). The inset shows the gross image of the corresponding cell-laden hydrogel. Scale bar: 200 µm. (B) Degradation profile of 10-wt% dPEGDA hydrogels containing different numbers (0–4×10^5) of hMSCs. (C) Number of hMSCs released from dPEGDA hydrogels containing varying numbers of encapsulated hMSCs. Reproduced from reference 114 with permission from Elsevier.

1.3.4 Diels-Alder cycloaddition: The addition of a conjugated diene to an activated double bond (dienophile) is referred to as a Diels–Alder cycloaddition. The most commonly used Diels–Alder reaction for cross-linking hydrogels involves the reaction between maleimide and furan functionalized precursors.[115,116,55] Diels-Alder reactions occur spontaneously under physiological conditions and are highly selective and relatively biorthogonal, aside from free thiol groups present at relatively low concentration in proteins.[117] Although Diels-Alder adducts are considered dynamic covalent bonds, reversibility of the formed adduct requires elevated temperatures beyond physiological temperature.[117] However, hydrogel degradation can be promoted under physiological conditions if the diffusion of hydrogel degradation products shifts the equilibrium towards the reverse Diels-Alder reaction. An illustrative example of the use of Diels-Alder chemistry for PEG hydrogels was recently reported by the groups of Bowman and Anseth.[118] The hydrogel network was formed using thiol-Michael chemistry, cross-linking a 4-arm PEG maleimide with a 4-arm PEG thiol. The maleimide functional groups are cross-reactive in Diels-Alder chemistry and thus provide a tethering site for a furan-modified RGD peptide (See Figure 1.4). By exploiting the reversible nature

of the Diels-Alder bond and le Châtelier's principle, the peptide could be release from the hydrogel with a release rate that is simply controlled by the excess of unreacted maleimide groups in the formed hydrogel network. For example, doubling the amount of maleimide groups present in the hydrogel decreased the amount of peptide released from approximately 60% to about 40%. Consequently, this example elegantly demonstrates how two different cross-link chemistries (i.e. thiol-Michael and Diels-Alder) can be used to independently control the rate of hydrogel degradation as well as release.

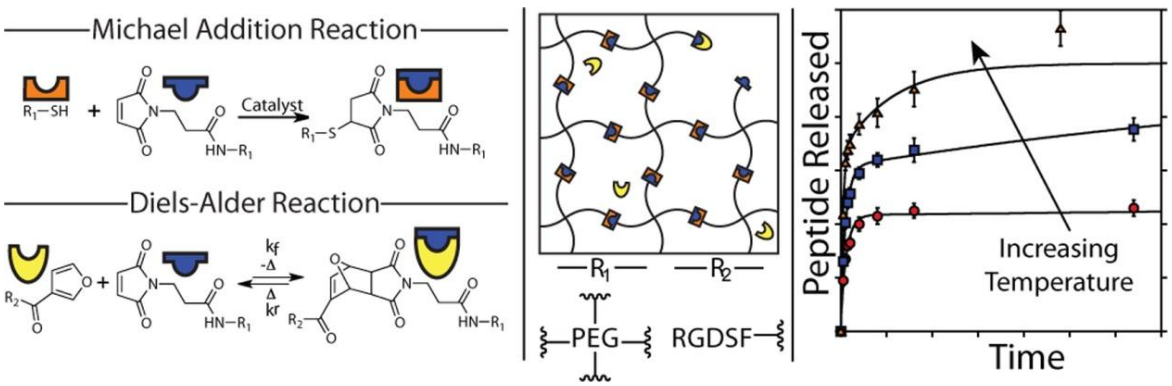

Figure 1.4. The formation of PEG hydrogels using thiol-Michael addition and the functionalization with a releasable fluorescent RGD peptide using Diels-Alder chemistry. A schematic representation of the hydrogel network and the release kinetics as a function of the temperature are also shown. Reproduced from reference 55 with permission from ACS publishing.

1.3.5 Schiff Base Formation: The nucleophilic addition of a nitrogen from an amine or hydrazide (or similar derivatives) to the carbonyl group of a ketone or aldehyde is referred to as a Schiff base or imine bond.[119] Schiff-bases are considered dynamic covalent bonds with the advantages of fast and tunable gelation kinetics[120] in the absence of a catalyst and complete reversibility. Conventional Schiff base formation between a carbonyl and a primary amine offers only limited hydrolytic stability and thus results in relatively fast hydrogel degradation.[119] Increased hydrolytic stability is achievable by increasing the nucleophilicity of the amine derivative, with the majority of the Schiff base cross-linked hydrogels reported have been based on hydrazone bond formation between a hydrazide and an aldehyde.[48,81,119,] An example of a PEG-based Schiff base hydrogel was reported by Saito and co-workers[37] for the delivery of doxorubicin. A doxorubicin-loaded hydrogel was prepared by conjugating doxorubicin to a low molecular weight PEG dialdehyde (5 kDa) using Schiff base chemistry, followed by mixing with a solution of a high molecular weight poly(vinylamine) (PVam)

(Figure 1.5). The precursor gelled quickly upon mixing and the resulting hydrogel showed sufficient hydrolytic stability at physiological pH for the targeted application. Prolonged doxorubicin was demonstrated up to 100 hours.[37] However, the functional groups used in Schiff base formation (in particular aldehydes) are cross-reactive with functional groups on biomacromolecules (e.g. amines), such that care must be taken in designing the precursor polymers and gelation times in order to avoid potential toxicity.[121]

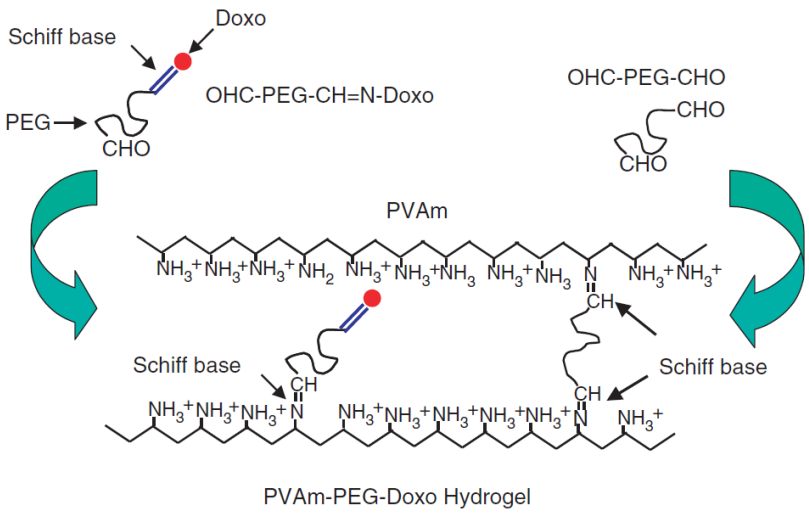

Figure 1.5. Schematic representation of the formation of poly(vinylamine) (PVAm)-poly(ethylene glycol) (PEG)-doxorubicin(doxo) hydrogels using Schiff base chemistry. Reproduced from reference 37 with permission from SAGE journals.

1.3.6 Oxime Chemistry: Oxime bonds form rapidly between an aldehyde or ketone and a hydroxylamine under physiological conditions and offer enhanced hydrolytic stability relative to Schiff base cross-linking strategies at the cost of requiring an acid catalyst in order to proceed at an appreciable rate. Grover and co-workers[59] have used oxime chemistry to synthesize PEG hydrogels through the reaction of an 8-arm aminooxy PEG with glutaraldehyde (Figure 1.6). The mechanical properties, gelation kinetics, and water swelling ratios could be tuned according to the weight fraction of precursor polymers and the pH, and hydrogels modified with RGD successfully supported hMSC cell encapsulation. The *in vivo* potential of oxime cross-linked hydrogels formed between a 4-arm aminooxy PEG and a 4-arm PEG ketone was subsequently evaluated in myocardial tissue by introducing the hydrogel using a catheter.[90] While *in vitro* gelation rates ranged from 30 minutes at pH 4 to >50 hours at pH 7.4, *in vivo* gelation was observed within 20 minutes independent of the pH

of the injection solution (pH 6.0–7.4). This effect can be attributed to the more complex biological environment *in vivo* relative to *in vitro* experiments.

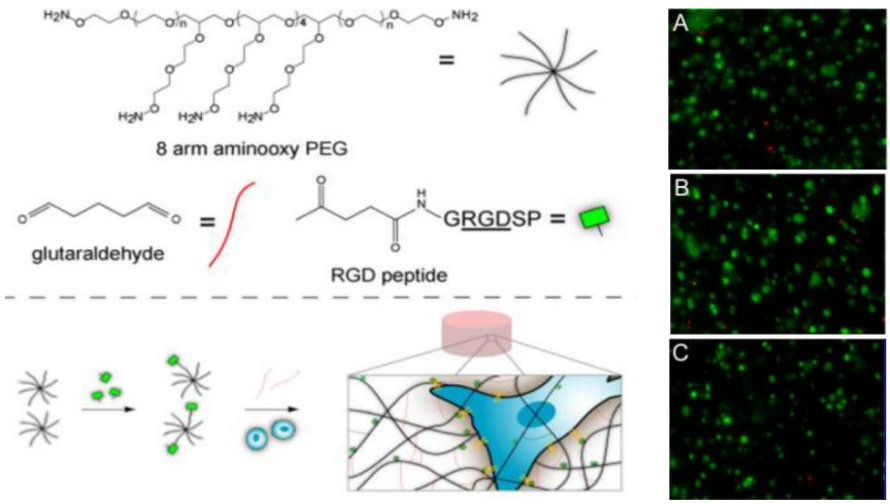

Figure 1.6. Synthesis and encapsulation of MSCs within RGD-functionalized oxime-cross-linked PEG hydrogels. Reproduced from reference 59 with permission from the American Chemical Society.

1.3.7 Hydrazone crosslinking chemistries: The use of hydrazone cross-linking chemistry for injectable hydrogels was first proposed by Bulpitt and Aeschlimann[122] and has been further developed by Langer's group[81,123] Hoare's group[124–127] and others[17,128,30,129] to a broad range of biopolymer, synthetic and composite hydrogel systems. Hydrazone chemistry offers significant benefits in terms of both its fast gelation kinetics (sometimes within seconds) and the pH-responsive hydrolytic reversibility of the hydrazone bond. Hydrazide and aldehyde functional groups can be introduced onto a range of synthetic and natural polymers using facile and few step copolymerization and post-polymerization modification strategies[48,130]. Furthermore, hydrazide and aldehyde functionalized precursors provide sufficient bio-orthogonality (even in the presence of potential Schiff-base formation between the pendant aldehydes and available amines on native proteins) such that it is atypical to see reports of any significant adverse reactions *in vitro* and *in vivo*.[15,131] This result has been attributed to the high reversibility of the aldehyde-amine Schiff base pair (i.e. a hydrazone bond will form preferentially to minimize free energy) and the fast gelation kinetics which rapidly consume a large fraction of the free aldehyde groups before proteins can diffuse into the hydrogel.

The clear advantages of hydrazone crosslinked hydrogels in terms of rapid gelation and hydrolytic degradation *in vivo* has resulted in their widespread recent use in drug delivery and tissue

engineering applications. For example, Zhu et al. developed a hydrazone crosslinked hydrogel comprised of a hydrazide-functionalized elastin-like protein (ELP) and aldehyde-functionalized hyaluronic acid (HA) for use as an injectable 3D scaffold for cartilage regeneration.[132] By increasing the amount of hyaluronic acid precursor polymer incorporated, an increase in sGAG deposition (integral for new chondrocyte formation) and a decrease in undesirable fibrocartilage accumulation was observed. Additionally, the biological and physiochemical properties of the HA gels could be decoupled (a common challenge associated with the use of HA hydrogels for applications requiring mechanical stability) to maintain gel mechanical stiffness by using an off-balance stoichiometric ratio of aldehyde:hydrazide groups (Figure 1.7).[132]

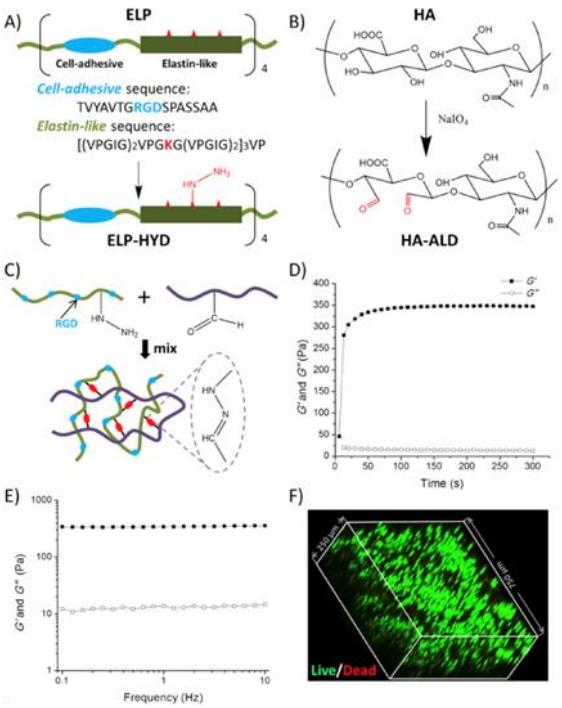

Figure 1.7. Design and characterization of protein hydrogels for 3D cell encapsulation. (A) Elastin-like protein (ELP) was designed with four modular repeats of cell-adhesive (blue) and structural elastin-like (green) sequences. Lysine residues (red) were used to generate hydrazide-modified ELP (ELP-HYD). (B) Synthesis of aldehyde-modified hyaluronic acid (HA-ALD). (C) ELP-HA hydrogel was formed via reaction between hydrazide groups on ELP-HYD and aldehyde groupss on HA-ALD to form dynamic covalent hydrazone linkages. (D & E) Rheological characterization of ELP-HA (1.8 wt%, 1.5 wt%) hydrogel during (D) an oscillatory time sweep at 25 °C demonstrates the onset of gelation and (E) an angular frequency sweep at 37 °C demonstrates gel stability at physiological conditions. Storage moduli (*G'*) are shown with filled symbols and loss moduli (*G"*) are shown with empty symbols. (F) Chondrocytes demonstrated round morphology and high viability after encapsulation in 3D ELP-HA hydrogels, as shown by confocal imaging of live/dead staining. Reproduced with permission from Elsevier.

Apostolides et al. demonstrated an alternative application of hydrazone crosslinked systems, using hydrazone chemistry to crosslink tetra-PEG hydrogels with self-healing properties.[133] Hydroxyl end-functionalized tetra-PEGs were activated by either an aldehydic phenol or by an aldehyde-protected acyhydrazide phenol to create tetrabenzaldehyde tetraPEG (TBPEG) and tetrabenzaacylhydrazide tetraPEG (TBAHPEG) precursor solutions, which were catalyzed with an acidic solution (pH~3.5) to form a gel within minutes. Interestingly, these hydrogels exhibited self-healing properties dependent on the pH of the gel solution (Figure 1.8), with self healing observed at low pHs where hydrazone bond exchange is sufficiently fast. It should be noted however that this formulation is not a good candidate for *in vivo* injection since gelation is very slow (i.e. over a few hours) at pH 7.0.

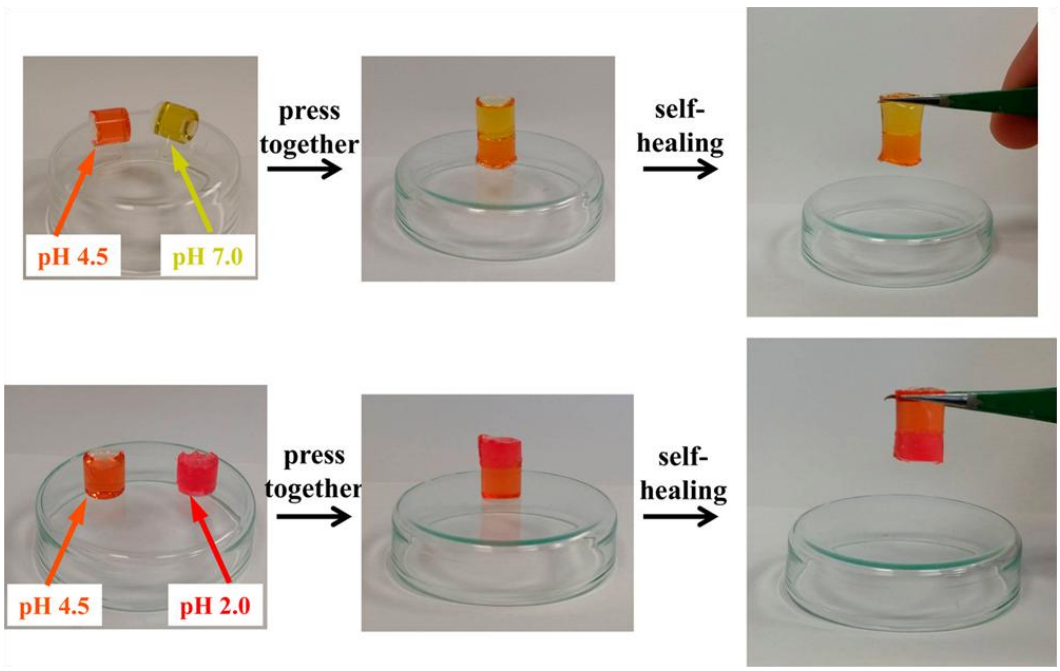

Figure 1.8. Self-healing between tetraPEG DYNAgels prepared at low pH values, without the need for added hydrazone bond exchange catalyst. The different colors are a direct result of the added universal pH indicator.[133] Reproduced with permission from the American Chemical Society.

1. 4. Poly(oligoethylene glycol methacrylate)-Based Hydrogels

Despite the obvious advantages of using PEG as a precursor polymer for the preparation of injectable hydrogels (specifically, its controlled molecular weight and protein repellent properties), PEG also suffers from a number of limitations. As PEG can only be selectively modified at the α,ω-hydroxyl chain ends, relatively expensive multi-arm PEG precursors must be used as precursor polymers to promote network formation at lower PEG concentrations. Furthermore, incorporation of specific functionalities (e.g. RGD peptide or other biomolecules) effectively competes with cross-linking since these functional tethers need to be incorporated at the same reactive sites; in this sense, the number of cross-links and functional tethers is inherently limited by the number of chain ends on the PEG starting materials, significantly limiting the mechanical strength of the resulting hydrogel. Consequently, we have started exploring injectable PEG analogue polymers that can be synthesized from free-radical polymerization as a potential system to improve upon PEG-based hydrogel designs.

In order to address challenges with injectable PEG hydrogels and PEG more broadly as a biomaterial, poly(oligoethylene glycol methacrylate) (POEGMA) is now being investigated as an alternative to PEG.[134,135] Unlike PEG, which is typically prepared via ring-opening polymerization and thus cannot readily be co-polymerized with other functional comonomers, POEGMA is synthesized from conventional (or controlled/living) free-radical polymerization,[134,135,136] offering excellent control over polymer composition, functionality, architecture and molecular weight distribution with a range of functional monomers to impart desired functionalities to the polymers. POEGMA can also be made thermoresponsive via the statistical copolymerization of oligo(ethylene glycol) methacrylate (OEGMA) monomers with varying lengths of ethylene oxide (EO) side chains (*n*).[135] For example, statistical copolymers of diethylene glycol methacrylate ($M(EO)_2MA$, n = 2) and OEGMA with an average molecular weight of 475 $g \cdot mol^{-1}$ ($OEGMA_{475}$, n = 8-9) display a cloud point in water according to a linear correlation between the cloud points of the respective $PM(EO)_2MA$ (~23°C) and $POEGMA_{475}$ (~90°C) homopolymers.[135] The reversible temperature transition shows little hysteresis[137] when compared to other thermoresponsive synthetic polymers such as *N*-isopropylacrylamide (NIPAAm) due to the lack of a hydrogen-bond donor.[138] This property is of potential interest both for the design of "smart", environmentally-responsive biomaterials for on-demand drug delivery, triggerable cell adhesion, etc. as well as more generally as PEG-based materials with significantly

improved bioadhesion in the absence of functional peptide tags. At the same time, POEGMA has been demonstrated to display similar bio-inert ("stealth")[139,140] and non-cytotoxic properties[141] when compared to PEG. One such example of use of POEGMA polymers to impart stealth properties, is the use of POEGMA brush layers applied as coatings to various surfaces to minimize protein adsorption. Specifically, surface-initiated ATRP (SI-ATRP) has been used to graft POEGMA brushes off of gold surfaces to decrease protein absorption and cell adhesion.[142] Recently, this same technique has been used to create POEGMA brush layers to construct a model surface to examine protein-surface interactions in a serum environment. The thickness of the hydrated brush layer could be well controlled by the polymerization time and density of surface initiators. Wang et al. used total internal reflection microscopy (TRIM) to investigate the degree to which newborn calf serum-coated polystyrene particles would associate with the hydrated POEGMA brush layer. The thicker the POEGMA coating of long chain OEGMA polymerized monomers (Figure 1.9 A-D), the stronger the repulsion to the protein coating polystyrene particles and the less overall adsorption observed. [143]

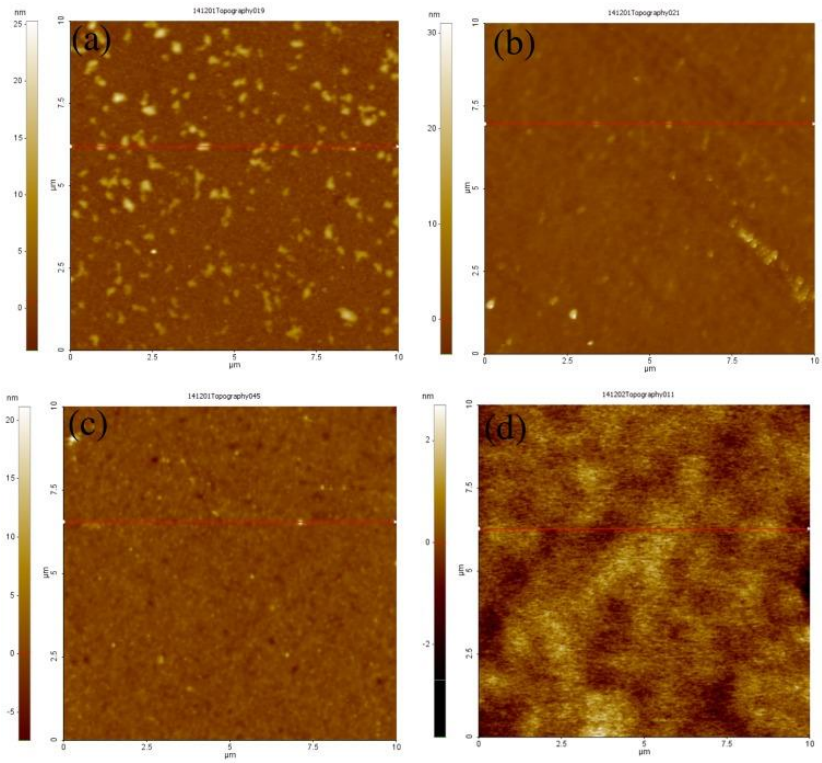

Figure 1.9. Atomic force microscope images of the POEGMA brush layer surfaces after TIRM measurements: (a) 4 nm-thick POEGMA brush layer, (b) 9 nm-thick POEGMA brush layer, (c) 17 nm-thick POEGMA brush, (d) 30 nm-thick POEGMA brush layer. Reproduced with permission from Elsevier.[143]

Building of the favourable biological properties of POEGMA polymers themselves, we and others have considered POEGMA polymers a promising platform for the synthesis of PEG-analogue hydrogels with improved control over the chemical, physical, and biological properties of the hydrogels.

A number of POEGMA-based hydrogels have been reported to-date,[144,145,146] including long-chain (PEG-like) gels targeting protein repellent coatings for protein seperation[147] and predominantly short-chain (PNIPAM-like) thermogelling hydrogels aiming to provide a biologically responsive matrix.[148,141,149] POEGMA hydrogels are typically prepared through controlled polymerization techniques to design POEGMA polymers to possess a LCST behavior and thus undergo a physical sol-gel transformation in the presence of heat.

Lutz et al. have done significant exploration of the use of POEGMA polymers to make biologically relevant hydrogels[135]. Using ATRP polymerization, they were able to create POEGMA polymers with well defined molecular weights and LCST behaviours. Lutz et al. further investigated varying the mol% of incorporation of $OEGMA_{475}$ (relative to the short-chain monomer $M(EO)_2MA$) within the POEGMA hydrogels in the presence of human hepatocellular carcinoma (HepG2) cells and shown high cell viabilities in each case. Of the linear polymers below, P(MEO_2MA-*co*-$OEGMA_{475}$) copolymers, will have collapsed at 37 °C and formed self-aggregated gels. (Figure 1.10)

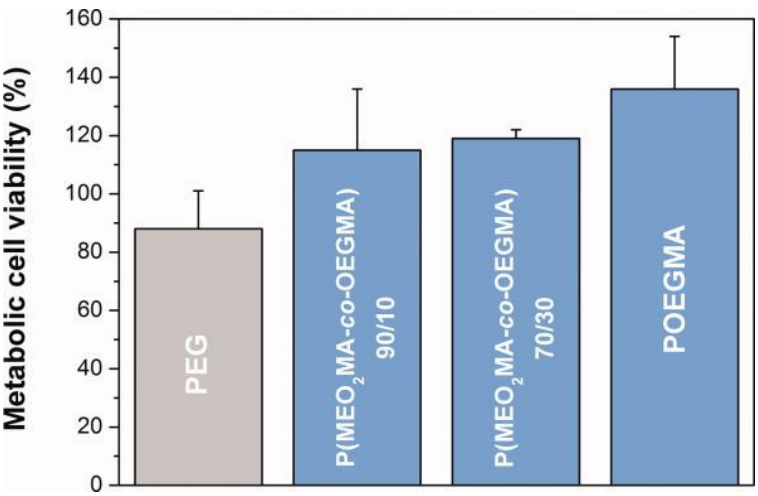

Figure 1.10. Metabolic cell viability measured for human hepatocellular carcinoma (HepG2) cell lines incubated at 37 °C in the presence of either a linear poly(ethylene glycol), a copolymer P(MEO_2MA-*co*-$OEGMA_{475}$) containing 10 mol % of $OEGMA_{475}$ units, a copolymer P(MEO_2MA-*co*-$OEGMA_{475}$) containing 30 mol % of $OEGMA_{475}$ units or a $POEGMA_{475}$ homopolymer. Reproduced with permission from Wiley Interscience.

Prior to the work performed in this thesis, injectable versions of POEGMA hydrogels were based on the thermoresponsive properties of POEGMA to drive physical gelation upon heating and, alternately, at the physiological temperature of 37°C.[150] The work of Fechler et al. is one such example, in which a 4-arm PEG-*b*-POEGMA polymer synthesized using ATRP in the presence of either linear or star-shaped PEG macroinitiators. By incorporating a 9:1 ratio of the short:long chain OEGMA monomers, Fechler et al. demonstrated the ability to precisely control the interactions between the polymers in water at different temperatures, ranging from the induction of strong thickening effects to macroscopic gelation depending on the macromolecular architecture of the polymers. [150] However, with the exception of a 4-arm PEG-*b*-POEGMA polymer reported by Fechler, which undergoes physical gelation at the physiological temperature of 37°C,[148] no previously reported POEGMA hydrogel was either injectable or degradable *in vivo*, severely limiting their potential clinical application.

1.5. Summary and Perspectives

PEG and PEG-analogue materials hold tremendous potential for the design of both *in vivo* scaffolds for drug delivery or tissue engineering as well as *in vitro* for cell culturing applications. Injectable analogues of such hydrogels offer even more promise both for effective 3D scaffolding of cells in these hydrogels by simple mixing as well as non-invasive administration *in vivo*, reducing the complexity of hydrogel use in the body as well as opening up potential uses of hydrogels in areas generally disfavored for routine surgical procedures if they are avoidable (e.g. the eye). Newer methods to incorporate multiple functional tethers (both physical and biological) on PEG-based hydrogels to direct cell responses in more precise and, in some cases, externally triggered ways suggest the potential use of PEG-based hydrogels in next-generation tissue engineering approaches. However, in our view, the significant synthetic challenges associated with functionalizing PEG, particularly in a manner that is independent of the cross-link density of the ultimate PEG-based hydrogel network, make PEG analogues such as POEGMA of increasing significance along the path of synthetically replicating (to the extent possible) natural cell microenvironments. To this end, an improved understanding of the similarities and differences between the well-established tissue responses and clearance mechanisms of PEG and those of POEGMA is essential to establish whether

or not the synthetic versatility offered by POEGMA-based hydrogels can truly be exploited in a broad range of potential biomedical applications.

1.6 Objectives

In light of the challenges with conventional PEG hydrogels and the opportunities posed by POEGMA-based materials, the central objective of this thesis is to develop a library of POEGMA precursor polymers based on hydrazide/aldehyde chemistry and explore how this library can be applied to generate functional hydrogel scaffolds with desirable properties for tissue engineering, cell delivery, or drug delivery applications. We hypothesize that this library of POEGMA polymers will allow for the design and development ofnovel functional biomaterials that exhibit extremely low protein adsorption, tunable cell interfacial properties, and favourable tissue responses while remaining amenable to minimally invasive injection-based delivery. Additionally, we hypothesize that the gel properties can be rationally tuned through the chemical manipulation of the POEGMA precursor polymers and by co-incorporating natural polymer dextran as one of the precursor polymers.

Chapter 2 describes the first reported development of injectable, degradable bulk POEGMA hydrogels based on covalent crosslinking, with gelation occurring due to the crosslinking of hydrazide and aldehyde group, formed through the incorporation of functional monomers acrylic acid (AA) and N-(2,2-dimethoxyethyl)methacrylamide (DMEMAm) with monomer oligothylene glycol methacrylate using free radical polymerization and then post-functionalized to provide hydrazide and aldehyde groups. This chapter aimed to show the cytocompatibility of the POEGMA precursor polymers and how the resultant POEGMA hydrogels formed through hydrazone crosslinking could (1) match the anti-fouling and positive cell interactive properties of conventional poly(ethylene glycol) hydrogels, but (2) create systematically tunable physiochemical properties (swelling, degradation, mechanics) through the facile incorporation of varying densities of functional monomer and/or polymer precursor concentration. By creating a system analogous to PEG-based hydrogel scaffolds, the further investigation of translation to biomedical applications could be pursued.

Chapter 3 represents a thorough investigation of the effect of varying the LCST behaviour of POEGMA precursor polymers and the effect of polymer LCST on both the physiochemical and biological properties of the POEGMA hydrogels. This chapter builds on the results from Chapter 2,

where we looked at one POEGMA hydrogel system with an LCST above 90˚ C, and thus does not exhibit a volume phase transition temperature around body temperature. This chapter describes the formulation of 2 new hydrogels based on the manipulation of LCST of the precursor polymers to form (1) a POEGMA hydrogel mimicking the volume phase transition temperature of PNIPAM, and (2) a POEGMA hydrogel already collapsed at room temperature. These new POEGMA hydrogels demonstrated that manipulation of temperature responsive properties could in fact affect both the physiochemical (swelling, degradation, mechanics) and biological (protein adsorption, cell adhesion, temperature-switchable cell delamination, and *in vivo* inflammatory responses) substantially.

Chapter 4 describes the further development of systematically tunable, modular mix-and-match hydrogel scaffolds based on the mixing of precursor polymers (PEG-like and PNIPAM-like) at different ratios. Specifically, we aimed to create an "off-the-shelf" concept hydrogel platform, with end-user biomedical companies in mind in which hydrogel properties could be easily tuned by simple mixing of precursor polymers with well-defined properties. Such an approach enables a hydrogel scaffold to be made easily application specific without the need for further synthetic synthesis of new precursor polymer. Macroscopically, bulk properties of a single precursor can be predicted based on the mixture of polymers that yield the same properties. Microscopically, the introduction of precursor polymers with different LCSTs leads to the formation of heterogeneity in microscale morphology within the systems leading to areas of more collapsed polymer that increase and modulate the protein adsorptive and adsorptive behaviours, cell adhesion, and *in vivo* inflammatory responses.

Chapter 5 describes the development of a new set of POEGMA precursor polymers that include both cationic (N-dimethylaminoethylmethacrylate, DMAEMA) and/or anionic (acrylic acid) (AA) functional comonoomers. The polymers were prepared using long-chain OEGMA (n=8-9) and functional monomer acrylic acid (leading to hydrazide groups) or N-(2,2-dimethoxyethyl)methacrylamide (DMEMAm, leading to aldehyde groups). Using these novel synthesized polymers, four uniquely charged hydrogel systems (neutral, cationic, amphoteric and anionic) were created and characterized via both bulk macroscopic measurements (swelling, degradation profiles, mechanical properties), and microscopic morphology assays (small angle neutron scattering (SANS) and isothermal titration calorimetry (ITC)). The structure-property

correlations between charge effects at varying lengths scales were described and developed to further develop the design of POEGMA hydrogels for targeted applications.

Chapter 6 describes the investigation of charge inclusion in the thermoresponsive POEGMA hydrogel platform firstly described in Chapter 3 to create functional hydrogels targeted for use as a cell delivery matrix. By using similar chemistry to Chapter 5 but using more short chain OEGMA monomer to create dual charged and thermoresponsive hydrogels, four new charged and thermoresponsive hydrogels (neutral, cationic, amphoteric and anionic were developed). The impact of charge on the physiochemical properties of the gels was analyzed, with specific note to characterize the effect of charge on the temperature response and the dual cross-linking (covalent and ionic) occurring in the amphoteric gel system. Cell adhesion of 3T3 mouse fibroblasts and cell viability/proliferative ability of ARPE-19 human retinal epithelial cells were both found to be enhanced in the charged hydrogels, with different charges influencing cell viability, clumping, and proliferation in subtly different ways over the 15 day time course observed. Additionally, the *in vivo* chronic tissue response following subcutaneous injection into BALB/c mice was mild for gels prepared with all charge types. The results of this chapter confirm the potential translatability of these POEGMA hydrogels for practical *in vivo* applications.

Chapter 7 describes the effects of incorporating a natural polymer (dextran) into the POEGMA gels by oxidizing dextran to expose aldehyde groups and forming gels using the same hydrazone chemistry. Our interest in such modification is to introduce native biological activity (e.g. enzymatic degradation) into such hydrogels while still maintaining the benefits of POEGMA. Dextran is shown to enhance cell adhesion to the gels while maintaining the thermoresponsive properties and low non-specific protein adsorption of POEGMA, at least when the residual aldehyde content of the gel is kept low. This chapter thus outlines the effect of including a natural polymer into the POEGMA gel system and the subsequent impacts of that natural polymer on the both the physiochemical and biological properties, offering the potential to better mimic cell extracellular matrices to control cell responses.

Chapter 8 summarizes the main conclusions of the thesis as well as proposes future experiments to extend this work.

1.7 References

(1) Van Vlierberghe, S.; Dubruel, P.; Schacht, E. Biopolymer-Based Hydrogels as Scaffolds for Tissue Engineering Applications: A Review. *Biomacromolecules* **2011**, *12*, 1387–1408.

(2) Tibbitt, M. W.; Anseth, K. S. Hydrogels as Extracellular Matrix Mimics for 3D Cell Culture. *Biotechnol. Bioeng.* **2009**, *103*, 655–663.

(3) Li, Z.; Guan, J. Hydrogels for Cardiac Tissue Engineering. *Polymers (Basel).* **2011**, *3*, 740–761.

(4) Lin, C.-C.; Anseth, K. S. PEG Hydrogels for the Controlled Release of Biomolecules in Regenerative Medicine. *Pharm. Res.* **2009**, *26*, 631–643.

(5) Hoare, T. R.; Kohane, D. S. Hydrogels in Drug Delivery: Progress and Challenges. *Polymer (Guildf).* **2008**, *49*, 1993–2007.

(6) Murua, A.; Orive, G.; Hernandez, R. M.; Pedraz, J. L. Epo Delivery by Genetically Engineered C2C12 Myoblasts Immobilized in Microcapsules. *Adv. Exp. Med. Biol.* **2010**, *670*, 54–67.

(7) Jiang, X.-J.; Wang, T.; Li, X.-Y.; Wu, D.-Q.; Zheng, Z.-B.; Zhang, J.-F.; Chen, J.-L.; Peng, B.; Jiang, H.; Huang, C.; *et al.* Injection of a Novel Synthetic Hydrogel Preserves Left Ventricle Function after Myocardial Infarction. *J. Biomed. Mater. Res. A* **2009**, *90*, 472–477.

(8) Dhandayuthapani, B.; Yoshida, Y.; Maekawa, T.; Kumar, D. S. Polymeric Scaffolds in Tissue Engineering Application: A Review. *Int. J. Polym. Sci.* **2011**, *2011*, 1–19.

(9) Lutolf, M. P.; Lauer-Fields, J. L.; Schmoekel, H. G.; Metters, A. T.; Weber, F. E.; Fields, G. B.; Hubbell, J. A. Synthetic Matrix Metalloproteinase-Sensitive Hydrogels for the Conduction of Tissue Regeneration: Engineering Cell-Invasion Characteristics. *Proc. Natl. Acad. Sci. U. S. A.* **2003**, *100*, 5413–5418.

(10) Lutolf, M. P.; Hubbell, J. A. Synthetic Biomaterials as Instructive Extracellular Microenvironments for Morphogenesis in Tissue Engineering. *Nat. Biotechnol.* **2005**, *23*, 47–55.

(11) Zhu, J. Bioactive Modification of Poly(ethylene Glycol) Hydrogels for Tissue Engineering. *Biomaterials* **2010**, *31*, 4639–4656.

(12) Boateng, J. S.; Matthews, K. H.; Stevens, H. N. E.; Eccleston, G. M. Wound Healing Dressings

and Drug Delivery Systems: A Review. *J. Pharm. Sci.* **2008**, *97*, 2892–2923.

(13) Wang, H.; Liu, Z.; Li, D.; Guo, X.; Kasper, F. K.; Duan, C.; Zhou, J.; Mikos, A. G.; Wang, C. Injectable Biodegradable Hydrogels for Embryonic Stem Cell Transplantation: Improved Cardiac Remodelling and Function of Myocardial Infarction. *J. Cell. Mol. Med.* **2012**, *16*, 1310–1320.

(14) Sivakumaran, D. N. Injectable In Situ Gellable Hydrogel-Microgel Composites For Drug Delivery. *Open Access Diss. Theses. Pap. 4439* **2010**.

(15) Smeets, N. M. B.; Bakaic, E.; Patenaude, M.; Hoare, T. Injectable and Tunable Poly(ethylene Glycol) Analogue Hydrogels Based on Poly(oligoethylene Glycol Methacrylate). *Chem. Commun.* **2014**, *50*, 3306–3309.

(16) Jiang, Y.; Chen, J.; Deng, C.; Suuronen, E. J.; Zhong, Z. Click Hydrogels, Microgels and Nanogels: Emerging Platforms for Drug Delivery and Tissue Engineering. *Biomaterials* **2014**, *35*, 4969–4985.

(17) Ossipov, D. A.; Hilborn, J. Poly(vinyl Alcohol)-Based Hydrogels Formed by "Click Chemistry." *Macromolecules* **2006**, *39*, 1709–1718.

(18) Malkoch, M.; Vestberg, R.; Gupta, N.; Mespouille, L.; Dubois, P.; Mason, A. F.; Hedrick, J. L.; Liao, Q.; Frank, C. W.; Kingsbury, K.; *et al.* Synthesis of Well-Defined Hydrogel Networks Using Click Chemistry. *Chem. Commun.* **2006**, 2774.

(19) Johnson, T. D.; Christman, K. L. Injectable Hydrogel Therapies and Their Delivery Strategies for Treating Myocardial Infarction. *Expert Opin. Drug Deliv.* **2013**, *10*, 59–72.

(20) Li, Y.; Rodrigues, J.; Tomás, H. Injectable and Biodegradable Hydrogels: Gelation, Biodegradation and Biomedical Applications. *Chem. Soc. Rev.* **2012**, *41*, 2193–2221.

(21) Yu, L.; Ding, J. Injectable Hydrogels as Unique Biomedical Materials. *Chem. Soc. Rev.* **2008**, *37*, 1473–1481.

(22) Patenaude, M. J.; Smeets, N.; Hoare, T.R. Designing Injectable, Covalently Cross-Linked Hydrogels for Biomedical Applications. *Macromol. Rapid Commun.* **2014**, *35,* 598-617.

(23) Chan, B. K.; Wippich, C. C.; Wu, C.; Sivasankar, P. M.; Schmidt, G. Robust and Semi-Interpenetrating Hydrogels from Poly(ethylene Glycol) and Collagen for Elastomeric Tissue Scaffolds. *Macromol. Biosci.* **2012**, *12*, 1490–1501.

(24) Pedroso, D. C. S.; Tellechea, A.; Moura, L.; Fidalgo-Carvalho, I.; Duarte, J.; Carvalho, E.; Ferreira,

L. Improved Survival, Vascular Differentiation and Wound Healing Potential of Stem Cells Co-Cultured with Endothelial Cells. *PLoS One*. **2011**, *6,* 1-12.

(25) Christman, K. L.; Fok, H. H.; Sievers, R. E.; Fang, Q.; Lee, R. J.; Ph, D. Fibrin Glue Alone and Skeletal Myoblasts in a Fibrin Scaffold Preserve Cardiac Function after Myocardial Infarction. *Tissue Engineering.***2004**, *10*. 403-409.

(26) Ossipov, D. A.; Piskounova, S.; Varghese, O. P.; Hilborn, J. Functionalization of Hyaluronic Acid with Chemoselective Groups via a Disulfide-Based Protection Strategy for In Situ Formation of Mechanically Stable Hydrogels. *Biomacromolecules* **2010**, *11*, 2247–2254.

(27) Shoichet, M. S.; Li, R. H.; White, M. L.; Winn, S. R. Stability of Hydrogels Used in Cell Encapsulation : An In Vitro Comparison of Alginate and Agarose. *Biotechnol. Bioeng.* **1996**, *50*, 374–381.

(28) Breger, J. C.; Fisher, B.; Samy, R.; Pollack, S.; Wang, N. S.; Isayeva, I. Synthesis Of “click” alginate Hydrogel Capsules and Comparison of Their Stability, Water Swelling, and Diffusion Properties with that of Ca(+2) Crosslinked Alginate Capsules. *J. Biomed. Mater. Res. B. Appl. Biomater.* **2014**, 1–13.

(29) Van Tomme, S. R.; Van Steenbergen, M. J.; De Smedt, S. C.; Van Nostrum, C. F.; Hennink, W. E. Self-Gelling Hydrogels Based on Oppositely Charged Dextran Microspheres. *Biomaterials* **2005**, *26*, 2129–2135.

(30) Ito, T.; Yeo, Y.; Highley, C. B.; Bellas, E.; Kohane, D. S. Dextran-Based in Situ Cross-Linked Injectable Hydrogels to Prevent Peritoneal Adhesions. *Biomaterials* **2007**, *28*, 3418–3426.

(31) Mackinnon, N. J. Investigation of Unilamellar Phospholipid Vesicle Interactions with PNIPAM Based Hydrogel Beads. *Langmuir.* **2009**, *26,* 1081-1089.

(32) Al-Haydari, M. D. Immune Response to Synthesized Pnipam-Based Graft Hydrogels Containing Chitosan and Hyaluronic Acid. *Open Access Diss. Th* **2010**, *1*, 4193.

(33) Lee, S.-W.; Tettey, K. E.; Kim, I. L.; Burdick, J. A.; Lee, D. Controlling the Cell-Adhesion Properties of Poly(acrylic acid)/Polyacrylamide Hydrogen-Bonded Multilayers. *Macromolecules* **2012**, *45*, 6120–6126.

(34) Lord, M. S.; Stenzel, M. H.; Simmons, A.; Milthorpe, B. K. The Effect of Charged Groups on Protein Interactions with poly(HEMA) Hydrogels. *Biomaterials* **2006**, *27*, 567–575.

(35) Binetti, V. R.; Fussell, G. W.; Lowman, A. M. Evaluation of Two Chemical Crosslinking Methods

of Poly(vinyl Alcohol) Hydrogels for Injectable Nucleus Pulposus Replacement. *J. Appl. Polym. Sci.* **2014**, *131,* 40943.

(36) Lin, C.-C.; Anseth, K. S. Cell-Cell Communication Mimicry with Poly(ethylene Glycol) Hydrogels for Enhancing Beta-Cell Function. *Proc. Natl. Acad. Sci. U. S. A.* **2011**, *108*, 6380–6385.

(37) Saito, H.; Hoffman, A. S.; Ogawa, H. I. Delivery of Doxorubicin from Biodegradable PEG Hydrogels Having Schiff Base Linkages . *J. Bioact. Compat. Polym.* **2007**, *22*, 589–601.

(38) Wang, J.; Sun, H.; Li, J.; Dong, D.; Zhang, Y.; Yao, F. Ionic Starch-Based Hydrogels for the Prevention of Nonspecific Protein Adsorption. *Carbohydr. Polym.* **2015**, *117*, 384–391.

(39) García, A. J. PEG-Maleimide Hydrogels for Protein and Cell Delivery in Regenerative Medicine. *Ann. Biomed. Eng.* **2014**, *42*, 312–322.

(40) Chen, Y.-C.; Su, W.-Y.; Yang, S.-H.; Gefen, A.; Lin, F.-H. In Situ Forming Hydrogels Composed of Oxidized High Molecular Weight Hyaluronic Acid and Gelatin for Nucleus Pulposus Regeneration. *Acta Biomater.* **2013**, *9*, 5181–5193.

(41) Xu, X.; Jha, A. K.; Harrington, D. A.; Farach-Carson, M. C.; Jia, X. Hyaluronic Acid-Based Hydrogels: From a Natural Polysaccharide to Complex Networks. *Soft Matter* **2012**, *8*, 3280–3294.

(42) Azagarsamy, M. A.; Anseth, K. S. Bioorthogonal Click Chemistry : An Indispensable Tool to Create Multifaceted Cell Culture Scaffolds. *ACS macro letters.* **2013**, *2,* 5-9.

(43) Fu, Y.; Kao, W. J. In Situ Forming Poly(ethylene Glycol)-Based Hydrogels via Thiol-Maleimide Michael-Type Addition. *J. Biomed. Mater. Res. A* **2011**, *98*, 201–211.

(44) Baskin, J. M.; Bertozzi, C. R. Bioorthogonal Click Chemistry: Covalent Labeling in Living Systems. *QSAR Comb. Sci.* **2007**, *26*, 1211–1219.

(45) Hoffmann, B.; Seitz, D.; Mencke, A.; Kokott, A.; Ziegler, G. Glutaraldehyde and Oxidised Dextran as Crosslinker Reagents for Chitosan-Based Scaffolds for Cartilage Tissue Engineering. *J. Mater. Sci. Mater. Med.* **2009**, *20*, 1495–1503.

(46) Bott, R. Injectable Microgel-Hydrogel Composites For Prolonged Small Molecule Drug Delivery. *Igarss.* **2014**, 1–5.

(47) Patenaude, M.; Hoare, T. Injectable, Degradable Thermoresponsive Poly(N -Isopropylacrylamide) Hydrogels. *ACS Macro Lett.* **2012**, *1*, 409–413.

(48) Patenaude, M.; Hoare, T. Injectable, Mixed Natural-Synthetic Polymer Hydrogels with Modular

Properties. *Biomacromolecules* **2012**, *13*, 369–378.

(49) Nguyen, M. K.; Lee, D. S. Injectable Biodegradable Hydrogels. *Macromol. Biosci.* **2010**, *10*, 563–579.

(50) Nimmo, C. M.; Shoichet, M. S. Regenerative Biomaterials That "click": Simple, Aqueous-Based Protocols for Hydrogel Synthesis, Surface Immobilization, and 3D Patterning. *Bioconjug. Chem.* **2011**, *22*, 2199–2209.

(51) Hodgson, S. M.; Bakaic, E.; Stewart, S. A.; Hoare, T.; Adronov, A. Properties of Poly(ethylene Glycol) Hydrogels Cross-Linked via Strain-Promoted Alkyne-Azide Cycloaddition (SPAAC). *Biomacromolecules* **2016**, *17*.

(52) Yang, J. A.; Yeom, J.; Hwang, B. W.; Hoffman, A. S.; Hahn, S. K. In Situ-Forming Injectable Hydrogels for Regenerative Medicine. *Prog. Polym. Sci.* **2014**, *39*, 1973–1986.

(53) Parker, J.; Mitrousis, N.; Shoichet, M. S. Hydrogel for Simultaneous Tunable Growth Factor Delivery and Enhanced Viability of Encapsulated Cells in Vitro. *Biomacromolecules* **2016**, *17*, 476–484.

(54) Koehler, K. C.; Anseth, K. S.; Bowman, C. N. Diels-Alder Mediated Controlled Release from a Poly (Ethylene Glycol) Based Hydrogel. *Biomacromolecules.* **2013,** *14,* 4–9.

(55) Truong, V. X.; Ablett, M. P.; Richardson, S. M.; Hoyland, J. A.; Dove, A. P. Simultaneous Orthogonal Dual-Click Approach to Tough, in-Situ -Forming Hydrogels for Cell Encapsulation. *J. Am. Chem. Soc.* **2015**, *137*, 1618–1622.

(56) Shu, X. Z.; Liu, Y.; Luo, Y.; Roberts, M. C.; Prestwich, G. D. Disulfide Cross-Linked Hyaluronan Hydrogels. *Biomacromolecules* **2002**, *3*, 1304–1311.

(57) Hu, Z.; Cai, T.; Chi, C. Thermoresponsive Oligo(ethylene Glycol)-Methacrylate- Based Polymers and Microgels. *Soft Matter* **2010**, *6*, 2115-2123.

(58) Grover, G. N.; Braden, R. L.; Christman, K. L. Oxime Cross-Linked Injectable Hydrogels for Catheter Delivery. *Adv. Mater.* **2014**, *25,* 2937-2942.

(59) Grover, G. N.; Lam, J.; Nguyen, T. H.; Segura, T.; Maynard, H. D. Biocompatible Hydrogels by Oxime Click Chemistry. *Biomacromolecules* **2012**, *13*, 3013–3017.

(60) Naghash, H. J.; Okay, O.; Yağci, Y. Gel Formation by Chain-Crosslinking Photopolymerization of Methyl Methacrylate and Ethylene Glycol Dimethacrylate. *Polymer (Guildf).* **1997**, *38*, 1187–1196.

(61) Keskinel, M.; Okay, O. Effects of Cyclization and Electrostatic Interactions on the Termination Rate of Macroradicals in Free-Radical Crosslinking Copolymerization. *Polym. Bull.* **1998**, *40*, 491–498.

(62) Okay, O.; Kurz, M.; Lutz, K.; Funke, W. Cyclization and Reduced Pendant Vinyl Group Reactivity during the Free-Radical Cross-Linking Polymerization of 1,4-Divinylbenzene. *Macromolecules* **1995**, *28*, 2728–2737.

(63) Naghash, H. J.; Okay, O.; Yildirim, H. Gel Formation in Free-radical Crosslinking Copolymerization. *J. Appl. Polym. Sci.* **1995**, *56*, 477–483.

(64) Discher, D. E.; Mooney, D. J.; Zandstra, P. W. Growth Factors, Matrices, and Forces Combine and Control Stem Cells. *Science* **2009**, *324*, 1673–1677.

(65) Kablik, J.; Monheit, G. D.; Yu, L. P.; Chang, G.; Gershkovich, J. Comparative Physical Properties of Hyaluronic Acid Dermal Fillers. *Dermatologic Surg.* **2009**, *35*, 302–312.

(66) Anseth, K. S.; Metters, A. T.; Bryant, S. J.; Martens, P. J.; Elisseeff, J. H.; Bowman, C. N. In Situ Forming Degradable Networks and Their Application in Tissue Engineering and Drug Delivery. *J. Control. Release* **2002**, *78*, 199–209.

(67) Matsusaki, M.; Akashi, M. Novel Functional Biodegradable Polymer IV: pH-Sensitive Controlled Release of Fibroblast Growth Factor-2 from a Poly(gamma-Glutamic Acid)-Sulfonate Matrix for Tissue Engineering. *Biomacromolecules* **2005**, *6*, 3351–3356.

(68) Temenoff, J. S.; Mikos, A. G. Injectable Biodegradable Materials for Orthopedic Tissue Engineering. *Biomaterials* **2000**, *21*, 2405–2412.

(69) Sawhney, A. S.; Pathak, C. P.; Hubbell, J. A. Bioerodible Hydrogels Based on Photopolymerized Poly(ethylene). *Macromolecules* **1993**, *26*, 581–587.

(70) Seliktar, D. Designing Cell-Compatible Hydrogels for Biomedical Applications. *Science* **2012**, *336*, 1124–1128.

(71) Babensee, J. E.; Anderson, J. M.; McIntire, L. V.; Mikos, A. G. Host Response to Tissue Engineered Devices. *Adv. Drug Deliv. Rev.* **1998**, *33*, 111–139.

(72) Seal, B. L.; Otero, T. C.; Panitch, A. Polymeric Biomaterials for Tissue and Organ Regeneration. **2001**, *34*, 147–230.

(73) Lutz, J.-F. Thermo-Switchable Materials Prepared Using the OEGMA-Platform. *Adv. Mater.* **2011**, *23*, 2237–2243.

(74) Vancoillie, G.; Frank, D.; Hoogenboom, R. Thermoresponsive Poly(oligo Ethylene Glycol Acrylates). *Prog. Polym. Sci.* **2014**, *39*, 1074–1095.

(75) Smeets, N. M. B.; Bakaic, E.; Patenaude, M.; Hoare, T. Injectable and Tunable Poly(ethylene Glycol) Analogue Hydrogels Based on Poly(oligoethylene Glycol Methacrylate). *Chem. Commun.* **2014**, *50*, 3306–3309.

(76) Ozcelik, B.; Brown, K. D.; Blencowe, A.; Daniell, M.; Stevens, G. W.; Qiao, G. G. Ultrathin Chitosan-Poly(ethylene Glycol) Hydrogel Films for Corneal Tissue Engineering. *Acta Biomater.* **2013**, *9*, 6594–6605.

(77) Konradi, R.; Acikgoz, C.; Textor, M. Polyoxazolines for Nonfouling Surface Coatings--a Direct Comparison to the Gold Standard PEG. *Macromol. Rapid Commun.* **2012**, *33*, 1663–1676.

(78) Ladd, J.; Zhang, Z.; Chen, S.; Hower, J. C.; Jiang, S. Zwitterionic Polymers Exhibiting High Resistance to Nonspecific Protein Adsorption from Human Serum and Plasma. *Biomacromolecules* **2008**, *9*, 1357–1361.

(79) Shao, Q.; Jiang, S. Molecular Understanding and Design of Zwitterionic Materials. *Advanced materials.* **2015**, *27*, 15–26.

(80) Damodaran, V. B.; Murthy, N. S. Bio-Inspired Strategies for Designing Antifouling Biomaterials. *Biomater. Res.* **2016**, *20*, 18.

(81) Hudson, S. P.; Langer, R.; Fink, G. R.; Kohane, D. S. Injectable in Situ Cross-Linking Hydrogels for Local Antifungal Therapy. *Biomaterials* **2010**, *31*, 1444–1452.

(82) Nicodemus, G. D.; Bryant, S. J. Cell Encapsulation in Biodegradable Hydrogels for Tissue Engineering Applications. *Tissue Eng. Part B. Rev.* **2008**, *14*, 149–165.

(83) Hutson, C. B.; Nichol, J. W.; Aubin, H.; Bae, H.; Yamanlar, S.; Al-Haque, S.; Koshy, S. T.; Khademhosseini, A. Synthesis and Characterization of Tunable Poly(ethylene Glycol): Gelatin Methacrylate Composite Hydrogels. *Tissue Eng. Part A* **2011**, *17*, 1713–1723.

(84) Paulusse, J. M. J.; Amir, R. J.; Evans, R. a; Hawker, C. J. Free Radical Polymers with Tunable and Selective Bio- and Chemical Degradability. *J. Am. Chem. Soc.* **2009**, *131*, 9805–9812.

(85) Murthy, N.; Thng, Y. X.; Schuck, S.; Xu, M. C.; Fréchet, J. M. J. A Novel Strategy for Encapsulation and Release of Proteins: Hydrogels and Microgels with Acid-Labile Acetal Cross-Linkers. *J. Am. Chem. Soc.* **2002**, *124*, 12398–12399.

(86) Rippe, C.; Rippe, A.; Torffvit, O.; Rippe, B. Size and Charge Selectivity of the Glomerular Filter in

Early Experimental Diabetes in Rats. *Am. J. Physiol. Renal Physiol.* **2007**, *293*, F1533–F1538.

(87) Varghese, O.; Sun, W. In Situ Cross-Linkable High Molecular Weight Hyaluronan−Bisphosphonate Conjugate for Localized Delivery and Cell-Specific Targeting: A Hydrogel Linked Prodrug. *J Am Chem Soc* **2009**, *4*, 8781–8783.

(88) Deshmukh, M.; Singh, Y.; Gunaseelan, S.; Gao, D.; Stein, S.; Sinko, P. J. Biodegradable Poly(ethylene Glycol) Hydrogels Based on a Self-Elimination Degradation Mechanism. *Biomaterials* **2010**, *31*, 6675–6684.

(89) Jokerst, J.; Lobovkina, T.; Zare, R. N.; Gambhir, S. S. Nanoparticle PEGylation for Imaging and Therapy. *Nanomedicine* **2011**, *6*, 715–728.

(90) Grover, G. N.; Braden, R. L.; Christman, K. L. Oxime Cross-Linked Injectable Hydrogels for Catheter Delivery. **2014**, *25*, 2937–2942.

(91) Polizzotti, B. D.; Fairbanks, B. D.; Anseth, K. S. Three-Dimensional Biochemical Patterning of Click-Based Composite Hydrogels via Thiolene Photopolymerization. *Biomacromolecules* **2008**, *9*, 1084–1087.

(92) DeForest, C. a; Polizzotti, B. D.; Anseth, K. S. Sequential Click Reactions for Synthesizing and Patterning Three-Dimensional Cell Microenvironments. *Nat. Mater.* **2009**, *8*, 659–664.

(93) Rizzi, S. C.; Hubbell, J. A. Recombinant Protein- *Co* -PEG Networks as Cell-Adhesive and Proteolytically Degradable Hydrogel Matrixes. Part I: Development and Physicochemical Characteristics. *Biomacromolecules* **2005**, *6*, 1226–1238.

(94) McCall, J. D.; Anseth, K. S. Thiol-Ene Photopolymerizations Provide a Facile Method to Encapsulate Proteins and Maintain Their Bioactivity. *Biomacromolecules* **2012**, *13*, 2410–2417.

(95) Kyburz, K. A.; Anseth, K. S. Three-Dimensional hMSC Motility within Peptide-Functionalized PEG-Based Hydrogels of Varying Adhesivity and Crosslinking Density. *Acta Biomater.* **2013**, *9*, 6381–6392.

(96) Matsunaga, T.; Sakai, T.; Akagi, Y.; Chung, U.; Shibayama, M. Structure Characterization of Tetra-PEG Gel by Small-Angle Neutron Scattering. *Macromolecules* **2009**, *42*, 1344–1351.

(97) Ruoslahti, E.; Pierschbacher, M. Arg-Gly-Asp: A Versatile Cell Recognition Signal. *Cell* **1986**, *44*, 517–518.

(98) Ruoslahti, E. RGD and Other Recognition Sequences for Integrins. *Annu. Rev. Cell Dev. Biol.* **1996**, *12*, 697–715.

(99) Wacker, B. K.; Alford, S. K.; Scott, E. a; Das Thakur, M.; Longmore, G. D.; Elbert, D. L. Endothelial Cell Migration on RGD-Peptide-Containing PEG Hydrogels in the Presence of Sphingosine 1-Phosphate. *Biophys. J.* **2008**, *94*, 273–285.

(100) Speers, A. E.; Adam, G. C.; Cravatt, B. F. Activity-Based Protein Profiling in Vivo Using a Copper (I) -Catalyzed Azide-Alkyne [3 + 2] Cycloaddition. *J. Am. Chem. Soc.* **2003**, *4*, 4686–4687.

(101) Adzima, B. J.; Tao, Y.; Kloxin, C. J.; DeForest, C. A.; Anseth, K. S.; Bowman, C. N. Spatial and Temporal Control of the Alkyne–azide Cycloaddition by Photoinitiated Cu(II) Reduction. *Nat. Chem.* **2011**, *3*, 258–261.

(102) Van Dijk, M.; Van Nostrum, C. F.; Hennink, W. E.; Rijkers, D. T. S.; Liskamp, R. M. J. Synthesis and Characterization of Enzymatically Biodegradable Peg and Peptide-Based Hydrogels Prepared by Click Chemistry. *Biomacromolecules* **2010**, *11*, 1608–1614.

(103) Sun, T. L.; Kurokawa, T.; Kuroda, S.; Ihsan, A. Bin; Akasaki, T.; Sato, K.; Haque, M. A.; Nakajima, T.; Gong, J. P. Physical Hydrogels Composed of Polyampholytes Demonstrate High Toughness and Viscoelasticity. *Nat. Mater.* **2013**, *12*, 932–937.

(104) Okumura, Y.; Ito, K. The Polyrotaxane Gel: A Topological Gel by Figure-of-Eight Cross-Links. *Adv. Mater.* **2001**, *13*, 485–487.

(105) Zheng, J.; Smith Callahan, L. A; Hao, J.; Guo, K.; Wesdemiotis, C.; Weiss, R. a; Becker, M. L. Strain-Promoted Crosslinking of PEG-Based Hydrogels via Copper-Free Cycloaddition. *ACS Macro Lett.* **2012**, *1*, 1071–1073.

(106) Dittmer, D. C.; Swain, C. G.; Benson, R. E.; Friedman, M.; Cavins, J. F.; Wall, J. S. Relative Nucleophilic Reactivities of Amino Groups and. *J. Am. Chem. Soc.* **1965**, *87*, 3672–3682.

(107) Buwalda, S. J.; Dijkstra, P. J.; Feijen, J. In Situ Forming Poly(ethylene Glycol)- Poly(L -Lactide) Hydrogels via Michael Addition: Mechanical Properties, Degradation, and Protein Release. *Macromol. Chem. Phys.* **2012**, *213*, 766–775.

(108) Kiick, K.; Baldwin, A. D. Tunable Degradation of Maleimide-Thiol Adducts in Reducing Environments. *Bioconjugate Chemistry.* **2012**, *22*, 1946–1953.

(109) Tsurkan, M. V.; Chwalek, K.; Prokoph, S.; Zieris, A.; Levental, K. R.; Freudenberg, U.; Werner, C. Defined Polymer-Peptide Conjugates to Form Cell-Instructive Starpeg-Heparin Matrices in Situ. *Adv. Mater.* **2013**, *25*, 2606–2610.

(110) Phelps, E. A.; Enemchukwu, N. O.; Fiore, V. F.; Sy, J. C.; Murthy, N.; Sulchek, T. A.; Barker, T. H.;

García, A. J. Maleimide Cross-Linked Bioactive PEG Hydrogel Exhibits Improved Reaction Kinetics and Cross-Linking for Cell Encapsulation and in Situ Delivery. *Adv. Mater.* **2012**, *24*, 64–70, 2.

(111) Levit, R. D.; Landázuri, N.; Phelps, E. A.; Brown, M. E.; García, A. J.; Davis, M. E.; Joseph, G.; Long, R.; Safley, S. A.; Suever, J. D.; *et al.* Cellular Encapsulation Enhances Cardiac Repair. *J. Am. Heart Assoc.* **2013**, *2*, e000367.

(112) Yu, J.; Xu, X.; Yao, F.; Luo, Z.; Jin, L.; Xie, B.; Shi, S.; Ma, H.; Li, X.; Chen, H. In Situ Covalently Cross-Linked PEG Hydrogel for Ocular Drug Delivery Applications. *Int. J. Pharm.* **2014**, *470*, 151–157.

(113) Choh, S.-Y.; Cross, D.; Wang, C. Facile Synthesis and Characterization of Disulfide-Cross-Linked Hyaluronic Acid Hydrogels for Protein Delivery and Cell Encapsulation. *Biomacromolecules* **2011**, *12*, 1126–1136.

(114) Kar, M.; Vernon Shih, Y. R.; Velez, D. O.; Cabrales, P.; Varghese, S. Poly(ethylene Glycol) Hydrogels with Cell Cleavable Groups for Autonomous Cell Delivery. *Biomaterials* **2016**, *77*, 186–197.

(115) Wei, H.-L.; Yang, Z.; Zheng, L.-M.; Shen, Y.-M. Thermosensitive Hydrogels Synthesized by Fast Diels–Alder Reaction in Water. *Polymer (Guildf).* **2009**, *50*, 2836–2840.

(116) Nimmo, C. M.; Owen, S. C.; Shoichet, M. S. Diels-Alder Click Cross-Linked Hyaluronic Acid Hydrogels for Tissue Engineering. *Biomacromolecules* **2011**, *12*, 824–830.

(117) Baldwin, J. E.; Herchen, S. R.; Schulz, G.; Falshaw, C. P.; King, T. J. Jack E. Baldwin,* Stephen R. Herchen, Giinter Schulz. *J. Am. Chem. Soc.* **1980**, *102*, 7816–7817.

(118) Koehler, K. C.; Anseth, K. S.; Bowman, C. N. Diels-Alder Mediated Controlled Release from a Poly(ethylene Glycol) Based Hydrogel. *Biomacromolecules* **2013**, *14*, 538–547.

(119) Xin, Y.; Yuan, J. Schiff's Base as a Stimuli-Responsive Linker in Polymer Chemistry. *Polym. Chem.* **2012**, *3*, 3045-3055.

(120) Kale, A. A.; Torchilin, V. P. Design, Synthesis, and Characterization of pH-Sensitive PEG-PE Conjugates for Stimuli-Sensitive Pharmaceutical Nanocarriers: The Effect of Substitutes at the Hydrazone Linkage on the pH Stability of PEG-PE Conjugates. *Bioconjug. Chem.* **2007**, *18*, 363–370.

(121) Huang Lee, L. L. H.; Cheung, D. T.; Nimni, M. E. Biochemical Changes and Cytotoxicity

Associated with the Degradation of Polymeric Glutaraldehyde Derived Crosslinks. *J. Biomed. Mater. Res.* **1990**, *24*, 1185–1201.

(122) Bulpitt, P.; Aeschlimann, D. New Strategy for Chemical Modification of Hyaluronic Acid: Preparation of Functionalized Derivatives and Their Use in the Formation of Novel Biocompatible Hydrogels. J Biomed Mater Res. 1999;47:152–69. *J Biomed Mater Res* **1999**, *47*, 152–69.

(123) Luo, Y.; Kobler, J. B.; Heaton, J. T.; Jia, X.; Zeitels, S. M.; Langer, R. Injectable Hyaluronic Acid-Dextran Hydrogels and Effects of Implantation in Ferret Vocal Fold. *J. Biomed. Mater. Res. B. Appl. Biomater.* **2010**, *93*, 386–393.

(124) Urosev, I.; Bakaic, E.; Alsop, R. J.; Rheinstädter, M. C.; Hoare, T. Tuning the Properties of Injectable Poly(oligoethylene Glycol Methacrylate) Hydrogels by Controlling Precursor Polymer Molecular Weight. *J. Mater. Chem. B* **2016**, *4*, 6541–6551.

(125) Bakaic, E.; Smeets, N. M. B.; Dorrington, H.; Hoare, T. "Off-the-Shelf" thermoresponsive Hydrogel Design: Tuning Hydrogel Properties by Mixing Precursor Polymers with Different Lower-Critical Solution Temperatures. *RSC Adv.* **2015**, *5*. 33364-33376.

(126) Yang, X.; Bakaic, E.; Hoare, T.; Cranston, E. D. Injectable Polysaccharide Hydrogels Reinforced with Cellulose Nanocrystals: Morphology, Rheology, Degradation, and Cytotoxicity. *Biomacromolecules* **2013**, *14*, 4447-4455.

(127) Smeets, N. M. B.; Bakaic, E.; Patenaude, M.; Hoare, T. Injectable Poly(oligoethylene Glycol Methacrylate)-Based Hydrogels with Tunable Phase Transition Behaviours: Physicochemical and Biological Responses. *Acta Biomater.* **2014**, *10*. 4143-4155

(128) Alves, M. H.; Young, C. J.; Bozzetto, K.; Poole-Warren, L. A.; Martens, P. J. Degradable, Click Poly(vinyl Alcohol) Hydrogels: Characterization of Degradation and Cellular Compatibility. *Biomed. Mater.* **2012**, *7*, 24106.

(129) Wang, S.; Oommen, O. P.; Yan, H.; Varghese, O. P. Mild and Efficient Strategy for Site-Selective Aldehyde Modi Fi Cation of Glycosaminoglycans: Tailoring Hydrogels with Tunable Release of Growth Factor. *Biomacromolecules.* **2013**, *14,* 2427-2432.

(130) Gilbert, T.; Smeets, N. M. B.; Hoare, T. Injectable Interpenetrating Network Hydrogels via Kinetically Orthogonal Reactive Mixing of Functionalized Polymeric Precursors. *ACS Macro Lett.* **2015**, *4*, 1104–1109.

(131) Smeets, N. M. B.; Patenaude, M.; Kinio, D.; Yavitt, F. M.; Bakaic, E.; Yang, F.-C.; Rheinstädter, M.; Hoare, T. Injectable Hydrogels with in Situ-Forming Hydrophobic Domains: Oligo(D , L -Lactide) Modified Poly(oligoethylene Glycol Methacrylate) Hydrogels. *Polym. Chem.* **2014**, *5*, 6811–6823.

(132) Zhu, D.; Wang, H.; Trinh, P.; Heilshorn, S. C.; Yang, F. Elastin-like Protein-Hyaluronic Acid (ELP-HA) Hydrogels with Decoupled Mechanical and Biochemical Cues for Cartilage Regeneration. *Biomaterials* **2017**, *127*, 132–140.

(133) Apostolides, D. E.; Sakai, T.; Patrickios, C. S. Dynamic Covalent Star Poly(ethylene Glycol) Model Hydrogels: A New Platform for Mechanically Robust, Multifunctional Materials. *Macromolecules* **2017**, *50*, 2155–2164.

(134) Lutz, J.-F. Polymerization of Oligo(ethylene Glycol) (Meth)acrylates: Toward New Generations of Smart Biocompatible Materials. *J. Polym. Sci. Part A Polym. Chem.* **2008**, *46*, 3459–3470.

(135) Lutz, J.-F.; Hoth, A. Preparation of Ideal PEG Analogues with a Tunable Thermosensitivity by Controlled Radical Copolymerization of 2-(2-Methoxyethoxy)ethyl Methacrylate and Oligo(ethylene Glycol) Methacrylate. *Macromolecules* **2006**, *39*, 893–896.

(136) Becer, C. R.; Hahn, S.; Fijten, M. W. M.; Thijs, H. M. L.; Hoogenboom, R.; Schubert, U. S. Libraries of Methacrylic Acid and Oligo (Ethylene Glycol) Methacrylate Copolymers with LCST Behavior. *J. Polym. Sci. Part A Polym. Chem.* **2008**, 7138–7147.

(137) Lutz, J.-F.; Akdemir, O.; Hoth, A. Point by Point Comparison of Two Thermosensitive Polymers Exhibiting a Similar LCST: Is the Age of poly(NIPAM) Over? *J. Am. Chem. Soc.* **2006**, *128*, 13046–13047.

(138) Sun, S.; Wu, P. On the Thermally Reversible Dynamic Hydration Behavior of Oligo(ethylene Glycol) Methacrylate-Based Polymers in Water. *Macromolecules* **2013**, *46*, 236–246.

(139) Banerjee, P.; Irvine, D. J.; Mayes, A. M.; Griffith, L. G. Polymer Latexes for Cell-Resistant and Cell-Interactive Surfaces. *J. Biomed. Mater. Res.* **2000**, *50*, 331–339.

(140) Hyun, J.; Ma, H.; Zhang, Z.; Beebe Jr., T. P.; Chilkoti, A. Universal Route to Cell Micropatterning Using an Amphiphilic Comb Polymer. *Adv. Mater.* **2003**, *15*, 576–579.

(141) Lutz, J.-F.; Andrieu, J.; Üzgün, S.; Rudolph, C.; Agarwal, S. Biocompatible, Thermoresponsive, and Biodegradable: Simple Preparation of “All-in-One” Biorelevant Polymers. *Macromolecules* **2007**, *40*, 8540–8543.

(142) Ma, H.; Hyun, J.; Stiller, P.; Chilkoti, A. “Non-Fouling” Oligo(ethylene Glycol)- Functionalized Polymer Brushes Synthesized by Surface-Initiated Atom Transfer Radical Polymerization. *Adv. Mater.* **2004**, *16*, 338–341.

(143) Wang, Z.; Luan, Y.; Gan, T.; Gong, X.; Chen, H.; Ngai, T. Long-Range Interactions between Protein-Coated Particles and POEGMA Brush Layers in a Serum Environment. *Colloids Surfaces B Biointerfaces* **2017**, *150*, 279–287.

(144) Lei, J.; Mayer, C.; Freger, V.; Ulbricht, M. Synthesis and Characterization of Poly(ethylene Glycol) Methacrylate Based Hydrogel Networks for Anti-Biofouling Applications. *Macromol. Mater. Eng.* **2013**, *298*, 967–980.

(145) París, R.; Quijada-Garrido, I. Swelling Behaviour of Thermo-Sensitive Hydrogels Based on Oligo(ethylene Glycol) Methacrylates. *Eur. Polym. J.* **2009**, *45*, 3418–3425.

(146) Yoon, J. A.; Gayathri, C.; Gil, R. R.; Kowalewski, T.; Matyjaszewski, K. Comparison of the Thermoresponsive Deswelling Kinetics of Poly(2-(2-Methoxyethoxy)ethyl Methacrylate) Hydrogels Prepared by ATRP and FRP. *Macromolecules* **2010**, *43*, 4791–4797.

(147) Huang, R.; Ferhan, A. R.; Guo, L.; Qiu, B.; Lin, Z.; Kim, D.-H.; Chen, G. In Situ Synthesis of Protein-Resistant Poly(oligo(ethylene Glycol)methacrylate) Films in Capillary for Protein Separation. *RSC Adv.* **2014**, *4*, 4883.

(148) Zhou, T.; Wu, W.; Zhou, S. Engineering Oligo(ethylene Glycol)-Based Thermosensitive Microgels for Drug Delivery Applications. *Polymer (Guildf).* **2010**, *51*, 3926–3933.

(149) Uhlig, K.; Wischerhoff, E.; Lutz, J.-F.; Laschewsky, A.; Jaeger, M. S.; Lankenau, A.; Duschl, C. Monitoring Cell Detachment on PEG-Based Thermoresponsive Surfaces Using TIRF Microscopy. *Soft Matter* **2010**, *6*, 4262-4267.

(150) Fechler, N.; Badi, N.; Schade, K.; Pfeifer, S.; Lutz, J.F. Thermogelation of PEG-Based Macromolecules of Controlled Architecture. *Macromolecules* **2009**, *42*, 33–36.

Chapter 2: Injectable and Tunable Poly(ethylene glycol) Analogue Hydrogels Based on Poly(oligoethylene glycol methacrylate)

Preface:

This chapter has been reproduced from the original publication of a communication describing the indepth synthesis and characterization of physiochemical and biological properties of injectable poly(oligoethylene glycol methacrylate) (POEGMA) hydrogels. This chapter outlines the design of hydrazide and aldehyde functionalized POEGMA precursor polymers, that when mixed or injected from a double barrel syringe, form injectable and degradable hydrogels with tunable gelation kinetics, swelling and degradation profiles and mechanics based on the variation of concentration or reactive monomer incorporation. This chapter also describes the further investigation of comparable protein adsorption and cell viability responses to typical poly(ethylene glycol) hydrogels, making them non-fouling and cytocompatible. The ease of adhesive peptide RGD conjugation to increase 3T3 fibroblast cell adhesion as well as the in vivo acute and chronic responses are also discussed.

Niels M.B. Smeets‡, Emilia Bakaic‡, Mathew Patenaude and Todd Hoare

Department of Chemical Engineering, McMaster University, 1280 Main St. W, Hamilton, Ontario, Canada L8S 4L7

‡ These authors contributed equally

[‡]Smeets, N.M.B.; [‡]Bakaic, E.; Patenaude, M.; Hoare, T. "Injectable and Tunable Poly(ethylene glycol)-Analogue Hydrogels Based on Poly(oligoethylene glycol methacrylate)". *Chemical Communications*, 2014, *50*, 3306-3309.

Abstract

Injectable PEG-analogue hydrogels based on poly(oligoethylene glycol methacrylate) have been developed based on complementary hydrazide and aldehyde reactive polymeric precursors. These hydrogels display the desired biological properties of PEG, form covalent networks *in situ* following injection, and are easily modulated for improved control over their functionality and physiochemical properties.

2.1 Introduction

Poly(ethylene glycol) (PEG) hydrogels have been extensively studied as matrices for the controlled release of therapeutics and as scaffolds for promoting tissue regeneration.[1] PEG hydrogels are hydrophilic, non-cytotoxic and non-immunogenic and can effectively mask the material from the host's immune system.[2] A significant drawback of PEG, however, is that the polymer lacks chemical versatility given that functionalization is limited to the hydroxyl chain end(s).[3] PEG hydrogels are predominantly synthesized *via* step-growth polymerization of complimentary α,ω-functionalized PEG precursors using a range of different chemistries.[4] Although step-growth polymerization minimizes network non-idealities, chemical modification of linear PEG precursors is limited and there is increasing interest in polymers with similar (biological and physicochemical) properties that can be synthesized in a facile manner with improved control over the polymer functionality.[5]

Hereto, we prepared PEG-analogue hydrogels based on poly(oligoethylene glycol methacrylate) (POEGMA) that exhibit all of the desirable protein and cell-repellent properties of conventional PEG hydrogels while also being injectable, degradable, and easily chemically and mechanically tunable, enabling facile preparation of hydrogels, useful from the perspective of injectable tissue engineering matrices, drug delivery vehicles for local small molecule or macromolecule delivery, or joint lubricants, among other potential applications. POEGMA is synthesized via simple free radical copolymerization[6] and has been demonstrated to serve as an effective PEG analogue, exhibiting corresponding non-immunogenic, non-cytotoxic and protein repellent properties to PEG.[7] A number of POEGMA-based hydrogels have been reported to-date;[8] however, none are covalently cross-linked while also being injectable and degradable *in vivo*, severely limiting their potential clinical application.

2.2 Results and Discussion

Our PEG-analogue hydrogels are based on hydrazide and aldehyde functionalized POEGMA precursors that rapidly form a hydrogel network through reversible hydrazone bond formation[9] upon co-extrusion (see Scheme 1).

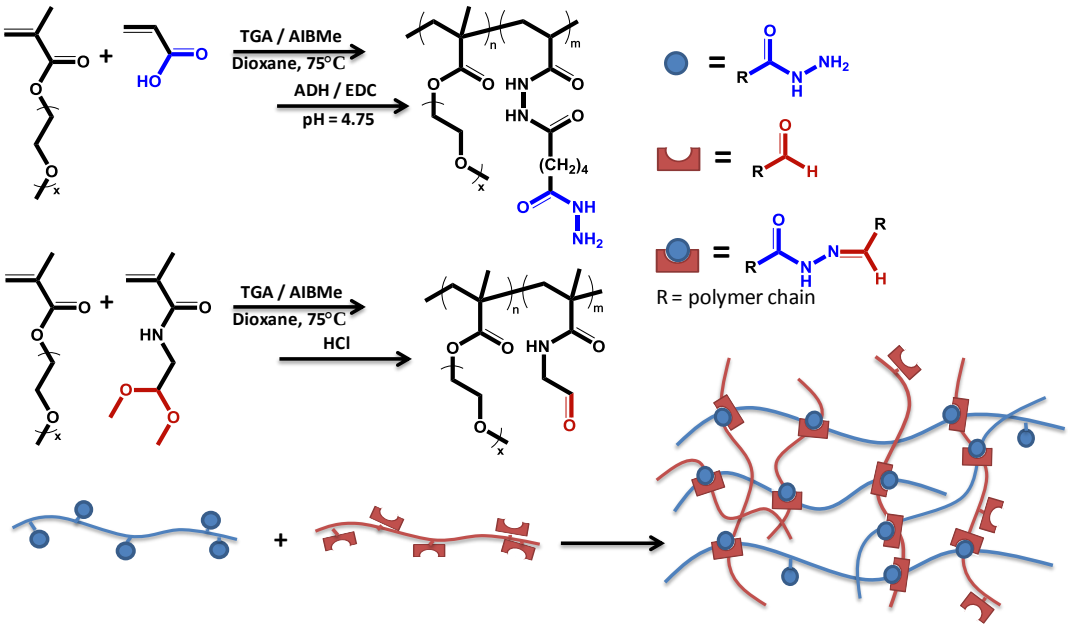

Scheme 2.1 Preparation of injectable PEG analogue hydrogels

The injectable, *in situ* gelling nature of this system is useful to circumvent many of the issues concerning surgical implantation of bulk hydrogel-based materials. The hydrazide-functionalized POEGMA precursors ($PO_{100}H_y$) were synthesized by copolymerizing $OEGMA_{475}$ (EO repeat units, *n* = 8-9) with acrylic acid (AA) and subsequent post-polymerization modification using EDC chemistry with a large excess of adipic acid dihydrazide. The aldehyde-functionalized POEGMA precursors ($PO_{100}A_y$) were synthesized by copolymerizing $OEGMA_{475}$ with a functional acetal monomer (*N*-(2,2-dimethoxyethyl)methacrylamide, DMEMAm) and subsequently converting the acetal to the corresponding aldehyde by acid-catalyzed hydrolysis (Scheme 2.1). The degree of functionality of the $PO_{100}H_y$ and $PO_{100}A_y$ precursors was controlled by varying the AA and DMEMAm content from y = 20 to 40 mol% (Supporting Information, Table S.2.1 and Fig. S2.1). The number-average molecular weight of the precursor polymers was controlled to be lower than 20×10^3 g/mol, well below the renal clearance limit of $40\text{-}50\times10^3$ g/mol to

facilitate polymer elimination following gel degradation.[10]

POEGMA hydrogels were prepared by co-extruding $PO_{100}H_y$ and $PO_{100}A_y$ solutions in 10 mM PBS using a double-barrel syringe. Gelation occurs over time frames ranging from a several hours (~ 8 hours) to a few minutes (< 10 min) (Supporting Information, Table S2), The hydrogels swell in PBS following preparation (Fig. 2.1E-J), indicating high water affinity. For POEGMA hydrogels prepared with precursors containing 25, 30 or 40 mol% functional groups (either hydrazide or aldehyde), the equilibrium mass-based swelling ratio (Q_m) is reached within 30 h (Supporting Information, Fig. S2.2) and decreases systematically with both the degree of chain functionalization and the concentration of precursor polymers used to prepare the hydrogel (Fig. 2.1A). This result suggests that facile tuning of the hydrogel water content at equilibrium is possible based on the types and concentrations of precursor polymers used (see Supporting Information for a more detailed explanation).

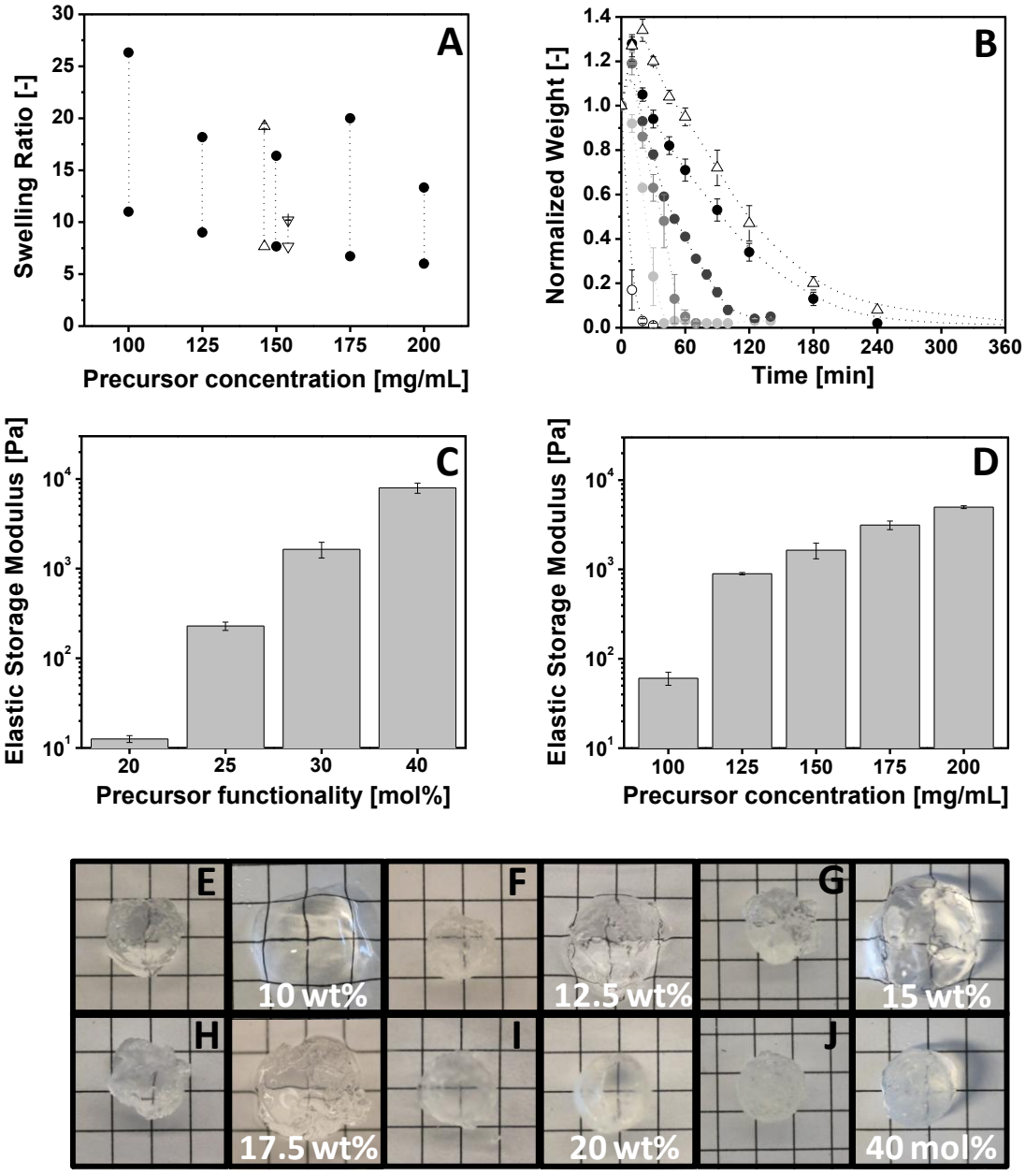

Fig 2.1 Physiochemical characterization of injectable POEGMA hydrogels. A) Bottom point = Initial swelling and top point = equilibrium swelling (△) 25 mol%, (●) 30 mol% and (▽) 40 mol%. B) Degradation kinetics at 30 mol% functionality in 100 mM HCl (○) 100 mg/mL,(●) 125 mg/mL, (●) 150 mg/mL, (●) 175 mg/mL, (●) 200 mg/mL and (△) 150 mg/mL and 40 mol%. C-D) Elastic storage modulus as a function of the precursor functionalization (C) and concentration (D). E-J) Photographs of the unswollen and swollen hydrogels (grid = 0.5 mm x 0.5 mm)

The injectable POEGMA hydrogels are cross-linked through the formation of dynamic hydrazone bonds, which are reversible in an aqueous environment. Aqueous size exclusion chromatography of the degradation products of a hydrogel prepared from $PO_{100}H_{30}$ and $PO_{100}A_{30}$ confirmed that the molecular weight distribution (MWD) of the degradation products is virtually identical to the combined MWDs of both precursor polymers (see Supporting Information, Fig. S2.3). Consequently, the $PO_{100}H_y$ and $PO_{100}A_y$ polymers represent both the hydrogel precursors are well as the hydrogel degradation products. MTT assay results following exposure of 3T3 mouse fibroblasts to $PO_{100}H_y$ and $PO_{100}A_y$ confirm that these materials do not impart any significant *in vitro* toxicity up to a concentration of 2000 µg/mL (Supporting Information, Fig. S2.4), suggesting that both the precursors and degradation products of the hydrogels are compatible with cells.

The degradation rate of the POEGMA hydrogels is governed by the cross-link density and thus by the degree of functionalization and concentration of the $PO_{100}H_y$ and $PO_{100}A_y$ precursors (Fig. 2.1B). Hydrogels prepared with precursors at low concentrations (< 125 mg/mL) or with low degrees of functionalization (< 30 mol%) degrade in <1 min. in 100 mM HCl, while hydrogels prepared with precursors at a high concentration (200 mg/mL) or with a high degree of functionalization (40 mol%) degrade significantly slower, requiring approximately 5 hours to fully degrade under acid-catalyzed conditions (Fig. 2.1B). Long-term incubation showed that the hydrazone cross-linked POEGMA hydrogels (150 mg/mL and 30 mol% reactive hydrazide and aldehyde groups) are stable for at least 5 months under physiological conditions *in vitro* but degrade within 4 weeks *in vivo* following subcutaneous injection in BALB/c mice.

The $PO_{100}H_y$ and $PO_{100}A_y$ precursors yield hydrogels with elastic moduli that can be tuned depending on the number of reactive functional groups as well as the precursor concentration. G' values range from 0.23 ± 0.02 kPa (150 mg/mL, 25 mol%) to 8.0±1.0kPa (150 mg/mL, 40 mol%) (Fig. 2.1C-D and Supporting Information Figs. S2.5 and S2.6). For comparison, the G' of conventional PEG hydrogels prepared from multi-arm and di-functional PEG precursors at comparable concentrations typically ranges from 0.25 to 6.0 kPa,[4b,4c,4f,4k] analogous to the range reported here. However, the modulus of these POEGMA

hydrogels can be tuned independently of polymer concentration (and thus hydrogel osmotic pressure) if desired by modifying the precursor functionality, not possible using conventional PEG chemistry.

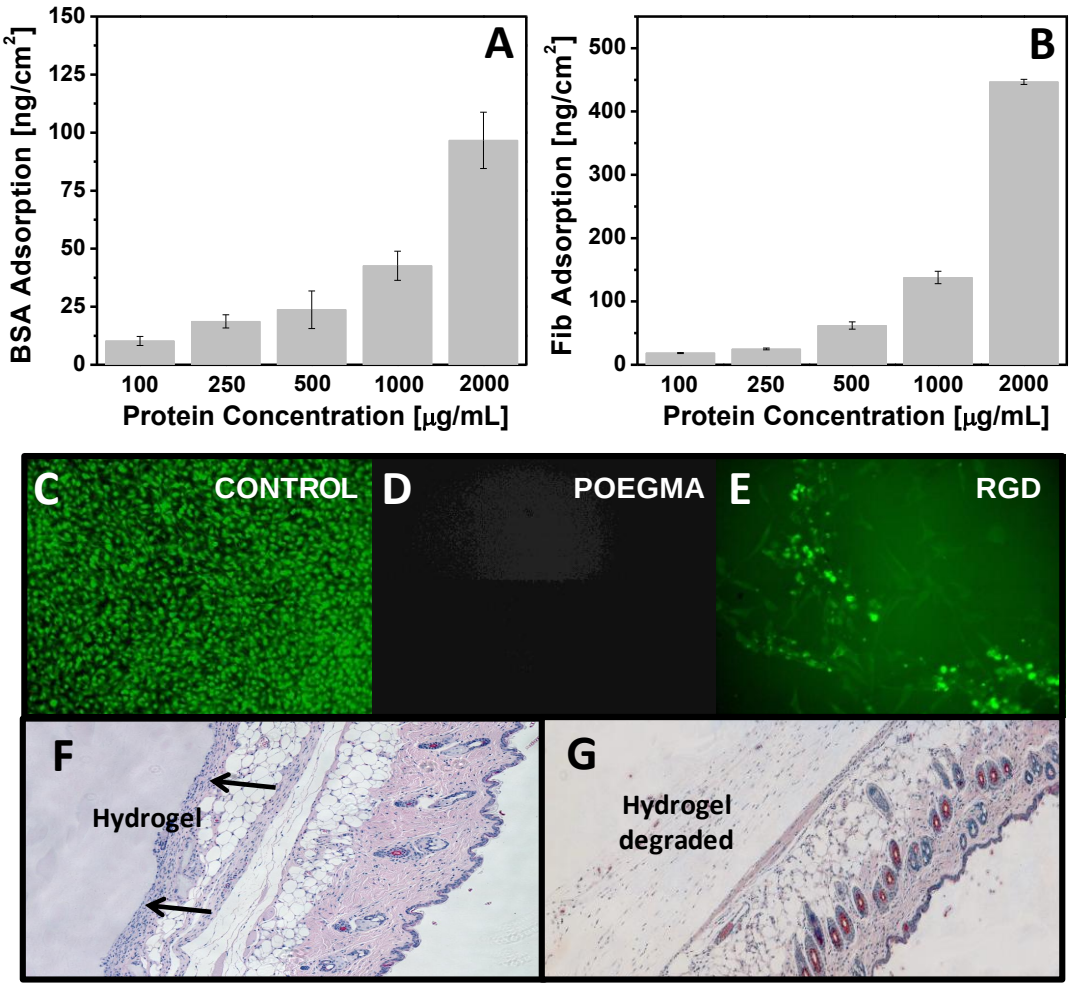

Fig.2.2 Biological properties of injectable POEGMA hydrogels (based on $PO_{100}H_{30}$ and $PO_{100}A_{30}$ at 150 mg/mL). A-B) Adsorption of BSA (A) and Fibrinogen (B). C-E) Fibroblast adhesion after 7 days to a polystyrene control (C), POEGMA hydrogel (D) and an RGD-functionalized hydrogel (E). F-G) acute (F) and chronic (G) i*n vivo* response to POEGMA hydrogels.

The biointerfacial properties of the injectable POEGMA hydrogels (prepared at 150 mg/mL and 30 mol% functional groups) were evaluated using protein adsorption (Fig. 2.2A-B) and cell adhesion (Fig. 2.2C-E) assays. POEGMA hydrogels were incubated with bovine

serum albumin (BSA) and fibrinogen (Fib) at varying concentrations. BSA and Fib adsorption to the POEGMA hydrogel is maintained below 100 and 500 ng/cm^2, respectively, even upon exposure to a 2000 μg/mL protein solution (Fig. 2.2A-B), comparable to adsorption values reported for conventional PEGylated surfaces.[11] Note that protein *absorption* is also likely to occur for POEGMA hydrogels, suggesting that the true protein adsorption on the hydrogel surface is likely even lower than reported in Fig. 2.2A-B. Furthermore, negligible adhesion of fibroblast cells (noted to adhere particularly strongly to many biomaterials due to their inherent ability to produce extracellular matrix)[12] is observed to the POEGMA hydrogels, with 6 ± 1 cells/mm^2 (n = 6) observed on POEGMA hydrogel interfaces (Fig. 2.2D and Supporting Information Fig. S2.7) compared to 2400 ± 130 cells/mm^2 (n = 6) for tissue culture polystyrene interfaces (Fig. 2.2C) after 7 days of incubation. The presence of reactive functional groups in the POEGMA hydrogel precursor polymers facilitates facile tuning of the cell-hydrogel interactions achievable with POEGMA hydrogels. For example, $PO_{100}A_{30}$-RGD precursors (average of 1 RGD sequence per chain) were synthesized to prepare POEGMA hydrogels containing 1.2 mM RGD, comparable to other RGD functionalized hydrogels reported previously.[13] At this concentration, RGD promotes a 6-fold increase in 3T3 mouse fibroblast adhesion to the injectable POEGMA hydrogel, as 36 ± 1 cells/mm^2 (n = 6) adhere (Fig. 2.2E). Note that the average degree of RGD functionalization can be increased independent of the cross-link density, simply by functionalizing the precursors with a larger fraction of aldehyde groups, making cell-hydrogel interactions easily tunable using a POEGMA-based hydrogel system. Thus, the injectable POEGMA hydrogels reported herein can either suppress or support cell adhesion, consistent with other PEG-based hydrogels reported in literature that are typically non-injectable and significantly more limited in terms of compositional diversity.

The *in vivo* response to the POEGMA precursors and hydrogel was evaluated by subcutaneous injection using a double-barrel syringe in BALB/c mice. Stable hydrogels were formed in the subcutaneous space of the mice with minimal leukocytotic infiltration at the hydrogel-tissue interface (< 100 cells/mm^2), suggesting a relatively mild acute inflammatory response 3 days post-injection (Fig. 2.2F). The POEGMA hydrogel fully degraded after one

month (Fig. 2.2G), with no signs of chronic inflammation (i.e. macrophages, foreign body giant cells, granulation tissue) or fibrous capsule formation observed histopathologically. This result suggests that injectable POEGMA hydrogels are well-tolerated *in vivo*, again analogous to conventional PEG hydrogels. It should be emphasized that *in vitro* degradation studies suggest that the degradation lifetime of the POEGMA hydrogels can be tuned based on the number of cross-linkable groups incorporated in the hydrogel (Fig. 2.1B); in this sense, hydrogel clearance kinetics *in vivo* may also be engineered.

In conclusion, we have prepared injectable, hydrazone cross-linked hydrogels based on POEGMA that exhibit the same favourable biological properties of conventional PEG-based hydrogels (i.e. facilitating minimal protein adsorption, no significant cellular adhesion, and no significant chronic inflammatory responses *in vivo*) while offering the significant advantages of facile synthesis, rapid *in situ* gelation following injection, tunable mechanics, tunable degradation times, and excellent control over chemical composition and functionalizability. These results suggest the potential of these POEGMA-based hydrogels as a platform for the design of engineered hydrogels for a variety of biomedical applications now served by conventional PEG hydrogels.

2.3 References

1. (*a*) C.-C. Lin and K. S. Anseth, *Pharm Res*, 2009, **26**, 631-643; (*b*) J. L. Drury and D. J. Mooney, *Biomaterials*, 2003, **24**, 4337–4351; *(c*) N. A. Peppas, J. Z. Hilt, A. Khademhosseini, and R. Langer, *Adv. Mater*, 2006, **18**, 1345–1360.
2. J. V. Jokerst, T. Lobovkina, R. N. Zare, and S. S. Gambhir, *Nanomedicine*, 2011, **6**, 715–728.
3. C. R. Nuttelman, M. A. Rice, A. E. Rydholm, C. N. Salinas, D. N. Shah, and K. S. Anseth, *Prog. Poly. Sci*, 2008, **33**, 167–179.
4. See for example: (*a*) M. Malkoch, R. Vestberg, N. Gupta, L. Mespouille, P. Dubois, A. F. Mason, J. L. Hedrick, Q. Liao, C. W. Frank, K. Kingsbury, and C. J. Hawker, *Chem. Commun.*, 2006, 2774–2776; (*b*) J. D. McCall and K. S. Anseth, *Biomacromolecules*, 2012, **13**, 2410–2417; (*c*) A. A. Aimetti, A. J. Machen, and K. S. Anseth, *Biomaterials*, 2009, **30**, 6048–6054; (*d*) M. P. Lutolf and J. A. Hubbell, *Biomacromolecules*, 2003, **4**, 713–722; (*e*) B. D. Polizzotti, B. D. Fairbanks, and K. S. Anseth, *Biomacromolecules*, 2008, **9**, 1084–1087; (*f*) K. C. Koehler, K. S. Anseth, and C. N. Bowman, *Biomacromolecules*, 2013, **14**, 538–547; (*g*) G. N. Grover, J. Lam, T. H. Nguyen, T. Segura, and H. D. Maynard, *Biomacromolecules*, 2012, **13**, 3013–3017.

5 B. L. Farrugia, K. Kempe, U. S. Schubert, R. Hoogenboom, and T. R. Dargaville, *Biomacromolecules*, 2013, **14**, 2724–32.

6 (*a*) M. Luzon, C. Boyer, C. Peinado, T. Corrales, M. Whittaker, L. E. I. Tao, and T. P. Davis, *J. Polym. Sci. Part A*, 2010, **48**, 2783–2792; (*b*) A. H. Soeriyadi, G.-Z. Li, S. Slavin, M. W. Jones, C. M. Amos, C. R. Becer, M. R. Whittaker, D. M. Haddleton, C. Boyer, and T. P. Davis, *Poly. Chem.*, 2011, **2**, 815–822; (*c*) J. K. Oh, K. Min, and K. Matyjaszewski, *Macromolecules*, 2006, **39**, 3161–3167; (*d*) J.-F. Lutz and A. Hoth, Macromolecules, 2006, 39, 893–896.

7. J.-F. Lutz, J. Andrieu, S. Üzgün, C. Rudolph, and S. Agarwal, *Macromolecules*, 2007, **40**, 8540–8543.
8. (*a*) J. Lei, C. Mayer, V. Freger, and M. Ulbricht, *Macromol. Mater. Eng.*, 2013, **298**, 967–980; (*b*) R. París and I. Quijada-Garrido, *Eur. Polym. J.*, 2009, **45**, 3418–3425; (*c*) J. A. Yoon, T. Kowalewski, K. Matyjaszewski, C. Gayathri, and R. R. Gil, *Macromolecules*, 2010, **43**, 4791–4797; (*d*) J. A. Yoon, T. Kowalewski, and K. Matyjaszewski, *Macromolecules*, 2011, **44**, 2261–2268; (*e*) J.-F. Lutz, K. Weichenhan, Ö. Akdemir, and A. Hoth, *Macromolecules*, 2007, **40**,

2503–2508; (*f*) N. Fechler, N. Badi, K. Schade, S. Pfeifer, and J.-F. Lutz, *Macromolecules*, 2009, **42**, 33–36.

9. (*a*) Patenaude, M.; Hoare, T. *ACS Macro Lett*. **2012**, *1*, 409–413; (*b*) Patenaude, M.; Hoare, T. *Biomacromolecules* **2012**, *13*, 369–78; (*c*) Ito, T.; Yeo, Y.; Highley, C. B.; Bellas, E.; Kohane, D. S. *Biomaterials* **2007**, *28*, 3418–26; (*d*) Ossipov, D. A.; Hilborn, J. *Macromolecules* **2006**, *39*, 1709–1718.
10. G. Pasut and F. M. Veronese, *Prog. Polym. Sci.*, 2007, **32**, 933–961.
11. (*a*) S. Pasche, S. M. de Paul, J. Voros, N. D. Spencer, and M. Textor, *Langmuir*, 2003, **22**, 9216–9225; (*b*) Y. Chung and Y. Chiu, *J. Med. Biol. Eng*, 2009, **29**, 320–324; (*c*) K. Y. Suh, J. Seong, A. Khademhosseini, P. E. Laibinis, and R. Langer, *Biomaterials*, 2004, **25**, 557–563; (*d*) E. Tziampazis, J. Kohn, and P. V. Moghe, *Biomaterials*, 2000, **21**, 511–520; (*e*) H. Du, P. Chandaroy, and S. W. Hui, *Biochim. Biophys. Acta*, 1997, **1326**, 236–248.
12. N. Faucheux, R. Schweiss, K. Lützow, C. Werner, and T. Groth, *Biomaterials*, 2004, **25**, 2721–2730.
13. (*a*) M. D. Pierschbacher and E. Ruoslahti, Nature, 1984, 309, 30–33; (*b*) F. Yang, C. G. Williams, D. Wang, H. Lee, P. N. Manson, and J. Elisseeff, *Biomaterials*, 2005, **26**, 5991–5998; (*c*) J. A. Burdick and K. S. Anseth, *Biomaterials*, 2002, **23**, 4315–4323; (*d*) D. Guarnieri, A. De Capua, M. Ventre, A. Borzacchiello, C. Pedone, D. Marasco, M. Ruvo, and P. A. Netti, *Acta Biomaterialia*, 2010, **6**, 2532–2539.

2.4 Supporting Information

S2.1 Experimental

S2.1.1 Materials: Oligo(ethylene glycol) methyl ether methacrylate with an average number-average molecular weight of 475 g/mol ($OEGMA_{475}$, Sigma Aldrich, 95%) was purified by passing it over a column of basic aluminum oxide (Sigma Aldrich, type CG-20) to remove the methyl ether hydroquinone (MEHQ) and butylated hydroxytoluene (BHT) inhibitors. Acrylic acid (AA, Sigma Aldrich, 99%), thioglycolic acid (TGA, Sigma Aldrich, 98%) and 2,2-azobisisobutryic acid dimethyl ester (AIBMe, Wako Chemicals, 98.5%), adipic acid dihydrazyde (ADH, Alfa Aesar, 98%), *N*'-ethyl-*N*-(3-dimethylaminopropyl)-carbodiimide (EDC, Carbosynth, Compton CA, commercial grade), sodium cyanoborohydride ($NaBH_3CN$, Sigma Aldrich, reagent grade), aminoacetaldehyde dimethyl acetal (Sigma Aldrich, 99%), 2,2,6,6-tetramethyl-1-piperidinyloxy (TEMPO, Sigma Aldrich, 98%), methacryloyl chloride (Sigma Aldrich, purum), bovine serum albumin (BSA, Sigma Aldrich, >96%), fibrinogen from human plasma (Sigma Aldrich), Arg-Gly-Asp (RGD, Sigma Aldrich, ≥97%)and fluorescein isothiocyanate (FITC, Sigma Aldrich, 90%) were all used as received. For all experiments Milli-Q grade distilled deionized water (DIW) was used. Dimethyl sulfoxide (DMSO, reagent grade) was purchased from Caledon Laboratory Chemicals (Georgetown, ON). Hydrochloric acid (1M) was received from LabChem Inc. (Pittsburgh, PA). 3T3mouse fibroblasts were obtained from ATCC: Cederlane Laboratories (Burlington, ON). Cell proliferation media, recovery media, and trypsin-EDTA were obtained from Invitrogen (Burlington, ON). Media contents included Dulbecco's Modified Eagle Medium-high glucose (DMEM), fetal bovine serum (FBS), penicillin streptomycin (PS), and trypsin-EDTA and were purchased from Invitrogen Canada (Burlington, ON). Thiazolyl blue tetrazolium bromide (MTT) was purchased from Sigma Aldrich (Oakville, ON). LIVE/DEAD assay for cell viability were purchased from Invitrogen Canada (Burlington).

S2.1.2 Chemical Characterization: Aqueous size exclusion chromatography (SEC) was performed on a system consisting of a Waters 515 HPLC pump, Waters 717 plus autosampler, three Ultrahydrogel columns (30 cm × 7.8 mm i.d.; exclusion limits: 0–3 kDa, 0–50 kDa, 2–300 kDa) and a Waters 2414 refractive index detector. A mobile phase consisting of 0.3 M sodium

nitrate and 0.05 M phosphate buffer (pH 7) at a flow rate of 0.8 mL/min was used for all polymers analyzed, and the system was calibrated with narrow-dispersed poly(ethylene glycol) standards ranging from 106 to 584×10^3 g/mol (Waters). ^{1}H-NMR was performed on a Bruker AVANCE 600 MHz spectrometer using deuterated chloroform as the solvent. The acrylic acid content of the polymers was determined using base-into-acid conductometric titration (ManTech Associates) using 50 mg of polymer dissolved in 50 mL of 1 mM NaCl as the analysis sample and 0.1 M NaOH as the titrant.

S2.1.3 Synthesis of N-(2,2-dimethoxyethyl)methacrylamide (DMEMAm): The *N*-(2,2-dimethoxyethyl)methacrylamide (DMEMAm) monomer was synthesized by adding aminoacetaldehyde dimethylacetal (50 mL, 461 mmol) and 100 mg of TEMPO to a concentrated sodium hydroxide solution (100 mL) at 10 °C. Methacryloyl chloride (47.08 mL, 486 mmol) was then added drop-wise over a period of 2 hours under nitrogen, and the resulting mixture was allowed to react for 24 hours under nitrogen at room temperature. Subsequently, the mixture was extracted with 150 mL of petroleum ether to remove impurities. The aqueous phase was then saturated with sodium chloride and extracted three times with 75 mL tert-butyl methyl ether. The organic phase was dried with magnesium sulfate, filtered, and concentrated under reduced pressure, yielding an orange oil as the final product. This product was stored in the dark at 10 °C until use. Purity (determined from ^{1}H-NMR) = >99%. ^{1}H-NMR (DMSO, 600 MHz): δ = 1.75 (s, 3H, -CH3), δ = 2.92 – 3.23 (m, 8H, O-CH3 and –N(H)-CH2), δ = 4.33 (t, 1H, -CH), δ = 5.24 (s, 1H, =CH2) , δ = 5.57 (s, 1H, =CH2) , δ = 7.89 (s, 1H, -NH).

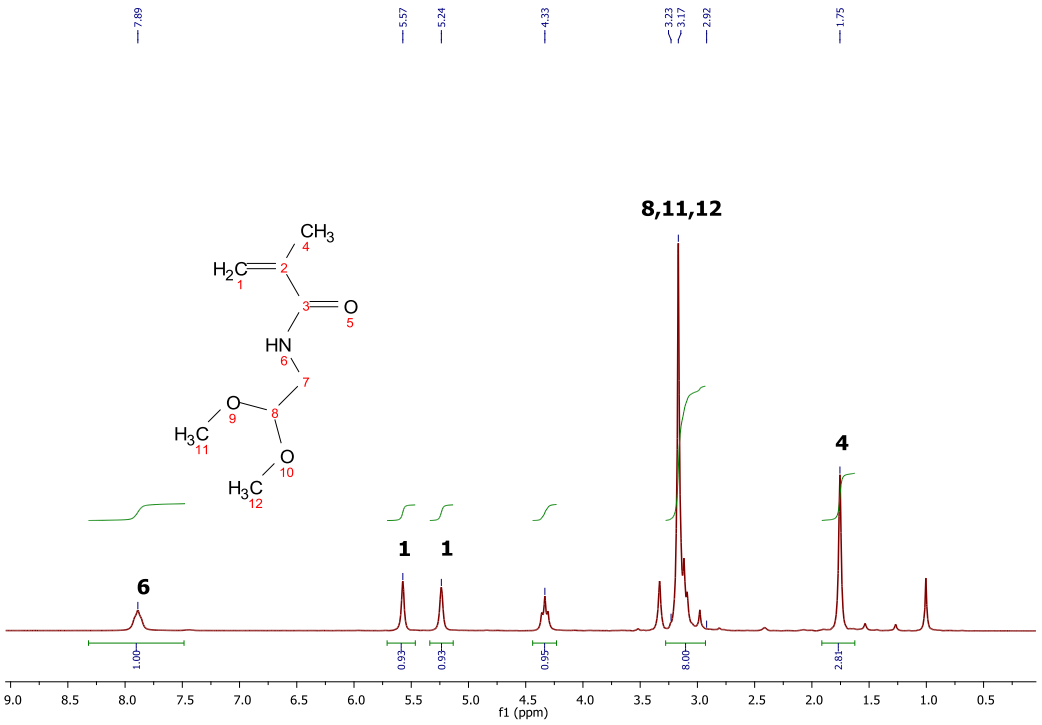

S2.1.4 Synthesis of the hydrazide-functionalized precursor ($PO_{100}H_y$): $PO_{100}H_y$ precursors were prepared by adding AIBMe (37 mg, 0.14 mmol), $OEGMA_{475}$ (4.0 g, 8.4 mmol), AA (0.25 g, 3.5 mmol, for $PO_{100}H_{30}$), and TGA (1 µL, 0.02 mmol) to a 50 mL Schlenk flask. Dioxane (20 mL) was added and the solution was purged with nitrogen for at least 30 minutes. Subsequently, the flask was sealed and submerged in a pre-heated oil bath at 75°C for 4 hours under magnetic stirring. After the solvent was removed, the resulting poly(OEGMA-co-AA) polymer was purified by dialysis against DIW for a minimum of 6 (6+ hour) cycles and lyophilized to dryness. The carboxylic acid groups of POH precursor were subsequently converted to hydrazide groups via a carbodiimide-mediated conjugation of a large excess of adipic acid dihydrazide. The polymer (3.8 g) was dissolved in 100 mL DIW and added to a 250 mL round-bottom flask. ADH (2.65 g, 15.2 mmol, 5 mol eq.) was added and the pH of the solution adjusted to pH = 4.75 using 0.1 M HCl. Subsequently, EDC (1.18 g, 7.6 mmol, 2.5 mol eq.) was added and the pH maintained at pH = 4.75 by the dropwise addition of 0.1 M HCl over 4 hours. The solution was left to stir overnight, dialyzed against DIW for a minimum of 6 (6+ hour) cycles, and lyophilized. The degree of functionalization was determined from conductometric base-into-acid titration. The polymers were stored as 20 w/w% solutions in PBS at 4°C.

S2.1.5 Synthesis of the aldehyde-functionalized precursor ($PO_{100}A_y$): $PO_{100}A_y$ precursors were prepared by adding AIBMe (60 mg, 0.26 mmol), $OEGMA_{475}$ (4.0 g, 8.4 mmol), DMEMAm (0.60 g, 3.5 mmol, for $PO_{100}A_{30}$) and TGA (1 µL, 0.02 mmol) to a 50 mL Schlenk flask. Dioxane (20 mL) was added and the solution was purged with nitrogen for at least 30 minutes. Subsequently, the flask was sealed and submerged in a pre-heated oil bath at 75°C for 4 hours under magnetic stirring. After polymerization, the solvent was removed and the poly(OEGMA-co-DMEMAm) polymer was purified by dialysis against DIW for a minimum of 6 (6+ hour) cycles and lyophilized to dryness. The acetal groups of $PO_{10}A$ were subsequently converted to aldehydes by dissolving 3.5 g of the copolymer prepared above in 75 mL DIW and 25 mL 1.0 M HCl in a 250 mL round-bottom flask. The solution was left to stir for 24 hours, dialyzed for a minimum of 6 (6+ hour) cycles and lyophilized to dryness. The polymer was stored at 20 w/w% in PBS at 4°C.

S2.1.6 Synthesis of RGD labelled POA: RGD labelled POA precursor ($PO_{100}A_{30}$-RGD) was prepared by incubating a solution of $PO_{100}A_{30}$ (0.6 g) and RGD (10 mg, 28.9 µmol) in 50 mL distilled deionized water for 24 hours under continuous agitation. Subsequently, sodium cyanoborohydride (18.2 mg, 0.29 mmol, 10 mol eq. to RGD) was added and the solution was stirred for another 48 hours. The solution was dialyzed for a minimum of 6 (6+ hour) cycles and lyophilized to dryness. The polymer was stored as 20 w/w% solution in PBS at 4°C.

S2.1.7 Synthesis of fluorescein-isothiocyanate labelled proteins: Fluorescein-isothiocyanate (FITC)-labelled bovine serum albumin (BSA-FITC) and fibrinogen (Fib-FITC) were prepared by dissolving 50 mg of the protein in a 100 mL carbonate buffer at pH = 9.0. FITC (1 mg) was added and the solution was incubated at room temperature for at least 12 h under gentile mechanical agitation. The FITC-labelled protein was subsequently dialyzed against distilled deionized water 6 (6+ hour) cycles and lyophilized to dryness. The isolated conjugated protein was stored at -4°C in the dark. For both proteins, a calibration curve was prepared to relate their concentration in PBS to the fluorescence signal measured at λ = 495nm and 535nm, with linear calibration

curves (R^2>0.99) observed in the concentration range of 2 to 10 µg/mL and 10 to 100 µg/mL respectively for BSA and fibrinogen.

S2.1.8 Preparation of injectable hydrogels: POEGMA hydrogels were prepared via co-extrusion of hydrazide-functionalized (POH) and aldehyde-functionalized (POA) precursors dissolved in 10 mM PBS. Intensive mechanical mixing of both polymer precursor solutions was achieved through the use of a double barrel syringe fitted with a static mixer at the outlet (Medmix Systems). Hydrogel disks for all *in vitro* testing were prepared by extrusion of the reactive polymer precursors through the double barrel syringe into cylindrical silicone rubber molds (diameter = 7 mm, volume = 300 µL) and incubated at room temperature for at least 12 hours to ensure complete gelation prior to testing.

S2.1.9 Swelling kinetics: Swelling of POEGMA hydrogels was determined at 22°C in 10 mM PBS at pH 7.4. Hydrogels (n = 4) were placed into cell culture inserts that are then placed in a 12-well cell culture plate and completely submerged with PBS (4 mL/well). At predetermined time intervals, the cell culture inserts were removed from the well, the PBS drained, and the hydrogel gently dried to wick off non absorbed PBS prior to weighing of the hydrogel. Subsequently, the hydrogels were resubmerged in a fresh 4 mL of PBS solution and tested repeatedly until equilibrium swelling was reached (generally ~30 hours). Error bars represent the standard deviation of the replicate measurements. The mass-based swell ratio (Q_m) was calculated by dividing the mass of the hydrogel at any given time point (m_h) by the dry mass of polymer in the hydrogel (m_p = initial hydrogel mass $\times$ (1 – water content)).

S2.1.10 Degradation kinetics: Degradation of POEGMA hydrogels was determined at 37°C in 100 mM HCl at pH 1.0; these acid-catalyzed conditions were used to compare the degradation properties of the hydrogels on a more measurable time frame. Hydrogels (n = 4) were placed into cell culture inserts that are subsequently placed in a 12-well cell culture plate and completely submerged with the HCl solution (4 mL per well). At predetermined time intervals, the cell culture inserts were removed from the well, the PBS drained and the hydrogel gently

dried to wick off non absorbed solution prior to weighing of the hydrogel. Subsequently, the hydrogels were resubmerged in fresh HCl solution (4 mL/well) until the hydrogel was completely degraded (i.e. no separate phase was observed between the hydrogel and the HCl bath solution). Error bars represent the standard deviation of the replicate measurements.

S2.1.11 Hydrogel rheology*:* The rheological properties of the hydrogels were measured using an ARES rheometer (TA Instruments) operating under parallel-plate geometry with a plate diameter of 7 mm and a plate spacing of 1 mm. Rheological properties were measured by first conducting a strain sweep from 0.1−100% strain at 1 Hz to identify the linear viscoelastic range of the hydrogels. A strain was then selected from within this linear range and set as a constant to perform a frequency sweep from 1 to 100 rad/s to measure shear elastic (G′) and loss (G″) moduli. All measurements were conducted at 22 °C and in triplicate, with error bars representing the standard deviation of the replicate measurements.

S2.1.12 Cytotoxicity assay: The cytocompatibility of POH and POA precursors (n = 4) was quantified using a MTT assay. NIH 3T3 fibroblasts were maintained in tissue culture flasks in DMEM supplemented with 10% FBS and 1% penicillin. Cytotoxicity of the linear polymers (at concentrations ranging from 200 to 2000 μg/mL) was evaluated using an MTT assay over a 1-day exposure time. NIH 3T3 fibroblasts were plated at density of 1.0×10^4 cells per well in a 24-well plate and maintained in DMEM media supplemented with 10% FBS and 1% penicillin. Cell viability was then characterized by removing the polymer solution, adding the MTT solution, and incubating over four hours. The absorbance of the MTT solution was read using a Biorad microplate reader (model 550) at 570 nm, normalized against a 630 nm baseline, and compared to that measured in cell-only wells in which no materials were added to estimate relative cell viability. Each experiment (hydrogels as well as controls) were done in quadruplicate, with reported errors representing the standard deviation of the replicates.

S2.1.13 In vitro protein adsorption assay: Protein absorption to the POEGMA hydrogels was assayed in 96 well plates. POH and POA polymer solutions (150 mg/mL) were sterilized and 60

µL of each precursor solution was extruded into each well and left overnight to ensure complete gelation. Once gelation was complete, 60µL of 10 mM PBS was added to each well and hydrogels were allowed to swell to equilibrium prior to protein addition (over 30 hours). Unabsorbed PBS was then removed, and 60µL of either BSA-FITC or Fib-FITC solution (125, 250 or 500 µg/mL) was added. The hydrogels were incubated for 2 hours at 37°C. After 2 hours, the hydrogels were rinsed to remove unadsorbed protein and the fluorescence signal was measured using a VICTOR 3 multi-label microplate reader and compared to the stock solution controls. Each experiment (hydrogels as well as controls) were done in quadruplicate, with reported errors representing the standard deviation of the replicates.

S2.1.14 In vitro cell adhesion assay: Cell adhesion to the POEGMA hydrogels and RGD-functionalized POEGMA hydrogels was assayed in 48-well plates using 3T3 fibroblasts as a model cell line. Hydrogels were directly extruded into each well, with 100 µL of each sterilized polymer precursor solution (150 mg/mL in 10 mM PBS) added and then left overnight to ensure complete gelation. Gels were then washed with DMEM culture media prior to cell addition. Cells were plated on top of the hydrogels at a density of 2.0×10^4 cells per well together with 400 µL of DMEM and incubated for 24 hours at 37ºC. After incubation, a LIVE/DEAD assay was conducted to visualize cells using microscopy and quantify adhesion. After staining, each well was washed three times with sterile 10 mM PBS to remove any non-adherent cells from the gels. Once washed, the resulting fluorescence of the cells on the gels was quantified using a VICTOR 3 multi-label microplate reader and compared to the cell-only TCPS control. All experiments were conducted in quadruplicate and multiple images (minimum 10) were taken per well for analysis, with error ranges reported representing the standard deviation associated with the cell counts in the replicate measurements. Cell morphology on the hydrogels was visualized using a Zeiss Axiovert 200M fluorescence/live cell imaging microscope.

S2.1.15 In vivo tolerability assay: The *in vivo* toxicity of the POEGMA hydrogels was assessed using a mouse subcutaneous injection model. A total of four BALB/c mice (22-24 g, Charles River Laboratories) were injected with 0.35 mL samples of a 150 mg/mL hydrogel precursor (30

mol% reactive groups) using a double-barrel syringe. Four additional mice were injected with 0.15M NaCl to serve as controls for comparing the tissue response to the hydrogels. Animals were also visually observed to identify any systemic toxic response. Both treated and control animals were sacrificed after 3 days (acute response) and 1 month (chronic response) after injection. A tissue sample that includes skin, underlying tissue, and residual material was recovered from the animals and subjected to histological analysis using hematoxylin and eosin staining. Animals were cared for in compliance with protocols approved by the Animal Research Ethics Board at McMaster University and regulations of the Animals for Research Act of the Province of Ontario and the guidelines of the Canadian Council on Animal Care.

Table S2.1. Chemical characterization of the various POEGMA precursors

	Functional Group [-]	**Theoretical Functional Monomer [mol%]** [a]	**Actual $OEGMA_{475}$ [mol%]**	**Actual Functional Monomer [mol%]**[b]	**M_n [$x10^3$ $g \cdot mol^{-1}$]**[c]	***Đ*** **[-]**[d]	**Average # of Functional Groups/Chain**
$PO_{100}H_{20}$	$NHNH_2$	20.0	81.8	18.2	16.9	2.66	8
$PO_{100}H_{25}$	$NHNH_2$	25.0	77.9	22.1	18.1	2.43	10
$PO_{100}H_{30}$	$NHNH_2$	30.0	72.8	27.2	19.4	2.35	16
$PO_{100}H_{40}$	$NHNH_2$	40.0	64.4	35.6	19.1	3.15	20
$PO_{100}A_{20}$	CHO	20.0	82.7	17.3	19.5	3.15	7
$PO_{100}A_{25}$	CHO	25.0	75.2	24.8	17.9	2.87	9
$PO_{100}A_{30}$	CHO	30.0	71.9	28.1	19.3	2.43	12
$PO_{100}A_{40}$	CHO	40.0	60.2	39.8	20.3	3.21	17

Nomenclature: PO_xH_y; x represents the mol fraction of $OEGMA_{475}$ of the OEGMA monomers used and y represents the theoretical mol fraction of functional monomer (hydrazide or aldehyde). [a] Theoretical degree of functionalization in mol%, [b] Experimental degree of functionalization as determined from conductometric base-into-acid titration for the hydrazide precursors or from ^{1}H-NMR for the aldehyde precursors, [c] Determined using aqueous GPC with a mobile phase consisting of 0.3 M sodium nitrate and 0.05 M phosphate buffer at pH 7, [d] Dispersity (*Đ*) as determined from aqueous GPC

Table S2.2. Gelation times of the various POEGMA hydrogels measured at 37°C.

Hydrazide precursor	Aldehyde precursor	Concentration [mg/mL]	Functionality [mol%]	Gelation time [min]
$PO_{100}H_{30}$	$PO_{100}A_{30}$	100	30	160
$PO_{100}H_{30}$	$PO_{100}A_{30}$	125	30	85
$PO_{100}H_{30}$	$PO_{100}A_{30}$	150	30	45
$PO_{100}H_{30}$	$PO_{100}A_{30}$	175	30	10
$PO_{100}H_{30}$	$PO_{100}A_{30}$	200	30	2
$PO_{100}H_{20}$	$PO_{100}A_{20}$	150	20	420
$PO_{100}H_{25}$	$PO_{100}A_{25}$	150	25	140
$PO_{100}H_{40}$	$PO_{100}A_{40}$	150	40	0.75

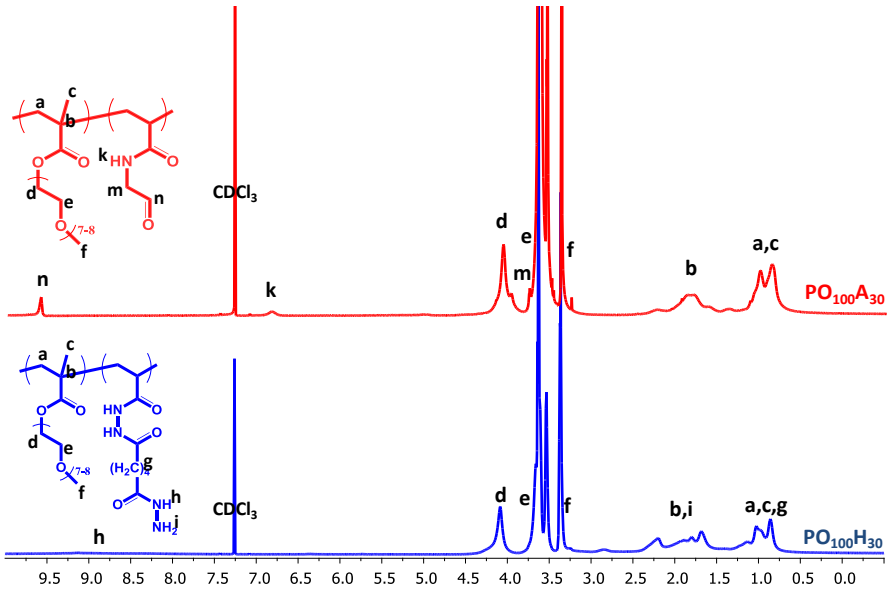

Figure S2.1 ^{1}H-NMR spectra of $PO_{100}H_{30}$ (blue, bottom) and $PO_{100}A_{30}$ (red, top).

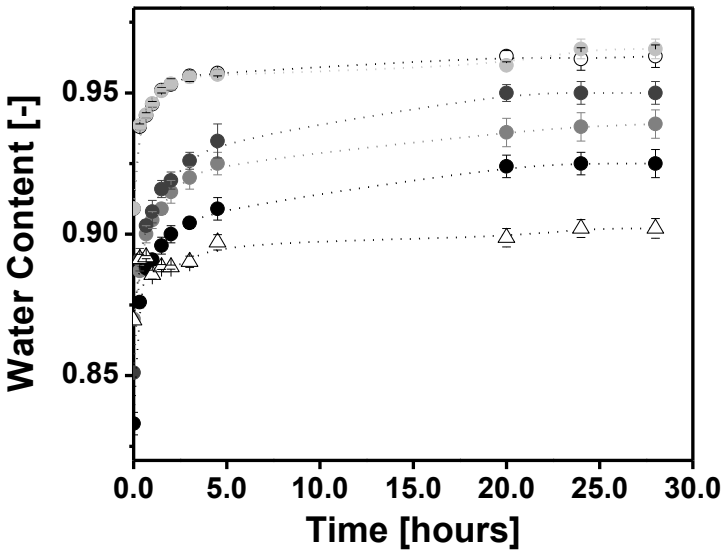

Figure S2.2. Swelling kinetics of the POEGMA hydrogels prepared at different precursor concentrations and precursor degrees of functionalization. (○) 100 mg/mL, 30 mol%, (●) 125 mg/mL, 30 mol%, (●) 150 mg/mL, 30 mol%, (●) 175 mg/mL, 30 mol%, (●) 200 mg/mL, 30 mol% and (△) 150 mg/mL, 40 mol%.

Note that the Q_m of hydrogels prepared from $PO_{100}H_{20}$ and $PO_{100}A_{20}$ precursors could not be determined under the experimental conditions due to the rapid dissolution of these hydrogels. The hydrogel prepared at 175 mg/mL precursor concentration ($PO_{100}H_{30}$ and $PO_{100}A_{30}$) is not consistent with the trend of decreasing swelling with increasing precursor concentration reported in the article and undergoes a dramatic change in appearance and a tripling in weight as it swells in PBS (see Fig. 1H of the manuscript); this result was consistent across three independent preparations of this hydrogel. While the reason for this behavior remains unclear, swelling in hydrogels prepared from the same precursors at different mass distributions should primarily be governed by a combination of the osmotic pressure influences (higher concentration = higher osmotic pressure) and the cross-link density (higher concentration = higher number of cross-links forming, as chains are on average closer together); the 175 mg/mL precursor concentration may shift the balance of these effects to favour osmotic swelling relative to additional cross-linking.

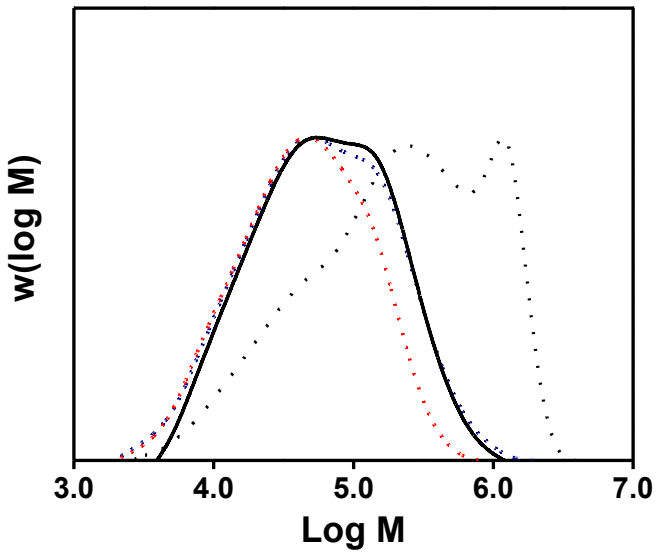

Fig S2.3. Molecular weight distributions of $PO_{100}H_{30}$ (blue), $PO_{100}A_{30}$ (red) and the hydrogel degradation products after intermediate degradation (black, dotted line) and complete degradation (black, solid line) as measured by aqueous size exclusion chromatography.

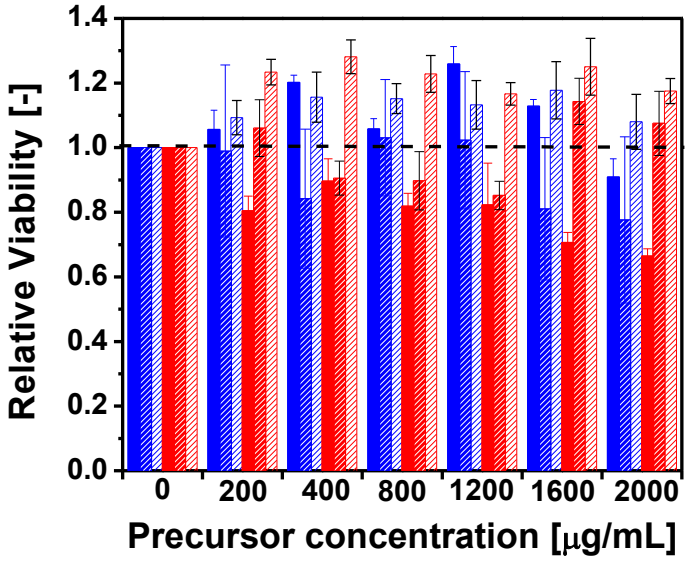

Figure S2.4. Relative cell viability of $PO_{100}H_{30}$ (blue) and $PO_{100}A_{30}$ (red) as determined from an MTT assay on 3T3 mouse fibroblasts

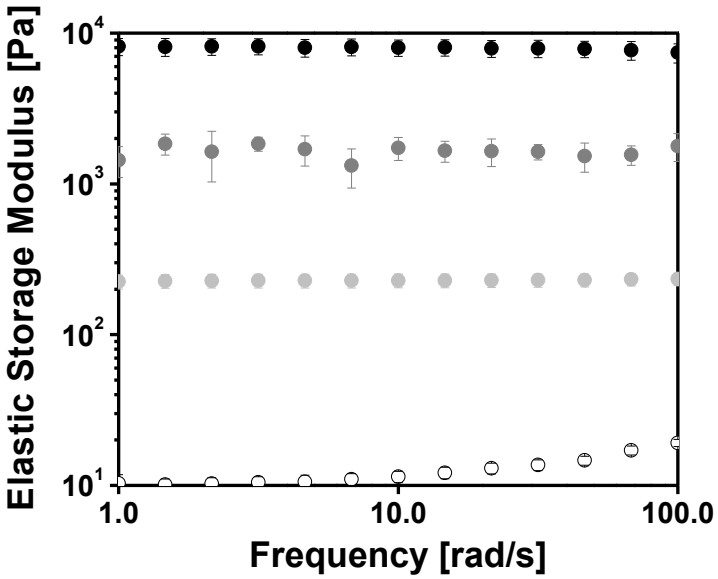

Figure S2.5. Elastic storage modulus of the POEGMA hydrogels prepared at 150 mg/mL with precursors with varying degree of functionality. (○) 20 mol%, (●) 25 mol%, (●) 30 mol% and (●) 40 mol%.

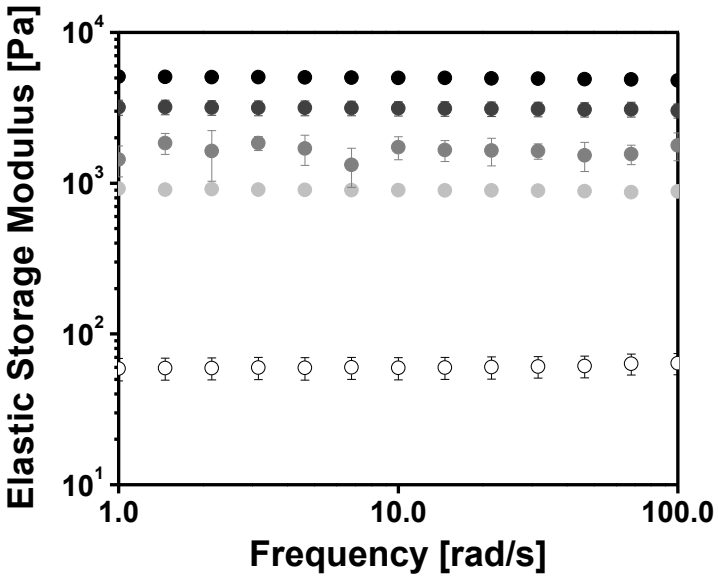

Figure S2.6. Elastic storage modulus of the POEGMA hydrogels prepared at varying precursor concentrations with from precursors functionalized with 30 mol% functional groups. (○) 100 mg/mL, (●) 125 mg/mL, (●) 150 mg/mL, (●) 175 mg/mL and (●) 200 mg/mL.

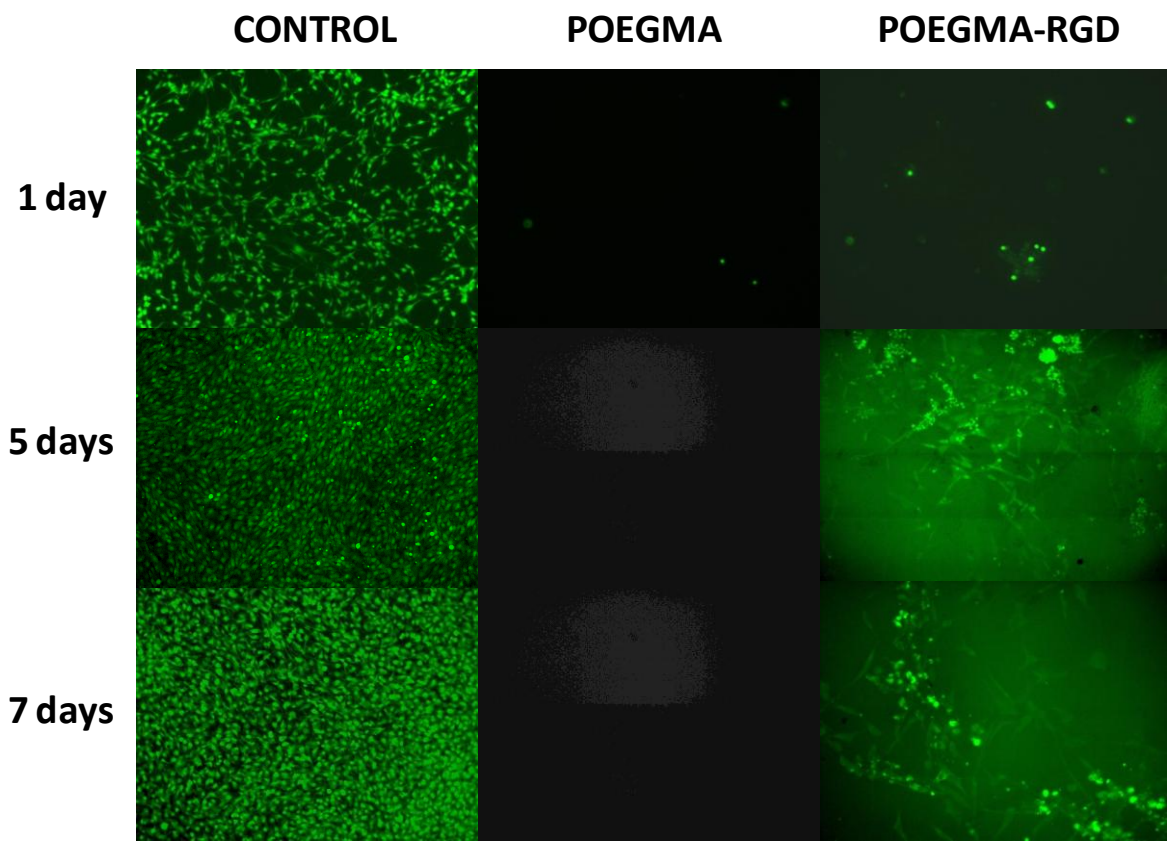

Figure S2.7. In-vitro fibroblast cell adhesion to a poly(styrene) control, POEGMA hydrogel and RGD-functionalized POEGMA hydrogel determined after 1, 5 and 7 days.

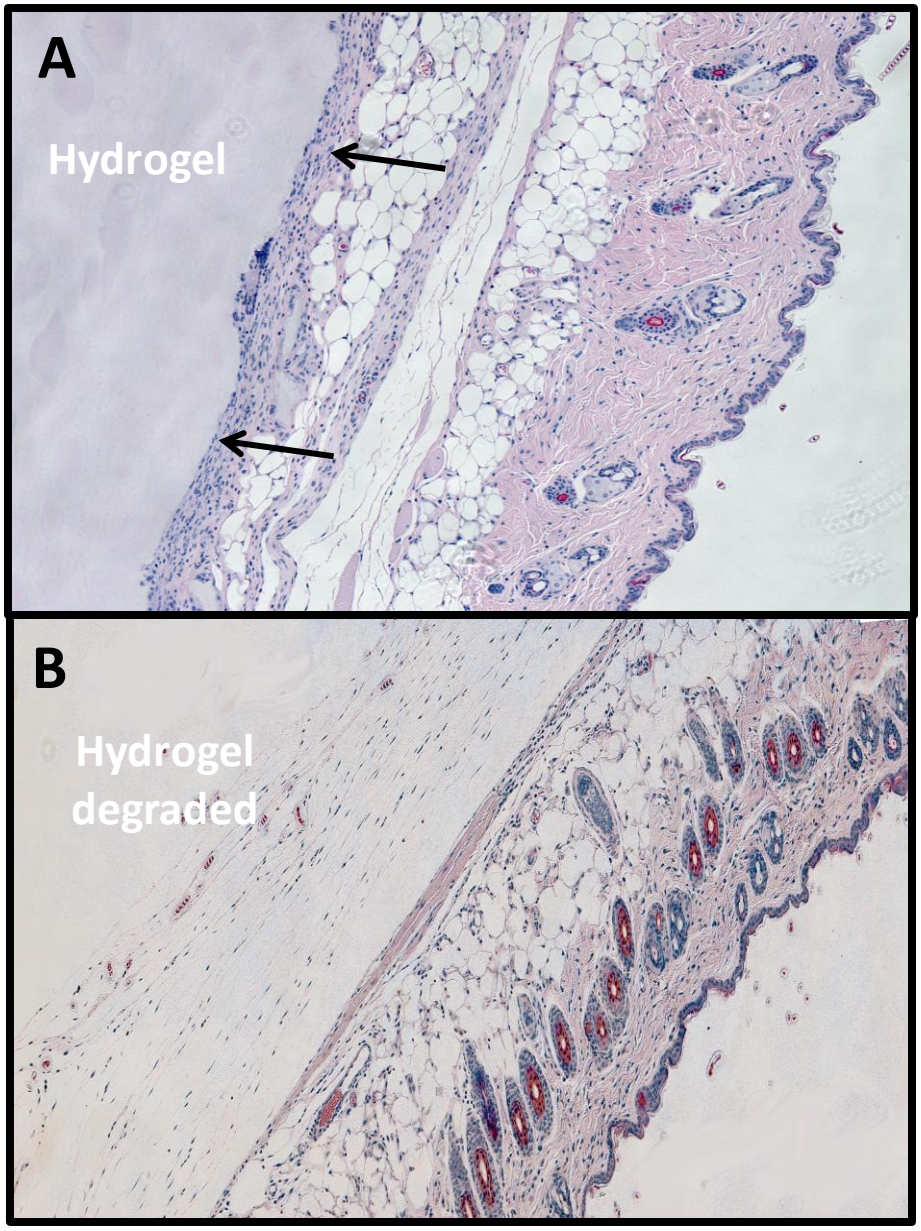

Figure S2.8 Enlarged images of Fig. 2F (A) and Fig. 2G (B) of the manuscript.

Chapter 3: Injectable Poly(oligoethylene glycol methacrylate)-Based Hydrogels With Tunable Phase Transition Behaviors: Physicochemical and Biological Responses

Preface:

This chapter describes the effect of varying the lower critical solution temperature (LCST) of the hydrazide and aldehyde functionalized poly(oligoethylene glycol methacrylate) (POEGMA) hydrogel precursors on the physiochemical and biological properties of injectable POEGMA hydrogels. This chapter investigates the ability to tune the VPTT of the POEGMA hydrogels from below to above physiological temperature to expand the potential use of POEGMA hydrogels for biomedical applications. Here, we also demonstrate the ability of the individual gel systems to mimic two advantageous properties of two model hydrogel systems; poly(ethylene glycol) (PEG) and poly(*N*-isopropylacrylamide) (pNIPAM).

Niels M.B. Smeets‡, Emilia Bakaic‡, Mathew Patenaude and Todd Hoare

Department of Chemical Engineering, McMaster University, 1280 Main St. W, Hamilton, Ontario, Canada L8S 4L7

‡ These authors contributed equally

[‡]Smeets, N.M.B.; [‡]Bakaic, E.; Patenaude, M.; Hoare, T. "Injectable Poly(oligoethylene glycol methacrylate)-Based Hydrogels With Tunable Phase Transition Behaviors: Physicochemical and Biological Responses". *Acta Biomaterialia*, 2014, *10*, 4143-4155.

Keywords

Hydrogels; thermoresponsive materials; poly(oligoethylene glycol methacrylate); *in situ* gelling hydrogels; protein adsorption

Abstract

The effect of the lower critical solution temperature of hydrazide and aldehyde functionalized poly(oligoethylene glycol methacrylate) (POEGMA) hydrogel precursors on the physiochemical and biological properties of injectable POEGMA hydrogels is evaluated. Three hydrogels were prepared with a volume-phase transition temperature (VPTT) below (= PO_0), close to (= PO_{10}) and well above (= PO_{100}) physiological temperature. Significant differences are observed between the swelling, degradation and mechanical properties of these hydrogels despite their comparable theoretical cross-link densities. Hydrogels with VPTTs close to and above physiological temperature exhibit biological properties similar to those typically observed for poly(ethylene glycol) (PEG) hydrogels (i.e. low protein adsorption, low cell adhesion, and minimal inflammatory responses *in vivo*) while hydrogels with VPTTs lower than physiological temperature exhibit biological properties more analogous to poly(*N*-isopropylacrylamide) above its phase transition temperature (temperature-switchable cell adhesion, higher protein adsorption, and somewhat more acute inflammation *in vivo*). As such, the use of POEGMA precursors with varying chain lengths of ethylene oxide grafts offers a versatile platform for the design of hydrogels with tunable physiological properties via simple copolymerization.

3.1. Introduction

Hydrogels, in part due to their high water content, controllable porosity, and mechanical and (potentially) compositional similarity to native tissues,[1] have been extensively studied as synthetic matrices for the controlled release of therapeutics and as scaffolds for promoting tissue regeneration.[2–5] However, the inherent elasticity of hydrogels limits their ability to be delivered via a minimally invasive (i.e. non-surgical) route. Consequently, there has been wide-spread interest in the development of injectable, *in situ* gelling hydrogel systems that can be delivered *in vivo* via injection, thereby reducing pain and minimizing healing time, scarring and the risk of infection as a result of the therapy.[6–8] Injectability offers the additional advantage that the hydrogel can be molded *in situ* to the match existing cavities and/or tissue defects in the neighbouring tissue. Finally, injectable hydrogels are highly modular and desired components can be introduced into the scaffold by simple mixing of the ingredients prior to injection.[9]

While many synthetic polymers have been explored for the synthesis of (injectable) hydrogels, two of the most popular for biomedical applications are poly(*N*-isopropylacrylamide) (PNIPAM)[10] and poly(ethylene glycol) (PEG).[11] PNIPAM is a thermoresponsive polymer which shows a lower critical solution temperature (LCST) in aqueous media.[12] PNIPAM-based hydrogels are, by analogy, also thermoresponsive, providing these hydrogels with switchable hydrophobicity (used, for example, for reversible cell adhesion/detachment)[13–15] and switchable pore sizes (used, for example, for the triggered release of therapeutics).[16,17] In contrast, PEG is a hydrophilic, non-immunogenic, and non-cytotoxic polymer widely studied for the controlled release of therapeutics and as scaffolds for promoting tissue regeneration.[18–20] The success of PEG in biomedical applications has largely been attributed to its “stealth”-like biological properties in terms of its capacity to significantly reduce protein adsorption (and thus subsequent inflammatory responses) relative to most other materials tested.[21]

Despite the obvious advantages that PNIPAM and PEG offer for the design of hydrogels (and biomaterials in general), there are limitations to the use of each polymer. While PNIPAM can be synthesized through facile free-radical (co)polymerization and offers thermoresponsivity,

concerns regarding the acute toxicity of the monomer *N*-isopropylacrylamide (NIPAM) as well as the chronic toxicity of degradation products of PNIPAM *in vivo* have hampered clinical use.[22,23] On the other hand, while PEG is FDA approved for many clinical uses, since PEG is an uncharged and unreactive polymer, chemical modification is necessary for hydrogel formation[24] (predominantly achieved through condensation reactions of α,ω functionalized PEG precursors),[25–34] or to incorporate other functional groups (e.g. ionic groups, acid/base responsive groups, or reactive functional groups to facilitate additional cross-linking) into the macromolecular design.

Poly(oligoethylene glycol methacrylate) (POEGMA)[35] offers a potential alternative to the use of PNIPAM and PEG for the design of hydrogels for biomedical applications. Similar to PNIPAM, POEGMA polymers can be synthesized through facile free radical polymerization and display an LCST in aqueous media that is governed by the ethylene oxide chain length (*n*) of the oligo(ethylene glycol) methacrylate (OEGMA) monomer.[36,37] Through the statistical copolymerization of diethylene glycol methacrylate ($M(EO)_2MA$, n = 2) and $OEGMA_{475}$ (n = 8,9),[38–40] hydrogels can be prepared that display a volume phase transition temperature (VPTT) ranging anywhere from ~23°C to ~90°C.[35,41–44] Recently, we reported an injectable PEG-analogue hydrogel based on $OEGMA_{475}$ (n = 8,9),[45] synthesized via the *in situ*-gelation of hydrazide and aldehyde functionalized linear polymer precursors,[9,46,47] that displayed all the advantageous non-immunogenic, non-cytotoxic and protein (and consequently cell) repellent properties of PEG. Furthermore, the hydrogel and degradation products were well tolerated *in vivo*,[45] demonstrating the potential versatility of these biomaterials for future clinical application. Consequently, we postulate that by changing the VPTT of POEGMA-based hydrogels, it should be possible to fabricate *in situ* gelling hydrogels that can match the physiochemical and biological properties of both PNIPAM and PEG but avoid the challenges of chemical modifying conventional PEG hydrogels and the toxicity concerns surrounding PNIPAM-based materials in terms of their use as biomaterials.

Herein, we evaluate the effect of the LCST of the POH (hydrazide-functionalized) and POA (aldehyde-functionalized) precursors on the physiochemical and biological properties of

injectable POEGMA hydrogels. Specifically, we have prepared three hydrogels with VPTT values (1) well below body temperature (i.e. the hydrogel will completely collapse once injected *in vivo*), (2) analogous to PNIPAM (i.e. the hydrogel will partly collapse after injection) and (3) analogous to PEG (i.e. the hydrogel remains highly swollen *in vivo*). While the degree of chemical functionality of each POH and POA precursor prepared is similar, the physiochemical and biological properties of the hydrogels are significantly different, with properties directly correlated to the VPTT of the hydrogel and, by extension, the LCST of the polymer precursors. The use of POEGMA thus offers a versatile platform for the design of both PEG-analogue hydrogels (with significantly more facile synthesis and modification) and PNIPAM-analogue hydrogels (with significantly lower concerns regarding material biocompatibility *in vivo*).

3.2. Materials and Methods

3.2.1 Materials: Di(ethylene glycol) methyl ether methacrylate ($M(EO)_2MA$, Sigma Aldrich, 95%) and oligo(ethylene glycol) methyl ether methacrylate with an average number-average molecular weight of 475 $g \cdot mol^{-1}$ ($OEGMA_{475}$, Sigma Aldrich, 95%) were purified by passing over a column of basic aluminum oxide (Sigma Aldrich, type CG-20) to remove the methyl ether hydroquinone (MEHQ) and butylated hydroxytoluene (BHT) inhibitors. *N*-(2,2-dimethoxyethyl) methacrylamide (DMAEAm, Sigma Aldrich, 98%) was synthesized according to a previously reported procedure.[45] Acrylic acid (AA, Sigma Aldrich, 99%), adipic acid dihydrazyde (ADH, Alfa Aesar, 98%), *N*'-ethyl-*N*-(3-dimethylaminopropyl)-carbodiimide (EDC, Carbosynth, Compton CA, commercial grade), thioglycolic acid (TGA, Sigma Aldrich, 98%), bovine serum albumin (BSA, Sigma Aldrich, >96%), fibrinogen from human plasma (Sigma Aldrich) fluorescein isothiocyanate (FITC, Sigma Aldrich, 90%) and 2,2-azobisisobutryic acid dimethyl ester (AIBMe, Wako Chemicals, 98.5%) were used as received. 3T3 *Mus musculus* mouse cells were obtained from ATCC: Cederlane Laboratories (Burlington, ON). Media contents including Dulbecco's Modified Eagle Medium-high glucose (DMEM), fetal bovine serum (FBS) and penicillin streptomycin (PS) as well as trypsin-EDTA were purchased from Invitrogen Canada (Burlington, ON). Thiazolyl blue tetrazolium bromide (MTT) was purchased from Sigma Aldrich (Oakville, ON). A LIVE/DEAD assay kit was purchased from Invitrogen Canada (Burlington). Dimethyl sulfoxide (DMSO, reagent grade) and dioxane (reagent grade) was purchased from Caledon Laboratory Chemicals

(Georgetown, ON). Hydrochloric acid (1M) was received from LabChem Inc. (Pittsburgh, PA). For all experiments Milli-Q grade distilled deionized water (DIW) was used.

3.2.2 Synthesis of hydrazide functionalized poly(oligoethylene glycol methacrylate) (POH): In a typical experiment (Table 1, entry $PO_{10}H_{30}$) the polymer was prepared by adding AIBMe (37 mg, 0.14 mmol), $M(EO)_2MA$ (3.5 g, 18.6 mmol), $OEGMA_{475}$ (0.50 g, 1.1 mmol), AA (0.60 g, 8.3 mmol), and TGA (8 µL, 0.12 mmol) to a 100 mL Schlenk flask. Dioxane (20 mL) was added and the solution was purged with nitrogen for at least 30 minutes. Subsequently, the flask was sealed and submerged in a pre-heated oil bath at 75°C for 4 hours under magnetic stirring. After removing the solvent, the resulting poly(ethylene glycol methacrylate-co-acrylic acid) polymer was purified by dialysis against DIW for a minimum of 6 cycles and lyophilized to dryness. The carboxylic acid groups on the acrylic acid residues were subsequently converted to hydrazide groups via a carbodiimide-mediated conjugation using a 5-fold molar excess of adipic acid dihydrazide. The polymer (3.0 g) was dissolved in 150 mL DIW in a 500 mL round-bottom flask. ADH (3.6 g, 20.5 mmol) was added and the pH of the solution was adjusted to pH = 4.75 using 0.1 M HCl. Subsequently, EDC (1.6 g, 10.2 mmol) was added and the pH maintained at pH = 4.75 by the dropwise addition (as required) of 0.1 M HCl over 4 hours. The solution was left to stir overnight, dialyzed against DIW for a minimum of 6 cycles, and lyophilized. The degree of functionalization was determined from conductometric base-into-acid titration. The polymers were stored as 20 w/w% solutions in PBS at 4°C. The PO_0H_{30} and $PO_{100}H_{30}$ polymers were synthesized in a similar manner, maintaining a total mass of 4 g of OEGMA monomer(s) in each polymerization conducted.

3.2.3 Synthesis of poly(oligoethylene glycol methacrylate-co-DMEMAm) (POA): In a typical experiment, (Table 3.1, entry $PO_{10}A_{30}$) the polymer was prepared by adding AIBMe (32 mg, 0.14 mmol), $M(EO)_2MA$ (3.10 g, 16.5 mmol), $OEGMA_{475}$ (0.90 g, 1.9 mmol), DMEMAm (1.30 g, 7.5 mmol) and TGA (7.5 µL, 0.12 mmol) to a 100 mL Schlenk flask. Dioxane (20 mL) was added and the solution purged with nitrogen for at least 30 minutes. Subsequently, the flask was sealed and submerged in a pre-heated oil bath at 75°C for 4 hours under magnetic stirring. After

polymerization, the solvent was removed and the polymer was purified by dialysis against DIW for a minimum of 6 (6+ hour) cycles and lyophilized to dryness. The acetal groups of $PO_{10}A$ were subsequently converted to aldehydes by dissolving 3.5 g of the copolymer prepared above in 50 mL DIW and 50 mL 1.0 M HCl in a 500 mL round-bottom flask. The solution was left to stir for 24 hours, dialyzed for a minimum of 6 (6+ hour) cycles, and lyophilized to dryness. The polymer was stored as 20 w/w% solution in PBS at 4°C. The PO_0A_{30} and $PO_{100}A_{30}$ polymer were synthesized in a similar manner, maintaining a total of mass of 4 g of OEGMA monomer(s) in each polymerization conducted

Table 3.1. Chemical synthesis of the POEGMA polymer precursors

	Functionality [-]	**$M(EO)_2MA$[a] [g]**	**$OEGMA_{475}$[a] [g]**	**AA [g]**	**DMEMAm [g]**	**TGA [µL]**	**AIBMe [mg]**
PO_0H_{30}	$NHNH_2$	4.00	0.0	0.65	-	7.5	3.7
$PO_{10}H_{30}$	$NHNH_2$	3.10	0.90	0.55	-	7.5	37
$PO_{100}H_{30}$	$NHNH_2$	0.0	4.0	0.30	-	1.0	37
PO_0A_{30}	CHO	4.00	0.0	-	1.50	7.5	50
$PO_{10}A_{30}$	CHO	3.10	0.90	-	1.30	7.5	50
$PO_{100}A_{30}$	CHO	0.0	4.0	-	0.60	1.0	50

All polymerizations performed at 75ºC for 4 hours in 20 mL dioxane. Sample codes PO_xH/A_y indicate the theoretical mole fraction of $OEGMA_{475}$ (*x*) and mole fractions of hydrazide (H) or aldehyde (A) functional groups (*y*) in each polymer according to the recipes used.

3.2.4 Synthesis of fluorescein-isothiocyanate labelled proteins: Fluorescein-isothiocyanate (FITC)-labelled bovine serum albumin (BSA-FITC) and fibrinogen (Fib-FITC) were prepared by dissolving 50 mg of the protein in 100 mL of a 10 mM carbonate buffer at pH = 9.0. FITC (1 mg) was added and the solution was incubated at room temperature for at least 12 h under gentile mechanical agitation. The FITC-labelled protein was subsequently dialyzed against distilled deionized water and lyophilized to dryness. The isolated labelled protein was stored at -4°C in the dark. For both proteins, a calibration curve was prepared to relate their concentration in PBS to the fluorescence signal measured at λ = 495 nm and 535 nm, with linear calibration

curves (R^2 > 0.999) observed in the concentration range of 1 to 100 µg/mL for BSA-FITC and 2 to 100 µg/mL for Fib-FITC.

3.2.5 Characterization of functionalized POEGMA polymers: Aqueous size exclusion chromatography (SEC) was performed on a system consisting of a Waters 515 HPLC pump, a Waters 717 Plus autosampler, three Ultrahydrogel columns (30 cm × 7.8 mm i.d.; exclusion limits: 0–3 kDa, 0–50 kDa, 2–300 kDa) and a Waters 2414 refractive index detector. A mobile phase consisting of 0.3 M sodium nitrate and 0.05 M phosphate buffer (pH 7) at a flow rate of 0.8 mL/min was used for all polymers analyzed, and the system was calibrated with narrow-dispersed poly(ethylene glycol) standards ranging from 106 to 584×10^3 g/mol (Waters). THF-SEC was performed using a Waters 2695 separations module equipped with a Waters 2996 photodiode array detector, a Waters 2414 refractive index detector, a Waters 2475 multi λ fluorescence detector and four Polymer Labs PLgel individual pore size columns maintained at 40°C, with 5 µm bead size and pore sizes of 100, 500, 103 and 105Å. Tetrahydrofuran (THF) was used as the eluent at a flow rate of 1.0 mL/min, and polystyrene standards were used to calibrate the instrument.

^{1}H-NMR was performed on a Bruker AVANCE 600 MHz spectrometer using deuterated chloroform as the solvent. The mole fraction of $M(EO)_2MA$ (n) and $OEGMA_{475}$ (m) incorporated into each polymer was calculated using the methodology reported by the Wang group.[48] Briefly, the integral values of the -OCH_3 signal (A = 3n + 3m, δ = 3.35-3.45 ppm), -OCH_2-CH_2 (B = 6n + 34m, δ = 3.5-3.8 ppm) and –OCH_2 (C = 2n + 2m, δ = 4.0-4.4 ppm) were used to the calculate the number of protons originating from $M(EO)_2MA$ and $OEGMA_{475}$. The acrylic acid content of the polymers was determined using base-into-acid conductometric titration (ManTech Associates) using 50 mg of polymer dissolved in 50 mL of 1 mM NaCl as the analysis sample and 0.1 M NaOH as the titrant. A Variant Cary Bio 100 UV-vis spectrophotometer was used to measure the LCST. The polymers were dissolved at a concentration of 1 mg/mL in PBS (pH = 7.4) and the absorbance of the polymer solution was recorded at 500 nm at every 0.5°C over a temperature range of 10°C to 80°C, with the temperature ramped at a rate of 1°C/min.

3.2.6 Preparation of injectable hydrogels: The different POEGMA hydrogels (PO_0, PO_{10} and PO_{100}) were prepared via co-extrusion of the corresponding hydrazide-functionalized (POH) and aldehyde-functionalized (POA) precursors dissolved in 10 mM PBS. Intensive mechanical mixing of both polymer precursor solutions was achieved through the use of a double barrel syringe fitted with a static mixer at the outlet (Medmix Systems). Hydrogel disks for all *in vitro* testing were prepared by extrusion of the reactive polymer precursors through the double barrel syringe into cylindrical silicone rubber molds (diameter = 7 mm, volume = 300 µL) and incubated at room temperature for at least 12 hours to ensure complete gelation prior to testing.

3.2.7 Swelling kinetics: The swelling kinetics were determined at 22°C in 10 mM PBS at pH 7.4. The POEGMA hydrogels were placed into cell culture inserts that are then placed in a 12-well cell culture plate and completely submerged with PBS (4 mL/well). At predetermined time intervals, the cell culture inserts were removed from the well, the PBS drained, and the hydrogel gently dried to wick off non absorbed PBS prior to weighing of the hydrogel. Subsequently, the hydrogels were resubmerged in a fresh 4 mL of PBS solution and tested repeatedly until equilibrium swelling was reached (generally ~30 hours). Error bars represent the standard deviation of the replicate measurements (n = 4). The mass-based swell ratio (Q_m) was calculated by dividing the mass of the hydrogel at any given time point (m_h) by the dry mass of polymer in the hydrogel (m_p = initial hydrogel mass $\times$ (1 – water content)).

3.2.8 Degradation kinetics: Degradation kinetics were determined at 37°C in 1 M HCl. The POEGMA hydrogels were placed into cell culture inserts that are subsequently placed in a 12-well cell culture plate and completely submerged with the HCl solution (4 mL per well). At predetermined time intervals, the cell culture inserts were removed from the well, the PBS drained and the hydrogel gently dried to wick off non absorbed solution prior to weighing of the hydrogel. Subsequently, the hydrogels were resubmerged in fresh HCl solution (4 mL/well) until the hydrogel was completely degraded (i.e. no separate phase was observed between the

hydrogel and the HCl bath solution). Error bars represent the standard deviation of the replicate measurements (*n* = 4).

3.2.9 Hydrogel rheology: The rheological properties of the hydrogels were measured using an ARES rheometer (TA Instruments) operating under parallel-plate geometry with a plate diameter of 7 mm and a plate spacing of 1 mm. Rheological properties were measured by first conducting a strain sweep from 0.1−100% strain at 1 Hz to identify the linear viscoelastic range of the hydrogels. A strain was then selected from within this linear range and set as a constant to perform a frequency sweep from 1 to 100 rad/s to measure shear elastic (G') and loss (G") moduli. All measurements were conducted at 22 °C and in triplicate, with error bars representing the standard deviation of the replicate measurements (*n* = 4).

3.2.10 In vitro cytotoxicity assay: The cytocompatibility of polymer precursors and hydrogels was assessed using a MTT assay. NIH 3T3 fibroblasts were plated at density of 1.0×10^4 cells per well in a 24-well plate and maintained in DMEM media supplemented with 10% FBS and 1% penicillin. Polymer concentrations ranging from 200 to 2000 μg/mL were transferred into wells with cultured cells and incubated for 24 hours. Cell viability was then characterized using a modified MTT assay. The absorbance of the MTT solution was read using a Biorad microplate reader (model 550) at 570 nm and normalized against a 630 nm baseline to account for any non-specific scattering. Error bars represent the standard deviation of the measured cell viability percentages (*n* = 4).

3.2.11 In vitro cell adhesion assay: Cell adhesion was assayed using NIH 3T3 mouse fibroblasts as a model adherent-dependent cell. 100 μL of each sterilized polymer precursor was extruded directly into a 48-well plate through a double-barrel syringe, left to gel for 8 hours, and then swelled to equilibrium for 24 hours with 200 μL of sterile PBS. The gels were washed with culture media, after which cells were plated on top of the hydrogel at a density of 1.0×10^4 cells per well together with 400 μL of DMEM media. Following incubation for 24 hours at 37ºC, a LIVE/DEAD assay was performed to stain all cells (both adhered and non-adhered) according to

the manufacturer-suggested protocol, after which each well was washed three times with sterile PBS to remove non-adherent cells. Residual cells were then imaged in both the live (525 nm) and dead (470 nm) channels of an Olympus inverted microscope to assess cell adhesion to the gels. The number of cells per mm^2 was counted and compared to the TCPS (tissue culture polystyrene) control for relative adherence values. The average and standard deviation of the density of adhered cells on each interface are reported (n = 4).

3.2.12 In vitro cell delamination assay: Temperature-induced cell delamination to PO_0 hydrogels was assayed using NIH 3T3 mouse fibroblasts. 100 µL of each sterilized polymer precursor was extruded directly into a 48-well plate through a double-barrel syringe, left to gel for 8 hours, and then swelled to equilibrium for 24 hours with 200 µL of sterile PBS. The gels were washed with culture media, after which cells were plated on top of both a PO_0 hydrogel at a density of 1.0×10^4 cells per well together with 400 µL of DMEM media and incubated for 24 hours at 37°C under a humidified atmosphere of 5% CO_2. The same cell density was also plated in unmodified tissue culture polystyrene wells for use as a control. Cells were then treated in one of the following two ways: (i) Conventional delamination: the media was removed and 200 µL of trypsin was applied to the gels and left for 5 minutes. After complete detachment of the cells (confirmed using microscopy), the culture medium containing the detached cells was transferred to a new 48 well plate (without hydrogel). 800 µL of fresh DMEM media was then added to each cell suspension to ensure complete trypsin neutralization and nutrient support for the delaminated cells, and cells were incubated for 16 hours to allow for attachment. (ii) Thermal delamination: cells were incubated at 4°C for 15 minutes to induce cell delamination. After 15 minutes, the culture medium containing the detached cells was transferred to a new 48 well plate (without hydrogel) and incubated for 16 hours at 37°C to allow for cell re-attachment. The number of cells adhered to the new 48 well plates following both delamination procedures (indicative of the number of cells delaminated from the original test surfaces) was determined via microscopy using calcein AM LIVE staining according to the manufacturer-suggested protocol (Invitrogen). Reattached cells were imaged in the live (525 nm) channel of an Olympus inverted microscope to assess viability and morphology. The

number of cells per mm^2 was counted and compared to the trypsinized controls for relative delamination values (% delamination = number of cells recovered following thermal delamination / number of cells recovered following trypsinization, with the latter number representing all cells originally adhered to both hydrogel and tissue culture polystyrene interfaces). The average and standard deviation of the density of adhered cells on each interface are reported (*n* = 6).

3.2.13 In vivo tolerability assay: The *in vivo* response of the injectable PO_{10} and PO_{100} hydrogels was determined histopathologically following co-extrusion of POA and POH functionalized polymer precursors into the subcutaneous space of BALB/c mice (Charles River, Montreal; *n* = 4 for every material tested). The co-injected precursor solutions consisted of 15 w/w% of PO_0H_{30} and PO_0A_{30}, 15 w/w% of $PO_{10}H_{30}$ and $PO_{10}A_{30}$, or 15 w/w% $PO_{100}H_{30}$ and $PO_{100}A_{30}$. All mice used were 3 weeks of age and weighed 22-24 g at the time of initial injection. Mice were euthanized by carbon dioxide asphyxiation after both acute (2 days) and chronic (30 day) time intervals. Tissue samples were recovered from euthanized mice and were subjected to eosin and hematoxylin staining prior to histological analysis. Animals were cared for in compliance with protocols approved by the Animal Research Ethics Board at McMaster University in accordance with the regulations of the Animals for Research Act of the Province of Ontario and the guidelines of the Canadian Council on Animal Care.

3.3 Results and Discussion

3.3.1 Synthesis of hydrogel precursors: Thermoresponsive poly(oligoethylene glycol methacrylate) (POEGMA) hydrogel precursors were synthesized via facile free radical copolymerization of oligoethylene glycol methacrylate (OEGMA) monomers with varying ethylene glycol side chain lengths (*n*) together with other functional (meth)acrylate monomers. To control the LCST of the polymer precursors (and ultimately the volume phase transition temperature (VPTT) of the injectable hydrogels), different mole ratios of diethylene glycol methacrylate ($M(EO)_2MA$, *n* = 2) and oligoethylene glycol methacrylate ($OEGMA_{475}$ *n* = 8-9) were used to synthesize poly($M(EO)_2MA$) with a target LCST close to room temperature (~24°C;

100 mol% $M(EO)_2MA$), statistical poly($M(EO)_2MA$-co-$OEGMA_{475}$ copolymers with a target LCST similar to PNIPAM (~32°C; 90 mol% $M(EO)_2MA$)[12] and poly($OEGMA_{475}$) with a target LCST similar to PEG (> 100°C; 0 mol% $M(EO)_2MA$).[49,50] Hydrazide-functionalized POEGMA precursors (PO_xH_y; where *x* equals the mole fraction of $OEGMA_{475}$ and *y* equals the mol fraction of reactive groups) with different LCSTs were synthesized by (co)polymerizing $M(EO)_2MA$, $OEGMA_{475}$ and acrylic acid (AA) and subsequent post-polymerization modification using EDC chemistry with a large excess of adipic acid dihydrazide.[9] Aldehyde-functionalized POEGMA precursors with different LCSTs (PO_xA_y) were synthesized by copolymerizing $M(EO)_2MA$, $OEGMA_{475}$ and an acetal monomer (*N*-(2,2-dimethoxyethyl)methacrylamide, DMEMAm),[51] which is subsequently converted to the corresponding aldehyde by acid catalyzed hydrolysis. Each PO_xH_y and PO_xA_y precursor reported in this paper is functionalized with *y* = 30 mol% functional hydrazide or aldehyde functional groups (equivalent to 18 ± 4 hydrazide or aldehyde functional groups per polymer chain, see Table 3.2), such that the theoretical cross-link density in each resulting hydrogel is the same among the three hydrogels assessed. The number-average molecular weight (M_n) of the polymer precursors is also consistent between the different precursors and is controlled to be less than 20×10^3 g/mol (Table 3.2), well below the renal clearance limit of 40-50×10^3 g/mol to facilitate polymer elimination following gel degradation.[52] As such, the precursor polymers tested are chemically equivalent aside from the ratio between the short and long chain OEGMA monomers.

Table 3.2. Chemical characterization of synthesized POEGMA polymer precursors

	Funct. Mon [-]	**$M(EO)_2MA$[a] [mol%]**	**$OEGMA_{475}$[a] [mol%]**	**Funct. monomer [mol%]**	**M_n [10^3 g·mol^{-1}]**	***D*** **[-]**	**Funct. groups [#/chain]**	**LCST[c] [°C]**
PO_0H_{30}	$NHNH_2$	77.1	0.0	22.9[b]	16.2	2.41	24	51.0
$PO_{10}H_{30}$	$NHNH_2$	72.5	5.9	21.6[b]	17.0	1.59	22	63.1
$PO_{100}H_{30}$	$NHNH_2$	0.0	72.8	27.2[b]	19.4[d]	2.35[d]	16	> 80[e]
PO_0A_{30}	CHO	80.6	0.0	19.4[a]	16.9	2.49	17	40.1
$PO_{10}A_{30}$	CHO	70.4	5.7	23.9[a]	13.0	2.03	19	53.6
$PO_{100}A_{30}$	CHO	0.0	71.9	28.1[a]	18.3[d]	2.43[d]	16	> 80[e]

[a] Determined by ^{1}H-NMR, [b] Determined from conductometric titration [c] Determined at 95% transmittance at 1 mg/mL in PBS [d] Measured in aqueous-SEC using an acetate buffer [e] no LCST was observed up to 80°C.

The lower-critical solution temperature (LCST) of the PO_xH_{30} and PO_xA_{30} precursors was determined in 10 mM PBS. It can be seen from Table 3.2 that the measured LCSTs of the aldehyde and hydrazide-functionalized precursors differ substantially from what was expected based solely on the mole fraction of $OEGMA_{475}$ in the polymer,[36] owing to the presence of the (hydrophilic) hydrazide or aldehyde functional groups. Although the $PO_{10}H_{30}$ and $PO_{10}A_{30}$ precursors (10 mol% $OEGMA_{475}$) display an LCST in 10 mM PBS of 63.0°C and 53.5°C respectively (see Supporting Information, Figure S1), these values are comparable to the LCST of hydrazide and aldehyde-functionalized PNIPAM precursors with the same degree of functionalization (58.2°C and 40.4°C respectively, see Supporting Information Figure S3.2). The LCSTs of the PO_0H_{30} and PO_0A_{30} polymer precursors (0 mol% $OEGMA_{475}$) in 10 mM PBS were 51.0°C and 40.1°C, respectively, significantly lower than for the equivalent PNIPAM precursors. The functionalized $PO_{100}H_{30}$ and $PO_{100}A_{30}$ precursors (100 mol% $OEGMA_{475}$) continue to display no LCST in water up to 80°C, as expected.

3.3.2 Physiochemical properties of the POEGMA hydrogels: Hydrogels were prepared by co-extruding the PO_xH_{30} and PO_xA_{30} precursors as solutions (dissolved at 150 mg/mL in 10 mM PBS) into silicone molds. Gelation occurred rapidly, with gelation times ranging from < 10

seconds for PO_0 and PO_{10} to ~20 minutes for PO_{100}; the significantly longer gelation time required for PO_{100} is likely attributable to the steric inhibition of functional group reactions by the long PEG side chains on this polymer. Following 28 hours of incubation in 10 mM PBS at 22°C, the equilibrium water content decreased from 0.870 at gel formation to 0.823 ± 0.010 and 0.861 ± 0.002 for PO_0 and PO_{10}, respectively; in contrast, the equilibrium water content of PO_{100} increased from 0.870 to 0.939 ± 0.003 (see Supporting Information Figure S3.3), the latter corresponding to a weight increase of 215 ± 20%. Thus, consistent with the LCST values of the respective precursors used to prepare the hydrogels, the PO_{100} hydrogels are considerably more hydrophilic than the PO_0 and PO_{10} hydrogels. Subsequent incubation at 37°C lowered the water content for all hydrogels, with the PO_{10} (PNIPAM-analogue) hydrogel deswelling the most (33% of its initial weight, final water content 0.822 ± 0.005) as anticipated. In comparison, the PO_0 hydrogel deswelled only 15% by weight (given that it was already largely collapsed at 22°C) and PO_{100} hydrogel lost 25% of its initial weight, although the water content remained extremely high (0.921 ± 0.002) analogous to a PEG hydrogel. Hydrogel deswelling occurs significantly faster than swelling (Supporting Information, Figure S3.3), consistent with previous observations with PNIPAM-based hydrogels.[9]

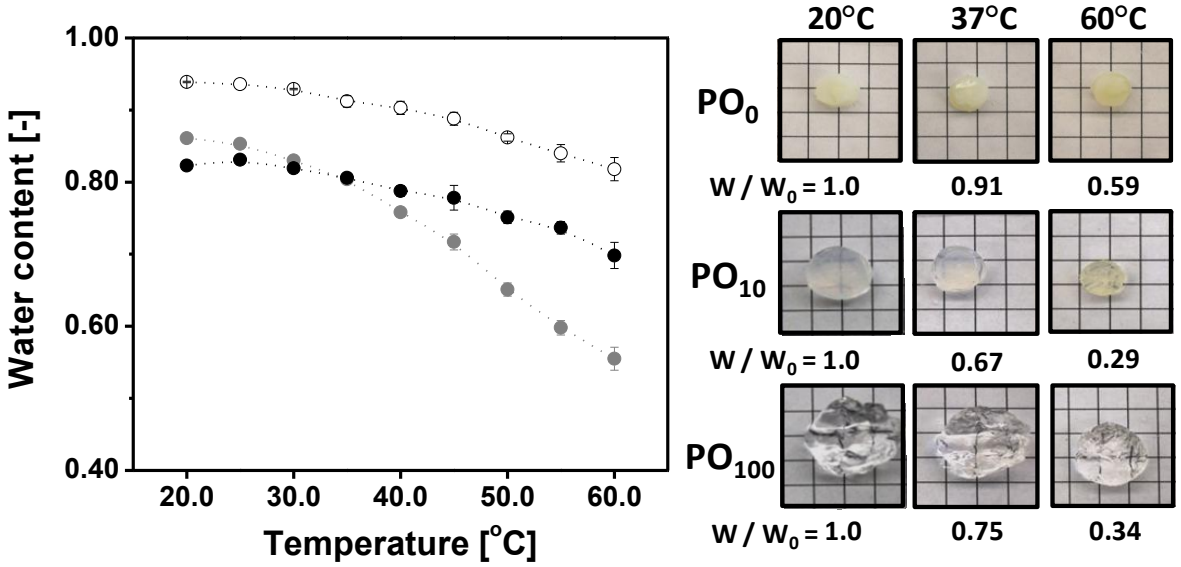

Figure 3.1. Thermoresponsive properties of the POEGMA hydrogels. Graph displays the decrease in water content as a function of the temperature (●) PO_0, (●) PO_{10} and (○) PO_{100}. The photos display the physical appearance of the hydrogels at 20°C, 37°C and 60°C (grid = 5 mm x 5 mm). The relative weight of the hydrogels (W / W_0, normalized to 20°C) is given under each photo.

The thermoresponsive behavior of the PO_0, PO_{10} and PO_{100} hydrogels was quantified by a step-wise temperature ramp (allowing 12 hours per interval to reach equilibrium conditions) from 20°C to 60°C in 5°C intervals, as shown in Figure 3.1. Although the water content slowly decreases for all hydrogels at lower temperature (< 30°C), there is a clear difference in the thermoresponsive behavior at higher temperature. For PO_{10}, an accelerated collapse of the hydrogel network is observed close to the physiological temperature that is absent for PO_0 and PO_{100}, consistent with the PO_{10} hydrogel having a volume phase transition temperature (VPTT) of approximately 32-33°C, analogous to PNIPAM. The PO_0 and PO_{100} hydrogels, with expected VPTTs of approximately 26°C and 90°C, do not display a clear volume phase transition when heated from 20°C to 60°C but rather gradually deswell as the temperature is ramped, consistent with responsive hydrogels above (PO_0) or below (PO_{100}) their phase transition temperatures.

The rheological properties of the swollen and non-swollen PO_0, PO_{10} and PO_{100} hydrogels are shown in Figure 2A (plateau modulus) and Supporting Information, Figure S3.5

(G' versus frequency profiles). The plateau elastic storage modulus (G') increases from 1.6 kPa for PO_{100} to 8.1 kPa for PO_{10} to 19.0 kPa for PO_0 as the LCST of the precursors decreases. Following equilibration of the hydrogels in 10 mM PBS at 22°C for 28 hours, plateau G' moduli change consistent with changes in the mass-based swelling ratio (Q_m) of the hydrogels (Table 3.3). For PO_0 (deswelling) and PO_{100} (swelling), a significant ($p < 0.05$) difference in G' upon equilibration was observed; in comparison, the plateau G' modulus of PO_{10} (minimal deswelling, with $Q_m = 7.69$ upon preparation compared to $Q_m = 7.18$ after equilibration) is not significantly influenced by hydrogel swelling/de-swelling ($p > 0.05$).

The cross-link density (v) of each hydrogel can be estimated from the measured G' values using rubber elasticity theory.[3,53] Calculations suggest that swollen PO_0 and PO_{10} hydrogels have relatively high cross-link densities of $(63.5 \pm 1.4)\times10^{17}$ cm^{-3} and $(20.3 \pm 1.8)\times10^{17}$ cm^{-3}, respectively, while the swollen PO_{100} hydrogels have a much lower cross-link density of $(4.7\pm 0.8)\times10^{17}$ cm^{-3} (Table 3.3). Additional quantification of the network structure of the PO_0, PO_{10} and PO_{100} hydrogels can be achieved by calculating the average molecular weight between cross-links (M_c)[54] and the network porosity (ξ)[55] using the Flory-Rehner equation[54] and the approach of Canal and Peppas.[55] Hydrogel properties were estimated using the measured volumetric swelling ratios (Q_v, Table 3.3), the measured molecular weights of the PO_xH_{30} and PO_xA_{30} precursors (Table 3.2), and under the assumption that the interaction parameter of POEGMA-water is similar to the interaction parameter of PEG-water (χ_1 = 0.426).[56] Table 3 shows the resulting mesh sizes calculated from the model, which are strongly dependent on the LCST of the precursors used. For PO_{10}, the mesh size at equilibrium decreases significantly from 3.1 nm at 20°C to 1.5 nm at 37°C, consistent with the significant collapse of the hydrogel network as shown in Fig. 3.1. The PO_0 hydrogel shows a strong decrease in mesh size after incubation at 22°C, reflective of its low (< room temperature) transition temperature, with minimal additional deswelling observed upon incubation at 37°C. In contrast, the PO_{100} hydrogels are in a highly hydrated state at both 22°C and 37°C; consequently, these hydrogels show a marked increase in the mesh size during swelling at 20°C (from 2.5 nm to 4.5 nm), followed by a small decrease in mesh size when heated to 37°C.

Table 3.3 Chemical characterization of synthesized POEGMA polymer precursors.

Hydrogel	Temperature [°C]	Q_m [a] [-]	Q_v [b] [-]	M_c [10^3 g·mol^{-1}]	N [c] [-]	ξ [nm]	υ [10^{17} cm^{-3}]
PO_0	20[d]	7.69	8.49	3.25	35	3.5	46.6
	20	5.62	6.17	2.00	22	2.5	63.5
	37	4.83	5.29	1.50	16	2.0	N/A
PO_{10}	20[d]	7.69	8.49	3.12	31	3.3	20.2
	20	7.18	7.92	2.85	29	3.1	20.3
	37	3.96	4.32	0.97	10	1.5	N/A
PO_{100}	20[d]	7.69	8.49	3.41	18	2.5	4.0
	20	16.47	18.33	6.88	35	4.5	4.7
	37	13.43	14.92	6.07	31	4.0	N/A

[a] Swell ratio based on hydrogel mass, [b] Volume swell ratio calculated based on the densities of water and the density of PEG, [c] Number of carbons between a cross-link and [d] Q_m calculated directly after preparation of the hydrogels. Note that the cross-link density at 37°C was not measured since water evaporation from the samples made mechanical testing highly variable.

The difference in mechanical properties and cross-link densities is mimicked in the degradation kinetics of the PO_0, PO_{10} and PO_{100} hydrogels, as shown in Figure 2b. In the presence of acid catalyst (1 M HCl), PO_{100} hydrogels (low cross-link density) fully degrade within 10 minutes, while the PO_{10} hydrogels (higher cross-link density) degrade within one hour. The PO_0 hydrogels, in comparison, degrade on the time scale of days (>7 days to full degradation, even in the presence of concentrated acid); we expect this difference is attributable to the large amount of deswelling (i.e. lower water accessibility for hydrolysis) and the higher local cross-link density observed for PO_0. This difference in degradation kinetics is striking, given that the number of potential (theoretical) cross-links per polymer chain is the same between the different hydrogels (18±4, see Table 3.2). When incubated *in vitro* in PBS, all three hydrogels showed no signs of macroscopic degradation for at least 3 months. The *in vivo* stability, determined upon injection of the PO_0, PO_{10} and PO_{100} hydrogels in BALB/c mice, shows that the PO_{100} hydrogels fully degraded within a month while the PO_0 and PO_{10} hydrogels were still present, although showing indications of degradation (to be discussed further later in conjunction with the histology analysis). The presence of the more complex biological

environment thus clearly accelerates degradation compared to the *in vitro* degradation experiments in phosphate buffered saline.

The PO_0 hydrogel shows a marked change in appearance during the initial stages of the degradation study (see Fig. 3.2D). While the hydrogel is completely opaque, it gradually becomes translucent as the hydrogel is incubated in 1 M HCl. We account this change in optical properties to the liberation of hydrazide and aldehyde functional groups as the dynamic hydrazone bonds are broken. Although the VPTT of the PO_0 hydrogel is well below physiological temperature, both linear precursors (PO_0H_{30} and PO_0A_{30}) have a LCST above 37°C (see Table 3.2). As hydrazone bonds degrade, the liberated hydrazone and aldehyde functional groups increase the LCST of the primary chains in the hydrogel from a collapsed, de-swollen state to a more hydrated state, resulting in a macroscopic increase in the VPTT of the hydrogel and ultimately in a decrease in the hydrogel translucency. The rate at which this optical transition happens can be governed by the cross-link density of the hydrogel, offering potential opportunities for programmed changes in light transmission through hydrogels over time.

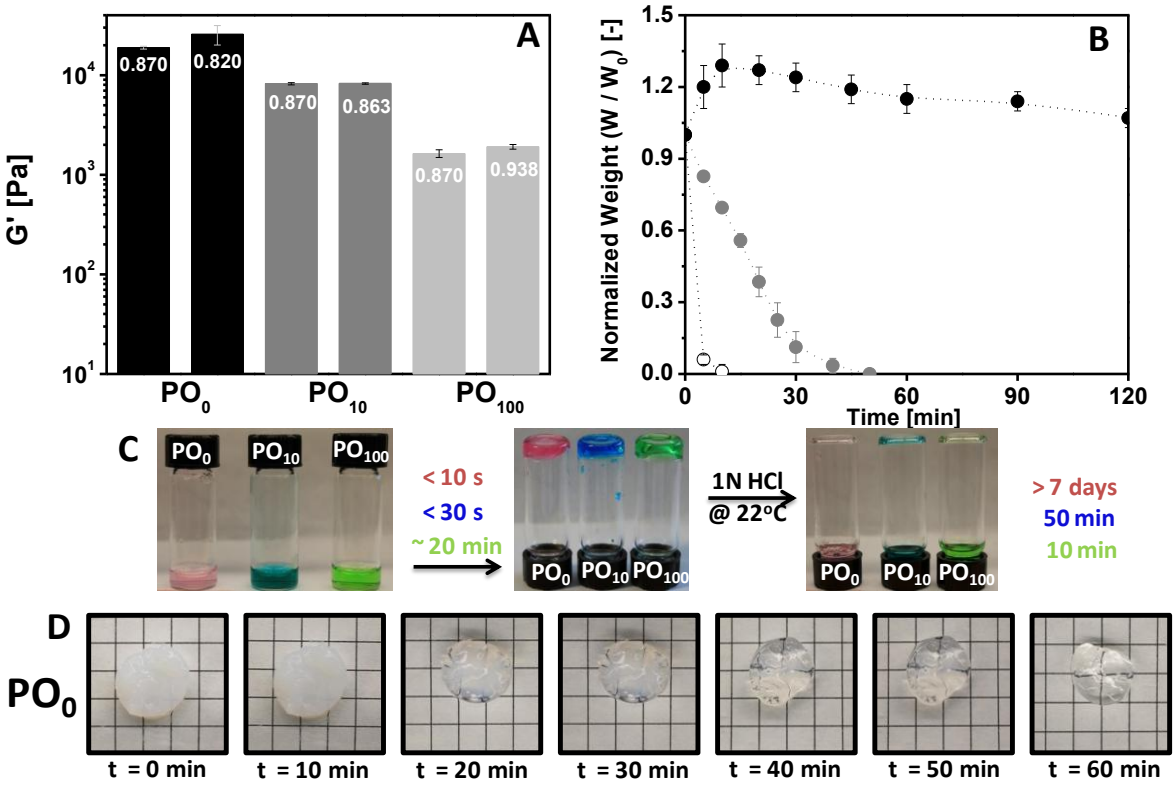

Figure 3.2. A) Shear storage modulus (G') of the PO_0, PO_{10} and PO_{100} hydrogels measured directly after preparation and after swelling for 24 hours. The numbers in the columns represent the equilibrium water content of each hydrogel. B) Degradation profiles for (●) PO_0, (●) PO_{10} and (○) PO_{100} in 1 M HCl. C) Gelation and degradation of PO_0 (red), PO_{10} (blue) and PO_{100} (green); colors are induced via the addition of food coloring and serve simply as guides to the eye. D) Optical appearance of PO_0 over the first 60 minutes of incubation in 1 M HCl (grid = 5 mm x 5 mm).

3.3.3 Protein adsorption to POEGMA hydrogels: Protein adsorption to the PO_0, PO_{10} and PO_{100} hydrogels was investigated from PBS solutions of bovine serum albumin (BSA) and fibrinogen (Fib) (Figures 3.3A and 3.3B respectively). BSA and fibrinogen are among the two most abundant proteins in human plasma (BSA: 20-40 mg/mL and Fib: 1-2 mg/mL) and adsorb onto surfaces within seconds to minutes, associated with subsequent inflammatory processes.

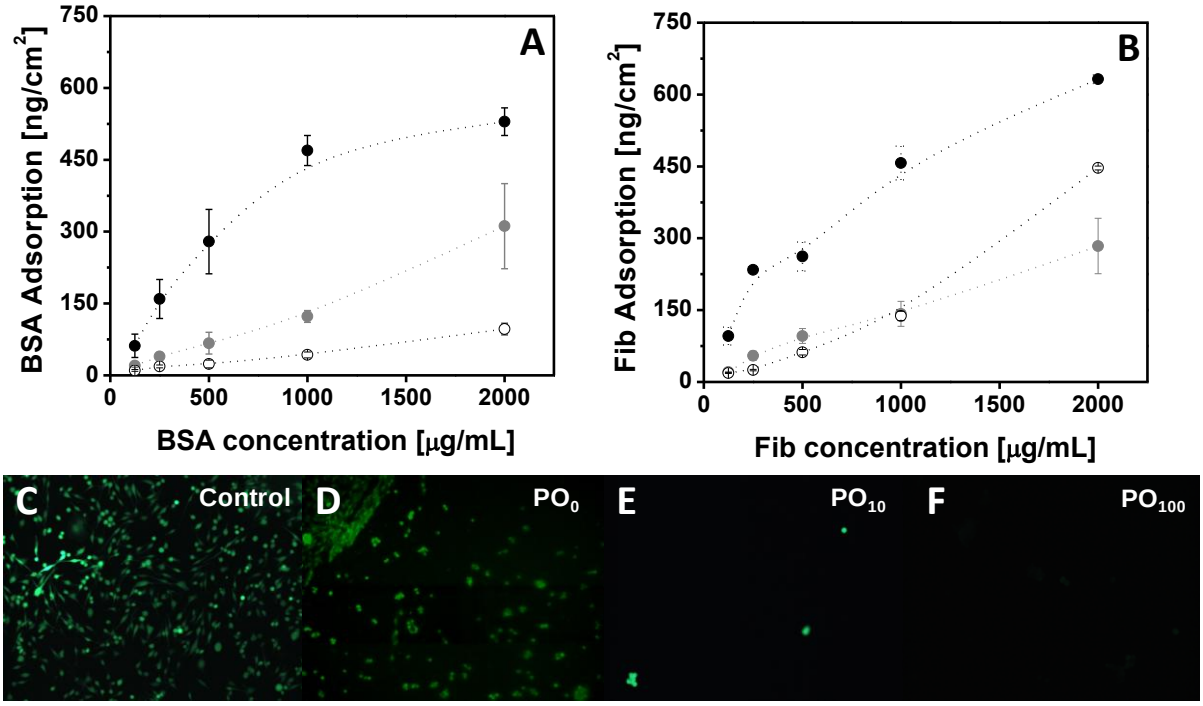

Figure 3.3. A) Bovine serum albumin (BSA) and B) fibrinogen (Fib) adsorption onto the PO_{10} and PO_{100} hydrogels at 37°C as function of the protein concentration in the loading solution. (C-F) 3T3 mouse fibroblast adhesion onto C) a tissue culture polystyrene control, and D) PO_0, E) PO_{10} and F) PO_{100} hydrogels.

BSA adsorption increases with increasing protein concentration in the loading solution for all hydrogels (Fig. 3.3A). For PO_{100}, BSA adsorption increases from approximately 10 ng/cm^2 to 100 ng/cm^2 over the range of concentrations tested, corresponding to a normalized adsorption of 3.8% ± 1.2% based on the loading solution concentration. BSA adsorption for PO_0 and PO_{10} is significantly higher, with 9.4%±1.1% (310 ng/cm^2) and 31.0%±8.9% (530 ng/cm^2) of the BSA in the 2000 μg/mL loading solution adsorbing to each respective hydrogel. The results for Fib follow a similar trend as observed for BSA (Fig. 3.3B), with up to 9.4±3.0% for PO_{100}, 11.0%±2.1% for PO_{10} and 38.4%±16.0% for PO_0 of Fib adsorbed onto the hydrogel at the highest concentration protein solution tested (2000 μg/mL). Thus, increased protein adsorption is observed as the VPTT of the temperature is decreased, consistent with the increased hydrophobicity of the hydrogel at 37°C.

3.3.4 Cell adhesion to POEGMA hydrogels: Adhesion of 3T3 mouse fibroblasts was studied by plating the cells on top of swollen PO_0 (Fig. 3.3D), PO_{10} (Fig. 3.3E) and PO_{100} (Fig. 3.3F) hydrogels, with a control experiment (for reference) performed using a tissue culture polystyrene plate (Fig. 3.3C). Following rinsing to remove non-adhered cells, negligible cell adhesion occurs to both the PO_{10} (23 ± 8 cells/mm^2, n = 6) and PO_{100} (6 ± 1 cells/mm^2, n = 6) hydrogels, whereas significantly higher cell adhesion occurs on the PO_0 hydrogels (192 ± 8 cells/mm^2, n = 4). Thus, the injectable POEGMA hydrogels with a VPTT < 37°C are repellent to both protein adsorption and (by extension) cell adhesion. It should however be noted that cell adhesion is significantly lower for all POEGMA-based hydrogels compared to the polystyrene control (2400 ± 130 cells/mm^2, n = 6), indicating that even PO_0 remains reasonably hydrophilic.

The PNIPAM-like behavior of PO_0 was further evaluated by assessing the capacity of PO_0 to facilitate cell delamination following cooling, previously demonstrated as a mild, chemical-free method for cell recovery from PNIPAM-based hydrogel materials via the switch from a more hydrophobic interface above the VPTT to a more hydrophilic interface below the VPTT.[13,57,58] Figure 4 demonstrates effective delamination of 3T3 mouse fibroblasts from a PO_0 hydrogel following a very short cooling cycle (15 minutes at 4°C). Relative to a trypsinized control (Fig. 3.4A, by which microscopy confirmed that all cells originally adhered to the hydrogel are removed), 21.0% ± 2.5% of the total number of originally adhered cells are recovered following even this extremely short cooling cycle (Fig. 3.4B), with re-adhered cells demonstrating high viability and ideal morphology following thermal delamination and recovery. In comparison, again relative to a trypsinized control (Fig. 3.4C), only 1.6 ± 0.5% of adhered cells to bare tissue culture polystyrene delaminated over the same thermal treatment (Fig. 3.4D), clearly confirming the role of the hydrogel in facilitating cell delamination. Analogous results have been reported for POEGMA-modified surfaces by Uhlig and co–workers,[59] who observed the delamination of L929 mouse fibroblasts and MCF-7 breast cancer cells from poly(MEO_2MA-co-$OEGMA_{475}$)-coated gold substrates (with a MEO_2MA:$OEGMA_{475}$ mol ratio of 90:10 mol%)[60] after incubation at 22°C for 30 minutes, although to our knowledge this is the first reported observation of delamination from a POEGMA hydrogel. Of note, the delamination shown in Figure 3.4 is largely single cell

delamination whereas most prior papers (including those cited above) assess the delamination of a cell sheet, which is significantly easier to achieve. Based on this result, by varying the ratio of short (*n* = 2) to long (*n* = 8-9) EO side chain OEGMA monomers used to prepare the reactive polymer precursors, tunable cell adhesion responses can be achieved from this injectable POEGMA hydrogel platform.

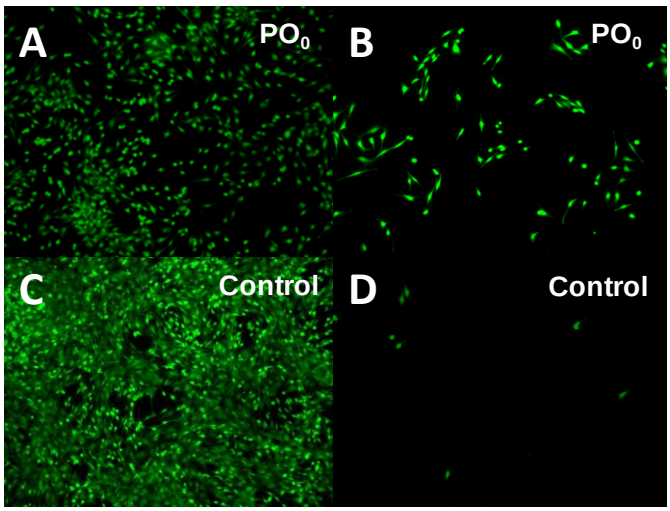

Figure 3.4. Cells recovered following delamination (replated in a new 48 well plate for 16 hours) from a PO_0 hydrogel interface (A,B) and tissue culture polystyrene surface (C,D) following trypsin treatment (A,C) and following thermal treatment at 4°C for 15 minutes (B,D).

3.3.5 In vitro cytotoxicity of POEGMA gel precursors: Prior to an *in vivo* evaluation of these injectable materials, the cytotoxicity of the polymer precursors was tested using an MTT assay on NIH 3T3 mouse fibroblasts (Figure 3.5). Results of the MTT assay demonstrate that none of the PO_xH_{30} nor the PO_xA_{30} precursors (which are also the degradation products following hydrolysis),[45] show substantial cytotoxicity up to 2000 µg/mL, an extremely high concentration of material to be screened via an *in vitro* cell-based assay. Coupled with the lack of cytotoxicity observed during the cell adhesion assay, suggesting that the PO_0, PO_{10} and PO_{100} hydrogels cause no adverse effects to cells *in vitro*.

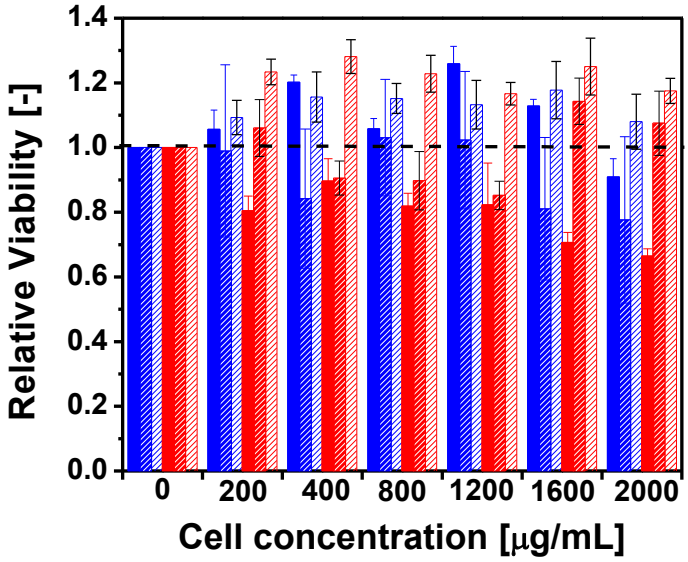

Figure 3.5. Cytotoxicity of the polymer precursors and degradation products via a MTT assay on 3T3 mouse fibroblasts. For each concentration, the order of the 6 bars is as follows: PO_0H_{30} (solid blue), $PO_{10}H_{30}$ (dense blue hatch), $PO_{100}H_{30}$ (light blue hatch), PO_0A_{30} (solid red), $PO_{10}A_{30}$ (dense red hatch), and $PO_{100}A_{30}$ (light red hatch).

3.3.6 Tissue response to POEGMA hydrogels: The *in vivo* response to the PO_0, PO_{10} and PO_{100} hydrogels was evaluated by subcutaneous injection of 150 mg/mL polymer precursor solutions using a double-barrel syringe in BALB/c mice. Co-injection of the precursor solutions resulted in the formation of stable gels within the subcutaneous space of the mice for each hydrogel tested, as confirmed via acute histopathological analysis (Figures 3.6A, 3.6C and 3.6E). Injection of the $PO_{100}H_{30}$ and $PO_{100}A_{30}$ precursors resulted minimal leukocytotic infiltration at the hydrogel-tissue interface (~100 mm^{-2}) two days post-injection (Fig. 3.6A), suggesting a relatively mild acute inflammatory reaction to the hydrogel. The PO_{100} hydrogel fully degraded within the subcutaneous space after one month (Fig. 3.6B) and no signs of chronic inflammation were observed at this time point (i.e. no macrophage, foreign body giant cells, fibrous capsule, or granulation tissue was observed histopathologically). Hence, PO_{100} appears to be very well-tolerated *in vivo*, analogous to conventional PEG hydrogels.

Co-injection of $PO_{10}H_{30}$ and $PO_{10}A_{30}$ precursors results in significantly higher leukocyte infiltration two days post-injection (~ 500 mm^{-2} at the hydrogel-tissue interface, Fig. 3.6C). The 30 day chronic time point data indicates that the gel remains present but exhibits evidence of

at least partial degradation, with clear ridging observed in the residual hydrogel sample (Fig. 3.6D). Cellular infiltration at the hydrogel-tissue interface is still present at this stage; however, the cellular density is significantly reduced (~75 mm^{-2}). However, no chronic foreign body response is observed at this time point, and the presence of polymorphonuclear neutrophils even 30 days post-injection demonstrates an ongoing infiltrative response toward the material likely mediated by the presence of precursor chains following its biodegradation. Thus, the PO_{10} gel both facilitates slower degradation and elicits a somewhat stronger inflammatory response than the high transition temperature PO_{100} gel, consistent with the relative hydrophilicities of both hydrogels suggested by *in vitro* swelling measurements. However, given that no fibrous capsule formation is observed and the degree of chronic inflammation is quite mild compared to many other biomaterials, the PO_{10} hydrogel is still relatively well-tolerated *in vivo*.

Co-injection of PO_0H_{30} and PO_0A_{30} reveals leukocyte infiltration toward the interface of the hydrogel at a cell concentration of ~500 mm^{-2}, similar to the PO_{10} gels but significantly higher than the PO_{100} gels. By contrast, however, histopathological analysis of the acute incubation of the PO_0 gels within the subcutaneous space shows that the gel remains fully intact over the span of 30 days (Fig. 3.6F). In addition, chronic inflammation of the tissue surrounding the injected hydrogel is apparent even at the chronic time interval, with a retained cell density of ~500 mm^{-2} along with the presence of granulation tissue and neovascularization. The adhesion of the gel to all surrounding tissue was also markedly increased by comparison to PO_{10} and PO_{100} hydrogels. Again, this result is consistent with the observed deswelling (i.e. enhanced hydrophobicity) of the PO_0 hydrogel *in vitro* (Fig. 3.1) as well as the significantly higher protein adsorption observed to PO_0 for both proteins tested (Figs. 3.3A and 3.3B).

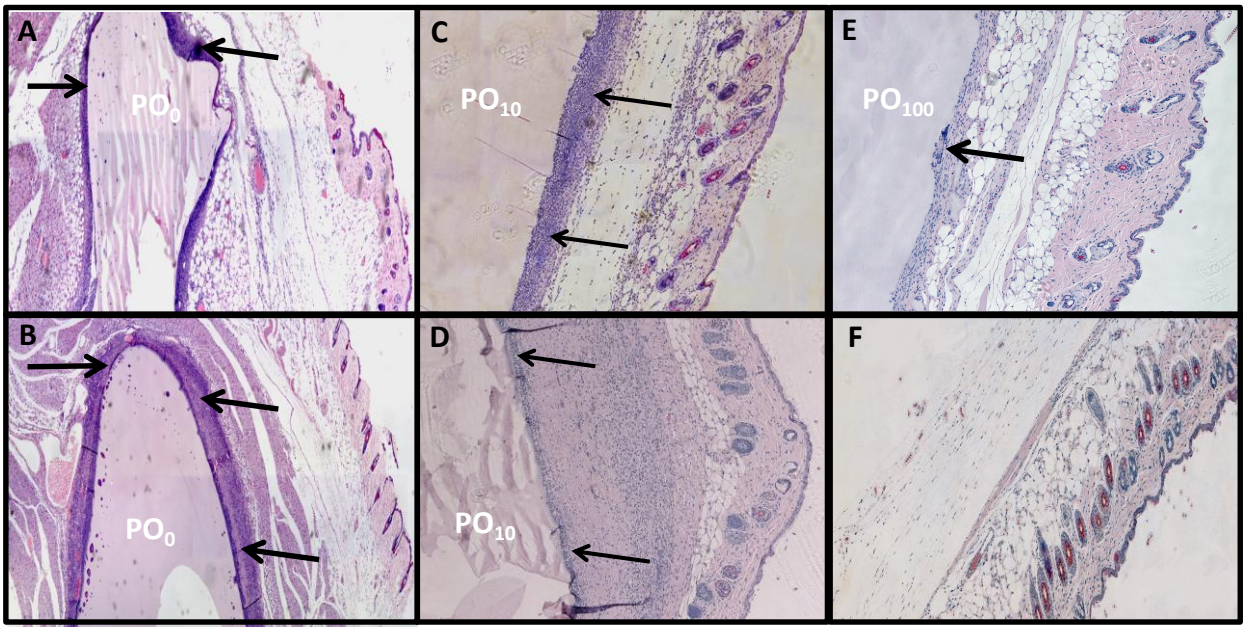

Figure 3.6. Histological sections of stained subcutaneous tissue samples following injection of PO_0 (A,B), PO_{10} (C,D) and PO_{100} (E,F), following acute (2 days; A,C,E) and chronic (30 days; B,D,F) time points. Arrows indicate the presence of leukocytes. Note that the PO_{100} hydrogel has completely degraded at the chronic time point. Evidence and localization of gelation was observed as a stable, firm, raised area of skin at the injection site.

3.4. Discussion

The results of this study suggest that both the physiochemical (i.e. swelling, temperature responsiveness, mechanical strength, and gelation and degradation kinetics) as well as the biological (i.e. protein adsorption and cell adhesion) properties of injectable POEGMA hydrogels can be controlled by the composition of the reactive precursors. The PO_0H_{30} and PO_0A_{30} precursors gel quickly (< 10 s) once co-extruded and form strong, densely cross-linked hydrogels (Fig. 3.2A) that slowly degrade (Fig. 3.2B) and have a phase transition temperature below room temperature (Fig. 3.1). Conversely, gelation of the $PO_{100}H_{30}$ and $PO_{100}A_{30}$ precursors occurs in approximately 20 minutes, with the resulting PO_{100} hydrogel swelling considerably (relative to its preparation condition) at both at 22°C and 37°C, with no discernable phase transition observed up to 60°C (Fig. 3.1). The lower G' (Fig. 3.2A) and fast degradation of this hydrogel in 1 M HCl suggest that the PO_{100} hydrogels are less densely cross-linked. The PO_{10} hydrogels display intermediate properties in terms of the G' (Fig. 3.2A) and degradation rate (Fig. 3.2B) to PO_0 and PO_{100}; furthermore, in contrast to PO_0 and PO_{100}

hydrogels, the PO_{10} hydrogel shows a clear volume phase transition close to physiological temperature (Fig. 3.1). As such, despite the elevated LCSTs of the $PO_{10}H_{30}$ (63.1°C) and the $PO_{10}A_{30}$ (53.6°C) precursors, the VPTT of the PO_{10} hydrogel was close to the targeted VPTT of PNIPAM hydrogels. This result suggests that the hydrazone bond formed upon gelation significantly reduces the phase transition temperature of the individual polymer chains to the point that the hydrogel collapses at a VPTT roughly predictable based on the relative mole fractions of the OEGMA monomers used to prepare the gel precursors (~35.8°C LCST based on a correlation reported by Lutz and Hoth[36] for a simple $M(EO)_2MA/OEGMA_{475}$ linear copolymer matching the composition of the PO_{10} polymer precursors as determined from ^{1}H-NMR analysis, Fig. S3.3). This result suggests that the VPTT of POEGMA-based injectable hydrogels can be controlled directly by choosing an appropriate copolymerization ratio between the two OEGMA monomers to prepare the reactive precursor polymers. In parallel, no volume phase transition was observed for PO_0 and PO_{100} on the temperature range 20°C < *T* < 60°C (Fig. 1), consistent with the predicted LCSTs of 24°C and 90°C of PO_0 and PO_{100} respectively. We also note that, upon degradation, all the hydrazide and aldehyde precursors have an LCST significantly higher than physiological temperature, preventing deposition and accumulation of these synthetic polymers by precipitation *in vivo*. Consequently, it is possible to design hydrogel systems (PO_0 and PO_{10}) that are collapsed *in vivo* but degrade into products that are likely to be cleared efficiently from the body once degraded.

Differences in the other physiochemical properties, such as the elastic storage modulus and the degradation rate, can be related to the cross-link density of the hydrogels (Fig. 3.2). Despite the identical theoretical cross-link density, an order of magnitude decrease in G' (and, analogously, in the crosslink density as calculated from rubber elasticity theory) is observed between the PO_0 and PO_{100} hydrogel. The $PO_{100}H_{30}$ and $PO_{100}A_{30}$ precursors are effectively comb-like copolymers due to the long ethylene glycol side chains (*n* = 8,9; side chain of 22 carbon and oxygen atoms); therefore, it is probable that a significantly higher fraction of the reactive hydrazide groups (side chain of 9 nitrogen and carbon atoms) and aldehyde groups (side chain of only 3 carbon and oxygen atoms) on the polymer backbone are sterically inaccessible for cross-linking. As a result the PO_{100} hydrogels have a lower effective cross-link

density and gelation requires longer periods of time relative to the PO_0 and PO_{10} hydrogels, despite the average number of reactive groups per polymer chain being similar for all precursors (Table 3.2).

The LCST of the precursors (and thus the VPTT of the hydrogel) also plays an important role in mediating protein adsorption. The PO_0 hydrogel (VPTT < 37°C) displays significantly more protein adsorption and cell adhesion than PO_{10} and PO_{100}, which are close to and well below their respective VPTTs at physiological temperature. This VPTT (or LCST) effect has been observed for POEGMA-grafted surfaces, to which protein adsorption and cell adhesion can be controlled by LCST of the polymer.[59–61] The collapsed, dehydrated and relatively hydrophobic PO_0 surface promotes protein adsorption and fouling due to enhanced hydrophobic interactions between the polymer and the protein. Interestingly, Figure 3 indicates that there is no significant difference in protein adsorption (Figs. 3.3A and 3.3B) or cell adhesion (Figs. 3.3C-F) between the PO_{10} and PO_{100} hydrogel ($p > 0.05$) suggesting that once the VPTT of the hydrogel is above the physiological temperature, fouling is limited regardless how close the VPTT lies to physiological temperature. Of note, the protein adsorption values observed for PO_{10} and (in particular) PO_{100} are comparable to those previously reported in the literature for PEGylated surfaces generally regarded as among the best biomaterials for mitigating protein adsorption;[62–66] BSA and Fib adsorption values in literature range for such interfaces lie in the range of 50 to 500 ng/cm^2 depending on concentration of the loading solution,[62–66] comparable to the values reported in Fig. 3.3A. It should also be noted that the results reported represent the sum of *adsorbed* and *absorbed* protein, with the latter potentially affecting results for the highly hydrated PO_{100} hydrogel in particular. However, while a clear trend in protein adsorption is observed as a function of OEGMA monomer ratio, all of these protein adsorption values reported (even for PO_0) are low relative to most biomaterials, indicating the potential of all of these POEGMA-based hydrogels for biomedical applications. Indeed, the effective delamination of cells observed when cell-cultured PO_0 hydrogel was subsequently cooled to 4°C suggests relatively weak binding of cells to even this more “hydrophobic” hydrogel, making this hydrogel of significant potential interest for the culturing and subsequent recovery of cells under very mild recovery conditions.

The *in vitro* protein adsorption and cell adhesion results were confirmed *in vivo* via subcutaneous injection (Fig. 3. 6). The PO_0 hydrogel, which is significantly more prone to protein and cell fouling, triggered a significant inflammatory response both at the acute and chronic time points; conversely, the protein and cell repellent PO_{10} and PO_{100} hydrogels show a mild inflammatory response at the acute time point and little to no inflammation at the chronic time point. Furthermore, given that the PO_{100} hydrogel completely degraded over the time scale of the experiment, the lack of local tissue toxicity supports the MTT assay result that the degradation products (i.e. the original precursors) are well tolerated by cells. As such, these injectable POEGMA-based hydrogels appear to have the potential to be viable biomaterials for *in vivo* use.

3.5. Conclusions

Injectable, hydrazone-crosslinked hydrogels based on poly(oligoethylene glycol methacrylate) prepared with mixtures of long (n = 8-9) and short (n = 2) ethylene oxide side chains have significant potential as flexible and easily tunable *in situ* gelling biomaterials. By tuning the $M(EO)_2MA$ (n = 2) : $OEGMA_{475}$ (n = 8-9) ratio in the preparation of reactive POEGMA gel precursors, the properties of the resulting hydrogels can be tuned to meet the needs of multiple potential biomedical applications. The variance in mechanical strength (1 kPa < G' < 25 kPa), swelling (4.0 < Q_m < 16.5) and degradation (10 min to > 7 days) achievable by incorporating $M(EO)_2MA$ monomer into the hydrogel is not achievable using solely $PO_{100}H_y$ and $PO_{100}A_y$ precursors over a range of potential gel preparation conditions (20 ≥ y ≥ 40 mol% and up to 200 mg/mL),[45] making such hydrogels of potential utility even in cases in which hydrogel thermoresponsivity of is not itself targeted. In addition, the ability to turn cell adhesion effectively on and off to these hydrogels by judicious selection of monomer ratio and (in the case of PO_0) temperature offers potential to apply these materials in (for example) tissue engineering applications not readily served by conventional PEG hydrogels. Finally, these POEGMA-based hydrogels offer the potential to reproduce the essential functional properties of PEG hydrogels (PO_{100}) and PNIPAM hydrogels (PO_0 or PO_{10}) while mitigating the challenges associated with each of those two polymers (i.e. effectively tuning cross-link density and

functionalization of PEG and ensuring the biocompatibility of PNIPAM *in vivo*). Together, these results suggest the potential that of POEGMA-based injectable hydrogels as a platform for the design of engineered hydrogels for drug delivery or tissue scaffolding applications.

3.6 Acknowledgements

Funding from 20/20 NSERC Ophthalmic Materials Research Network, Ontario Ministry of Research and Innovation (NMBS), and NSERC CREATE-IDEM (Integrated Design of Extracellular Matrices (EB) is gratefully acknowledged.

3.7 References

[1] Tibbitt MW, Anseth KS. Hydrogels as extracellular matrix mimics for 3D cell culture. Biotechnol Bioeng 2009;103:655–63.

[2] Langer R, Tirrell DA. Designing materials for biology and medicine. Nature 2004;428:487–92.

[3] Slaughter B V, Khurshid SS, Fisher OZ, Khademhosseini A, Peppas NA. Hydrogels in regenerative medicine. Adv Mater 2009;21:3307–29.

[4] Hoare TR, Kohane DS. Hydrogels in drug delivery: Progress and challenges. Polymer 2008;49:1993–2007.

[5] Hoffman AS. Hydrogels for biomedical applications. Adv Drug Deliv Rev 2002;54:3–12.

[6] Patenaude M, Smeets NMB, Hoare T. Designing Injectable, Covalently Cross-Linked Hydrogels for Biomedical Applications. Macromol Rapid Commun 2014.

[7] Li Y, Rodrigues J, Tomás H. Injectable and biodegradable hydrogels: gelation, biodegradation and biomedical applications. Chem Soc Rev 2012;41:2193–221.

[8] Overstreet DJ, Dutta D, Stabenfeldt SE, Vernon BL. Injectable hydrogels. J Polym Sci Part B Polym Phys 2012;50:881–903.

[9] Patenaude M, Hoare T. Injectable, Degradable Thermoresponsive Poly(N -isopropylacrylamide) Hydrogels. ACS Macro Lett 2012;1:409–13.

[10] Rzaev ZMO, Dinçer S, Pişkin E. Functional copolymers of N-isopropylacrylamide for bioengineering applications. Prog Polym Sci 2007;32:534–95.

[11] Milton J, editor. Poly(Ethylene Glycol) Chemistry: Biotechnical and Biomedical Applications. Springer; 1992.

[12] Schild HG. Poly(N-isopropylacrylamide): experiment, theory and application. Prog Polym Sci 1992;17:163–249.

[13] Cooperstein MA, Canavan HE. Biological cell detachment from poly(N-isopropyl acrylamide) and its applications. Langmuir 2010;26:7695–707.

[14] Da Silva RMP, Mano JF, Reis RL. Smart thermoresponsive coatings and surfaces for tissue engineering: switching cell-material boundaries. Trends Biotechnol 2007;25:577–83.

[15] Okano T, Yamada N, Okuhara M, Sakai H, Sakurai Y. Mechanism of cell detachment from temperature-modulated, hydrophilic-hydrophobic polymer surfaces. Biomaterials 1995;16:297–303.

[16] Ju X-J, Chu L-Y, Zhu X-L, Hu L, Song H, Chen W-M. Effects of internal microstructures of poly(N -isopropylacrylamide) hydrogels on thermo-responsive volume phase-transition and controlled-release characteristics. Smart Mater Struct 2006;15:1767–74.

[17] Makino K, Hiyoshi J, Ohshima H. Effects of thermosensitivity of poly (N-isopropylacrylamide) hydrogel upon the duration of a lag phase at the beginning of drug release from the hydrogel. Colloids Surf B Biointerfaces 2001;20:341–6.

[18] Lin C-C, Anseth KS. PEG hydrogels for the controlled release of biomolecules in regenerative medicine. Pharm Res 2009;26:631–43.

[19] Drury JL, Mooney DJ. Hydrogels for tissue engineering: scaffold design variables and applications. Biomaterials 2003;24:4337–51.

[20] Peppas NA, Hilt JZ, Khademhosseini A, Langer R. Hydrogels in Biology and Medicine: From Molecular Principles to Bionanotechnology. Adv Mater 2006;18:1345–60.

[21] Jokerst J V., Lobovkina T, Zare RN, Gambhir SS. Nanoparticle PEGylation for imaging and therapy. Nanomedicine 2011;6:715–28.

[22] Vihola H, Laukkanen A, Valtola L, Tenhu H, Hirvonen J. Cytotoxicity of thermosensitive polymers poly(N-isopropylacrylamide), poly(N-vinylcaprolactam) and amphiphilically modified poly(N-vinylcaprolactam). Biomaterials 2005;26:3055–64.

[23] Cooperstein MA, Canavan HE. Assessment of cytotoxicity of (N-isopropyl acrylamide) and Poly(N-isopropyl acrylamide)-coated surfaces - Springer. Biointerphases 2013;8.

[24] Nuttelman CR, Rice MA, Rydholm AE, Salinas CN, Shah DN, Anseth KS. Macromolecular Monomers for the Synthesis of Hydrogel Niches and Their Application in Cell Encapsulation and Tissue Engineering. Prog Polym Sci 2008;33:167–79.

[25] McCall JD, Anseth KS. Thiol-ene photopolymerizations provide a facile method to encapsulate proteins and maintain their bioactivity. Biomacromolecules 2012;13:2410–7.

[26] Aimetti AA, Machen AJ, Anseth KS. Poly(ethylene glycol) hydrogels formed by thiol-ene photopolymerization for enzyme-responsive protein delivery. Biomaterials 2009;30:6048–54.

[27] Fu Y, Kao WJ. In situ forming poly(ethylene glycol)-based hydrogels via thiol-maleimide Michael-type addition. J Biomed Mater Res A 2011;98:201–11.

[28] Cengiz N, Rao J, Sanyal A, Khan A. Designing functionalizable hydrogels through thiol-epoxy coupling chemistry. Chem Commun (Camb) 2013;49:11191–3.

[29] Lutolf MP, Hubbell JA. Synthesis and physicochemical characterization of end-linked poly(ethylene glycol)-co-peptide hydrogels formed by Michael-type addition. Biomacromolecules 2003;4:713–22.

[30] Zustiak SP, Leach JB. Hydrolytically degradable poly(ethylene glycol) hydrogel scaffolds with tunable degradation and mechanical properties. Biomacromolecules 2010;11:1348–57.

[31] Polizzotti BD, Fairbanks BD, Anseth KS. Three-dimensional biochemical patterning of click-based composite hydrogels via thiolene photopolymerization. Biomacromolecules 2008;9:1084–7.

[32] Malkoch M, Vestberg R, Gupta N, Mespouille L, Dubois P, Mason AF, et al. Synthesis of well-defined hydrogel networks using Click chemistry. Chem Commun 2006:2774–6.

[33] Grover GN, Lam J, Nguyen TH, Segura T, Maynard HD. Biocompatible hydrogels by oxime Click chemistry. Biomacromolecules 2012;13:3013–7.

[34] Saito H, Hoffman AS, Ogawa HI. Delivery of Doxorubicin from Biodegradable PEG Hydrogels Having Schiff Base Linkages. J Bioact Compat Polym 2007;22:589–601.

[35] Lutz J-F. Polymerization of oligo(ethylene glycol) (meth)acrylates: Toward new generations of smart biocompatible materials. J Polym Sci Part A Polym Chem 2008;46:3459–70.

[36] Lutz J-F, Hoth A. Preparation of Ideal PEG Analogues with a Tunable Thermosensitivity by Controlled Radical Copolymerization of 2-(2-Methoxyethoxy)ethyl Methacrylate and Oligo(ethylene glycol) Methacrylate. Macromolecules 2006;39:893–6.

[37] Sun S, Wu P. On the Thermally Reversible Dynamic Hydration Behavior of Oligo(ethylene glycol) Methacrylate-Based Polymers in Water. Macromolecules 2013;46:236–46.

[38] Luzon M, Boyer C, Peinado C, Corrales T, Whittaker M, Tao LEI, et al. Water-Soluble, Thermoresponsive, Hyperbranched Copolymers Based on PEG-Methacrylates : Synthesis, Characterization, and LCST Behavior. J Polym Sci Part A Polym Chem 2010;48:2783–92.

[39] Soeriyadi AH, Li G-Z, Slavin S, Jones MW, Amos CM, Becer CR, et al. Synthesis and modification of thermoresponsive poly(oligo(ethylene glycol) methacrylate) via catalytic chain transfer polymerization and thiol–ene Michael addition. Polym Chem 2011;2:815–22.

[40] Oh JK, Min K, Matyjaszewski K. Preparation of Poly(oligo(ethylene glycol) monomethyl ether methacrylate) by Homogeneous Aqueous AGET ATRP. Macromolecules 2006;39:3161–7.

[41] Lei J, Mayer C, Freger V, Ulbricht M. Synthesis and Characterization of Poly(ethylene glycol) Methacrylate Based Hydrogel Networks for Anti-Biofouling Applications. Macromol Mater Eng 2013;298:967–80.

[42] París R, Quijada-Garrido I. Swelling behaviour of thermo-sensitive hydrogels based on oligo(ethylene glycol) methacrylates. Eur Polym J 2009;45:3418–25.

[43] Yoon JA, Kowalewski T, Matyjaszewski K, Gayathri C, Gil RR. Comparison of the Thermoresponsive Deswelling Kinetics of Poly(2-(2-methoxyethoxy)ethyl methacrylate) Hydrogels Prepared by ATRP and FRP. Macromolecules 2010;43:4791–7.

[44] Yoon JA, Kowalewski T, Matyjaszewski K. Comparison of Thermoresponsive Deswelling Kinetics of Poly (oligo(ethylene oxide) methacrylate)-Based Thermoresponsive Hydrogels Prepared by " Graft-from " ATRP. Macromolecules 2011;44:2261–8.

[45] Smeets NM, Bakaic E, Patenaude M, Hoare T. Injectable and Tunable Poly(ethylene glycol) Analogue Hydrogels Based on Poly(oligoethylene glycol methacrylate). Chem Commun 2014;50:3306–9.

[46] Campbell SB, Patenaude M, Hoare T. Injectable superparamagnets: highly elastic and degradable poly(N-isopropylacrylamide)-superparamagnetic iron oxide nanoparticle (SPION) composite hydrogels. Biomacromolecules 2013;14:644–53.

[47] Sivakumaran D, Maitland D, Hoare T. Injectable microgel-hydrogel composites for prolonged small-molecule drug delivery. Biomacromolecules 2011;12:4112–20.

[48] Dong Y, Saeed AO, Hassan W, Keigher C, Zheng Y, Tai H, et al. "One-step" Preparation of Thiol-Ene Clickable PEG-Based Thermoresponsive Hyperbranched Copolymer for In Situ Crosslinking Hybrid Hydrogel. Macromol Rapid Commun 2012;33:120–6.

[49] Saeki S, Kuwahara N, Nakata M, Kaneko M. Upper and lower critical solution temperatures in poly (ethylene glycol) solutions. Polymer 1976;17:685–9.

[50] Ashbaugh HS, Paulaitis ME. Monomer Hydrophobicity as a Mechanism for the LCST Behavior of Poly(ethylene oxide) in Water. Ind Eng Chem Res 2006;45:5531–7.

[51] Zábranský J, Houska M, Kálal J. Aldehydes and acetals based on acryl- and methacrylamides as potential monomers. Macromol Chem Phys 1985;186:223–9.

[52] Pasut G, Veronese FM. Polymer–drug conjugation, recent achievements and general strategies. Prog Polym Sci 2007;32:933–61.

[53] Dealy JM, Larson RG. The Structure and Rheology of Molten Polymers: From Structure and Flow Behavior and Back Again, New York: Hansen Verlag; 2006, p. 152–8.

[54] Lu S, Anseth KS. Release Behavior of High Molecular Weight Solutes from Poly(ethylene glycol)-Based Degradable Networks. Macromolecules 2000;33:2509–15.

[55] Canal T, Peppas NA. Correlation between mesh size and equilibrium degree of swelling of polymeric networks. J Biomed Mater Res 1989;23:1183–93.

[56] Merrill EW, Dennison KA, Sung C. Partitioning and diffusion of solutes in hydrogels of poly(ethylene oxide). Biomaterials 1993;14:1117–26.

[57] Nash ME, Healy D, Carroll WM, Elvira C, Rochev YA. Cell and cell sheet recovery from pNIPAm coatings; motivation and history to present day approaches. J Mater Chem 2012;22:19376.

[58] Schmidt S, Zeiser M, Hellweg T, Duschl C, Fery A, Möhwald H. Adhesion and Mechanical Properties of PNIPAM Microgel Films and Their Potential Use as Switchable Cell Culture Substrates. Adv Funct Mater 2010;20:3235–43.

[59] Uhlig K, Wischerhoff E, Lutz J-F, Laschewsky A, Jaeger MS, Lankenau A, et al. Monitoring cell detachment on PEG-based thermoresponsive surfaces using TIRF microscopy. Soft Matter 2010;6:4262–7.

[60] Wischerhoff E, Uhlig K, Lankenau A, Börner HG, Laschewsky A, Duschl C, et al. Controlled cell adhesion on PEG-based switchable surfaces. Angew Chem Int Ed Engl 2008;47:5666–8.

[61] Sefcik LS, Kaminski A, Ling K, Laschewsky A, Lutz J-F, Wischerhoff E. Effects of PEG-Based Thermoresponsive Polymer Brushes on Fibroblast Spreading and Gene Expression. Cell Mol Bioeng 2013;6:287–98.

[62] Hou Y, Schoener CA, Regan KR, Munoz-pinto D, Mariah S, Grunlan MA. Photo-crosslinked PDMSstar-PEG Hydrogels: Synthesis, Characterization, and Potential Application for Tissue Engineering Scaffolds. Biomacromolecules 2010;11:648–56.

[63] Chung Y, Chiu Y. Protein adsorption and cell alignment on micropatterned phosphorylcholine surfaces. J Med Biol Eng 2009;29:320–4.

[64] Tziampazis E, Kohn J, Moghe P V. PEG-variant biomaterials as selectively adhesive protein templates: model surfaces for controlled cell adhesion and migration. Biomaterials 2000;21:511–20.

[65] Du H, Chandaroy P, Hui SW. Grafted poly-(ethylene glycol) on lipid surfaces inhibits protein adsorption and cell adhesion. Biochim Biophys Acta - Biomembr 1997;1326:236–48.

[66] Unsworth LD, Sheardown H, Brash JL. Protein resistance of surfaces prepared by sorption of end-thiolated poly(ethylene glycol) to gold: effect of surface chain density. Langmuir 2005;21:1036–41.

3.8 Table of contents image

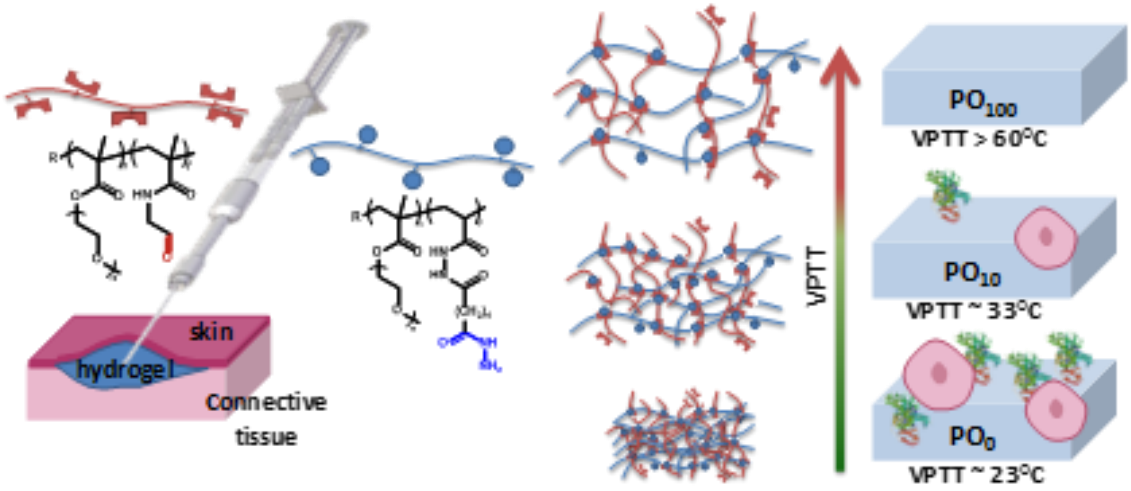

3.9 Supporting Information

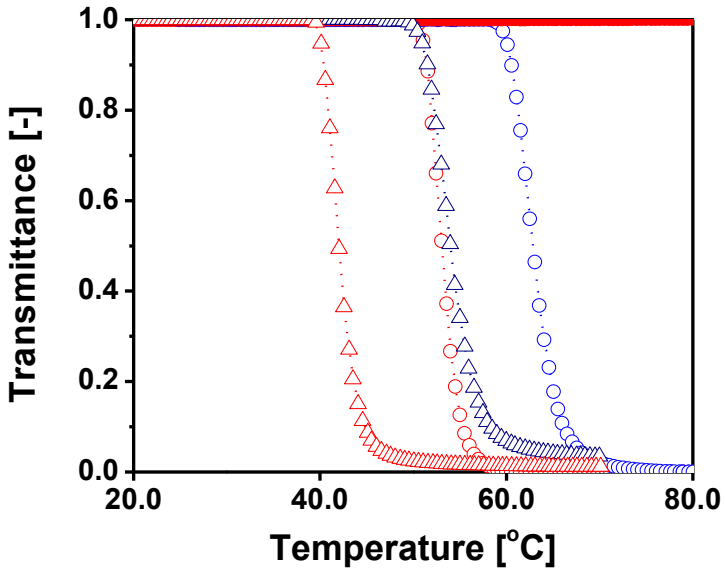

Fig. S3.1 Thermoresponsive properties of the linear POEGMA-precursor polymers. (△, blue) PO_0H, (○, blue) $PO_{10}H$, (●, blue) $PO_{100}H$, (△, red) PO_0H, (○, red) $PO_{10}A$ and (●, red) $PO_{100}A$ aldehyde.

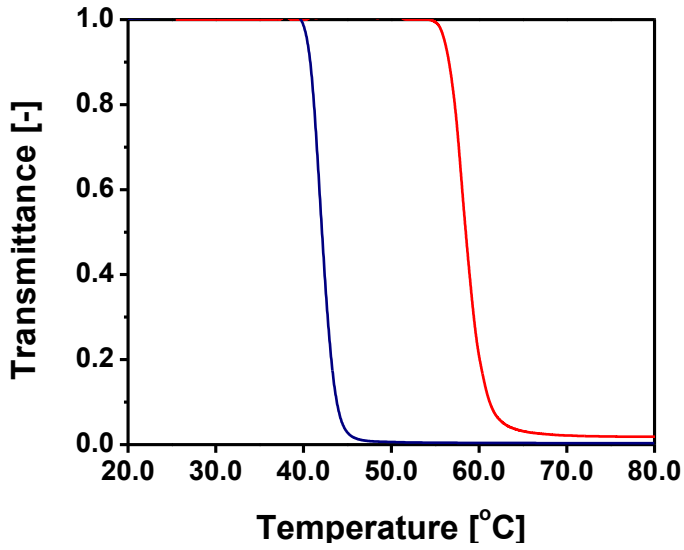

Fig. S3.2 LCST of hydrazide and aldehyde-functionalized PNIPAM as measured in PBS buffer at pH = 7.4. PNIPAM-hzd (red) and PNIPAM-ald (blue).

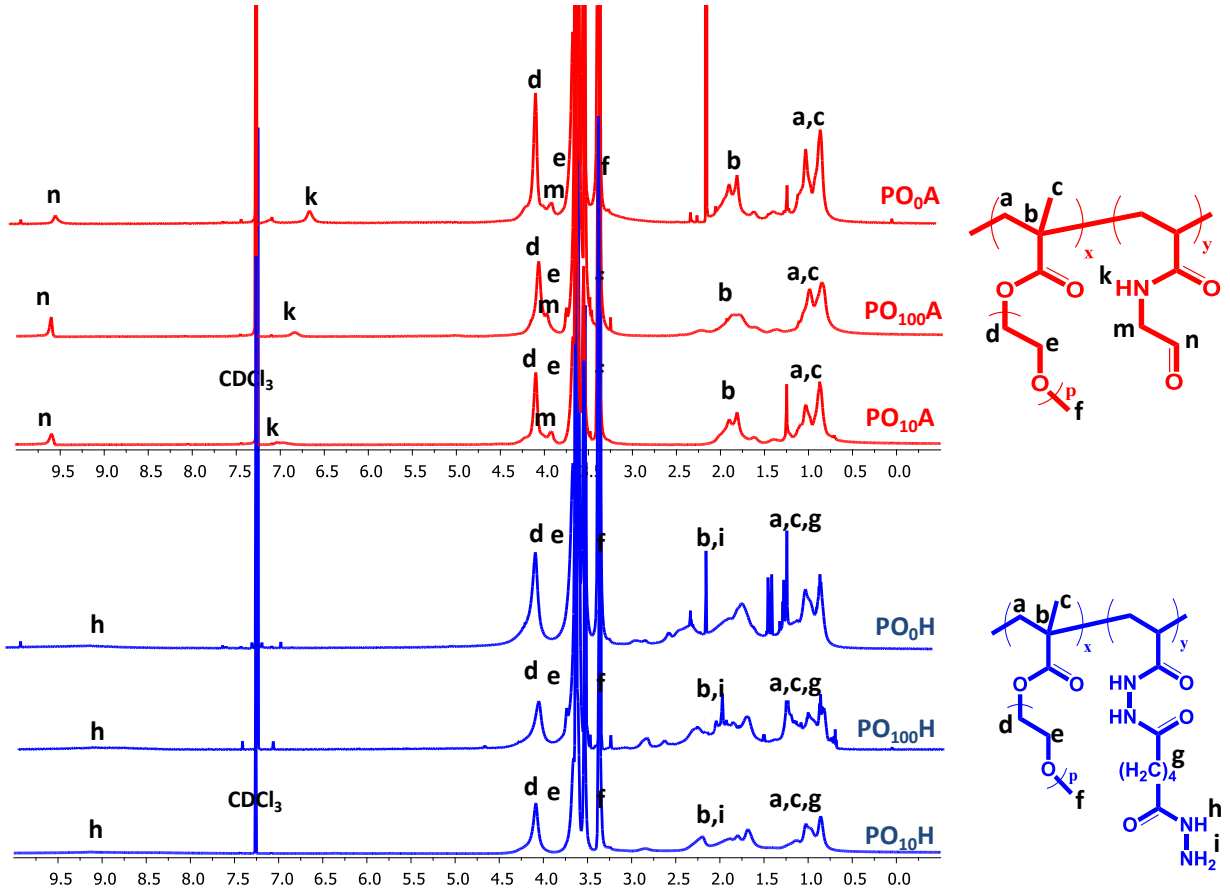

Fig. S3.3 ^{1}H-NMR of the hydrazide (blue) and aldehyde (red) POEGMA precursors.

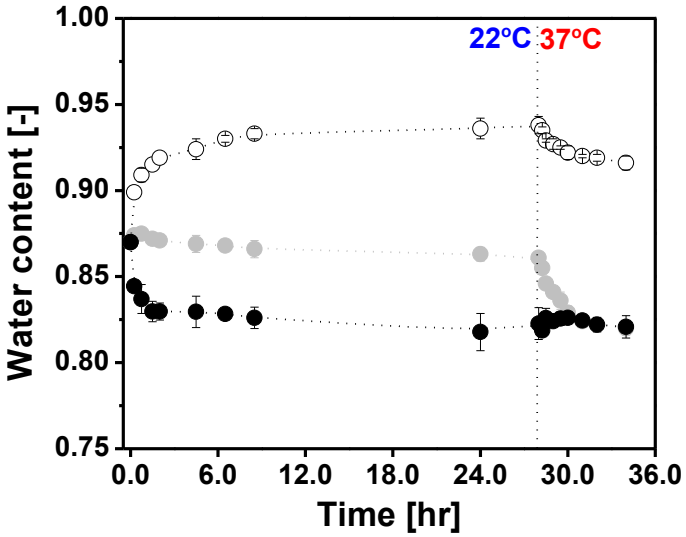

Fig. S3.4 Swelling and de-swelling kinetics of (●) PO_0, (●) PO_{10} and (○) PO_{100} hydrogels.

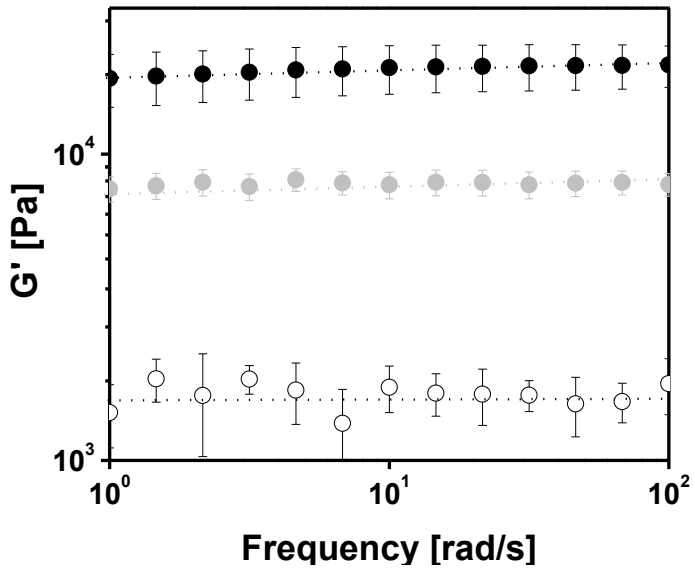

Fig. S3.5 Elastic storage modulus of (●) PO_0, (●) PO_{10} and (○) PO_{100} hydrogels.

Chapter 4: Tuning the Physicochemical, Pharmokinetic, and Biological Properties of Injectable Poly(oligoethylene glycol methacrylate) Hydrogels by Mixing Precursor Polymers with Different LCSTs

Preface:

This chapter builds and complements chapter 3. Here, we looked to investigate the capabilities of our system to be systematically tuned for an "Off-the-Shelf" 3D matrix scaffold for possible drug discovery applications. In this paper, we show that injectable and degradable POEGMA hydrogels have tunable, and well defined properties when the polymers precursors of temperature responsive (pNIPAM-like) and non temperature responsive (PEG-like) reactive precursors are mixed together in different ratios. Macroscopically, gelation rates, swelling kinetics, degradation kinetics, and mechanical properties of hydrogels produced by mixing different precursor polymers can be predicted by the simple rule of mixtures. Microscopically, phase separated domains result in localized phase transitions within hydrogels, inducing significant changes in protein affinity, drug release kinetics, transparency, and cell adhesion potentials.

Emilia Bakaic[‡], Dr. Niels M.B. Smeets[‡], Helen Dorrington, and Dr. Todd Hoare[*]

Department of Chemical Engineering, McMaster University, Department of Chemical Engineering, 1280 Main Street West, Hamilton, Ontario, L8S 4L8, Canada.

‡ These authors contributed equally

[‡]Bakaic, E.; [‡]Smeets, N.M.B.; Dorrington, H.E.; Hoare, T. "'Off-the-Shelf" Thermoresponsive Hydrogel Design: Tuning Hydrogel Properties by Mixing Precursor Polymers with Different Lower-Critical Solution Temperatures". *RSC Advances*, 2015, *5*, 33364 – 33376.

Keywords

Hydrogels, poly(oligoethylene glycol methacrylate), poly(ethylene glycol), *in situ* gelling hydrogels, drug release, protein affinity

Abstract

Injectable poly(oligoethylene glycol methacrylate) (POEGMA) hydrogels are prepared by mixing two sets of aldehyde and hydrazide-functionalized hydrogel precursors, one set with a low lower critical solution temperature (LCST) and one set with a high LCST. Macroscopically, gelation rates, swelling kinetics, degradation kinetics, and mechanical properties of hydrogels produced by mixing different precursor polymers can be predicted by the simple rule of mixtures. Microscopically, phase separated domains result in localized phase transitions within hydrogels, inducing significant changes in protein affinity, drug release kinetics, transparency, and cell adhesion. Injectable hydrogels with well-defined properties can thus be designed "off the shelf" by simple mixing of a limited number (four) of precursor polymers with different LCSTs, avoiding laborious polymerization steps each time a hydrogel with new properties is required.

4.1. Introduction

The development of easily tunable, well-defined synthetic hydrogel platforms is essential to rapidly customize hydrogels to applications such as cell delivery scaffolds,[1,2] functional tissues,[3,4,5] or wound dressings,[6] all of which demand highly specific properties to direct the desired local and systemic biological response. Indeed, successful cell maintenance, differentiation, and/or proliferation both in vitro and in vivo is strongly influenced by chemical, structural, and mechanical cues from the surrounding hydrogel scaffold.[7,8] Tunable degradation of the scaffold is also critical both in the context of tissue engineering (to prompt programmed changes in the cell microenvironment)[8,9] and drug delivery (to facilitate the desired kinetics of therapeutic release).[10]

Many commercially available natural polymers such as collagen,[11] fibrin,[12] hyaluronic acid,[13] alginate,[14,15] agarose,[16] and dextran[17,18] have been commonly used as biomaterial scaffolds, taking advantage in many cases of the inherent biological activity and degradability of those materials.[19,1] However, the unavoidable batch-to-batch variation in natural polymers can be problematic in terms of generating predictable biological responses. Instead, various synthetic polymers such as poly(*N*-isopropylacrylamide) (PNIPAM),[20] polyacrylamide (PAA),[21] and poly(ethylene glycol) (PEG)[22] have been used, typically cross-linked via biodegradable linkers to enforce at least some level of degradation in the materials.[23] PEG in particular has found wide-spread application in the design of biomaterials[24–26] due to its demonstrated non-cytotoxic and non-immunogenic properties[27] that effectively mask it from the host's immune system.[28] Hydrogels based on PEG have been demonstrated to act as excellent synthetic matrices for the controlled release of therapeutics and scaffolds for tissue regeneration.[29–31] However, given that conventional PEG-based hydrogels can only be cross-linked or functionalized through hydroxyl chain ends,[10,32–36] modification of PEG hydrogels to create more elastic hydrogels or modify cell-hydrogel interactions (for example, to promote cell adhesion or cell spreading)[37] can be synthetically challenging and/or directly affect the cross-link density of the hydrogel, especially problematic if higher graft contents and stiffer hydrogels are desired.

Recently, we reported injectable, *in situ* covalently cross-linked and degradable poly(oligoethylene glycol methacrylate) (POEGMA) hydrogels that address many of the synthetic challenges associated with conventional PEG hydrogels yet display the same desirable biological properties (i.e. significantly reduced protein adsorption, minimal cell adhesion, and a mild inflammatory response in vivo).[38,39] Our approach is based on the rapid cross-linking of complementary reactive POEGMA precursors exploiting hydrazide-aldehyde chemistry.[40–47] Depending on the number of ethylene oxide repeat units (*n*) in the oligo(ethylene glycol) methacrylate (OEGMA) monomer(s), hydrogels with PEG-like properties (*n* = 8,9)[38] or thermoresponsive, poly(*N*-isopropylacrylamide)-mimicking hydrogels[39] with lower critical solution temperatures (LCST) can be produced according to the statistical copolymerization of monomers with different side chain lengths (*n* = 2 and *n* = 8,9).[48,49] POEGMA offers the additional advantage of being synthesized using free-radical polymerization, allowing for facile functionalization with both multiple reactive hydrazide or aldehyde groups along the backbone as well as other functional tethers (e.g. charged co-monomers or grafted biomolecules to influence cell behavior).[50] These synthetic characteristics of POEGMA have directed the development of POEGMA hydrogels that display substantial differences in e.g. hydrophilicity, swelling, elastic storage modulus, degradation rate, and mesh size, as governed by the LCST and the degree of functionalization of the hydrogel precursors.[39,50]

One intrinsic advantage of our approach to injectable hydrogel formation is its inherent modularity, by which different hydrogel precursors[40,41] (and/or other desired components)[51,52] with the same hydrazide or aldehyde functionalization can be mixed together in one or both precursor solutions to form a hydrogel that exhibits the combined properties of the precursor mixture following simple co-extrusion. We have previously demonstrated this modular functionality in terms of mixing various aldehyde-functionalized carbohydrates with hydrazide-functionalized poly(*N*-isopropylacrylamide) to produce (for example) hydrogels with similar swelling responses but different enzymatic degradation rates or hydrogels with zero net swelling upon extended incubation in phosphate-buffered saline.[41] The facile synthesis of POEGMA building blocks with different LCST values offers another ideal opportunity to use this

mixing approach to generate injectable hydrogels with targeted and/or unique properties while minimizing the synthetic chemistry required.

To this end, given that we can facilely synthesize POEGMA-based precursor polymers with different phase transition temperatures, we hypothesize that mixing one high LCST and one low LCST precursor functionalized with each functional group (i.e. both hydrazide and aldehyde) will lead to hydrogels with unique functional morphologies. In such a system, phase separation can occur on the same timescale of gelation without negatively impacting the overall cross-linking potential of the system, providing a thermodynamic driving force for the formation of nanoscale or microscale domains. We recently reported the preparation and internal morphology of such injectable hydrogels using small-angle neutron scattering (SANS) and light scattering (LS).[53] Results indicated that hydrogels consisting of precursors with similar LCST were transparent and relatively homogeneous, whereas hydrogels consisting of precursors of different LCSTs were opaque and contained large inhomogeneities controlled by the hydrogel composition. Given the potential for nanoscale and microscale features to have significant impacts on cell-biomaterial responses and drug delivery kinetics,[54,55] we anticipate these novel "mixed precursor" morphologies may have useful properties as biomedical materials.

Herein, we explore the physicochemical, pharmacokinetic, and biological properties of hydrogels prepared from pairs of precursor polymers with different LCST values (i.e. in which gelation can occur together with phase separation), compared to hydrogels prepared with same-LCST precursor polymers as well as one high LCST and one low LCST polymer (i.e. gelation can only happen in the absence of phase separation). The results demonstrate that, on a macroscopic scale, mixing precursors with different LCSTs gives access to hydrogels with intermediate physiochemical and biological properties compared to the respective hydrogels consisting of precursors of similar LCST, providing a facile method to tune gel properties while circumventing the need to synthesize of a vast library of POEGMA precursor polymers. However, the biological properties of the hydrogels are significantly influenced by the phase-separated internal morphology of the hydrogels, leading to non-linear cell adhesion and protein adsorption responses. Furthermore, the heterogeneity induced by microscale phase separation

of low-LCST precursor polymers inside a matrix of high-LCST precursor polymers on the timescale of gelation was found to be relevant for tuning the pharmacokinetic properties of the hydrogels for the controlled, extended release of proteins.

4.2. Experimental Section

4.2.1 Materials: Di(ethylene glycol) methyl ether methacrylate ($M(EO)_2MA$, Sigma Aldrich, 95%) and oligo(ethylene glycol) methyl ether methacrylate with an average number-average molecular weight of 475 $g \cdot mol^{-1}$ ($OEGMA_{475}$, Sigma Aldrich, 95%) monomers were purified through a column of basic aluminum oxide (Sigma Aldrich, type CG-20) to remove inhibitors. Acrylic acid (AA, Sigma Aldrich, 99%), adipic acid dihydrazide (ADH, Alfa Aesar, 98%), *N*'-ethyl-*N*-(3-dimethylaminopropyl)-carbodiimide (EDC, Carbosynth, Compton CA, commercial grade), thioglycolic acid (TGA, Sigma Aldrich, 98%), bovine serum albumin (BSA, Sigma Aldrich, >96%), fibrinogen from human plasma (Sigma Aldrich)**,** Immunoglobulin G from human plasma (Sigma Aldrich), fluorescein isothiocyanate (FITC, Sigma Aldrich, 90%) and 2,2-azobisisobutryic acid dimethyl ester (AIBMe, Wako Chemicals, 98.5%) were used as received.*N*-(2,2-dimethoxyethyl) methacrylamide (DMAEAm, Sigma Aldrich, 98%) was synthesized according to a previously reported procedure.[50] For all experiments, Milli-Q grade distilled deionized water (DIW) was used. 3T3 mouse fibroblasts were obtained from ATCC: Cedarlane Laboratories (Burlington, ON). Media contents included Dulbecco's Modified Eagle Medium-high glucose (DMEM), fetal bovine serum (FBS), penicillin streptomycin (PS), and trypsin-EDTA and were purchased from Invitrogen Canada (Burlington, ON). Dimethyl sulfoxide (DMSO, reagent grade) was purchased from Caledon Laboratory Chemicals (Georgetown, ON). Hydrochloric acid (1M) was received from LabChem Inc. (Pittsburgh, PA). LIVE/DEAD assay kits for cell viability testing were purchased from Invitrogen Canada (Burlington).

4.2.2 Synthesis of hydrazide-functionalized poly(oligoethylene glycol methacrylate): $PO_{10}H_{30}$ and $PO_{100}H_{30}$ hydrazide functionalized POEGMA precurors were synthesized as described previously.[39] $PO_{55}H_{30}$ was synthesized by dissolving AIBMe (37 mg, 0.14 mmol), $M(EO)_2MA$ (1.0 g, 5.2 mmol), $OEGMA_{475}$ (3.0 g, 6.4 mmol), AA (0.36 g, 5.0 mmol), and TGA (2 µL, 0.03 mmol) in

1,4-dioxane (20 mL). After purging for at least 30 min, the flask was sealed and submerged in a pre-heated oil bath at 75°C for 4 hours under magnetic stirring. The solvent was removed and the polymer dissolved in 150 mL DIW. A large excess of adipic acid dihydrazide (4.4 g, 21 mmol) was then added, and the pH of the solution was adjusted to pH = 4.75 using 0.1 M HCl. Subsequently, EDC (1.6 g, 10.6 mmol) was added and the pH maintained at pH = 4.75 by the dropwise addition of 0.1 M HCl over 4 hours. The solution was left to stir overnight, dialyzed against DIW for a minimum of 6 (6+ hours) cycles, and lyophilized. The hydrazide-functionalized precursors were stored as 20 w/w% solutions in PBS at 4°C. The hydrazide functionalized precursors are labeled as PO_xH_y, where *x* denotes the mole fraction of $OEGMA_{475}$ among the OEGMA monomers used (the remainder being $M(EO)_2MA$) and *y* denotes the overall mole fraction of AA (among all comonomers) in the synthesis recipe.

4.2.3 Synthesis of aldehyde-functionalized poly(oligoethylene glycol methacrylate): $PO_{10}A_{30}$ and $PO_{100}A_{30}$ hydrazide functionalized POEGMA precursors were synthesized as described earlier.[39] $PO_{55}A_{30}$ was synthesized by dissolving AIBMe (60 mg, 0.26 mmol), $M(EO)_2MA$ (1.0 g, 5.2 mmol), $OEGMA_{475}$ (3.0 g, 6.4 mmol), DMEMAm (0.90 g, 5.2 mmol), and TGA (2 µL, 0.03 mmol) in 1,4-dioxane (20 mL). After purging for at least 30 min, the flask was sealed and submerged in a pre-heated oil bath at 75°C for 4 hours under magnetic stirring. The solvent was removed, and the polymer was subsequently dissolved in 100 mL of 0.5 M HCl. The solution was left to stir for 24 hours, dialyzed against DIW for a minimum of 6 cycles (6+ hours), and lyophilized. The degree of functionalization was determined from ^{1}H-NMR analysis. The aldehyde-functionalized precursors were stored as 20 w/w% solutions in PBS at 4°C. The aldehyde functionalized precursors are labeled as PO_xA_y, where *x* denotes the mole fraction of $OEGMA_{475}$ among the OEGMA monomers used (the remainder being $M(EO)_2MA$) and *y* denotes the overall mole fraction of DMEMAm (among all comonomers) in the synthesis recipe.

4.2.4 Synthesis of fluorescein isothiocyanate-labelled proteins: Fluorescein isothiocyanate (FITC)-labelled bovine serum albumin (BSA-FITC), immunoglobulin G (IgG-FITC) and fibrinogen (Fib-FITC) were prepared by dissolving 50 mg of the protein in a 100 mL 0.1 M carbonate buffer

at pH = 9.0. FITC (1 mg) was added, and the solution was incubated at room temperature for at least 12 h under gentile mechanical agitation. The FITC-labelled protein was subsequently dialyzed against distilled deionized water and lyophilized to dryness. The isolated conjugated proteins were stored at -20°C in the dark. Linear calibration curves were prepared for all proteins relating the protein concentration to the fluorescence signal (in PBS) at 495 nm and 519 nm for excitation and emission wavelengths. The linear concentration range for each protein and the goodness of fit parameter for each calibration are: BSA-FITC: 1 – 100 μg/mL R^2 = 0.999, IgG-FITC: 0.25 – 70 μg/mL R^2 = 0.997, Fib-FITC = 1 – 100 μg/mL R^2 = 0.999.

4.2.5 Chemical characterization: Aqueous size exclusion chromatography (SEC) was performed using a Waters 515 HPLC pump, Waters 717 Plus autosampler, three Ultrahydrogel columns (30 cm × 7.8 mm i.d.; exclusion limits: 0–3 kDa, 0–50 kDa, 2–300 kDa) and a Waters 2414 refractive index detector. A mobile phase consisting of 0.3 M sodium nitrate and 0.05 M phosphate buffer (pH 7) at a flow rate of 0.8 mL/min was used for all polymers analyzed, and the system was calibrated with narrow-dispersed poly(ethylene glycol) standards ranging from 106 to 584×10^3 g/mol (Waters). ^{1}H-NMR was performed using a Bruker AVANCE 600 MHz spectrometer and deuterated chloroform as the solvent. The acrylic acid content of the polymers was determined with conductometric titration (ManTech Associates), using 50 mg of polymer dissolved in 50 mL of 1 mM NaCl as the analysis sample and 0.1 M NaOH as the titrant. A TVariant Cary Bio 100 UV-vis spectrophotometer was used to measure the LCST of the polymer precursor chains. The polymers were dissolved at a concentration of 1 mg/mL in PBS (pH = 7.4), and the absorbance of the polymer solution was recorded at 500 nm at every 0.5°C over a temperature range of 10°C to 80°C (ramp speed 1°C/min.)

4.2.6 Hydrogel preparation: Hydrogels were prepared by co-extruding one or more hydrazide-functionalized precursor(s) ($PO_{10}H_{30}$, $PO_{55}H_{30}$ and/or $PO_{100}H_{30}$) with one or more aldehyde-functionalized precursor(s) ($PO_{10}A_{30}$, $PO_{55}A_{30}$ and/or $PO_{100}A_{30}$) using a double barrel syringe (Medmix), with each barrel containing polymer at a total concentration of 150 mg/mL in 10 mM PBS. Hydrogel disks for swelling and transparency measurements were prepared by extruding

the reactive polymer precursors through the double barrel syringe into cylindrical silicone rubber molds (diameter = 7 mm, volume = 300 µL). In all cases, gels were incubated at room temperature for at least 12 hours to ensure complete gelation prior to testing. Table 1 provides a complete summary of the hydrogel recipes evaluated, expressed in terms of the concentrations of each polymer precursor dissolved in each barrel of the double barrel syringe prior to gelation.

Three categories of hydrogels were prepared in the context of the current study. First, single precursor, same LCST hydrogels were prepared by co-extruding hydrazide and aldehyde precursors with the same OEGMA comonomer content (i.e. similar LCST values) (PO(100/0) = $PO_{10}H_{30}$ + $PO_{10}A_{30}$; PO_{55} = $PO_{55}H_{30}$ + $PO_{55}A_{30}$; PO(0/100) = $PO_{100}H_{30}$ + $PO_{100}A_{30}$). Second, single precursor, different LCST hydrogels were prepared by mixing precursors with different OEGMA comonomer contents (i.e. different LCST values) (PO(L/H) = $PO_{10}H_{30}$ + $PO_{100}A_{30}$; PO(H/L) = $PO_{100}H_{30}$ + $PO_{10}A_{30}$). Finally, mixed precursor hydrogels (PO(75/25), PO(50/50) and PO(25/75)) were prepared by mixing both high LCST (PO_{100}) and low LCST (PO_{10}) precursor polymers in both the hydrazide ($PO_{10}H_{30}$ and $PO_{100}H_{30}$) and aldehyde ($PO_{10}A_{30}$ and $PO_{100}A_{30}$) barrels of the double barrel syringe at the ratios indicated by the hydrogel sample code (PO_{10}/PO_{100} content) at a total concentration of 150 mg/mL in 10 mM PBS. The key difference between these groups is that each mixed precursor hydrogel is prepared by mixing four (2 hydrazide-functionalized and 2 aldehyde-functionalized) precursor polymers with different LCST values, while the single precursor hydrogels are prepared by mixing only two (1 hydrazide-functionalized and 1 aldehyde-functionalized) precursor polymers which may have the same or different LCST values (Table 1).

Table 4.1. Compositions of the various POEGMA hydrogels studied

	Hydrazide Barrel			**Aldehyde Barrel**		
	$PO_{10}H_{30}$ [mg/mL]	**$PO_{55}H_{30}$ [mg/mL]**	**$PO_{100}H_{30}$ [mg/mL]**	**$PO_{10}A_{30}$ [mg/mL]**	**$PO_{55}A_{30}$ [mg/mL]**	**$PO_{100}A_{30}$ [mg/mL]**
PO_{10} = PO(100/0)	150.0	-	-	150.0	-	-
PO(75/25)	112.5	-	37.5	112.5	-	37.5
PO(50/50)	75.0	-	75.0	75.0	-	75.0
PO(25/75)	37.5	-	112.5	37.5	-	112.5
PO_{100} = PO(0/100)	-	-	150.0	-	-	150.0
PO(L/H)	150.0	-	-	-	-	150.0
PO(H/L)	-	-	150.0	150.0	-	-
PO_{55}	-	150.0	-	-	150.0	-

4.2.7 Swelling kinetics: Hydrogel swelling was determined at 22°C and 37°C in 10 mM PBS at pH 7.4. Hydrogels were placed into cell culture inserts that were subsequently placed in a 12-well cell culture plate and completely submerged with PBS (4 mL/well). At predetermined time intervals, the cell culture inserts were removed from the well, the PBS drained, and the hydrogel gently dried to wick off non-absorbed PBS prior to weighing of the hydrogel. Subsequently, the hydrogels were resubmerged in a fresh 4 mL aliquot of PBS solution and tested repeatedly until equilibrium swelling was reached (generally ~30 hours). Error bars represent the standard deviation of the replicate measurements (n = 4). The mass-based swell ratio (Q_m) was calculated by dividing the mass of the hydrogel at any given time point (m_h) by the dry mass of polymer in the hydrogel (m_p = initial hydrogel mass $\times$ (1 – water content)).

4.2.8 Phase transition behavior: The volume phase transition temperature of the hydrogels was determined both spectroscopically (using the same approach described for measuring the linear precursor LCST values) and gravimetrically. For the latter measurement, hydrogels were placed inside scintillation vials filled with 12 mL of 10 mM PBS and submerged into a thermostatted water bath. After a 12-hour incubation period, the hydrogels were gently dried using a Kimwipe to remove non-absorbed PBS and weighed. A fresh aliquot of PBS was then added, the temperature of the water bath increased by 5°C, and the process repeated. The mass-loss of the hydrogels was calculated by comparing the mass of the hydrogel at any given

temperature to the initial mass of the same hydrogel, as measured at 22°C. Error bars represent the standard deviation of the replicate measurements (*n* = 4).

4.2.9 Degradation kinetics: Hydrogel degradation was determined in acid-accelerated conditions at 37°C in the presence of 100 mM HCl (pH 1.0); these acid-catalyzed conditions were used to compare the degradation properties of the hydrogels on a more measurable time frame to enable better comparisons between the hydrogel compositions rather than to model a specific in vivo environment. Hydrogels were placed into cell culture inserts that were subsequently placed in a 12-well cell culture plate and completely submerged with the HCl solution (4 mL per well). At predetermined time intervals, the cell culture inserts were removed from the wells, the PBS was drained, and the hydrogel gently dried to wick off non-absorbed liquid prior to weighing of the hydrogel. Hydrogels were resubmerged in fresh HCl solution (4 mL/well) until the hydrogel was completely degraded (i.e. no separate phase was observed between the hydrogel and the HCl bath solution). Error bars represent the standard deviation of the replicate measurements (*n* = 4).

4.2.10 Hydrogel rheology: The rheological properties of the hydrogels were measured using an ARES rheometer (TA Instruments) operating under parallel-plate geometry with a plate diameter of 7 mm and a plate spacing of 1 mm. A strain was selected within the linear viscoelastic range of each hydrogel and a frequency sweep was performed from 1 to 100 rad/s to measure the shear elastic (G') and loss (G") moduli of the hydrogel. All measurements were conducted at 25 °C, with error bars representing the standard deviation of the replicate measurements (*n* = 3).

4.2.11 Protein affinity: The protein affinity of pre-formed hydrogels was assayed in 96-well plates. POH and POA precursor solutions (150 mg/mL) were first sterilized via filtration through a 0.2 µm filter. Aliquots of 30 µL of each precursor solution were then extruded into each well and left overnight to ensure complete gelation. Once gelation was complete, 60 µL of 10 mM PBS was added to each well, and hydrogels were allowed to swell to equilibrium prior to

protein addition (over 30 hours, a time confirmed to correspond to equilibrium swelling for all hydrogels tested). Excess PBS was then removed, and 60 µL of either BSA-FITC, Fib-FITC or IgG-FITC solution (125, 250 or 500 µg/mL in PBS) was added. The hydrogels were incubated for 2 hours at 37°C. After 2 hours, the hydrogels were rinsed to remove free protein, and the fluorescence signal was measured using a VICTOR 3 multi-label microplate reader and compared to the stock solution controls. Each experiment (hydrogels as well as controls) were done in quadruplicate, with reported errors representing the standard deviation of the replicates.

4.2.12 Protein release kinetics: BSA-FITC, IgG-FITC, and Fib-FITC release from the POEGMA hydrogels was studied by dissolving the proteins (BSA-FITC 5 mg/mL, IgG-FITC 1.3 mg/mL and Fib-FITC 2.5 mg/mL) in the hydrazide precursor polymer solution and then forming hydrogel as described above, with the resulting gel incubated either at 22°C or at 37°C to allow for complete gelation. Note that the protein concentrations used vary due to the limited solubility of IgG-FITC and Fib-FITC in PBS; however, since the protein is present at the time of gelation, significantly higher loadings can be achieved using this direct loading method compared to the diffusion method. To compensate for this difference, all release results were normalized relative to the initial quantity of protein loaded into the hydrogel to enable direct comparisons. Upon complete gelation, the hydrogels (n = 4) were placed in cell culture inserts that were subsequently placed in a 12-well cell culture plate and completely submerged with PBS (4 mL/well, the release medium) and incubated at 37°C. At predetermined time intervals, the hydrogels were removed from the well, blotted to remove any unbound medium, and incubated in fresh PBS (4 mL, preheated at 37°C) to satisfy infinite-sink conditions throughout the release experiment. Protein release kinetics were assayed by measuring the fluorescence of the recovered release medium solutions at each time point using a VICTOR 3 multi-label microplate reader and comparing the results to each relevant calibration curve.

4.2.13 Cell adhesion: Cell adhesion to POEGMA hydrogels was assessed using mouse 3T3 fibroblast cells. Hydrogels were directly extruded into each well of a 48-well plate, with 100 µL

of each sterilized polymer precursor solution (150 mg/mL in 10 mM PBS) added and then left overnight to ensure complete gelation (*n* = 4). Gels were then incubated at 37ºC in 600µL of sterilized 10 mM PBS and allowed to equilibrate for 24 hours prior to cell plating. The PBS was then removed, and gels were washed with DMEM culture media prior to cell addition. Cells were plated on top of the hydrogels at a density of 1.0×10^4 cells per well together with 600 µL of DMEM and incubated for either 48 hours or one week at 37ºC. After the incubation period, a LIVE/DEAD assay was conducted to visualize cells using microscopy and quantify adhesion. Each well was washed three times with sterile 10 mM PBS to remove any non-adherent cells from the gels before staining. Once washed, fluorescent live cells were counted using a Zeiss Axiovert 200M fluorescence/live cell imaging microscope and ImageJ. All experiments were conducted in quadruplicate, with multiple images (minimum 10) taken per well for analysis; error ranges reported represent the standard deviation associated with the total cell counts (across the multiple images taken per replicate) in the replicate measurements. Cell morphology on the hydrogels was visualized using a Zeiss Axiovert 200M fluorescence/live cell imaging microscope.

4.3. Results and Discussion

4.3.1 Synthesis of hydrogel precursors: The six hydrogel precursor polymers were prepared according to a strategy reported previously.[39] Briefly, $PO_{10}H_{30}$, $PO_{55}H_{30}$ and $PO_{100}H_{30}$ were synthesized by copolymerizing diethylene glycol methacrylate ($M(EO)_2MA$, *n* = 2), oligoethylene glycol methacrylate ($OEGMA_{475}$, *n* = 8,9) and acrylic acid (AA), followed by post-polymerization modification using EDC chemistry with a large excess of adipic acid dihydrazide. $PO_{10}A_{30}$, $PO_{55}A_{30}$ and $PO_{100}A_{30}$ were prepared by copolymerizing $M(EO)_2MA$, $OEGMA_{475}$ and *N*-2,2-diethoxyethyl methacrylamide (DMEMAm) and subsequently deprotecting the acetal via acid-catalyzed hydrolysis to form an aldehyde. Chemical characterization of these four precursors is presented in Table 2. According to their $M(EO)_2MA$:$OEGMA_{475}$ composition, the hydrogel precursors are classified as low LCST (*x* = 10 mol%; $PO_{10}H_{30}$ and $PO_{10}A_{30}$), medium LCST (*x* = 55 mol%; $PO_{55}H_{30}$ and $PO_{55}A_{30}$) and high LCST (*x* = 100 mol%; $PO_{100}H_{30}$ and $PO_{100}A_{30}$). The average number of functional groups per polymer chain is similar for each precursor, such that differences in the micro-and macroscopic hydrogel properties are likely to be related to the

overall composition rather than the cross-link density of the hydrogel. In addition, given that the molecular weights of all precursor polymers is below the renal cut-off (~32 kDa) and the LCSTs of each precursor polymer lie well above physiological temperature (>50°C), kidney elimination of soluble oligomers offers a viable potential method for clearing the polymers following the degradation of the hydrogels.

Table 4.2. Chemical characterization of the synthesized POEGMA polymer precursors

	$M(EO)_2MA$[a] [mol%]	$OEGMA_{475}$[a] [mol%]	Functional Monomer [mol%]	M_n[c] [10^3 g/mol^{-1}]	$Đ$[c] [-]	Functional Groups [#/chain]	LCST[d] [°C]
$PO_{10}H_{30}$	72.5	5.9	21.6[b]	17.0	2.08	22	63.0
$PO_{55}H_{30}$	33.3	39.0	27.7[b]	15.4	2.47	16	> 80
$PO_{100}H_{30}$	0.00	72.8	27.2[b]	19.4	2.35	16	> 80
$PO_{10}A_{30}$	70.4	5.7	23.9[a]	13.0	2.03	19	53.5
$PO_{55}A_{30}$	35.5	40.1	24.4[a]	13.2	2.62	17	78.5
$PO_{100}A_{30}$	0.00	71.9	28.1[a]	18.3	2.43	16	> 80

[a] Determined by ^{1}H-NMR, [b] Determined from conductometric titration [c] Measured using aqueous-SEC using an acetate buffer, [d] Determined at 95% transmittance at a concentration of 1 mg/mL in PBS. Synthesis data partly reproduced from reference 17.

4.3.2 Preparation of poly(oligoethylene glycol methacrylate) hydrogels: The low and high LCST precursors were mixed in different proportions to prepare single and mixed precursor hydrogels (Table 4.1). Note that, given that the functional group density is similar for all PO_xH_{30} and PO_xA_{30} precursors synthesized (Table 4.2), a ~1:1 ratio of aldehyde:hydrazide functional groups is present within each hydrogel. Single precursor POEGMA hydrogels were prepared by mixing 2 precursors with the same $OEGMA_{475}$:$M(EO)_2MA$ percentage *x* (*x* = 10 mol% – PO_{10}, *x* = 55 mol% – PO_{55}, or *x* = 100 mol% - PO_{100}). For comparison, two additional hydrogels were prepared by mixing one low LCST and one high LCST precursor of opposite reactivity (PO(L/H), PO(H/L)), providing a control in which gelation can *only* occur via reaction between precursors with different LCST values. All of these single precursor hydrogels were found to be relatively homogeneous on both the microscopic (SANS) and macroscopic (UV-vis) scale.[53] Finally, mixed precursor POEGMA hydrogels were prepared by mixing 4 precursors such that (1) an equal

weight ratio of low LCST ($PO_{10}H_{30}$ and $PO_{10}A_{30}$) and high LCST ($PO_{100}H_{30}$ and $PO_{100}A_{30}$) precursors was added to both the hydrazide and aldehyde barrels of the double barrel syringe (2) the aldehyde (PO_xA_{30}) and the complementary hydrazide (PO_xH_{30}) precursor solutions were both prepared at a total concentration of 150 mg/mL, maintaining an approximate 1:1 ratio between the aldehyde and hydrazide functional groups in the final hydrogel. Note that for the mixed hydrogels gelation may occur without significant cross-reaction between the PO_xH_{30} and PO_xA_{30} precursors of different $M(EO)_2MA$:$OEGMA_{475}$ composition. The PO(75/25), PO(50/50) and PO(25/75) mixed POEGMA hydrogels were prepared by mixing the low LCST and high LCST precursors in 75/25, 50/50 and 25/75 weight ratios (for example, the 75/25 wt% hydrogel was prepared by mixing 75 w/w% $PO_{10}H_{30}$ with 25 w/w% $PO_{100}H_{30}$ in the hydrazide barrel and 75 w/w% $PO_{10}A_{30}$ and 25 w/w% $PO_{100}A_{30}$ in the aldehyde barrel and co-extruding the mixture through the mixing channel). Note that the PO_{10} and PO_{100} single precursor hydrogels can be regarded as the 100/0 w/w% and 0/100 w/w% mixed precursor hydrogels in this labeling scheme and are labeled PO(0/100) and PO(100/0) in the remainder of this manuscript. Contrary to the single precursor hydrogels, the mixed precursor hydrogels are all opaque (even below their respective VPTTs), suggesting the presence of large inhomogeneities in the hydrogel morphology that were confirmed by light scattering (LS) experiments. Furthermore, SANS analysis showed that these mixed precursor hydrogels are significantly more heterogeneous than the single precursor hydrogels on a smaller light scattering length scale.[53]

Based on these results (and the detailed SANS and LS study reported earlier),[53] we envisage the microscopic structures of the various POEGMA hydrogels as schematically presented in Scheme 4.1. PO_{10}, PO_{55} and PO_{100} as well as the PO(L/H) and PO(H/L) hydrogels (all prepared with only one hydrazide and one aldehyde gelling pair) consist of largely homogeneous networks and contain no large microphase separated domains. In comparison, the mixed precursor hydrogels prepared with two gelling pairs contain phase separated domains, with an excess of low LCST precursor causing inhomogeneities of high VPTT domains in a low VPTT hydrogel matrix (PO(75/25)) and an excess of high LCST precursor creating low VPTT domains inside a high VPTT matrix (PO(25/75)); the PO(50/50) hydrogel presents an

intermediate morphology. This schematic representation of the mixed precursor hydrogels will be used to interpret and explain the experimental observations made in this manuscript.

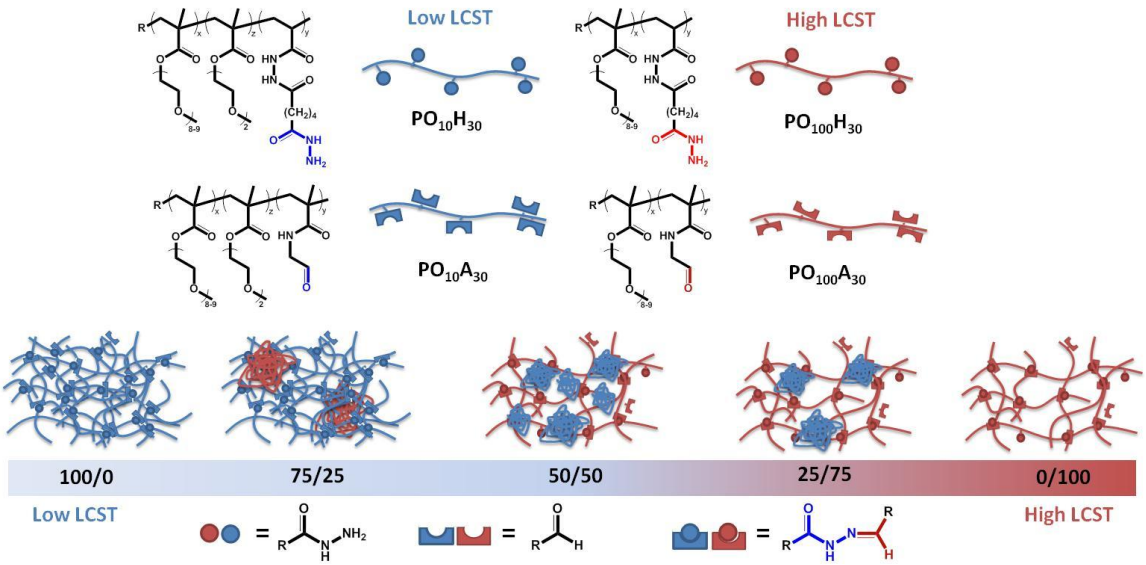

Scheme 4.1. Preparation and hypothesized internal morphologies of POEGMA hydrogels prepared by mixing precursor polymers with different phase transition temperatures

4.3.3 Physiochemical properties: The thermoresponsive swelling, rheology, and degradation properties of hydrogels prepared using both single and mixed precursor approaches are summarized in Table 4.3 and are discussed more specifically in the following sections.

4.3.3.1 Thermoresponsive swelling: POEGMA hydrogels were incubated in 10 mM PBS at 22°C and 37°C for 30 hours to monitor the swelling kinetics (Fig. 4.1). The PO(0/100) hydrogel (VPTT > 60°C, Table 4.3)[39] quickly adsorbs water, reaching a mass-based equilibrium swell ratio (Q_m) of 16.1±0.5 at 22°C and 13.5±0.1 at 37°C after 12 hours of incubation (a 16% decrease in volume upon heating). The PO(100/0) hydrogels have a VPTT close to physiological temperature (Table 4.3) and consequently swell less, reaching a Q_m of 7.2±0.1 at 22°C and 4.2±0.1 (at 37°C) after 30 hours of incubation; these results represent a 42% decrease in volume upon heating, clearly indicative of a VPTT. The mixed hydrogels show intermediate behavior, with Q_m decreasing in a linear fashion as the weight fraction of low LCST precursor is increased (Fig. 4.1 and Supporting Information Fig. S1, R^2 = 0.932 at 22°C and R^2 = 0.980 at 37°C). Of particular note, the PO(50/50)

hydrogel at 37°C shows only a marginal increase in water content during swelling, reaching a Q_m of 8.1±0.1 (compared to a Q_m = 7.7 upon preparation). Swelling kinetics of PO(50/50) analogue hydrogels revealed analogous results; PO(L/H), PO(H/L), and PO_{55} (all of which contain the same overall ratio of $M(EO)_2MA$:$OEGMA_{475}$ but distribute those monomers differently between the precursor chains) all exhibited near-zero swelling at 37°C relative to their preparation state, reaching equilibrium Q_m values of 8.0±0.2, 7.6±0.1 and 7.4±0.1, respectively (see Supporting Information, Fig. S4.2). These results suggest that hydrogels can be designed for space-filling applications in vivo (such as vitreous humor replacement, for which hydrogel swelling/de-swelling over time must be avoided to avoid glaucoma) by simple mixing of precursors, removing the need for extensive precursor synthesis.

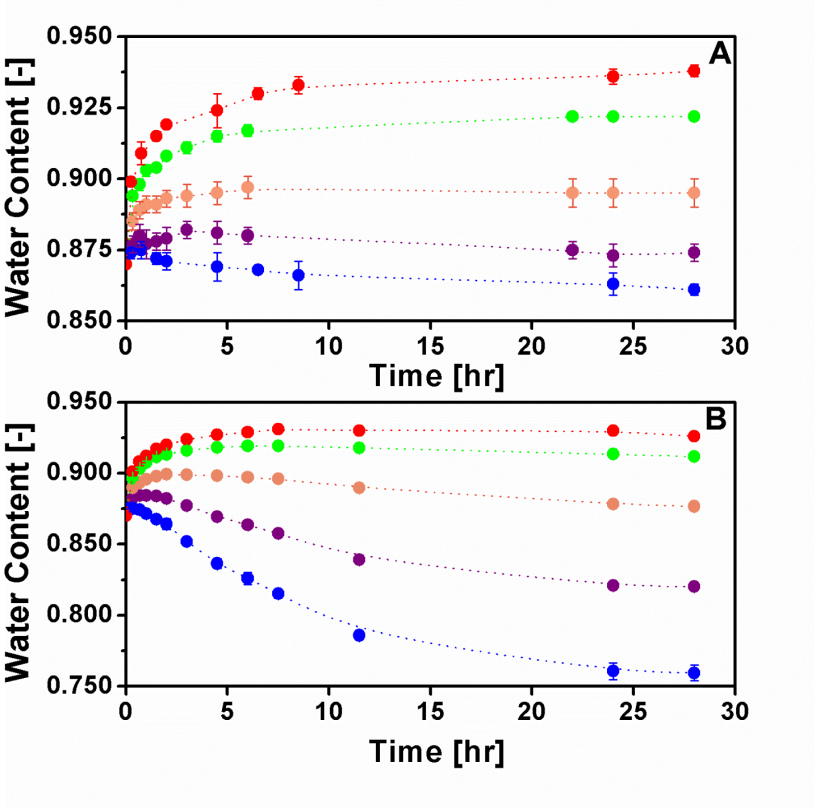

Figure 4.1. Swelling kinetics of POEGMA hydrogels in 10 mM PBS at (A) 22°C and (B) 37°C: (●, blue) PO(100/0); (●, purple) PO(75/25); (●, orange) PO(50/50); (●, green) PO(25/75) and (●, red) PO(0/100).

4.3.3.2 Rheological properties: The rheological properties and average elastic storage moduli (*G'*) of the fully swollen POEGMA hydrogels (pre-incubated for at least 12 hours in PBS prior to testing to ensure equilibrium swelling measurements) are shown in Fig. 4.2 and Supporting Information Fig. S4.3. Comparable to the equilibrium swelling results (Supporting Information Fig. 1), there is a linear decrease (R^2 = 0.984) in *G'* from the PO(100/0) hydrogel (8.25 ± 0.66 kPa) to the PO(0/100) hydrogel (1.63 ± 0.25 kPa), related to significant differences in the average cross-link density (*v*) in the hydrogels. As the weight fraction of low LCST precursors in the hydrogel is increased, *v* increases by almost one order of magnitude (see Table 4.3). Although the different precursor polymers are similar in terms of the average number of functional groups per chain (approximately 19±3 hydrazide and 18±2 aldehyde groups for each precursor), increased steric hindrance is observed as the mole fraction of $OEGMA_{475}$ (*n* = 8,9) increases, preventing some reactive groups from cross-linking. Of note, the presence of heterogeneous microscale hydrogel morphology (i.e. the distribution of the high and low transition temperature OEGMA comonomers between the component precursor chains) has no significant impact on the mechanical strength of the hydrogel, with *G'* observed to be directly correlated with the ratio of low LCST and high LCST comonomers used in the hydrogel formulation independent of their distribution (Supporting Information Fig. 4.4). This result suggests that it is the continuous network structure and not the network inhomogeneities that primarily govern the mechanical properties of the hydrogels.

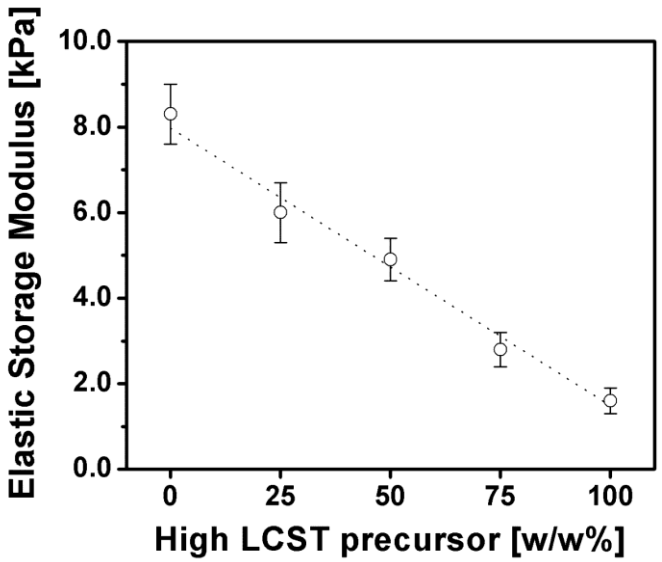

Figure 4.2. Average elastic storage moduli (*G*') of the fully swollen mixed precursor POEGMA hydrogels as a function of the weight fraction of high LCST precursor polymers used to prepare the hydrogels. Correlation: $G' = 7.97\pm0.33 - (0.065\pm0.004)x$; $R^2 = 0.984$.

4.3.3.3 Degradation: The hydrolytically cleavable hydrazone cross-link used to gel the polymers facilitates degradation of the hydrogels into their precursors over time, key for most in vivo applications. Hydrogels were incubated in 100 mM HCl at 37°C to monitor the relative degradation kinetics of the mixed precursor hydrogels (Fig. 4.3). The weakly cross-linked PO(0/100) hydrogel degrades rapidly and is fully degraded within 1 hour. The addition of 25 w/w% low LCST precursor (PO(25/75)) increases the overall cross-link density (Table 3) and delays complete degradation to approximately 2 hours, although the shape of the degradation curve is similar. However, increasing the weight fraction of low LCST precursor to > 25 w/w% induces a marked change in the degradation kinetics (Fig. 4.3). The PO(100/0) hydrogel is densely cross-linked and de-swells when incubated at 37°C in PBS (Fig. 4.1B), resulting in a weight loss of ~30% in the first 8 hours; incubation of this hydrogel in 100 mM HCl resulted in essentially the same mass change trend, suggesting that degradation is extremely slow for these hydrogels. In contrast, while the PO(50/50) and PO(75/25) hydrogels also deswelled at 37°C in PBS (albeit not to the same extent as the PO(100/0) hydrogel, Fig. 4.1B), in the presence of 100 mM HCl these hydrogels initially swell prior to the onset of macroscopic degradation (Fig. 4.3). We hypothesize that this degradation kinetic profile can be explained by the presence

of domains of high LCST precursors within PO(75/25) and PO(50/50) that degrade relatively rapidly (analogous to the PO(0/100) hydrogel), resulting in the observed initial swelling due to a decrease in local cross-link density within these domains. However, following this initial change, the remaining, more densely cross-linked domains rich in low LCST precursor polymer domains degrade significantly more slowly (analogous to the PO(100/0) hydrogel). These results suggest that degradation of the mixed precursor hydrogels depends on both the degree and type of phase separation that occurs as well as the overall cross-link density of the hydrogel. Of note, regardless of the relative degradation kinetics, all POEGMA hydrogels could be fully degraded upon longer acid exposure times into their original precursor polymers, which have previously been demonstrated to be non-cytotoxic in vitro (MTT assay) and well tolerated in vivo (subcutaneous injection in Balb/c mice).[39]

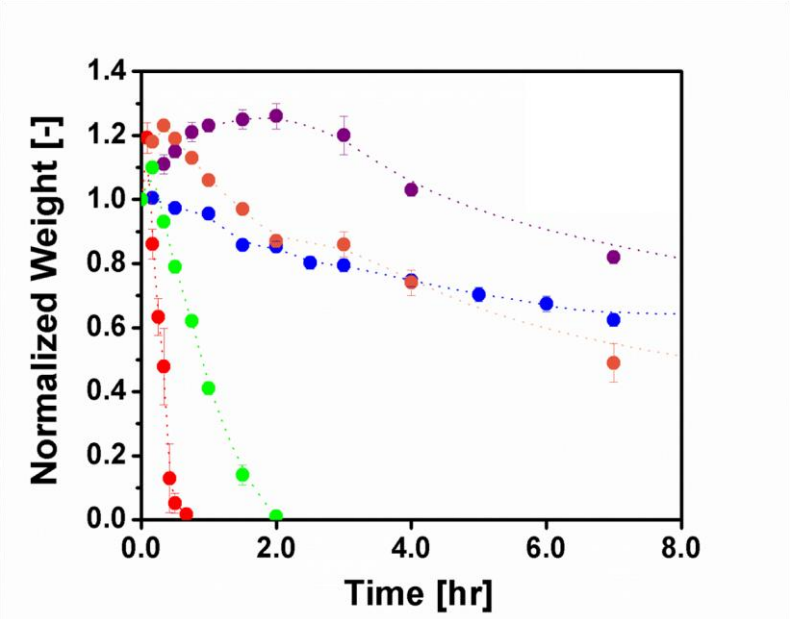

Figure 4.3. Degradation kinetics of single and mixed precursor POEGMA hydrogels at 37°C and 100 mM HCl: (●, blue) PO(100/0); (●, purple) PO(75/25); (●, orange) PO(50/50); (●, green) PO(25/75) and (●, red) PO(0/100).

Overall, on the macroscopic scale, the mixed precursor POEGMA hydrogels demonstrate intermediate Q_m and G' values similar to those predicted by the simple rule of mixtures (Figs. 4.1 and 4.2 and Supporting Information Fig. S4.1), relatively independently of the degree of phase separation observed. As such, provided transparency is not an issue, injectable hydrogels

with well-defined properties can be designed “off the shelf” by simple mixing of precursor polymers with different LCST, avoiding laborious polymerization steps each time a property change is required. Alternately, if transparency is critical to the proposed application, this modular mixing approach can be used to rapidly identify the $M(EO)_2MA$:$OEGMA_{475}$ composition required to achieve a particular degree of swelling but maintain transparency in the hydrogel, again avoiding the need for repetitive, trial-and-error polymer synthesis. As an example, the PO(50/50) mixed precursor hydrogel exhibited near-zero swelling as a function of time at physiological temperature (Fig. 4.1B) and has an opaque appearance at 37°C;[53] a corresponding injectable hydrogel prepared with 55 mol% $OEGMA_{475}$ precursors (identical to the overall monomer ratio in the PO(50/50) hydrogel) not only also exhibits near-zero swelling (Supporting Information Fig. S4.2) and very similar mechanical properties to PO(50/50) (Supporting Information Fig. S4.4), but maintains transparency (Supporting Information Fig. S4.5). Interestingly though, the phase separated microdomains do impose significant impacts on the degradation kinetics (Fig. 4.3), with high transition temperature domains locally degrading significantly faster than low transition temperature domains and thus significantly impacting the overall rate of degradation depending on the mass distribution within the hydrogel.

4.3.4 Pharmokinetic properties: The pharmokinetic properties of the single and mixed component hydrogels were assessed with regards to both their affinity and their capacity to load and release model proteins of different molecular weights and properties.

4.3.4.1 Protein affinity: The affinity of the various POEGMA hydrogels to proteins was evaluated using bovine serum albumin (BSA), fibrinogen (Fib) and immunoglobulin G (IgG) absorption assays (Fig. 4.4). These three proteins were selected due to their different isoelectric points (BSA ~4.7, fibrinogen ~5.1-6.3, and IgG ~6.4-9) and molecular weights (BSA ~66 kDa, IgG ~ 150 kDa, and fibrinogen ~340 kDa) that span the range of typical proteins of interest for therapeutic delivery.

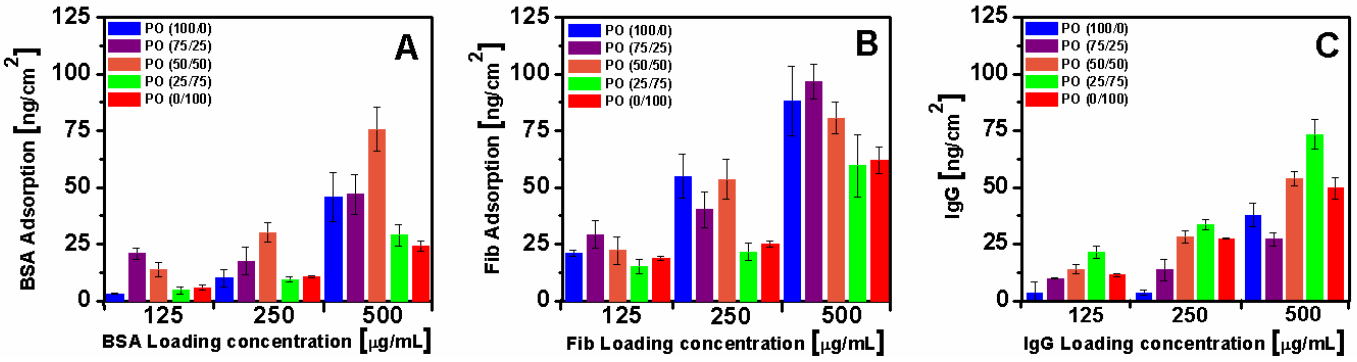

Figure 4.4. (A) Bovine serum albumin (BSA), (B) fibrinogen (Fib), and (C) immunoglobulin G (IgG) uptake (expressed as ng per cross-sectional area of hydrogel) to POEGMA hydrogels: (■, blue) PO(100/0); (■, purple) PO(75/25); (■, orange) PO(50/50); (■, green) PO(25/75) and (■, red) PO(0/100).

Although BSA, Fib, and IgG uptake all increase with increasing protein concentration in the loading solution, adsorption values for all single component hydrogels remain below 50 ng/cm^2 for BSA and IgG and 100 ng/cm^2 for Fib, comparable to the 10 to 100 ng/cm^2 range (depending on concentration of the loading solution) reported for protein adsorption to PEG-grafted surfaces.[56–58] Thus, the homogeneous hydrogels have low affinity to protein uptake analogous to PEG hydrogels that typically exhibit rapid protein release.[59,60] In comparison, BSA affinity to PO(50/50) is significantly higher than BSA affinity to either of the PO(100/0) and PO(0/100) hydrogels at all protein concentrations tested (p > 0.05, Fig. 4.4A), despite this hydrogel having an intermediate composition compared to the other two hydrogels. A similar but less extreme trend is observed for both fibrinogen (Fig. 4.4B), for which the PO(50/50) hydrogel exhibits the same protein affinity as the low-VPTT PO(100/0) hydrogel despite being (on an overall basis) significantly more hydrophilic, as well as IgG (Fig. 4.4C), which exhibits a clear absorption maximum at the PO(25/75) composition relative to the single component hydrogels. Since the PO(100/0) (all low LCST precursor) hydrogel exhibits significantly lower BSA adsorption than any of the mixed precursor hydrogels and BSA is well-known to interact with hydrophobic domains in hydrogels,[61] it is unlikely that this result is associated purely with the phase transition temperature of the hydrogels. We hypothesize that the increased protein affinity at these intermediate ratios may instead be attributable to the presence of

inhomogeneities at the hydrogel-water interface. Differences in cross-link density between the low LCST precursor-rich phase (higher cross-link density) and the high LCST precursor-rich phase (lower cross-link density) increase the interfacial roughness of the hydrogel, which has been reported to enhance protein uptake to metal surfaces[62,63] as well as a hyaluronic acid hydrogel modified with poly(L-lysine).[64] The PO(50/50) hydrogel is structurally the most inhomogeneous (consisting of 50/50 w/w% low LCST and high LCST precursors) and would, on this basis, support significantly more protein uptake than the other heterogeneous or homogeneous hydrogels, as primarily observed.

4.3.4.2 Protein release: Based on these non-linear protein affinity results, we hypothesized that hydrogel heterogeneity could prove advantageous for controlled release applications both in terms of facilitating potential drug partitioning into the heterogeneous phases as well as inducing potential changes in the effective diffusional path lengths as the cross-link density varies throughout the hydrogel. In order to test this hypothesis, fluorescein-labeled bovine serum albumin (BSA-FITC, MW = 67kDa, pI = 4.7, ellipsoid 14 x 4 x 4 nm^3) was loaded into the hydrogels by simple mixing of the proteins with the precursor polymers, facilitating entrapment of the proteins inside the gel during the gelation process. Protein release kinetics were assessed from both the two single precursor hydrogels (PO(100/0) and PO(0/100)) as well as the three mixed precursor hydrogels (PO(75/25), PO(50/50) and PO(25/75)) to evaluate whether the macroscopic properties or the microscopic morphology primarily governs protein release (Fig. 4.5A-B and Supporting Information Fig. S4.6). The hydrogels were prepared in two different ways: (*i*) the hydrogel precursors were extruded and gelled at 22°C, followed by incubation in 10 mM PBS at 37°C (Fig. 5A) or (*ii*) the hydrogel precursors were pre-incubated, extruded and gelled all at 37°C, followed by incubation in 10 mM PBS at 37°C (Fig. 4.5B).

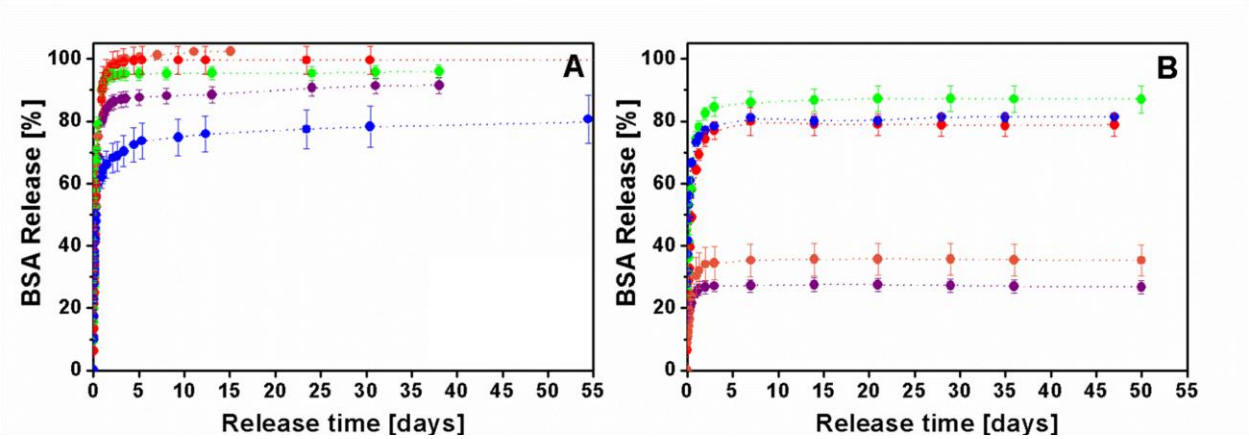

Figure 4.5. BSA release kinetics at 37°C for the POEGMA hydrogels prepared at (A) 22°C and (B) 37°C: (●, blue) PO(100/0); (●, purple) PO(75/25); (●, orange) PO(50/50); (●, green) PO(25/75) and (●, red) PO(0/100). See Supporting Information Fig. S4.6 for a zoom of the initial 12 hours of release.

For hydrogels prepared at 22°C, BSA release increases systematically with increasing weight fractions of high LCST precursor in the hydrogel formulation (Fig. 4.5A). The PO(100/0) hydrogel shows the slowest release, with 81.0±7.9% of protein released after 61 days, followed by the PO(75/25) hydrogel which releases 91.5±2.6% of loaded BSA after 38 days. The PO(50/50), PO(25/75) and PO(0/100) hydrogels all display very similar release rates and reach nearly complete release in 5 days. As such, BSA release from the heterogeneous hydrogels prepared at room temperature is governed by the macroscopic properties of the hydrogels, specifically the cross-link density and swelling kinetics of the respective hydrogels. Of note, similar trends are observed for fibrinogen (340 kDa, dimeric 47.5 x 6 x 9 nm^3) and IgG (~150 kDa, Y-shaped), although total release is lower at any time point for higher molecular weight proteins (Supporting Information, Figs. S4.7 and S4.8). The gap between the release observed with PO(100/0) and PO(0/100) is significantly smaller with IgG, consistent with the similar protein affinity observed between those two hydrogels at higher protein loadings such as those used here (Fig. 4.4C).

When the precursor polymers were pre-incubated and gelled at 37°C, the BSA release profile from the PO(100/0) (low VPTT) hydrogel was not significantly changed. In contrast, the release curve plateaus for the PO(0/100) (high VPTT) hydrogel was observed at a significantly

lower percentage release (78.5±3.5% compared to 99.5±4.4% for gelation at 22°C). Since the LCST values of all polymer precursors lie well above 37°C (the lowest is 53.6°C for $PO_{10}A_{30}$, Table 4.2), the precursor chains should be in a similar state of chain expansion in all cases at the onset of gelation. Instead, we speculate that this result can be attributed to the residual stresses present in the hydrogel network when the hydrogel precursors are pre-incubated at the same temperature as is used for the ultimate release experiment. When the precursors are extruded and gelled at 37°C, the hydrogels will be close to their equilibrium temperature (and thus equilibrium water content, Fig. 4.1) prior to incubation in the release medium for drug release (i.e. t = 0 of the kinetics experiment). The PO(100/0) hydrogel forms quickly (within several seconds) and collapses quickly (with significant deswelling occurring within tens of minutes) when incubated at 37°C; as such, the temperature of gel preparation (22°C versus 37°C) has little effect on the release kinetics (Fig. 4.5A and 4.5B) aside from slightly accelerating the burst release portion of the kinetic profile. In contrast, the PO(0/100) hydrogel gels more slowly (over tens of minutes as opposed to seconds) and swells relatively slowly (on the same time scale of protein release) such that the initial (gelation) conditions of the hydrogel more significantly impact release. Specifically, the slight thermal deswelling observed for PO(0/100) (~17% mass decrease between 22°C-37°C, Fig. 4.1) reduces the average pore size of the hydrogel throughout the release process for hydrogels prepared at 37°C, contributing to the somewhat lower plateau release value observed at 37°C.

In contrast, the mixed precursor hydrogel release behavior changes dramatically depending on whether gels are formed at 22°C or 37°C. Most notably, very slow release profiles with minimal burst release are observed for PO(75/25) and PO(50/50) when the hydrogels are prepared at 37°C (Fig. 4.5B). The differences in the BSA release profiles for the heterogeneous hydrogels as a function of the gelation temperature are likely governed by the degree of phase separation achieved prior to gelation and the resulting impact of that phase separation on the hydrogel morphology. SANS results suggested that the PO(25/75) hydrogel consists of (a relatively small fraction of) low VPTT domains contained within a high VPTT hydrogel matrix.[53] When the hydrogel is prepared at 22°C, the low VPTT domains will quickly collapse upon incubation at 37°C and expel any BSA contained in these phases by convective

mass transfer. Conversely, when the hydrogel is prepared at 37°C, these microdomains are already collapsed and will better retain the BSA entrapped in these phases. Consequently, BSA release from the PO(25/75) hydrogel plateaus at a somewhat lower release value relative to PO(0/100) (86.9±4.3% compared to 99.5±4.4%) but follows similar kinetics, as the more continuous high VPTT domain phase of the hydrogel is structurally similar in both cases.

For the mixed precursor hydrogels prepared with higher fractions of low LCST precursors, the hydrogel structure would consist of a mixture of domains throughout (PO(50/50)) or predominantly high VPTT domains within a low VPTT matrix (PO(75/25)), depending on the relative mole fractions of high and low LCST precursors used to prepare each hydrogel. When gelation is performed at 22°C (< VPTT of both phase-separated domains), a significant burst release is observed for both PO(75/25) and PO(50/50) hydrogels following incubation at 37°C and the hydrogels deswell, releasing 91.4±2.1% and 99.5±1.1% respectively over 30 days due to the local collapse and thus convective transport of protein out of the low VPTT domains. However, when gelled at 37°C (> VPTT of the low VPTT domains), the low VPTT domains are already largely formed and collapsed either prior to or during the gelation process rather than at the incubation step; as a result, both PO(75/25) and PO(50/50) hydrogels facilitate significantly enhanced entrapment of BSA and significantly lower plateau release values (26.9±2.1% and 35.4±5.0% for PO(75/25) and PO(50/50) respectively) relative to the other hydrogels tested. We hypothesize that the larger fraction of high VPTT domains in PO(50/50) drives the slightly higher burst release observed in this hydrogel relative to PO(75/25). Considered together, these results suggest that significant modifications in drug release kinetics can be achieved by preparing hydrogels using precursor polymers with different phase transition temperatures or using the same precursor polymers gelled at different temperatures, providing a facile modular, mix-and-match approach to “dialing in” specific protein release kinetics of interest based on a minimal number of precursor polymers.

4.3.5 Biological Properties: We have previously shown that none of the precursor polymers used herein are significantly cytotoxic to 3T3 mouse fibroblast cells[17]. Here, based on the significantly different protein affinity results observed depending on phase separation, we

investigated the potential for adhesion of 3T3 fibroblasts to the single and mixed precursor hydrogels (Fig. 4.6).

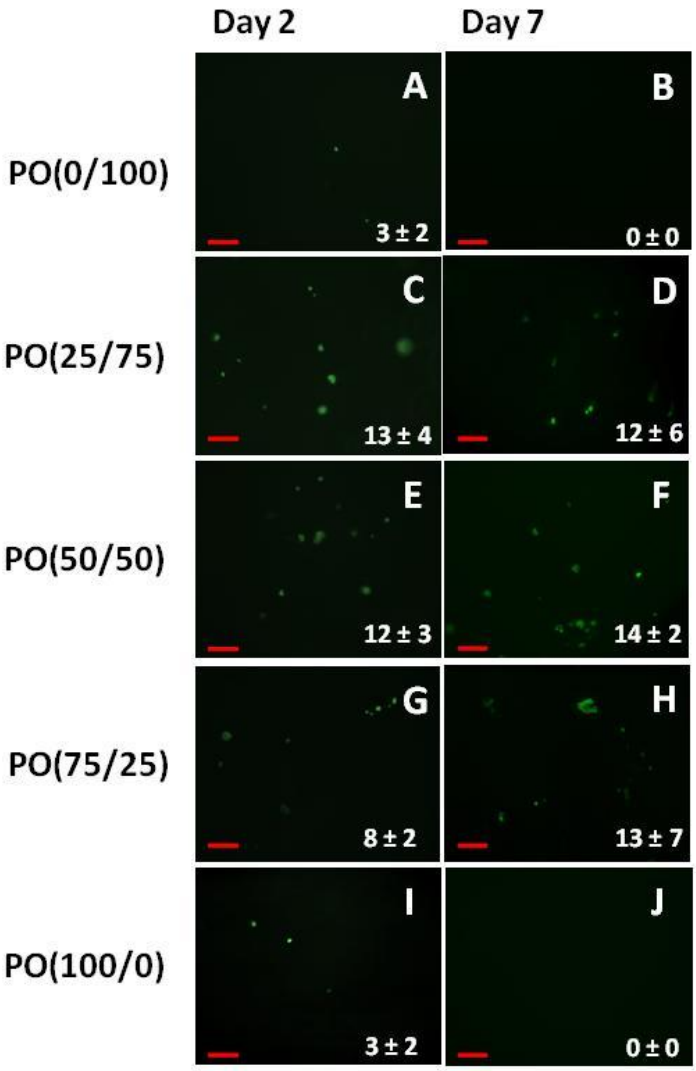

Figure 4.6. 3T3 fibroblast cell adhesion to POEGMA hydrogels after 2 days ((A) PO(0/100); (C) PO(25/75); (E) PO(50/50); (G) PO(75/25); (I) PO(100/0)) and 7 days ((B) PO(0/100); (D) PO(25/75); (F) PO(50/50); (H) PO(75/25); (J) PO(100/0)). Numbers of adhered, viable cells per/cm^2 measured at each time point (n = 4) are given on each graph. Scale bars measure 100µm.

At shorter time points (2 days), the increased protein affinity to the mixed precursor hydrogels (Fig. 4.4) was echoed by a small but statistically significant increase in cell adhesion to the hydrogels, with 13 ± 4 cells/cm^2 adsorbed to PO(25/75), 12 ± 3 cells/cm^2 area adsorbed to PO(50/50), and 8 ± 2 cells/cm^2 adsorbed to PO(75/25) compared to 3 ± 2 cells/cm^2 area for PO(100/0) and 3 ± 2 cells/cm^2 for PO(0/100). By day 7 following addition of the cells to the hydrogels, this trend of increased cell adhesion to the mixed precursor gels is still observed, although the cell numbers adhered to each gel do not significantly change from day 2 ($p > 0.05$ for each mixed precursor gel). This result indicates that these mixed precursor hydrogels are not effective for promoting cell proliferation but can support limited cell adhesion; in contrast, no cells whatsoever were observed on either the PO(100/0) or PO(0/100) gels after seven days of incubation. Thus, analogous to the protein absorption results, the presence of phase-separated microdomains in the mixed precursor hydrogels significantly enhances cell adhesion relative to more homogeneous hydrogels prepared from either of the two single phases comprising the phase separated gels. As with the protein absorption results, we hypothesize that increased mechanical roughness of phase separated gels on the length scale of cells and/or cellular binding domains can account for these differences. However, it must be emphasized that the number of cells adhered to the mixed precursor hydrogels remains orders of magnitude lower than that observed on tissue culture polystyrene (790 ± 170 cells/cm^2 on day 2 and 1150 ± 15 cells/cm^2 on day 7). Thus, from an in vivo application perspective, the mixed precursor hydrogels support significantly enhanced protein affinity (Fig. 4.4) and significantly prolonged protein release kinetics (Fig. 4.5) while still largely resisting cell adhesion, which is typically associated with lower inflammatory responses in vivo.[65]

4.4. Conclusions

By preparing injectable hydrogels using mixtures of POEGMA precursors with high and low LCST values, the properties of the hydrogels can be tuned on multiple length scales to be appropriate for different biomedical applications. Macroscopically, in terms of swelling kinetics/equilibria or hydrogel mechanics, hydrogels can be produced with intermediate properties that are largely predictable using the simple rule of mixtures based on the properties

of hydrogels prepared with the constituent polymers alone. In contrast, on a microscopic scale, the observed phase separation of the high and low LCST precursor polymers into domains results in significant changes in degradation kinetics, protein affinity, and drug release kinetics, according to the relative ratios of the high and low LCST precursors used as well as the temperature at which those precursors are gelled. Specifically, from an applications perspective, significant increases in protein affinity and decreases in burst protein release are observed when high and low LCST precursor polymers are mixed together, all while minimally changing the nature of cell-hydrogel interactions with the materials. Alternately, mixing different LCST precursors together in different ratios can be used to readily identify the composition of a single precursor composition that will have the same macroscopic properties (swelling response, mechanics) but will maintain transparency. Together, we believe these results demonstrate the utility of a "modular" approach to hydrogel design in which a very limited number of precursor polymers (in this case, 4) can achieve a wide variety of hydrogel properties depending on the ratios at which they are mixed and the temperatures at which they are gelled. This approach both avoids the need to synthesize new precursor for different application criteria and/or costly and time-consuming trial-and-error synthesis to prepare hydrogels with specific targeted properties, in addition to facilitating the expression of new hydrogel properties not achievable with either of the precursor polymers alone.

4.4.1 Supporting information: Swelling kinetics and mechanical data for the PO(50/50) analogue hydrogels, rheological data, VPTT of the POEGMA hydrogels as measured by UV-vis spectrophotometry, optical transparency data, and protein release kinetics for BSA, Fib and IgG are provided.

4.5 Acknowledgements

Funding from 20/20: NSERC Ophthalmic Materials Research Network, the Ontario Ministry of Research and Innovation Postdoctoral Fellowship program (NMBS), and NSERC CREATE-IDEM (Integrated Design of Extracellular Matrices) (EB) is gratefully acknowledged.

4.6 References

(1) Hernández, R. M. A.; Orive, G.; Murua, A.; Pedraz, J. L. Microcapsules and Microcarriers for in Situ Cell Delivery. *Adv. Drug Deliv. Rev.* **2010**, *62*, 711–730.

(2) Jiang, X.-J.; Wang, T.; Li, X.-Y.; Wu, D.-Q.; Zheng, Z.-B.; Zhang, J.-F.; Chen, J.-L.; Peng, B.; Jiang, H.; Huang, C.; et al. Injection of a Novel Synthetic Hydrogel Preserves Left Ventricle Function after Myocardial Infarction. *J. Biomed. Mater. Res. A* **2009**, *90*, 472–477.

(3) Lutolf, M. P.; Lauer-Fields, J. L.; Schmoekel, H. G.; Metters, A. T.; Weber, F. E.; Fields, G. B.; Hubbell, J. A. Synthetic Matrix Metalloproteinase-Sensitive Hydrogels for the Conduction of Tissue Regeneration: Engineering Cell-Invasion Characteristics. *Proc. Natl. Acad. Sci. U. S. A.* **2003**, *100*, 5413–5418.

(4) Lutolf, M. P.; Hubbell, J. A. Synthetic Biomaterials as Instructive Extracellular Microenvironments for Morphogenesis in Tissue Engineering. *Nat. Biotechnol.* **2005**, *23*, 47–55.

(5) Zhu, J. Bioactive Modification of Poly(ethylene glycol) Hydrogels for Tissue Engineering. *Biomaterials* **2010**, *31*, 4639–4656.

(6) Boateng, J. S.; Matthews, K. H.; Stevens, H. N. E.; Eccleston, G. M. Wound Healing Dressings and Drug Delivery Systems: A Review. *J. Pharm. Sci.* **2008**, *97*, 2892–2923.

(7) Janson, I. A.; Putnam, A. J. Extracellular Matrix Elasticity and Topography: Material-Based Cues That Affect Cell Function via Conserved Mechanisms. *J. Biomed. Mater. Res. A* **2014**, 1–13.

(8) Lavik, E. B.; Klassen, H.; Warfvinge, K.; Langer, R.; Young, M. J. Fabrication of Degradable Polymer Scaffolds to Direct the Integration and Differentiation of Retinal Progenitors. *Biomaterials* **2005**, *26*, 3187–3196.

(9) Kloxin, A. M.; Kasko, A. M.; Salinas, C. N.; Anseth, K. S. Photodegradable Hydrogels for Dynamic Tuning of Physical and Chemical Properties. *Science* **2009**, *324*, 59–63.

(10) Aimetti, A. A.; Machen, A. J.; Anseth, K. S. Poly(ethylene glycol) Hydrogels Formed by Thiol-Ene Photopolymerization for Enzyme-Responsive Protein Delivery. *Biomaterials* **2009**, *30*, 6048–6054.

(11) Ghezzi, C. E.; Marelli, B.; Donelli, I.; Alessandrino, A.; Freddi, G.; Nazhat, S. N. The Role of Physiological Mechanical Cues on Mesenchymal Stem Cell Differentiation in an Airway Tract-like Dense Collagen-Silk Fibroin Construct. *Biomaterials* **2014**, *35*, 6236–6247.

(12) Godier-Furnémont, A. F. G.; Martens, T. P.; Koeckert, M. S.; Wan, L.; Parks, J. Composite Scaffold Provides a Cell Delivery Platform for Cardiovascular Repair. *Proc. Natl. Acad. Sci.* **2011**, *108*, 7974–7979.

(13) Vercruysse, K. P.; Marecak, D. M.; Marecek, J. F.; Prestwich, G. D. Synthesis and in Vitro Degradation of New Polyvalent Hydrazide Cross-Linked Hydrogels of Hyaluronic Acid. *Bioconjug. Chem.* **2000**, *8*, 686–694.

(14) Venkatesan, J.; Bhatnagar, I.; Manivasagan, P.; Kang, K.-H.; Kim, S.-K. Alginate Composites for Bone Tissue Engineering: A Review. *Int. J. Biol. Macromol.* **2014**, 1–13.

(15) Lee, K. Y.; Mooney, D. J. Alginate: Properties and Biomedical Applications. *Prog. Polym. Sci.* **2012**, *37*, 106–126.

(16) Shoichet, M. S.; Li, R. H.; White, M. L.; Winn, S. R. Stability of Hydrogels Used in Cell Encapsulation: An In Vitro Comparison of Alginate and Agarose. **1996**, *50*, 374–381.

(17) Lévesque, S. G.; Shoichet, M. S. Synthesis of Cell-Adhesive Dextran Hydrogels and Macroporous Scaffolds. *Biomaterials* **2006**, *27*, 5277–5285.

(18) Liu, Y.; Chan-Park, M. B. A Biomimetic Hydrogel Based on Methacrylated Dextran-Graft-Lysine and Gelatin for 3D Smooth Muscle Cell Culture. *Biomaterials* **2010**, *31*, 1158–1170.

(19) Coviello, T.; Matricardi, P.; Marianecci, C.; Alhaique, F. Polysaccharide Hydrogels for Modified Release Formulations. *J. Control. Release* **2007**, *119*, 5–24.

(20) Jiang, X.; Bai, J.; Gittens, S. A.; Uludağ, H. Growth of Bone Marrow Stromal Cells on RGD-Grafted Thermoreversible (NiPAM) Polymers. *Materwiss. Werksttech.* **2006**, *37*, 462–468.

(21) Lee, S.-W.; Tettey, K. E.; Kim, I. L.; Burdick, J. A.; Lee, D. Controlling the Cell-Adhesion Properties of Poly(acrylic acid)/Polyacrylamide Hydrogen-Bonded Multilayers. *Macromolecules* **2012**, *45*, 6120–6126.

(22) Fairbanks, B. D.; Schwartz, M. P.; Halevi, A. E.; Nuttelman, C. R.; Bowman, C. N.; Anseth, K. S. A Versatile Synthetic Extracellular Matrix Mimic via Thiol-Norbornene Photopolymerization. *Adv. Mater.* **2009**, *21*, 5005–5010.

(23) Jiang, Y.; Chen, J.; Deng, C.; Suuronen, E. J.; Zhong, Z. Click Hydrogels, Microgels and Nanogels: Emerging Platforms for Drug Delivery and Tissue Engineering. *Biomaterials* **2014**, *35*, 4969–4985.

(24) Pasut, G.; Veronese, F. M. State of the Art in PEGylation: The Great Versatility Achieved after Forty Years of Research. *J. Control. Release* **2012**, *161*, 461–472.

(25) Bhadra, D.; Bhadra, S.; Jain, P.; Jain, N. K. Pegnology: A Review of PEG-Ylated Systems. *Pharmazie* **2002**, *57*, 5–29.

(26) Knop, K.; Hoogenboom, R.; Fischer, D.; Schubert, U. S. Poly(ethylene glycol) in Drug Delivery: Pros and Cons as Well as Potential Alternatives. *Angew. Chem. Int. Ed. Engl.* **2010**, *49*, 6288–6308.

(27) Monfardini, C.; Veronese, F. M. Stabilization of Substances in Circulation. *Bioconjug. Chem.* **1998**, *9*, 418–450.

(28) Jokerst, J. V.; Lobovkina, T.; Zare, R. N.; Gambhir, S. S. Nanoparticle PEGylation for Imaging and Therapy. *Nanomedicine* **2011**, *6*, 715–728.

(29) Lin, C.-C.; Anseth, K. S. PEG Hydrogels for the Controlled Release of Biomolecules in Regenerative Medicine. *Pharm. Res.* **2009**, *26*, 631–643.

(30) Lee, K. Y.; Mooney, D. J. Hydrogels for Tissue Engineering. *Chem. Rev.* **2001**, *101*, 1869–1880.

(31) Slaughter, B. V; Khurshid, S. S.; Fisher, O. Z.; Khademhosseini, A.; Peppas, N. A. Hydrogels in Regenerative Medicine. *Adv. Mater.* **2009**, *21*, 3307–3329.

(32) Nuttelman, C. R.; Rice, M. A.; Rydholm, A. E.; Salinas, C. N.; Shah, D. N.; Anseth, K. S. Macromolecular Monomers for the Synthesis of Hydrogel Niches and Their Application in Cell Encapsulation and Tissue Engineering. *Prog. Polym. Sci.* **2008**, *33*, 167–179.

(33) McCall, J. D.; Anseth, K. S. Thiol-Ene Photopolymerizations Provide a Facile Method to Encapsulate Proteins and Maintain Their Bioactivity. *Biomacromolecules* **2012**, *13*, 2410–2417.

(34) Lutolf, M. P.; Hubbell, J. A. Synthesis and Physicochemical Characterization of End-Linked Poly(ethylene glycol)-Co-Peptide Hydrogels Formed by Michael-Type Addition. *Biomacromolecules* **2003**, *4*, 713–722.

(35) Grover, G. N.; Lam, J.; Nguyen, T. H.; Segura, T.; Maynard, H. D. Biocompatible Hydrogels by Oxime Click Chemistry. *Biomacromolecules* **2012**, *13*, 3013–3017.

(36) Cengiz, N.; Rao, J.; Sanyal, A.; Khan, A. Designing Functionalizable Hydrogels through Thiol-Epoxy Coupling Chemistry. *Chem. Commun.* **2013**, *49*, 11191–11193.

(37) Missirlis, D.; Spatz, J. Combined Effects of PEG Hydrogel Elasticity and Cell-Adhesive Coating on Fibroblast Adhesion and Persistent Migration. *Biomacromolecules* **2014**, *15*, 195–205.

(38) Smeets, N. M. B.; Bakaic, E.; Patenaude, M.; Hoare, T. Injectable and Tunable Poly(ethylene Glycol) Analogue Hydrogels Based on Poly(oligoethylene Glycol Methacrylate). *Chem. Commun.* **2014**, *50*, 3306–3309.

(39) Smeets, N. M. B.; Bakaic, E.; Patenaude, M.; Hoare, T. Injectable Poly(oligoethylene Glycol Methacrylate)-Based Hydrogels with Tunable Phase Transition Behaviours: Physicochemical and Biological Responses. *Acta Biomater.* **2014**, *10*, 4143–4155.

(40) Patenaude, M.; Hoare, T. Injectable, Degradable Thermoresponsive Poly(N -Isopropylacrylamide) Hydrogels. *ACS Macro Lett.* **2012**, *1*, 409–413.

(41) Patenaude, M.; Hoare, T. Injectable, Mixed Natural-Synthetic Polymer Hydrogels with Modular Properties. *Biomacromolecules* **2012**, *13*, 369–378.

(42) Ito, T.; Yeo, Y.; Highley, C. B.; Bellas, E.; Kohane, D. S. Dextran-Based in Situ Cross-Linked Injectable Hydrogels to Prevent Peritoneal Adhesions. *Biomaterials* **2007**, *28*, 3418–3426.

(43) Alves, M. H.; Young, C. J.; Bozzetto, K.; Poole-Warren, L. A.; Martens, P. J. Degradable, Click Poly(vinyl Alcohol) Hydrogels: Characterization of Degradation and Cellular Compatibility. *Biomed. Mater.* **2012**, *7*, 024106.

(44) Ossipov, D. A.; Hilborn, J. Poly(vinyl Alcohol)-Based Hydrogels Formed by "Click Chemistry."*Macromolecules* **2006**, *39*, 1709–1718.

(45) Oommen, O. P.; Wang, S.; Kisiel, M.; Sloff, M.; Hilborn, J.; Varghese, O. P. Smart Design of Stable Extracellular Matrix Mimetic Hydrogel: Synthesis, Characterization, and In Vitro and In Vivo Evaluation for Tissue Engineering. *Adv. Funct. Mater.* **2013**, *23*, 1273–1280.

(46) Hudson, S. P.; Langer, R.; Fink, G. R.; Kohane, D. S. Injectable in Situ Cross-Linking Hydrogels for Local Antifungal Therapy. *Biomaterials* **2010**, *31*, 1444–1452.

(47) Lee, K. Y.; Bouhadir, K. H.; Mooney, D. J. Degradation Behavior of Covalently Cross-Linked Poly(aldehyde Guluronate) Hydrogels. *Macromolecules* **2000**, *33*, 97–101.

(48) Lutz, J.-F. Polymerization of Oligo(ethylene Glycol) (meth)acrylates: Toward New Generations of Smart Biocompatible Materials. *J. Polym. Sci. Part A Polym. Chem.* **2008**, *46*, 3459–3470.

(49) Lutz, J.-F.; Weichenhan, K.; Akdemir, Ö.; Hoth, A. About the Phase Transitions in Aqueous Solutions of Thermoresponsive Copolymers and Hydrogels Based on 2-(2-Methoxyethoxy)ethyl Methacrylate and Oligo(ethylene Glycol) Methacrylate. *Macromolecules* **2007**, *40*, 2503–2508.

(50) Smeets, N. M. B.; Bakaic, E.; Patenaude, M.; Hoare, T. Probing the Internal Morphology of Injectable Poly(oligoethylene Glycol Methacrylate) Hydrogels by Light and Small-Angle Neutron Scattering. *Macromolecules* **2014**, *47*, 6017–6027.

(51) Sivakumaran, D.; Maitland, D.; Hoare, T. Injectable Microgel-Hydrogel Composites for Prolonged Small-Molecule Drug Delivery. *Biomacromolecules* **2011**, *12*, 4112–4120.

(52) Campbell, S. B.; Patenaude, M.; Hoare, T. Injectable Superparamagnets: Highly Elastic and Degradable poly(N-Isopropylacrylamide)-Superparamagnetic Iron Oxide Nanoparticle (SPION) Composite Hydrogels. *Biomacromolecules* **2013**, *14*, 644–653.

(53) Smeets, N. M. B.; Bakaic, E.; Yavitt, F. M.; Yang, F.-C.; Rheinstädter, M. C.; Hoare, T. Probing the Internal Morphology of Injectable Poly(oligoethylene Glycol Methacrylate) Hydrogels by Light and Small-Angle Neutron Scattering. *Macromolecules* **2014**, *47*, 6017–6027.

(54) Schwall, C. T.; Banerjee, I. A. Micro- and Nanoscale Hydrogel Systems for Drug Delivery and Tissue Engineering. *Materials* **2009**, *2*, 577–612.

(55) Kim, Y.; Abuelfilat, A.Y.; Hoo, S. P.; Al-Abboodi, A.; Liu, B.; Ng, T.; Chan, P.; Fu, J. Tuning the Surface Properties of Hydrogel at the Nanoscale with Focused Ion Irradiation. *Soft Matter* **2014**, *10*, 8448–8456.

(56) Hou, Y.; Schoener, C. A.; Regan, K. R.; Munoz-pinto, D.; Mariah, S.; Grunlan, M. A. Photo-Crosslinked PDMSstar-PEG Hydrogels: Synthesis, Characterization, and Potential Application for Tissue Engineering Scaffolds. *Biomacromolecules* **2010**, *11*, 648–656.

(57) Unsworth, L. D.; Sheardown, H.; Brash, J. L. Protein Resistance of Surfaces Prepared by Sorption of End-Thiolated Poly(ethylene glycol) to Gold: Effect of Surface Chain Density. *Langmuir* **2005**, *21*, 1036–1041.

(58) Du, H.; Chandaroy, P.; Hui, S. W. Grafted Poly-(ethylene glycol) on Lipid Surfaces Inhibits Protein Adsorption and Cell Adhesion. *Biochim. Biophys. Acta - Biomembr.* **1997**, *1326*, 236–248.

(59) Weber, L. M.; Lopez, C. G.; Anseth, K. S. Effects of PEG Hydrogel Crosslinking Density on Protein Diffusion and Encapsulated Islet Survival and Function. *J. Biomed. Mater. Res. A* **2009**, *90*, 720–729.

(60) Peppas, N. A.; Keys, K. B.; Torres-Lugo, M.; Lowman, A. M. Poly(ethylene Glycol)-Containing Hydrogels in Drug Delivery. *J. Control. Release* **1999**, *62*, 81–87.

(61) Smeets, N. M. B.; Patenaude, M.; Kinio, D.; Yavitt, F. M.; Bakaic, E.; Yang, F.-C.; Rheinstädter, M.; Hoare, T. Injectable Hydrogels with in Situ-Forming Hydrophobic Domains: Oligo(D , L -Lactide) Modified Poly(oligoethylene Glycol Methacrylate) Hydrogels. *Polym. Chem.* **2014**, *5*, 6811–6823.

(62) Scopelliti, P. E.; Borgonovo, A.; Indrieri, M.; Giorgetti, L.; Bongiorno, G.; Carbone, R.; Podestà, A.; Milani, P. The Effect of Surface Nanometre-Scale Morphology on Protein Adsorption. *PLoS One* **2010**, *5*, e11862.

(63) Rechendorff, K.; Hovgaard, M. B.; Foss, M.; Zhdanov, V. P.; Besenbacher, F. Enhancement of Protein Adsorption Induced by Surface Roughness. *Langmuir* **2006**, *22*, 10885–10888.

(64) Yamanlar, S.; Sant, S.; Boudou, T.; Picart, C.; Khademhosseini, A. Surface Functionalization of Hyaluronic Acid Hydrogels by Polyelectrolyte Multilayer Films. *Biomaterials* **2011**, *32*, 5590–5599.

(65) Anderson, J.; Rodriguez, A.; Chang, D. Foreign Body Reaction to Biomaterials. **2009**, *20*, 86–100.

4.7 Table of contents image

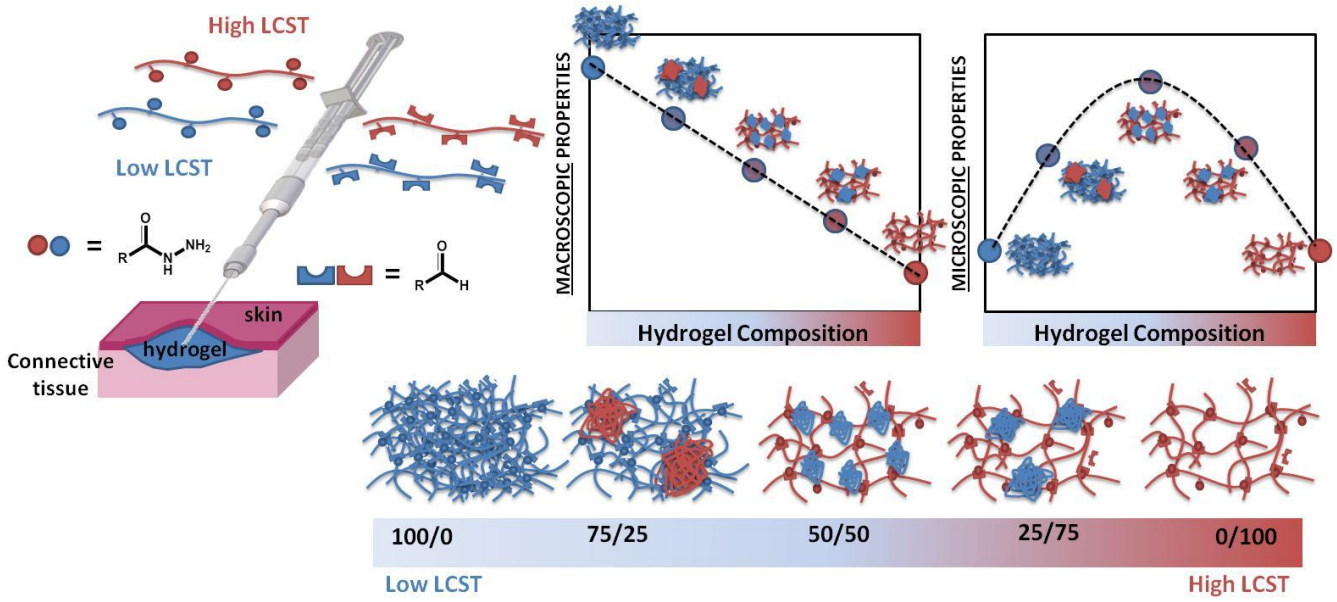

Mixing poly(oligoethylene glycol methacrylate) (POEGMA) precursor polymers with different lower critical solution temperatures leads to linear changes in macroscopic gel properties (e.g. mechanics, swelling) but non-linear changes in properties dependent on gel microstructure (e.g. transparency, protein adsorption, cell adhesion, drug release). Hydrogels with desired properties can be formed a priori by simple mixing of a limited number (4) of precursor polymers.

Chapter 5: pH-Ionizable *In situ*-Gelling Poly(Oligo ethylene glycol methacrylate)-Based Hydrogels: The Role of Internal Network Structures in Controlling Macroscopic Properties

Preface:

This chapter describes the design of POEGMA precursor polymers containing either *N,N*-dimethylaminoethyl methacrylate (DMAEMA) or acrylic acid (AA) to produce cationic and anionic charged polymers respectively. By mixing the charged precursors in different combinations, we create four charged POEGMA hydrogels; cationic, amphoteric, anionic and neutral. In this chapter, we show the potential to leverage our capacity to precisely control hydrogel charge content in this manner to create injectable and degradable POEGMA hydrogels with highly tunable physicochemical properties. Furthermore, to better understand the mechanistic and structural reasons behind the effects of ionic functional groups on the gel properties, we use isothermal titration calorimetry (ITC) and small angle neutron scattering (SANS) to investigate intermolecular interactions within the gel.

Emilia Bakaic[1], Niels M.B. Smeets[1], Owen Barrigar[1], Richard Alsop[2], Maikel C. Rheinstädter[2] and Todd Hoare[1]*

[1]*Department of Chemical Engineering, McMaster University, 1280 Main Street West, Hamilton, Ontario, Canada L8S 4L8.*

[2]*Department of Physics and Astronomy, McMaster University, 1280 Main Street West, Hamilton, Ontario, Canada L8S 4M1.*

Keywords

Hydrogels, charge density, small angle neutron scattering, poly(oligoethylene glycol methacrylate), structure-property correlation.

Abstract

The incorporation of charge within *in situ* covalently gelling poly(oligoethylene glycol methacrylate) (POEGMA) precursor polymers enables the fabrication of hydrogels that exhibit both pH-responsive swelling as well as tunable network structures due to multi-mechanism crosslinking interactions. The gelation times, swelling responses, degradation kinetics, and mechanics of the resulting gels were strongly influenced by both the type of charge(s) incorporated and pH, with both amphoteric gels and anionic gels showing clear evidence of dual network formation. While the amphoteric dual network was anticipated due to charge interactions, the mechanism of the five-fold enhancement in mechanical properties observed with the anionic gel relative to the neutral gel was revealed by isothermal titration calorimetry and small angle neutron scattering to relate to the formation of a zippered chain structure based on dipole-dipole interactions. Consequently, rational design of the chemistry and the microscopic network structure results in controllable macroscopic properties amenable to potential biomedical applications.

Introduction

Poly(ethylene glycol) (PEG)-based hydrogels have been widely used as biologically relevant mimics of native human tissues given their inherently high water contents and anti-fouling properties that are highly relevant to both therapeutic delivery and tissue engineering applications.[1–3] Despite the widespread use of PEG-based hydrogels as biomedical scaffolds, their chemistry is inherently limited given the step-growth mechanism of polymerization that effectively constrains the presence of reactive functional groups for both crosslinking and gel functionalization at the chain ends.[4,5] We,[6–8] and others,[9–11] have recently explored the use of poly(oligo ethylene glycol methacrylate) (POEGMA) hydrogels as a PEG hydrogel mimic that can exhibit the same general favorable properties of PEG hydrogels while exploiting the chain growth mechanism of OEGMA polymerization (and thus facile capacity for copolymerization) to enable polymer functionalization. Our particular interest lies in the design of in situ-gelling POEGMA hydrogels prepared by simple mixing of hydrazide and aldehyde-functionalized gel precursor polymers.[6] In this context, copolymerization of functional comonomers has been demonstrated to enable precise control over the density of reactive functional groups for covalent crosslinking,[12] hydrophobic grafts to induce physical crosslinking,[13] biological ligands to direct cell behavior,[12] and other types of functional groups. Furthermore, the capacity of POEGMA to exhibit both PEG-like properties as well as thermoresponsive properties (tunable based on the number of ethylene oxide repeat units on the polymer backbone)[10] opens up a new set of potential applications of POEGMA hydrogels, including reversible cell binding-delamination[7] and mixing-based introduction of heterogeneous domains within hydrogels due to thermally-induced phase separation on the same time scale as to enable regulation of drug release.[6,7]

Aside from the hydrophobic or covalent crosslinking strategies previously applied to modify in situ-gelling POEGMA hydrogels, inclusion of charge is also interesting in several contexts. From an application perspective, introducing pH-responsive charges within the polymer matrix can promote prolonged drug release by electrostatically enhancing drug-polymer interactions and/or environmentally-responsive drug delivery in targeted pH environments that drive gel swelling (to reduce diffusion resistance to drug release) and/or

switch the charge-based affinity between the drug and the gel on and off.[14–16] Similarly, from a tissue engineering or cell scaffolding perspective, charged hydrogels have been noted to alter cell adhesion properties (again, potentially in a pH-dependent manner) and/or introduce antibacterial properties into hydrogels,[16] although higher cationic charge in particular have been correlated with high protein adsorption and thus upregulated inflammatory reactions in vivo.[17] Alternately, if both pH-responsive cationic and anionic charges are present in the gel network (i.e. amphoteric hydrogels), ionic crosslinks can form that can be reversed to drive gel swelling in targeted biological environments according to the pK_a values of the respective charged groups.[18,19] In addition, given the mixing-based gelation approach used for the design of in situ-gelling POEGMA hydrogels, charge interactions may also induce the formation of physical heterogeneities (i.e. microdomains) within the gel network either prior to or on the same timescale as covalent gelation, potentially creating domains with defined charge densities within a bulk hydrogel matrix. Such charge-driven phase separation has been observed in poly(N-isopropylacrylamide-co-acrylic acid) (NIPAM-AA) gels, in which varying the amount of anionic charge substantially affects the microdomain structure and thus the release rate of encapsulated drug.[20]

Given the multi-faceted impacts of introducing charge into in situ-gelling hydrogel networks, developing an understanding of how incorporated charges and/or the interaction between charges affects the nanoscale morphologies and, by extension, the bulk properties of such hydrogels would significantly expand our capacity to more rationally engineer a hydrogel ideally suited to a particular biological (or even non-biological) application. Such understanding requires an analytical method suitable for probing the nanoscale morphology of these hydrogels. Scattering methods such as small angle neutron scattering (SANS), small angle X-ray scattering (SAXS) and light scattering (LS) are extensively used to analyze structure-property correlations in conventional hydrogels created using free radical copolymerization,[13,21–23] with SANS particularly advantageous for the microstructural characterization of hydrogels on the length scale of typical gel homogeneities. SANS has been successfully used on PEG-based hydrogels to enable quantifiable characterization of hydrogel parameters including characteristic network mesh size, solvent affinity, and the size of heterogeneous domains,

among other features.[22,24] We have also previously applied SANS to gain insight into the morphology of (neutral) POEGMA-based injectable hydrogels.[25] However, given the previously outlined multiple ways in which polymer charge can alter the network structure, SANS analysis on charged POEGMA networks is expected to yield significant insight into the effect of charge on the network morphology and, in turn, the key physical properties of these hydrogels.

Herein we report on the characterization of both the macrostructural physicochemical properties as well as the microstructural morphologies of cationic, amphoteric and anionic injectable POEGMA hydrogels crosslinked via hydrazone chemistry. A specific focus is placed on characterizing the microstructure (using SANS) to correlate the gel morphology with the bulk gel properties (e.g. swelling, degradation, etc.) at different degrees of ionization of the incorporated charges. We highlight evidence of both the anticipated ionic double network crosslinking observed in amphoteric gels as well as a surprising mechanical enhancement in anionically-functionalized injectable POEGMA gels that we extensively characterize via both conventional physicochemical gel measurements, SANS, and isothermal titration calorimetry. The structure-property correlations identified can subsequently be leveraged to design hydrogel systems that better mimic native tissues and/or regulate the release kinetics of biological therapeutics.

5.2. Experimental

5.2.1 Materials. All chemicals were purchased from Sigma Aldrich (Oakville, Ontario, Canada) unless otherwise stated. Oligo(ethylene glycol) methyl ether methacrylate ($OEGMA_{475}$, 95%) with a number-average molecular weight of 475 g/mol was purified through a basic aluminum oxide packed column (type CG-20) to remove the methyl ether hydroquinone (MEHQ) and butylated hydroxytoluene (BHT) inhibitors. N-(2,2-dimethoxyethyl) methacrylamide (DMAEAm, 98%) was synthesized as previously reported.[26] Functional monomers acrylic acid (AA, 99%) and N,N-dimethylaminoethyl methacrylate (DMAEMA, 98%) as well as adipic acid dihydrazyde (ADH, Alfa Aesar, 98%), N'-ethyl-N-(3-dimethylaminopropyl)-carbodiimide (EDC, Carbosynth, Compton CA, commercial grade), thioglycolic acid (TGA, 98%), and 2,2-azobisisobutryic acid

dimethyl ester (AIBMe, Wako Chemicals, 98.5%) were used as received. For all experiments, Milli-Q grade distilled deionized water (DIW, 18.2 MΩ cm resistivity) was used.

5.2.2 Synthesis and characterization of neutral and charged hydrazide-functionalized POEGMA precursor polymers (POH and POH(+)). Linear neutral ($PO_{100}H_{30}$) and cationic ($PO_{100}H_{30}(+)_{20}$) hydrazide-functionalized POEGMA precursor polymers were synthesized based on our previously reported method.[26] Briefly, AIBMe (37 mg), $OEGMA_{475}$ (4.0 g), functional monomer DMAEMA (0 µL for $PO_{10}H_{30}$, 591 µL for $PO_{10}H_{30}(+)_{20}$), AA (286 µL for $PO_{100}H_{30}$, 333 µL for $PO_{100}H_{30}(+)_{20}$), and TGA (1.0 µL) were dissolved in a 100 mL round-bottom flask in 1,4-dioxane (20 mL). Note that the amount of AA (used to conjugate hydrazide groups to enable crosslinking) is adjusted in the POH(+) recipe to maintain an equivalent 30 mol% functionalization of crosslinkable groups in both POH and POH(+). After nitrogen purging for 30 min, the flask was sealed and submerged in a pre-heated oil bath at 75°C for 4 hours under magnetic stirring. Subsequently, the solvent was removed by rotary evaporation, and the polymer was re-dissolved in 100 mL DIW. ADH (5x molar excess of polymer-bound –COOH groups) was then added and the pH was lowered to ~4.75 using 0.1 M HCl, after which EDC (3.5x molar excess of polymer-bound –COOH content) was added; the pH was maintained at pH = 4.75 over the following 4 hours. The solution was left to stir overnight, dialyzed (molecular weight cut-off MWCO= 3500 g/mol) against DIW for a minimum of 6 cycles, and lyophilized. The polymers were stored as 20 w/w% solutions in PBS at 4°C. The degree of hydrazide functionalization was determined from conductometric base-into-acid titration (ManTech Associates) using 0.1 M NaOH as the titrant and 50 mg of polymer dissolved in 50 mL of 1 mM NaCl as the analysis sample. Quantification of hydrazide functionalization was achieved by comparing the –COOH content of the polymer before and after the ADH conjugation reaction, assuming that 1 mol ADH reacts with 1 mol –COOH group (i.e. no crosslinking occurs, as is likely based on the 5x molar excess of small molecule ADH added). Precursor polymer molecular weights were estimated by aqueous size exclusion chromatography (SEC) using a Waters 515 HPLC pump, Waters 717 Plus autosampler, three Ultrahydrogel columns (30 cm × 7.8 mm i.d.; exclusion limits: 0–3 kDa, 0–50 kDa, 2–300 kDa) and a Waters 2414 refractive index detector. A

mobile phase consisting of 0.3 M sodium nitrate and 0.05 M phosphate buffer (pH 7) running at a flow rate of 0.8 mL/min was used for all polymers analyzed. Molecular weights were calculated based on narrow-dispersed poly(ethylene glycol) standards (Waters).

5.2.3 Synthesis and characterization of neutral and charged aldehyde-functionalized POEGMA precursors (POA and POA(-)). Linear neutral ($PO_{100}A_{30}$) and anionic ($PO_{100}A_{30}(-)_{20}$) aldehyde-functionalized POEGMA precursor polymers were synthesized based on previously described method.[26] Briefly, AIBMe (37 mg), $OEGMA_{475}$ (4.0 g), functional monomer DMAEAm (0.60 g for $PO_{10}A_{30}$, 0.82 g for $PO_{10}A_{30}(-)_{20}$), AA (0 g for $PO_{100}A_{30}$, 0.23 g for $PO_{100}A_{30}(-)_{20}$), and TGA (1.0 µL for $PO_{10}A_{30}$ and $PO_{10}A_{30}(-)_{20}$) were dissolved in a 100 mL round-bottom flask using 1,4-dioxane (20 mL) as the solvent. As with POH/POH(+), the amount of DMAEAm added was adjusted to maintain 30 mol% of the functional crosslinking monomer in both POA and POA(-). After purging with nitrogen for at least 30 min, the flask was sealed and the reaction carried out at 75°C for 4 hours under magnetic stirring. The solvent was then removed via rotary evaporation and subsequently re-dissolved in 100 mL of 0.5 M HCl to cleave the acetal groups on the DMAEAm monomer to aldehydes. The solution was left to stir for 24 hours, dialyzed (MWCO= 3500 g/mol) against DIW for a minimum of 6 cycles, and lyophilized. The polymers were stored as 20 w/w% solutions in PBS at 4°C. The degree of functionalization was determined from ^{1}H-NMR analysis (Bruker AVANCE 600 MHz spectrometer, $CDCl_3$) by comparing the integral values of the $–OCH_3$ signal (3H, δ=3.35-3.45 ppm) and the –OCH signal (1H, δ=9.50-10.0 ppm). Molecular weights were estimated using the same SEC protocol described for POH/POH(+).

5.2.4 Degree of ionization. The degrees of ionization of $PO_{100}H_{30}(+)_{20}$ (cationic charge) and $PO_{100}A_{30}(-)_{20}$ (anionic charge) as a function of pH were calculated individually by potentiometric titration using the same titration conditions outlined previously, normalizing the results to a blank titration (no polymer).[27]

5.2.5 Isothermal titration calorimetry (ITC). ITC was performed using a Nano ITC low-volume system (TA Instrument). Experiments were conducted by performing 20 successive 2.5 µL injections of POA or POA(-) (1 wt % in 10 mM PBS) into a reaction cell containing 170 µL of a 0.1 wt % of POH or POH(+), with all solutions degassed prior to testing. All experiments were performed at room temperature under constant stirring at 350 rpm. Titration heat signals were processed by NanoAnalyze software (TA Instruments–Waters LLC, Newcastle, DE). Data from the first injection was disregarded, avoiding errors originating from the diffusion of titrant into the calorimetric cell.[28] The heat of dilution associated with adding each charged or uncharged POEGMA precursor polymer solution titrant (prepared in 10 mM PBS) into 10 mM PBS without dissolved polymer was used as a blank, with those measured heats of dilution subtracted from the enthalpies measured for each polymer run to enable isolation of polymer interaction heat effects. The molar heats of injection (ΔH, kJ mol^{-1}) were determined by integrating the area under each individual injection peak to find the heat (Q) associated with each injection and dividing by the number of moles of polymer titrated into the sample ((concentration of polymer (mM) x injection volume (µL))/M_w of polymer); this type of analysis has been done for other polymer systems.[29]

5.2.6 Hydrogel preparation. Both neutral and charged hydrogels were prepared via co-extrusion of hydrazide-functionalized (POH and/or POH(+)) and aldehyde-functionalized (POA and/or POA(-)) precursor polymers, both dissolved at 150 mg/mL in 10 mM PBS, via a double barrel syringe equipped a static mixer at the outlet to ensure mechanical mixing of the precursor polymers prior to gelation (Medmix L series, 2.5 mL volume). Hydrogel disks for swelling and degradation testing were prepared by extruding the reactive precursor polymers directly into cylindrical silicone rubber molds (diameter = 7 mm, volume = 300 µL); gels were incubated at room temperature for at least 4 hours to ensure complete gelation prior to testing. Hydrogel disks for mechanical testing were extruded into similar but thinner silicone molds (diameter = 7 mm, volume = 150 µL) to fit the parallel plate geometry of the rheometer.

5.2.7 Hydrogel gelation kinetics. Gelation times were assessed using a simple vial inversion test following the mixing of 200 µL aliquots of each combination of reactive hydrazide and aldehyde precursor polymers into a 2 mL Eppendorf tube and vortexing the mixture immediately upon addition of the second precursor polymer solution to ensure complete mixing (2 s vortexing per sample). Following, the tube was rotated manually every 5 seconds, with the gelation time defined as the time at which the hydrogel visually no longer flows on the time scale of the rotation (5 s).

5.2.8 pH-dependent swelling kinetics. Hydrogel swelling was determined at 37°C in buffered solutions maintained at 10 mM pH 3 (citrate), 7.4 (phosphate) and 10 (carbonate). Hydrogels disks were loaded into cell culture inserts that were subsequently placed into a 12-well cell culture plate and completely submerged in buffer solutions (4 mL/well). At predetermined time intervals, the cell culture inserts were removed from the well, excess solution inside the insert was drained, and the hydrogel was gently dried with a Kimwipe to wick off any non-absorbed buffer. The gel + insert mass was then measured, after which the hydrogels were resubmerged into a fresh 4 mL of buffered solution and tested repeatedly until equilibrium swelling was reached (~30 hours). The mass-based swelling ratio Q_m was calculated using Equation (1):

$$Q_m = \frac{M_s}{M_d} \quad (1)$$

where M_s is the mass of the swollen hydrogel and M_d is the initial dry hydrogel mass. Using the calculated Q_m, a volumetric swelling ratio Q_v was subsequently calculated using Equation (2):

$$Q_v = 1 + \frac{Pp}{Ps}(Q_m - 1) \quad (2)$$

where P_p is the weight average of the densities of the constituent precursor polymers used to prepare the hydrogels (1.01 g/cm^3 for POH(+) and 1.05 g/cm^3 for POA(-) polymers, as estimated based on a weighted average of the densities of $OEGMA_{475}$, DMAEMA, and AA) and P_s is the

density of the solvent (~1 g/cm^3 for water). Error bars represent the standard deviation of the replicate measurements (n = 4).

5.2.9 Calculation of hydrogel mesh size. The Peppas-Merill equation was used to calculate the mesh size of the charged POEGMA hydrogel systems. First, the molecular weight between crosslinking points M_c was determined for the neutral PO_{100} hydrogel using Equation (3):[30]

$$\frac{1}{\overline{Mc}} = \frac{2}{\overline{Mn}} + \frac{\left(\frac{\bar{v}}{V_1}\right)[\ln(1-v_{2,s})+v_{2,s}+\chi_1 v_{2,s}^2]}{v_{2,r}\left[\left(\frac{v_{2,s}}{v_{2,s}}\right)^{\frac{1}{3}}-\left(\frac{v_{2,s}}{2v_{2,s}}\right)\right]} \quad (3)$$

Here, M_n is the molecular weight of the POEGMA precursor polymer (measured via SEC), V_1 is the molar volume of the solvent (~18 cm^3/mol), $v_{2,S}$ is the polymer volume fraction at equilibrium swelling, $v_{2,r}$ is the polymer volume fraction in a relaxed state (defined as the state of the polymer immediately after crosslinking but before swelling), v is the specific volume of the polymer (P_s/P_p), and χ_1 is the polymer-solvent interaction parameter (approximated by that measured for PEG-water systems, 0.426).[31]

As the presence of ionic moieties in hydrogels makes the theoretical approximation of swelling behavior much more complex, Equations 4 and 5 have been derived to aid in more accurate determinations of M_c for the charged hydrogels by incorporating terms to describe the ionic contributions to the chemical potential of the system through Brannon-Peppas model for ionic gels:[30]

$$\frac{V_1}{4IM_r} = \left(\frac{v_{2,s}}{\bar{v}}\right)^2 \left(\frac{K_b}{10^{pH-14}-K_a}\right)^2 =$$

$$\left[\ln(1-v_{2,s})+v_{2,s}+\chi 1 v_{2,s}^2\right]+\left(\frac{V_1}{v\overline{M_c}}\right)\left(1-\frac{2\overline{M_c}}{\overline{M_n}}\right) \quad v_{2,r}\left[\left(\frac{v_{2,s}}{v_{2,s}}\right)^{\frac{1}{3}}-\left(\frac{v_{2,s}}{2v_{2,s}}\right)\right] \quad (4)$$

$$\frac{V_1}{4IM_r} = \left(\frac{v_{2,s}}{\bar{v}}\right)^2 \left(\frac{K_a}{10^{-pH} - K_a}\right)^2 =$$

$$\left[\ln(1 - v_{2,s}) + v_{2,s} + \chi_1 v_{2,s}^2\right] + \left(\frac{V_1}{v\overline{M_c}}\right)\left(1 - \frac{2\overline{M_c}}{\overline{M_n}}\right) \quad v_{2,r}\left[\left(\frac{v_{2,s}}{v_{2,s}}\right)^{\frac{1}{3}} - \left(\frac{v_{2,s}}{2v_{2,s}}\right)\right] \tag{5}$$

Here, I is the ionic strength, K_a and K_b are the dissociation constants for the acid and base respectively (calculated based on the pK_a of the polymers as determined by potentiometric titration), and M_r is the molecular weight of the repeating unit (taken as a weighted average of the molecular weights of the monomers).

The mesh size of the hydrogel networks can subsequently be estimated based on Equation (6):

$$\xi = v_{2,s}^{-\frac{1}{3}} \left(\frac{2C_n M_c}{M_r}\right)^{\frac{1}{2}} l \tag{6}$$

where C_n is the characteristic ratio between the observed end-to-end distance and the end-to-end distance of a freely jointed chain composed of n bonds of step length l, the bond length of a carbon-carbon bond (1.54 Å). [30]

5.2.10 Degradation kinetics. Hydrogel degradation was determined in acid-accelerated conditions at 37°C in the presence of 100 mM HCl (pH = 1.0); these acid-catalyzed conditions were used to enable comparisons of the degradation kinetics of the hydrogels via hydrazone hydrolysis on a more reasonably measurable time frame and are fully appreciated not to approximate any sort of in vivo-relevant degradation condition. Degradation was measured gravimetrically using the same method used to track swelling but 100 mM HCl (4 mL per well) as the submersing solvent. Measurements were continued until the hydrogel was completely degraded (i.e. no separate phase was observed between the hydrogel and the HCl bath solution). Error bars represent the standard deviation of the replicate measurements (n = 4).

5.2.11 Hydrogel rheology. The rheological properties of the hydrogels were measured using an ARES rheometer (TA Instruments) operating under parallel-plate geometry using a plate

diameter of 7 mm and a plate spacing of 1 mm. A strain sweep was first conducted from 0.1−100% strain at 1 Hz to identify the linear viscoelastic range of the hydrogels. Following, a strain was selected within this range and set as a constant to perform a frequency sweep from 1 to 100 rad/s to measure shear elastic (G') and loss (G") moduli. All measurements were conducted at 25°C, with error bars representing the standard deviation of the replicate measurements (n = 3).

5.2.12 Small-angle neutron scattering (SANS). SANS experiments were conducted on the 30 m SANS NGB instrument at the National Institute of Standards and Technology Center for Neutron Research (NIST NCNR, Gaithersburg, MD, USA). Sample-to-detector distances of 1 m (2 min collection time, 6 Å neutron wavelength), 4 m (5 min collection time, 6 Å neutron wavelength) and 13 m (13 min collection time with lenses and 20 min collection time without lenses, 8.4 Å neutron wavelength) were used to measure an effective q-range of ~10^{-3} $Å^{-1}$ to ~10^{0} $Å^{-1}$. Samples were prepared by co-extruding ~300 µL of charged and/or neutral precursor polymers prepared at concentrations of 150 mg/mL in 10 mM deuterated PBS directly into the sample cells, standard quartz window chambers (4.32 x 3.49 x 2.16 cm^3) with a sample thickness of 1 mm (blank transmission = 0.61). The four ranges of data collected were merged using the DAVE on-site data reduction tool. The scattering intensity (I(q)) of the charged POEGMA hydrogel networks was modeled based on Porod theory by Equation (7):

$$I(q) = \frac{A}{q^n} + \left(\frac{1}{q^s}\right)\frac{C}{1+(\xi q)^m} + B \quad (7)$$

where I(q) is the scattering intensity, q is the scattering vector, B is the background scattering, n is the Porod exponent, s is the stretch factor, m is the Lorentzian exponent, and ξ is the Lorentzian screening length.[32,33] The Porod exponent characterizes the fractal structure of the gel, related to the local clustering of polymer chains of degree n. The stretch factor relates to the stretch or ordering of polymer chains on a scale of 0 to 1, where s = 0 describes fully unstretched (globular) chains and s = 1 describes chains that are fully stretched. Note that this term is not required to fit neutral POEGMA hydrogels and was included in this model to account

for the effects of charge repulsion on expanding the polymer coils in the network. The Lorentzian exponent m indicates the affinity of the polymer chains in solution, with m = 2 typically describing high affinity between the polymer and solvent and m = 4 describing low polymer-solvent affinity due to slightly attractive or repulsive biased random walks.[33] The Lorentzian screening length ξ is the correlation length for polymer chains and is indicative of the mesh size (i.e. average distance between crosslinking points) in the gel. Note that crosslinking points in the charged hydrogel system may be either chemical (hydrazone crosslinks) or physical (charge-charge interactions or dipole-dipole/hydrogen bonding interactions). A variety of models have been developed specifically for charged hydrogel systems, including the Panyukov-Rabin,[34] Borue-Erukimovich[21] and Debye-Bueche[35–37] models. However, these models were not used here because the overall charge incorporation within our systems (~10 mol% of total monomers) is significantly less than that of typical PAA[38] or poly(NIPAM-co-AA)[39] systems previously fit with such models; instead, a simpler Porod model (albeit it one incorporating stretch) can accurately capture the features of the intensity profiles collected. Additionally, the use of 10 mM PBS solvent to better mimic biological systems increases charge screening within the gel, making the charged domains larger, shifting the polyelectrolyte contribution towards lower q values, and making the SANS spectra in the tested q range more similar to neutral systems.[40]

5.3 Results

5.3.1 Synthesis of hydrogel precursors. Each charged precursor polymer was prepared by copolymerizing a functional monomer to enable covalent crosslinking via hydrazide/aldehyde chemistry (AA, subsequently grafted with ADH to form hydrazide groups, or DMAEAm, subsequently hydrolyzed to form aldehyde groups) and a functional monomer to impart charge in the polymer (AA for anionic polymers, DMAEMA for cationic polymers). Each $PO_xH_y(+)_z$ and $PO_xA_y(-)_z$ precursor polymer reported in this paper is functionalized with y = 30 mol% functional hydrazide or aldehyde functional groups (i.e. the theoretical covalent cross-link density

potential is the same among all gels) and z = 20 mol % charged monomer; the remaining ~50 mol% of monomers in the charged precursor polymers or ~70 mol% of monomers in the uncharged gels is comprised of $OEGMA_{475}$, the n=8-9 long-chain comonomer which mimics PEG and does not exhibit any thermal phase transition. Table 5.1 indicates essentially quantitative incorporation of each of these comonomer components into the precursor polymers (see also Supporting Information Figs. S5.1 and S5.2), leading to functional precursor polymers with expected average pK_a values of ~7.5 (cationic) and ~5.1 (anionic) as per potentiometric titration (Supporting Information, Fig. S5.3). The number-average molecular weight (M_n) of the polymer precursors is also consistent between the different precursors and is controlled to be <30 kDa (Table 5.1), well below the renal clearance limit of 40-50 kDa.[51] As such, given the similar degrees of functionalization and molecular weights, the precursor polymers to be used for hydrogel fabrication are chemically equivalent aside from the incorporation of charged monomers.

Table 5.1. Chemical characterization of synthesized POEGMA polymer precursors

Polymer Precursor	**$OEGMA_{475}$ (mol%)** [b]	**Functional Reactive Group**	**Functional Reactive Group Content (mol%)**	**Charged Group**	**Charged Functional Monomer Content (mol%)**	**M_n (kDa)**	**Đ**	**pK_a**	**% Ionization at pH 7.4**
$PO_{100}H_{30}$ (POH)	70.7 [c]	$NHNH_2$	29.3 [a]	-	N/A	24.1	3.3	N/A	N/A
$PO_{100}H_{30}(+)_{20}$ (POH(+))	47.9 [c]	$NHNH_2$	28.3 [a]	DMAEMA	(+) 19.7 [a]	24.9	3.1	~7.5 [b]	55.1
$PO_{100}A_{30}$ (POA)	71.9 [c]	CHO	28.1 [c]	-	N/A	22.1	2.9	N/A	N/A
$PO_{100}A_{30}(-)_{20}$ (POA(-))	46.4 [c]	CHO	32.3 [c]	AA	(-) 19.3 [a]	23.8	3.1	~5.1 [b]	99.5

[a] Determined from conductometric titration; [b] Determined from potentiometric titration; [c] Determined by ^{1}H-NMR

5.3.2 Physiochemical properties of charged POEGMA hydrogels. Charged POEGMA hydrogels were prepared via co-extrusion of an equal total mass of one or more hydrazide (POH/POH(+)) and one or more aldehyde (POA/POA(-)) polymers using a double barrel syringe, as per the recipes shown in Table 2. All gels are labeled as $PO_{100\text{-}x/y}$, where x corresponds to the mass percentage of the overall hydrazide-functionalized polymer added that contains charge and y corresponds to the mass percentage of the overall aldehyde-functionalized polymer added that contains charge. For example, $PO_{100\text{-}100/0}$ was prepared by gelling 100% POH(+) (15 wt%) as the hydrazide component and 0% POA(-) (i.e. 100% POA, 15 wt%) as the aldehyde component, while $PO_{100\text{-}50/50}$ was prepared using 50% POH(+) (7.5 wt%) and 50% POH (7.5 wt%) as the hydrazide component and 50% POA(-) (7.5 wt%) and 50% POA (7.5 wt%) as the aldehyde component.

Table 5.2. Recipes and gelation times (by the vial inversion test) of charged POEGMA hydrogels

Hydrogel	**Hydrogel Type**	**Hydrazide Polymer(s)**	**Aldehyde Polymer(s)**	**% Charged monomer residues in gel**	**Ratio of cationic: anionic charge**	**Overall Polymer Concentration (mg/mL)**	**Gelation Time at pH=7.4 (seconds)**
PO_{100}	Neutral	$PO_{100}H_{30}$	$PO_{100}A_{30}$	0	N/A	150	1500
$PO_{100\text{-}100/0}$ ($PO_{100\text{-}cat}$)	Cationic	$PO_{100}H_{30}(+)_{20}$	$PO_{100}A_{30}$	10	∞	150	1200
$PO_{100\text{-}0/100}$ ($PO_{100\text{-}an}$)	Anionic	$PO_{100}H_{30}$	$PO_{100}A_{30}(-)_{20}$	10	0	150	30
$PO_{100\text{-}100/100}$ ($PO_{100\text{-}amp}$)	Amphoteric	$PO_{100}H_{30}(+)_{20}$	$PO_{100}A_{30}(-)_{20}$	20	1:1	150	300
$PO_{100\text{-}75/25}$	Amphoteric (mixed)	$PO_{100}H_{30}(+)_{20}$, $PO_{100}H_{30}$	$PO_{100}A_{30}(-)_{20}$, $PO_{100}A_{30}$	10	3:1	150	120
$PO_{100\text{-}50/50}$		$PO_{100}H_{30}(+)_{20}$, $PO_{100}H_{30}$	$PO_{100}A_{30}(-)_{20}$, $PO_{100}A_{30}$	10	1:1	150	90
$PO_{100\text{-}25/75}$		$PO_{100}H_{30}(+)_{20}$, $PO_{100}H_{30}$	$PO_{100}A_{30}(-)_{20}$, $PO_{100}A_{30}$	10	3:1	150	60

All gels were made using the same overall concentration of precursor polymer (150 mg/mL) and the same overall ~1:1 hydrazide:aldehyde ratio (Table 5.1) to ensure limited (or at least roughly equivalent) numbers of residual reactive groups were present after gelation. The charged precursor polymers both have a charged monomer content of ~20 mol%, leading to an overall charge content of ~10 mol% in the final PO_{100}-$_{100/0}$ (cationic) and PO_{100}-$_{0/100}$ (anionic) gels given that the complementary precursor polymer used to make these gels is uncharged. PO_{100}-$_{100/100}$ is an amphoteric gel which contains a 1:1 charge ratio and was prepared by mixing both charged precursor polymers together, resulting in double (~20 mol %) the overall charge in the final hydrogel. To compare gel properties on gels prepared with the same overall 10 mol% charge content as the single charge cationic and anionic gels, a series of amphoteric mixed hydrogels was also prepared by mixing different ratios of charged and uncharged polymers in each barrel to control the cationic:anionic charge ratio in the final hydrogel. Neutral gels were prepared by mixing $PO_{100}H_{30}$ and $PO_{100}A_{30}$, consistent with our previous work[12] and used as a control.

All gels were optically clear (Supporting Information, Fig. S5.4), suggesting no significant inhomogeneities on the visible light length scale. All of the gelation times for the charged precursor-containing gels were faster than the 25 minutes required to gel the neutral PO_{100} gels (Table 5.2 and Figure 5.1A). While the all-cationic PO_{100}-$_{100/0}$ hydrogel gelled only slightly faster (20 minutes) than PO_{100}, the inclusion of even a small fraction anionic precursor polymer substantially reduced gelation times. Specifically, including only 2.5 mol% anionic functional groups in the overall gel ($PO_{100\text{-}75/25}$) reduced the gelation time from ~20 minutes (PO_{100}-$_{100/0}$) to ~2 minutes; further increasing the amount of anionic functional groups in the gel from 2.5 mol% ($PO_{100\text{-}75/25}$) to 10 mol% (PO_{100}-$_{0/100}$) reduced the gelation time to as short as ~30 seconds. Interestingly, doubling the total charge content of the 1:1 charge ratio amphoteric gels from 10 mol% ($PO_{100\text{-}50/50}$) to 20 mol% (PO_{100}-$_{100/100}$) of total monomer residues increases the gelation time from ~1.5 minutes to ~5 minutes, a result we attribute to charge interactions between the precursor polymers sterically inhibiting covalent bond formation. These significant variations in gelation time are observed even though the theoretical covalent cross-linking density of each gel is identical (i.e. y = 30 mol % hydrazide and aldehyde groups total in each gel, Table 5.1).

The effect of charge on the equilibrium swelling ratio was measured gravimetrically and evaluated in three different pH buffers at pH = 3 (acetate), 7.4 (phosphate) and 10 (carbonate) at 37°C. These three specific pH values were chosen to bracket the pK_a values of the charged anionic (~5.1; ionization between pH 4.4 – 5.8) and cationic (~7.5; ionization between pH 6.2 - 8.0) precursor polymers as well as to mimic various in vivo environments such as stomach acid (pH = 1.5-3.5), blood (pH = 7.35-7.45), or basic lower intestines (pH = 7.5-9.0). Results are shown graphically in Figure 5.1B and summarized in Table 5.3. Note that the presence of the hydrazide groups (pK_a ~2.5-3.5) inductively lowers the average pK_a of the cationic precursor polymer (~7.1) from typical average pK_a observed for pDMEAMA homopolymers (~7.8).[41]

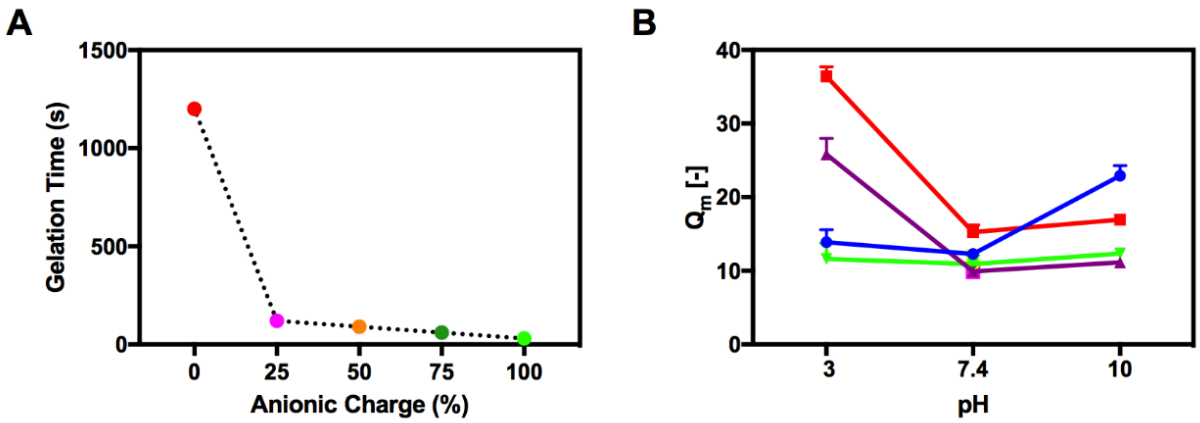

Figure 5.1. Physicochemical properties of injectable charged POEGMA hydrogels: (A) Gelation times assessed at pH 7.4 and 22°C as a function of the percentage of total charges in the gel that are anionic (10 mol% total charge): (red) $PO_{100\text{-}100/0}$ (0%); (magenta) $PO_{100\text{-}75/25}$ (25%); (orange) $PO_{100\text{-}50/50}$ (50%); (dark green) $PO_{100\text{-}25/75}$ (75%);. (green) $PO_{100\text{-}0/100}$ (100%). (B) Mass-based swelling ratio at pH = 3, 7.4 and 11 at 37°C: (blue) PO_{100}; (red) $PO_{100\text{-}100/0}$; (green) $PO_{100\text{-}0/100}$; (purple) $PO_{100\text{-}100/100}$.

Table 5.3. Measured (swelling ratios, shear storage modulus) and calculated (crosslink density, mesh size) physiochemical properties of charged POEGMA hydrogels

Hydrogel	**Q_m pH = 3**	**Q_m pH = 7.4**	**Q_m pH = 10**	**Q_v pH = 7.4**	**G' [kPa]**	**v [1/cm^3] (x 10^{17})**	**ξ_t [nm]**	**ξ_e [nm]**
PO_{100}	13.9 ± 1.7	12.3 ± 0.2	22.9 ± 1.3	13.6 ± 0.3	2.1 ± 0.1	5.2 ± 0.9	4.1	1.1
$PO_{100\text{-}100/0}$	36.4 ± 1.3	15.2 ± 0.9	16.9 ± 0.4	16.9 ± 1.0	2.7 ± 0.2	6.6 ± 0.7	5.0	0.9
$PO_{100\text{-}100/100}$	25.8 ± 2.2	9.9 ± 0.1	11.1 ± 0.5	10.9 ± 0.1	4.0 ± 0.3	9.8 ± 0.3	3.7	1.0
$PO_{100\text{-}75/25}$	-	10.8 ± 0.1	-	12.1 ± 0.1	2.4 ± 0.4	5.8 ± 0.8	4.2	1.0
$PO_{100\text{-}50/50}$	-	11.1 ± 1.6	-	10.1 ± 0.3	4.5 ± 0.2	11.1 ± 0.5	3.6	1.0
$PO_{100\text{-}25/75}$	-	9.86 ± 0.8	-	10.9 ± 0.8	6.7 ± 0.7	16.4 ± 1.7	4.1	1.0
$PO_{100\text{-}0/100}$	11.6 ± 2.1	10.8 ± 1.1	11.9 ± 0.5	12.1 ± 1.3	11.7 ± 1.5	28.7 ± 3.6	3.9	1.1

ξ_t = theoretical mesh size from Equation 6; ξ_e = experimental mesh size determined through SANS.

The neutral PO_{100} gel maintains a low Q_m at both pH =3 and 7.4 and is minimally affected by acidic pH as it contains no ionizable functional groups. Both the cationic and amphoteric gels exhibit increased swelling at acidic pH (Q_m = 36.4 ± 1.3 and 25.8 ± 2.2 respectively); this result is consistent with protonation of the cationic groups at low pH (and, in the case of the amphoteric gel, simultaneous protonation of the anionic groups), resulting in Donnan equilibrium-driven swelling.[42] When the cationic and anionic groups are simultaneously ionized in the amphoteric gels (pH 7.4), gels exhibited the lowest water content among all tested gels, consistent with the formation of charge complexes at intermediate pH values; slight reswelling was then observed at pH 10 as the cationic groups are deprotonated but the anionic groups remain fully ionized. In contrast, anionic gels remain collapsed at low pH when the –COOH groups are protonated and hydrogen bonding (e.g. between protonated –COOH groups and ether groups on the POEGMA side chain) can occur to further enhance the physical crosslink density, as anticipated. Once the pH was increased above the pK_a of the anionic polymer (pH 7.4 and 10), we expected the hydrogel to swell due to a similar Donnan repulsion mechanism described for the cationic gel under acidic conditions. Interestingly, such swelling is not observed to a significant extent, as Q_m remains roughly constant over the full pH range. This suggests the formation of a secondary network in these gels even at higher pH values.

The swelling kinetics of the neutral, cationic, amphoteric and anionic PO_{100} gels over a time scale of 30 hours, shown in Figure 5.2, show similar trends. $PO_{100\text{-}100/0}$ and $PO_{100\text{-}100/100}$ (both of which contain fully-charged, 10 mol% cationic precursor polymer at acidic pH) both swell significantly more than neutral or anionic gels at pH 3 (Fig. 5.2A), as expected. Even at pH 7.4, at which the degree of ionization of the cationic precursor polymer before gelation is ~ 55% (Fig. S5.3), the cationic $PO_{100\text{-}100/0}$ gel remains the hydrogel that exhibits the most swelling despite the anionic precursor polymer being 99% ionized at this same pH (Fig. 5.2B). The amphoteric $PO_{100\text{-}100/100}$ gel swells the least and slowest of all tested hydrogels at pH 7.4, consistent with internal ionic crosslinking being induced at this pH. The mixed PO_{100} gels incorporating different cationic:anionic charge ratios but the same overall 10 mol% of charged monomer residues (Fig. 5.2D) further demonstrate this ionic crosslinking mechanism as well as the controlling influence of the anionic functional groups in determining swelling; the swelling

kinetics of the 1:3, 1:1, and 3:1 cationic:anionic charge ratio hydrogels all exhibited reduced swelling similar to the anionic-only $PO_{100\text{-}0/100}$ hydrogel while the cationic $PO_{100\text{-}100/0}$ hydrogel swells substantially more. This result again suggests that secondary crosslinking interactions are occurring in both the amphoteric and anionic gel systems.

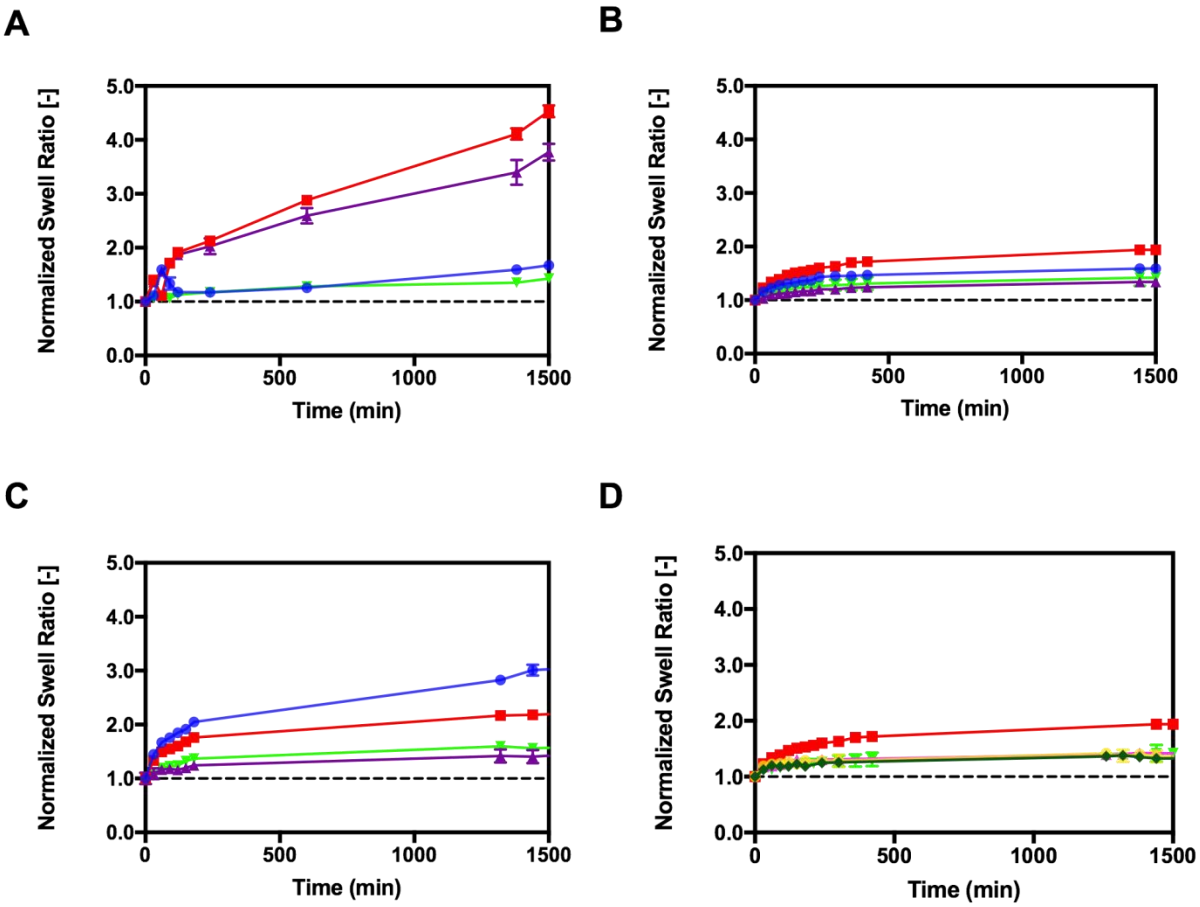

Figure 5.2. Swelling kinetics of POEGMA hydrogels in buffered solutions of (A) pH 3, (B) pH 7.4 and (C) pH 10 at 37°C: (blue) PO_{100}; (red) PO_{100}-cat; (green) PO_{100}-an; (purple) PO_{100}-amp, (D) Swelling kinetics of POEGMA hydrogels at pH 7.4, 37°C for hydrogels prepared by mixing cationic and anionic precursor polymers at different charge ratios (all 10 mol% charged monomer residues); (dark green) $PO_{100\text{-}75/25}$; (yellow) $PO_{100\text{-}50/50}$; (magenta) $PO_{100\text{-}25/75}$ (red and light green correspond to the same coding as A-C).

Degradation kinetics were evaluated gravimetrically in solutions of 0.1 M HCl, acid-catalyzed conditions used to enable direct comparisons of the degradation rates of the hydrogels on a more measurable time frame (Figure 5.3). Note that the acidic conditions used for this assay

correlate to full charge in the cationic hydrogels, a large net cationic charge (and swelling) in the amphoteric hydrogels, and full neutralization in the anionic hydrogels.

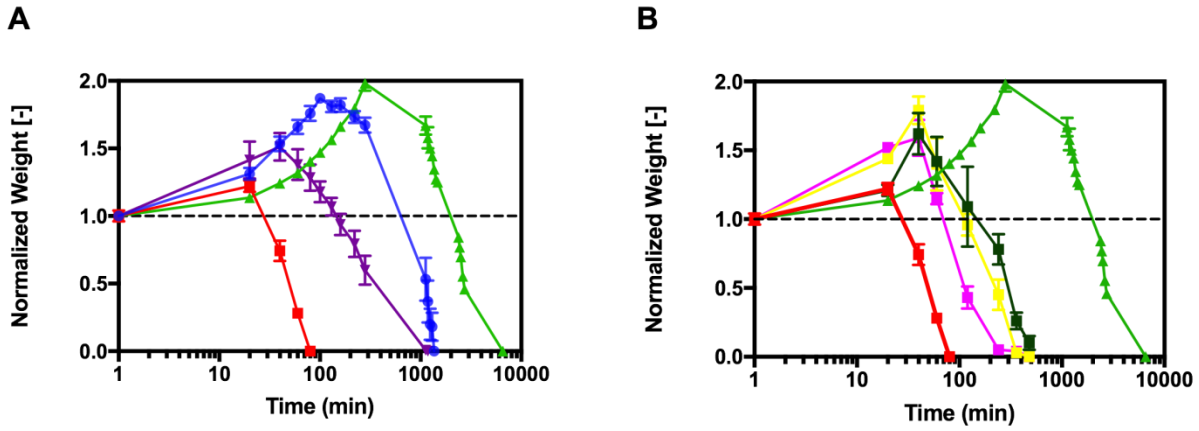

Figure 5.3. Comparative degradation profiles of charged POEGMA hydrogels in 0.1 M HCl: (A) comparison of cationic, anionic, neutral, and 50:50 amphoteric hydrogels: (blue) PO_{100}; (red) $PO_{100\text{-}100/0}$; (green) $PO_{100\text{-}0/100}$; (purple) $PO_{100\text{-}100/100}$; (B) comparison of hydrogels with same total charge but varying cationic:anionic charge ratios: (dark green) $PO_{100\text{-}25/75}$; (yellow) $PO_{100\text{-}50/50}$; (magenta) $PO_{100\text{-}75/25}$ (the red and light green series are the same gels denoted in A).

The degradation profiles of the charged PO_{100} hydrogels are substantially altered compared to that of the neutral gels (Fig. 5.3A). Accelerated degradation profiles are observed for both the cationic $PO_{100\text{-}100/0}$ (80 minutes) and amphoteric $PO_{100\text{-}100/100}$ (1180 minutes) hydrogels; here, the high degree of swelling observed in these (net cationic) hydrogels counteracts the repulsion between the gel network and the H^+ hydrolyzing ions, leading to faster degradation. However, based on the significant swelling observed in $PO_{100\text{-}100/0}$ even at high pH values, the presence of a lower effective covalent crosslink density in the cationic hydrogel cannot be ruled out. In contrast, all mixed amphoteric hydrogels regardless of charge ratio degrade at roughly equivalent rates consistent with the swelling results observed for this series (Fig. 5.3B), although marginally prolonged degradation rates are observed upon incorporating increasing amounts of anionic precursor. In comparison, the anionic hydrogels exhibit substantially prolonged degradation times, again suggestive of a secondary crosslinking mechanism in these gels.

The mechanics of the hydrogels also vary significantly as a function of the hydrogel charge (Figure 4). Here, gels are tested immediately after fabrication (without swelling) using 10 mM PBS buffer (pH 7.4) to dissolve the precursor polymers; this buffer choice results in largely (~55%) ionized cationic gels, nearly fully (>99%) ionized anionic gels, and amphoteric gels with a small net anionic charge.

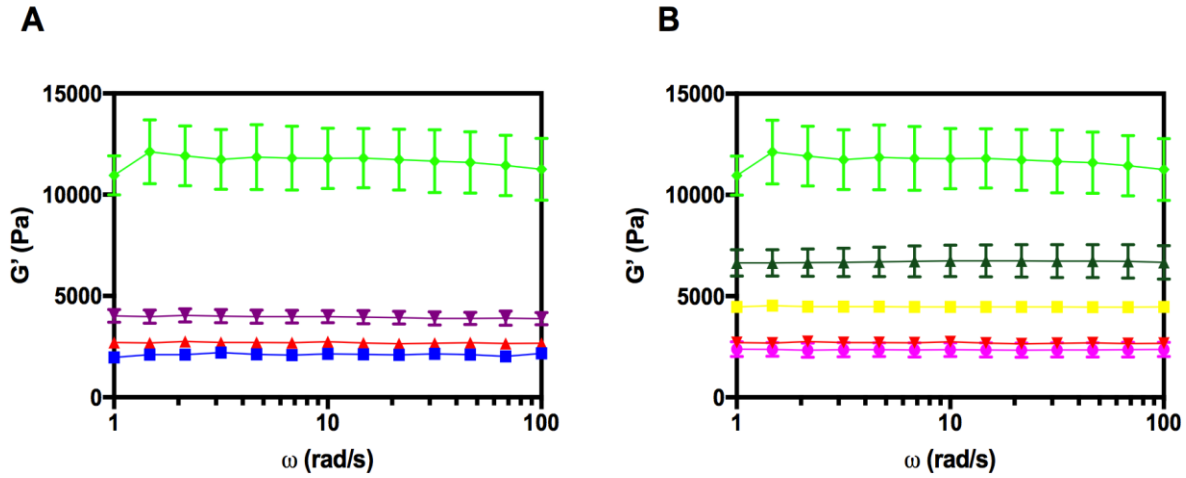

Figure 5.4. Shear storage moduli (G') of charged POEGMA hydrogels: (A) comparison of cationic, anionic, neutral, and 50:50 amphoteric hydrogels: (blue) PO_{100} ; (red) $PO_{100\text{-}cat}$; (green) $PO_{100\text{-}0/100}$; (purple) $PO_{100\text{-}100/100}$; (B) comparison of hydrogels with same total charge but varying cationic:anionic charge ratios: (dark green) $PO_{100\text{-}75/25}$; (yellow) $PO_{100\text{-}50/50}$; (magenta) $PO_{100\text{-}25/75}$ (red and light green series are the same gels denoted in A).

The shear storage modulus (G') increases with the incorporation of charge in all hydrogels. Cationic (2.7 ± 0.2 kPa), amphoteric (4.0 ± 0.3 kPa), and anionic (11.7 ± 1.5 kPa) gels all exhibit significantly stronger mechanical properties compared to the neutral gel (2.1 ± 0.1 kPa). The higher modulus of $PO_{100\text{-}100/100}$ relative to the neutral gel is consistent with reports of other amphoteric dual network systems in which the contribution of the second electrostatic network in addition to the covalently crosslinked system increases the shear storage modulus of the amphoteric gels.[43,44] However, the amphoteric charge enhances G' comparatively little compared to previous reports. This can be attributed to a combination of two factors. First, since covalent crosslinking occurs at the same time as ionic interactions between precursor polymers, ionic-based inhibition of chain mobility and thus lower effective covalent crosslink density can be observed that suppresses the overall modulus. We have observed similar

reductions in total covalent crosslink density in systems containing hydrophobic grafts that can physically gel as a comparable competitive networking mechanism.[13] Second, potential steric interference of the ionic associations due to the comb-like $OEGMA_{475}$ side chains may reduce the frequency of ionic bridging relative to that observed in other, less sterically hindered polymer chains. Interestingly, the anionic hydrogels produce by far the strongest networks, more than five-fold stronger than the neutral gel and three-fold stronger than the amphoteric gel (Fig. 5.4A); adding more anionic charge to the network was also observed to systematically increase the shear storage moduli of the mixed hydrogels (Fig. 5.4B). This is consistent with the suppressed swelling (Fig. 5.2) and prolonged degradation kinetics (Fig. 3) observed for $PO_{100\text{-}0/100}$ and again suggests a role of a secondary crosslinking interaction in strengthening the network that is not active in the other hydrogel formulations tested.

To further investigate the roles of covalent and non-covalent crosslinking within charged POEGMA hydrogels (and particularly the mechanism behind the apparently anomalous behavior of the anionic $PO_{100\text{-}0/100}$ hydrogel), isothermal titration calorimetry (ITC) was conducted (Figure 5; see Supporting Information Fig. S5 for the raw heat versus injection data). When the anionic POA(-) precursor polymer was titrated into an unfunctionalized POEGMA polymer (i.e. no potential for covalent crosslinking exists but secondary interactions associated with the anionic residues could be observed), a maximum injection enthalpy of -80 kJ/mol added polymer was measured. We attribute this energy to dipole-dipole interactions between the $-COO^-$ groups and the ether oxygen groups in the POEGMA side chain; the measured magnitude is consistent with that of stronger hydrogen bonds formed between charged entities.[45] In comparison, when (uncharged) hydrazide-functionalized POH and aldehyde-functionalized POA were mixed (i.e. potential for covalent crosslinking exists but no secondary interactions involving -COOH groups would be observed), the maximum injection enthalpy was significantly decreased to -1 kJ/mol added polymer, despite the obvious potential for covalent hydrazone bond formation. This number is considerably less than the typical magnitude associated with covalent crosslink formation (80-400 kJ/mol);[52] however, since the enthalpies were normalized based on a per added polymer chain molar basis, this low magnitude reflects incomplete crosslinking in the system as anticipated due to steric limitations. In comparison,

when the uncharged POH precursor polymer was mixed with the anionic POA(-) precursor polymer (i.e. the potential for both covalent and secondary interactions involving -COOH groups exists) an intermediate maximum injection enthalpy of -41 kJ/mol added polymer was measured. This result is consistent with covalent crosslinking sterically limiting the potential for polymer rearrangements to maximize the number of dipole-dipole interactions that can form, a steric limitation not present in the absence of crosslinking (thus resulting in more interactions and higher absolute enthalpies in that case). Collectively, these results suggest that strong dipole-dipole bonding (likely via hydrogen bonding) is the origin of the special responses observed in the anionic hydrogels reported. Previous work on the interactions between poly(methacrylic acid) (PMAA) and poly(ethylene glycol) (PEG) has identified the formation of hydrogen-bonded complexes stabilized by hydrophobic interactions,[46] forming a "zipped" morphology dependent on both the neutralization ratio and molecular weight.[47] We hypothesize that a similar interaction may be occurring here, with the hydrogen bonding contribution dominating the enthalpic signature of the interaction due to the relatively low effective crosslinking efficiency in this system.

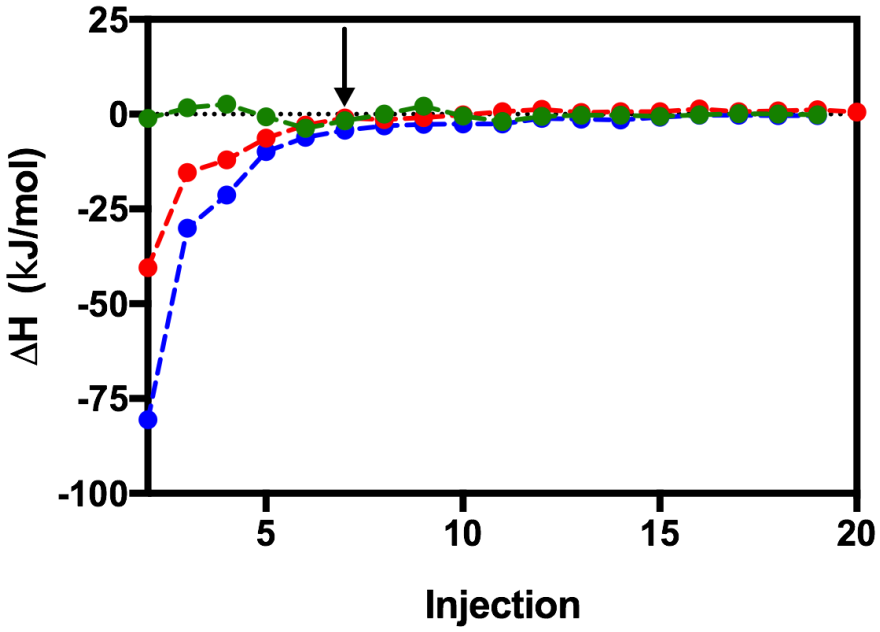

Figure 5.5. Enthalpies associated with mixing (green) POA + POH (uncharged but covalently crosslinkable), (red) POA(-) + POH (charged and covalently crosslinkable) and (blue) POA(-) + unfunctionalized POEGMA (charged, not covalently crosslinkable). Arrow denotes mass-based equivalence point.

5.3.3 Small angle neutron analysis of microstructure. To investigate the microstructure of the charged POEGMA hydrogels and support the hypotheses from the macroscopic hydrogel data above regarding the effects of charge on hydrogel macrostructure, SANS was employed to investigate and describe the nanometer-scale structure and domains within the gels. Table 5.5 shows the best-fit parameters based on the Porod model allowing stretch (Eq. 5.7, the simplest equation that gives reasonable fits to the data) for all hydrogels analyzed.

Table 5.5. Fitting parameters for the neutral, cationic, amphoteric and anionic networks at 22°C in D_2O PBS.

	Porod Scale	Porod Exponent (n)	Stretch Factor (s)	Lorentzian Scale (B)	Lorentzian Screening Length (Å) (ξ)	Lorentzian Exponent (m)	Bgd [1/cm] (C)
PO_{100}	1.03	3.0	0.05	1.86	10.6	4	0.22
PO_{100}-100/0	1.7	2.6	0	1.63	9.2	4	0.22
PO_{100}-100/100	53.25	2.8	0	1.84	9.5	4	0.19
PO_{100}-75/25	11.7	2.7	0.09	1.95	10.3	3.9	0.21
PO_{100}-50/50	1.23	2.6	0.09	1.59	10.1	4	0.19
PO_{100}-25/75	65.9	2.6	0.17	1.55	10.4	3.6	0.23
PO_{100}-0/100	1.268	3.0	0.22	1.50	10.9	3.6	0.16

Figure 5.6 shows the raw I(q) versus q plots for hydrogels prepared by mixing single hydrazide and aldehyde polymers (see Supporting Information, Fig. S5.6, for fitting curves).

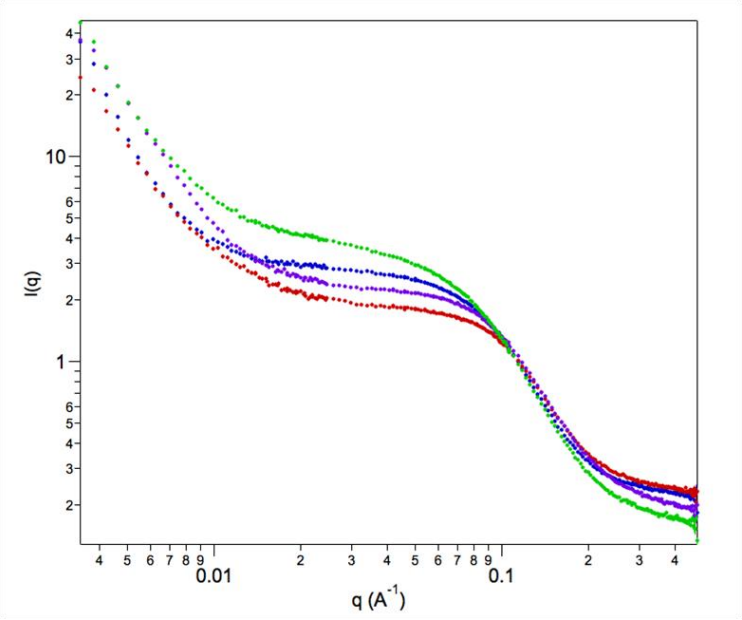

Figure 5.6. Comparison of neutron scattering intensity profiles of charged PO_{100} hydrogels prepared with single functional precursor polymers (pH 7.4, 10 mM D_2O PBS, 22˚C); (blue) PO_{100}; (red) PO_{100}-100/0; (green) PO_{100}-0/100; (purple) PO_{100}-100/100.

The Porod exponent (n) characterizes the fractal structure of the gel, related to the clustering of polymer chains of degree n, and is reflected by a decreased scattering intensity in the region $0.01 < q < 0.1$ (Fig. 6).[48] When n = 1, scattering describes rigid rods, while n = 4 describes a smooth surface. In the case of polymer coils, n is related to the excluded volume parameter v by the correlation $n = 1/v$. A slope of n = 2 is thus a signature of Gaussian chains in a dilute solvent environment, n = 5/3 represents fully swollen coils, and n = 3 represents collapsed polymer coils, or in presence and/or of random branching of polymer chains. A slope between 2 and 3, consistent with all gels tested (Table 5.5), represents "mass fractals" that are often ascribed to branched systems (gels and the POEGMA polymer itself) or networks.[49] A slightly lower Porod exponent was observed for charged hydrogels, reflective of looser networks and/or a more heterogeneous collapsed or branched morphologies (as expected when charged groups are present inside hydrogels).[50]

A qualitative difference in scattering response can also been seen upon the incorporation of charge. Horkay et al. previously demonstrated that, for polymer systems containing labile (and potentially hydrogen-bonding) protons such as NH and OH groups, the process of H-D exchange does not dramatically influence the overall shape of the scattering curve but does enhance the scattering contrast[40]. We clearly see this effect in terms of a significantly higher Porod scale for all charged hydrogels but in particular the anionic and amphoteric hydrogels in which secondary (non-covalent) interactions are observed, consistent with scattering theory (Table 5.5).

The proposed "zipped" morphology hypothesized to account for the higher modulus of the anionic gels can be further investigated via SANS using the stretch factor ($1/q^s$), which relates to the stretch or ordering of polymer chains; 0 describes globular chains while 1 describes chains that are fully stretched.[48] While both the cationic and amphoteric gels can be fit well with zero stretch, the incorporation of a stretch factor is required to fit the anionic hydrogel data as well as (to a lesser extent) amphoteric hydrogels with imbalanced charge contents (particularly those with a net excess of anionic groups) (Table 5.5). By far the largest stretch is observed in the anionic networks, consistent with the zipped morphology inferred

from the ITC results to contribute to the lower swelling (Fig. 5.2A), slower degradation (Fig. 5.3A), and significantly enhanced mechanics (Fig. 5.4A) observed for PO_{100}-$_{0/100}$.

The Lorentzian screening length ξ represents the correlation length for polymer chains and describes the gel mesh size or distance between crosslinking points. All gels, regardless of charge content, show similar Lorentzian screening lengths. This minimal difference observed between the individual gels is consistent with similar net crosslink densities (combined between covalent and ionic crosslinks) in each hydrogel, all of which were prepared at the same polymer concentration and based on precursor polymers with the same functional group density (~30 mol%). We hypothesize that the proposed zipper-like assembly in the anionic PO_{100}-$_{0/100}$ hydrogel is not reflected in the mesh size results since the larger-scale chain rearrangements involved in that interaction are occurring over a different length scale than that reflected by the Lorentzian exponent (ξ). However, there is a significantly higher scattering intensity in the $0.01 Å^{-1} < q < 0.1 Å^{-1}$ range data best fit using the Lorentzian component of the function for the PO_{100}-$_{0/100}$ hydrogel (Fig. 5.5A), reflective of a significant different morphology on the few to tens of nanometer length scale that suggests additional inter-chain interactions. Note that while the Lorentzian exponent is high (close to 4, typically representative of non-ideal solvent interactions around helix-like associations)[50], we hypothesize this is an artefact of the brush copolymer structure of the polymer itself. Each OEGMA monomer unit has n=8-9 ethylene oxide repeat units as a side chain, resulting in a dense comb-like structure that from a scattering perspective appears significantly more condensed than it actually is.[32]

Figure 5.7 shows the SANS data comparing the two 50:50 cationic:anionic charge density hydrogels PO_{100}-$_{50/50}$ (10 mol% total charge) and PO_{100}-$_{100/100}$ (20 mol% total charge), indicative of the effect of total charge on the network parameters. The best fits using the Porod model are shown in Table 5.5; see Supporting Information, Figure S5.6 for the fits to these profiles.

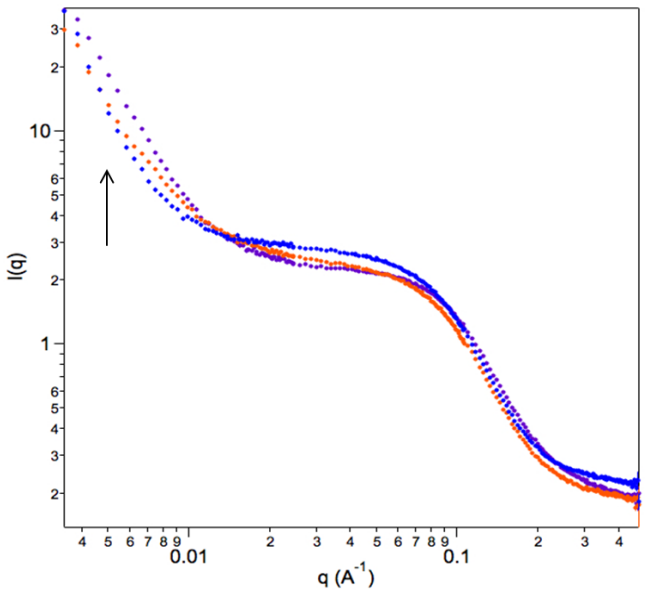

Figure 5.7. Comparison of neutron scattering intensity profiles for zero net charge density hydrogels with different overall charge contents (10 mM D_2O PBS, 22˚C): (blue) 0 mol% total charge (PO_{100}); (orange) 10 mol% total charge ($PO_{100\text{-}50/50}$) (purple) 20 mol% total charge ($PO_{100\text{-}100/100}$)

Here, the Porod exponent (n) decreases for both the $PO_{100\text{-}50/50}$ and $PO_{100\text{-}100/100}$ hydrogels compared with the neutral PO_{100} network, suggesting a more rigid network in these hydrogels consistent with the mechanical data (Fig. 5.4), the swelling data (Fig. 5.2), and the dual covalent/ionic crosslinking mechanism present in amphoteric hydrogels. Interestingly, a stretch parameter is required to fit the $PO_{100\text{-}50/50}$ but not the $PO_{100\text{-}100/100}$ (which has double the total charge density) or PO_{100} data (Table 5.5), suggesting the intermediate charge density hydrogel has a more efficiently ordered network. This result is consistent with the significantly higher G' value observed for the intermediate charge density $PO_{100\text{-}50/50}$ gel relative to $PO_{100\text{-}100/100}$ (Table 3, $p < 0.0001$). We interpret this result as the incorporation of more charge resulting in stronger ionic interactions on the length scale of covalent gelation, resulting in less covalent crosslinking in the $PO_{100\text{-}100/100}$ gel.

The effect of the cationic:anionic charge ratio on the scattering intensity profiles of charged hydrogels is shown in Figure 8 (see Supporting Information Fig. S5.6 for the fits to these profiles).

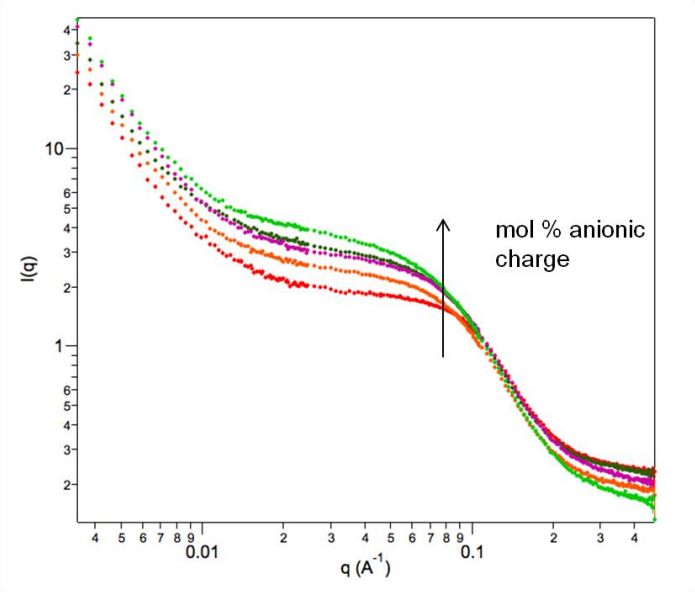

Figure 5.8. (A) Comparison of neutron scattering intensity profiles for hydrogels with same total charge but varying cationic:anionic charge ratios (10 mM D_2O PBS, 22˚C): (red) $PO_{100\text{-}100/0}$; (magenta) $PO_{100\text{-}75/25}$; (orange) $PO_{100\text{-}50/50}$; (dark green) $PO_{100\text{-}25/75}$; (green) $PO_{100\text{-}0/100}$.

The Porod exponent (n) increases from 2.6 to 3.0 as the cationic:anionic charge ratio decreases from 1 to 0, suggesting that increased anionic charge results in increased “pulling” of the gel network. This observation is reflected quantitively in the stretch value. The stretch (s) is the largest for the 1:3 cationic:anionic charge ratio $PO_{100\text{-}25/75}$ and the anionic $PO_{100\text{-}0/100}$ gel (and consistent with the increased scattering of these two systems in the mid q region of Fig. 5.8), indicative of increased ordering in the gel network as more anionic precursor polymer is added. These results are again consistent with enhanced dipole-dipole interactions between acrylic acid residues and ether groups on the $OEGMA_{475}$ chain indicated by the ITC results.

5.4 Discussion

The incorporation of charged co-monomers into hydrazide and aldehyde-functionalized POEGMA precursor polymers significantly alters the gel properties on both the macroscopic and microscopic length scale. Macroscopically, the inclusion of charge systematically changes the swelling, degradation, and mechanical properties of the hydrogels, including the capacity for

pH-responsive changes in swelling properties (Fig. 5.2). Such responses, coupled with the precise control over the actual charge balance in the hydrogel achievable by simple mixing of precursor polymers with well-defined charge densities (extending our concept of modular hydrogels)[6], offer potential of these materials in biomedical applications in which pH sensing is important (e.g. infection control or oral drug delivery). The significant changes observed in hydrogel mechanics (~5-fold enhancement, Fig. 5.4) and degradation kinetics (>2-fold prolongation of degradation under acidic conditions, Fig. 5.3) upon including just 10 mol% anionic co-monomer residues enables significant alteration of gel properties with minimal changes in gel chemistry.

Bulk hydrogel properties correlated well with small angle neutron scattering observations. For cationic and amphoteric gels, an increase in cationic charge content leads to increased swelling and weaker mechanics on the macroscale, directly related to the microscopic observations of less ordered, globular chains comprising the hydrogel based on the Porod exponent from the SANS fit. In contrast, the stiffer and slower-degrading anionic gel bulk properties are reflected in increased apparent ordering and alignment in these hydrogels, as inferred through the need for a stretch factor to achieve accurate fits and the higher Porod exponents observed from the SANS analysis as well as the different interaction enthalpies observed in the ITC measurements. These structure-property correlations relevant to in situ-gelling hydrogels from precursor polymers can aid in the rational design of injectable gels with defined properties for potential applications.

5.5 Conclusions

Incorporating charge into in situ covalently gelling POEGMA hydrogels can significantly alter the physicochemical properties of the gels through rational manipulation of the internal gel morphology. Macroscopically, gelation times, swelling responses, and degradation kinetics were greatly affected by charge incorporation, with gels containing more cationic charge density gelling slower, swelling more, and degrading faster. Amphoteric hydrogels can support secondary network formation via charge complexation, resulting in stronger mechanics and slower degradation times at physiological pH than the corresponding neutral gels. However,

the significant increase in mechanics and faster gelation times of anionic gels were less expected and motivated further investigation of the nanoscale interactions potentially leading to these properties. Isothermal titration calorimetry indicates significantly different mixing enthalpies between gels prepared with anionic or neutral aldehyde-functionalized precursor polymers, while small angle neutron scattering indicates stretching of the polymer chains in the anionic gels consistent with a zippered chain structure formed via secondary dipole-dipole/hydrogen bonding interactions. In addition to adding fundamental insight into how the balance between in situ covalent gelation and non-covalent interactions affects the properties of injectable hydrogels, the structure-property correlations developed herein will significantly inform the design of better defined matrices for potential drug delivery and tissue engineering applications.

Supporting Information Available. ^{1}H-NMR of the precursor polymers used, titration analysis of the degree of ionization as a function of pH for each charged precursor polymer, transparency images for the different gels studied, raw ITC data, and comparisons between raw and fitted SANS profiles are provided.

5.6 Acknowledgements

The Natural Sciences and Engineering Research Council of Canada (NSERC) is acknowledged for funding this work (Strategic Project Grant STPGP 447372 and Discovery Grant RGPIN 356609). This work utilized facilities supported in part by the National Science Foundation under Agreement No. DMR-1508249. We acknowledge the support of the National Institute of Standards and Technology, U.S. Department of Commerce, in providing the neutron research facilities used in this work and Boualem Hammouda of NCNR for his assistance with the SANS experiments.

5.7 References

(1) Papavasiliou, G.; Sokic, S.; Turturro, M. Synthetic PEG Hydrogels as Extracellular Matrix Mimics for Tissue Engineering Applications. *Interchopen* **2005**, 111-134.

(2) Raeber, G. P.; Lutolf, M. P.; Hubbell, J. A. Molecularly Engineered PEG Hydrogels: A Novel Model System for Proteolytically Mediated Cell Migration. *Biophys. J.* **2005**, 89, 1374–1388.

(3) Qiu, Y.; Lim, J. J.; Scott, L.; Adams, R. C.; Bui, H. T.; Temenoff, J. S. PEG-Based Hydrogels with Tunable Degradation Characteristics to Control Delivery of Marrow Stromal Cells for Tendon Overuse Injuries. *Acta Biomater.* **2011**, 7, 959–966.

(4) Nuttelman, C. R.; Rice, M. A; Rydholm, A. E.; Salinas, C. N.; Shah, D. N.; Anseth, K. S. Macromolecular Monomers for the Synthesis of Hydrogel Niches and Their Application in Cell Encapsulation and Tissue Engineering. *Prog. Polym. Sci.* **2008**, 33, 167–179.

(5) McCall, J. D.; Anseth, K. S. Thiol-Ene Photopolymerizations Provide a Facile Method to Encapsulate Proteins and Maintain Their Bioactivity. *Biomacromolecules* **2012**, 13, 2410–2417.

(6) Bakaic, E.; Smeets, N. M. B.; Dorrington, H.; Hoare, T. "Off-the-Shelf" thermoresponsive Hydrogel Design: Tuning Hydrogel Properties by Mixing Precursor Polymers with Different Lower-Critical Solution Temperatures. *RSC Adv.* **2015**, 5, 33364–33376.

(7) Smeets, N. M. B.; Bakaic, E.; Patenaude, M.; Hoare, T. Injectable Poly(oligoethylene Glycol Methacrylate)-Based Hydrogels with Tunable Phase Transition Behaviours: Physicochemical and Biological Responses. *Acta Biomater.* **2014**, 10, 4143–4155.

(8) Smeets, N. M. B.; Bakaic, E.; Yavitt, F. M.; Yang, F.; Rheinstädter, M. C.; Hoare, T. Probing the Internal Morphology of Injectable Poly(oligoethylene Glycol Methacrylate) Hydrogels by Light and Small-Angle Neutron Scattering. *Macromolecules* **2014**, 47, 6017–6027.

(9) Luzon, M.; Boyer, C.; Peinado, C.; Corrales, T.; Whittaker, M.; Tao, L. E. I.; Davis, T. P. Water-Soluble, Thermoresponsive, Hyperbranched Copolymers Based on PEG-Methacrylates : Synthesis , Characterization , and LCST Behavior. *J. Polym. Sci. Part A Polym. Chem.* **2010**, 48, 2783–2792.

(10) Lutz, J. F. Thermo-Switchable Materials Prepared Using the OEGMA-Platform. *Adv. Mater.* **2011**, 23, 2237–2243.

(11) Lutz, J. F. Polymerization of Oligo(ethylene Glycol) (Meth)acrylates: Toward New Generations of Smart Biocompatible Materials. *J. Polym. Sci. Part A Polym. Chem.* **2008**, 46, 3459–3470.

(12) Smeets, N. M. B.; Bakaic, E.; Patenaude, M.; Hoare, T. Injectable and Tunable Poly(ethylene Glycol) Analogue Hydrogels Based on Poly(oligoethylene Glycol Methacrylate). *Chem. Commun.* **2014**, 50, 3306–3309.

(13) Smeets, N. M. B.; Patenaude, M.; Kinio, D.; Yavitt, F. M.; Bakaic, E.; Yang, F. C.; Rheinstädter, M.; Hoare, T. Injectable Hydrogels with in Situ-Forming Hydrophobic Domains: Oligo(D , L -Lactide) Modified Poly(oligoethylene Glycol Methacrylate) Hydrogels. *Polym. Chem.* **2014**, 5, 6811–6823.

(14) Lord, M. S.; Stenzel, M. H.; Simmons, A.; Milthorpe, B. K. The Effect of Charged Groups on Protein Interactions with poly(HEMA) Hydrogels. *Biomaterials* **2006**, 27, 567–575.

(15) Van Tomme, S. R.; van Nostrum, C. F.; de Smedt, S. C.; Hennink, W. E. Degradation Behavior of Dextran Hydrogels Composed of Positively and Negatively Charged Microspheres. *Biomaterials* **2006**, 27, 4141–4148.

(16) Schneider, G. B.; English, A.; Abraham, M.; Zaharias, R.; Stanford, C.; Keller, J. The Effect of Hydrogel Charge Density on Cell Attachment. *Biomaterials* **2004**, 25, 3023–3028.

(17) Dadsetan, M.; Knight, A. M.; Lu, L.; Windebank, A. J.; Yaszemski, M. J. Stimulation of Neurite Outgrowth Using Positively Charged Hydrogels. *Biomaterials* **2009**, 30, 3874–3881.

(18) Samal, S. K.; Dash, M.; Van Vlierberghe, S.; Kaplan, D. L.; Chiellini, E.; van Blitterswijk, C.; Moroni, L.; Dubruel, P. Cationic Polymers and Their Therapeutic Potential. *Chem. Soc. Rev.* **2012**, 41, 7147–7194.

(19) Farahani, V. Hydrogels in Controlled Drug Delivery Systems. *Iranian Polym. J.* **2009**, 18, 63–88.

(20) Nasimova, I.; Karino, T.; Okabe, S.; Nagao, M.; Shibayama, M. Small-Angle Neutron Scattering Investigation of Pressure Influence on the Structure of Weakly Charged Poly(N -Isopropylacrylamide) Solutions and Gels. *Macromolecules* **2004**, 37, 8721–8729.

(21) Shibayama, M.; Kawakubo, K.; Ikkai, F.; Imai, M. Small-Angle Neutron Scattering Study on Charged Gels in Deformed State. *Macromolecules* **1998**, 31, 2586–2592.

(22) Matsunaga, T.; Sakai, T.; Akagi, Y.; Chung, U. Il; Shibayama, M. SANS and SLS Studies on Tetra-Arm PEG Gels in as-Prepared and Swollen States. *Macromolecules* **2009**, 42, 6245–6252.

(23) Shibayama, M. Small-Angle Neutron Scattering on Polymer Gels: Phase Behavior, Inhomogeneities and Deformation Mechanisms. *Polym. J*. **2011**, 43, 18–34.

(24) Matsunaga, T.; Sakai, T.; Akagi, Y.; Chung, U.; Shibayama, M. Structure Characterization of Tetra-PEG Gel by Small-Angle Neutron Scattering. *Macromolecules* **2009**, 42, 1344–1351.

(25) Smeets, N. M. B.; Bakaic, E.; Yavitt, F. M.; Yang, F.; Rheinstädter, M. C.; Hoare, T. Probing the Internal Morphology of Injectable Poly(oligoethylene Glycol Methacrylate) Hydrogels by Light and Small-Angle Neutron Scattering. *Macromolecules* **2014**, 47, 6017–6027.

(26) Smeets, N. M. B.; Bakaic, E.; Patenaude, M.; Hoare, T. Injectable and Tunable Poly(ethylene Glycol) Analogue Hydrogels Based on Poly(oligoethylene Glycol Methacrylate). *Chem. Commun*. **2014**, 50, 3306–3309.

(27) Hoare, T.; Pelton, R. Titrametric Characterization of pH-Induced Phase Transitions in Functionalized Microgels. *Langmuir* **2006**, 22, 7342–7350.

(28) Velazquez-Campoy, A.; Freire, E. Isothermal Titration Calorimetry to Determine Association Constants for High-Affinity Ligands. *Nat. Protoc.* **2006**, 1, 186–191.

(29) De France, K. J.; Chan, K. J. W.; Cranston, E. D.; Hoare, T. Enhanced Mechanical Properties in Cellulose Nanocrystal-Poly(oligoethylene Glycol Methacrylate) Injectable Nanocomposite Hydrogels through Control of Physical and Chemical Cross-Linking. *Biomacromolecules* **2016**, 17, 649–660.

(30) Peppas, N. A.; Hilt, J. Z.; Khademhosseini, A.; Langer, R. Hydrogels in Biology and Medicine: From Molecular Principles to Bionanotechnology. *Adv. Mater*. **2006**, 18, 1345–1360.

(31) Dong, Y.; Saeed, A. O.; Hassan, W.; Keigher, C.; Zheng, Y.; Tai, H.; Pandit, A.; Wang, W. “One-Step” Preparation of Thiol-Ene Clickable PEG-Based Thermoresponsive Hyperbranched Copolymer for In Situ Crosslinking Hybrid Hydrogel. *Macromol. Rapid Commun.* **2011**, 33, 120–126.

(32) Hammouda, B.; Ho, D. L.; Kline, S. Insight into Clustering in Poly (Ethylene Oxide) Solutions. *Macromolecules* **2004**, 6932–6937.

(33) Hammouda, B.; Ho, D. L. Insight Into Chain Dimensions in PEO/Water Solutions. *J. Polym. Sci. Part B Polym. Phys.* **2007**, 45, 1390–1398.

(34) Shibayama, M.; Ikkai, F.; Shiwa, Y.; Rabin, Y. Effect of Degree of Cross-Linking on Spatial Inhomogeneity in Charged Gels. I. Theoretical Predictions and Light Scattering Study. *J. Chem. Phys.* **1997**, 107, 5227.

(35) Hammouda, B. SANS from Polymers: Review of the Recent Literature. *Polym. Rev.* **2010**, 50, 14–39.

(36) Tirumala, V. R.; Ilavsky, J.; Ilavsky, M. Effect of Chemical Structure on the Volume-Phase Transition in Neutral and Weakly Charged Poly (N -Alkyl(meth)acrylamide) Hydrogels Studied by Ultrasmall-Angle X-Ray Scattering. *J. Chem. Phys.* **2006,** 124.

(37) Berts, I.; Gerelli, Y.; Hilborn, J.; Rennie, A. R. Structure of Polymer and Particle Aggregates in Hydrogel Composites. *J. Polym. Sci. Part B Polym. Phys.* **2013**, 51, 421–429.

(38) Hourdet, D.; L, F.; Durand, A.; Lafuma, F.; Audebert, R.; Cotton, J. Small-Angle Neutron Scattering Study of Microphase Separation in Thermoassociative Copolymers. *Macromolecules* **1998**, 31, 5323–5335.

(39) Shibayama, M. Small-Angle Neutron Scattering on Polymer Gels: phase behaviour, inhomogeneities and deformation mechanisms. *Polymer Journal.* **2011**, 1, 18-34.

(40) Horkay, F.; Hammouda, B. Small-Angle Neutron Scattering from Typical Synthetic and Biopolymer Solutions. *Colloid Polym. Sci.* **2008**, 286, 611–620.

(41) van de Wetering, P.; Zuidam, N. J.; van Steenbergen, M. J.; van der Houwen, O. A. G. J.; Underberg, W. J. M.; Hennink, W. E. A Mechanistic Study of the Hydrolytic Stability of Poly (2-(Dimethylamino) Ethyl Methacrylate). *Macromolecules* **1998**, 31, 8063–8068.

(42) Zhai, M.; Chen, Y.; Yi, M.; Ha, H. Swelling Behaviour of a New Kind of Polyampholyte Hydrogel Composed of Dimethylaminoethyl Methacrylate and Acrylic Acid. *Polym. Int.* **2004**, 53, 33–36.

(43) Shimoda, A.; Sawada, S.; Kano, A.; Maruyama, A.; Moquin, A.; Winnik, F. M.; Akiyoshi, K. Dual Crosslinked Hydrogel Nanoparticles by Nanogel Bottom-up Method for Sustained-Release Delivery. *Colloids Surf. B. Biointerfaces* **2012,** 99, 38–44.

(44) Jeon, O.; Samorezov, J. E.; Alsberg, E. Single and Dual Crosslinked Oxidized Methacrylated alginate/PEG Hydrogels for Bioadhesive Applications. *Acta Biomater.* **2014**, 10, 47–55.

(45) Desiraju, G. R. Chemistry beyond the Molecule. *Nature* **2001**, 412, 397–400.

(46) Mathur, A. M.; Drescher, B.; Scranton, A. B.; Klier, J. Polymeric Emulsifiers Based on Reversible Formation of Hydrophobic Units. *Nature* **1998**, 392, 367–370.

(47) Zeghal, M.; Auvray, L. Structure of Polymer Complexes in Water. *Europhys. Lett.* **1999,** 45, 482–487.

(48) Hammouda, B. Probing Nanoscale Structures-The SANS toolbox. National Institute of Standards and Technology Center for *Neutron Research***.2008**, 1-717.

(49) Wisotzki, E. I.; Tempesti, P.; Fratini, E.; Mayr, S. G. Influence of High Energy Electron Irradiation on the Network Structure of Gelatin Hydrogels as Investigated by Small-Angle X-Ray Scattering (SAXS). *Phys. Chem Chem. Phs.* **2017**, 19, 12064-12074.

(50) Hammouda, B.; Worcester, D. The Denaturation Transition of DNA in Mixed Solvents. *Biophys. J.* **2006**, 91, 2237–2242.

(51) Pasut, G.; Veronese, F.M. Polymer-drug conjugation, recent acheivements and strategies. *Prog. Polym. Sci.* **2007**, 32, 933–961.

(52) Ryde, U.; A Fundamental View of Enthalpy–entropy Compensation. *Medchemcomm.* **2014**, 5, 1324-1336.

5.8 TOC Graphic

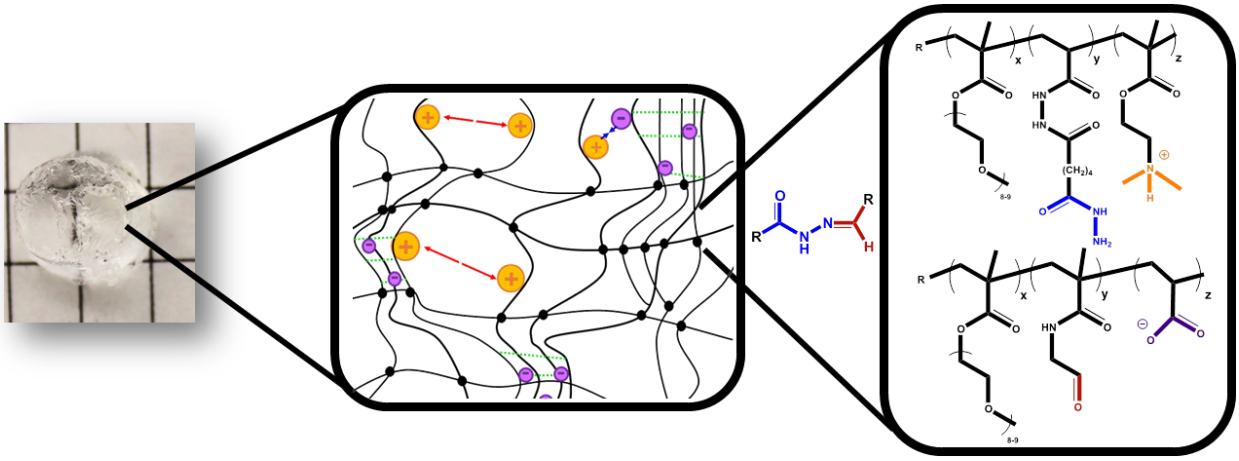

5.9 Supporting Information

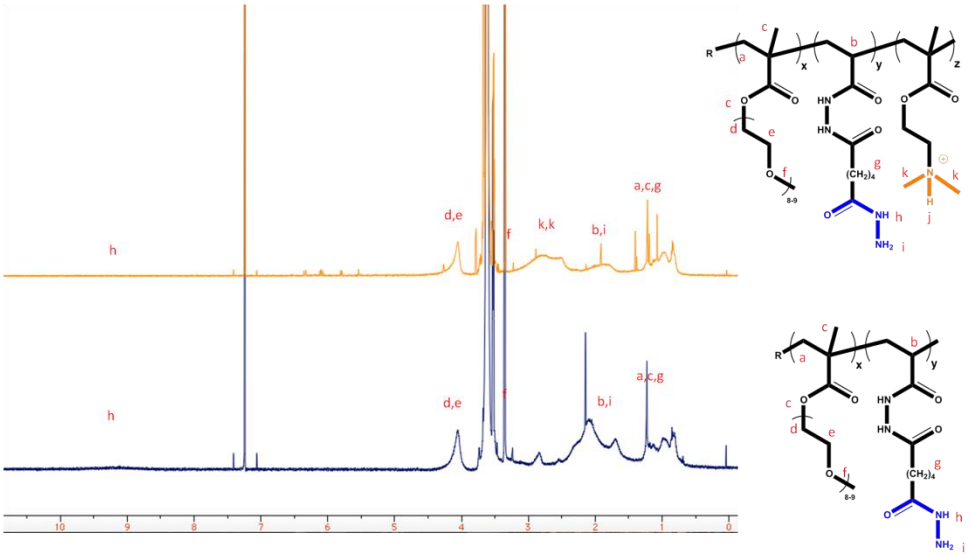

S5.1 ^{1}H-NMR spectra for (POEGMA-DMAEMA-ADH) (orange) and (POEGMA-ADH) (blue).

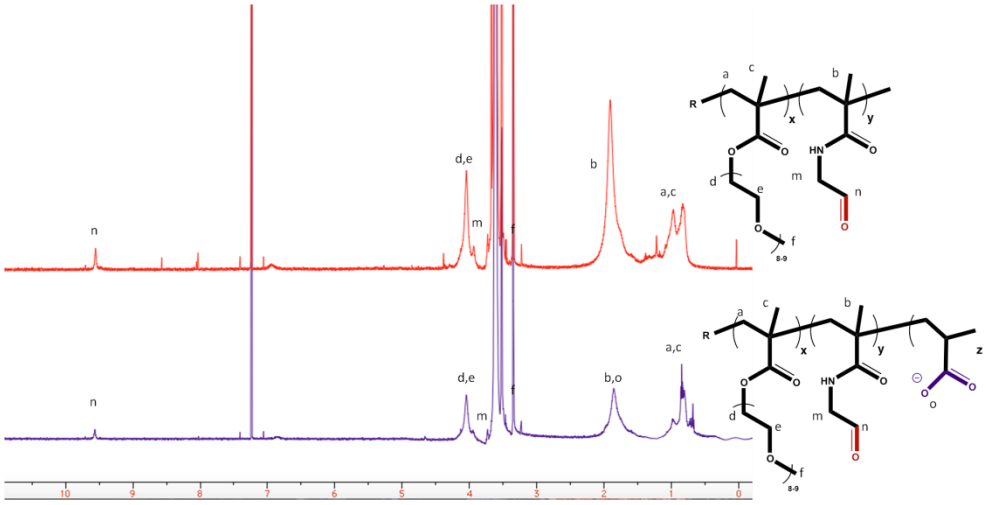

S5.2 ^{1}H-NMR spectra for (POEGMA-AA-Ald) (blue) and (POEGMA-Ald) (blue).

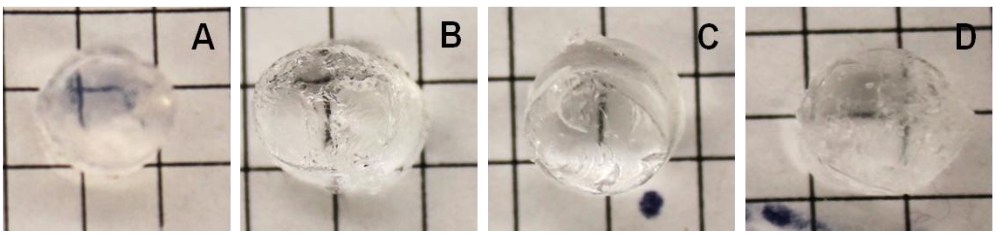

S5.3 Optical morphology of the (A) neutral and (B) cationic, (C) amphoteric and (D) anionic charged hydrogels.

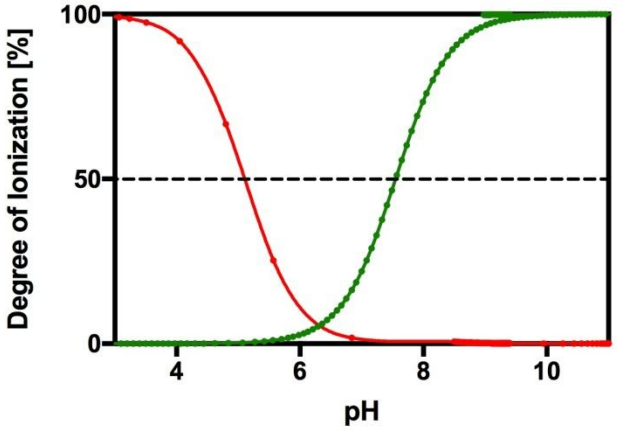

Figure S5.4: Degree of ionization measured using potentiometric titration with 0.1M NaOH at 22˚C of $PO_{100}H_{30}C_{20}$ (red) and $PO_{100}A_{30}D_{20}$ (green) precursor polymers.

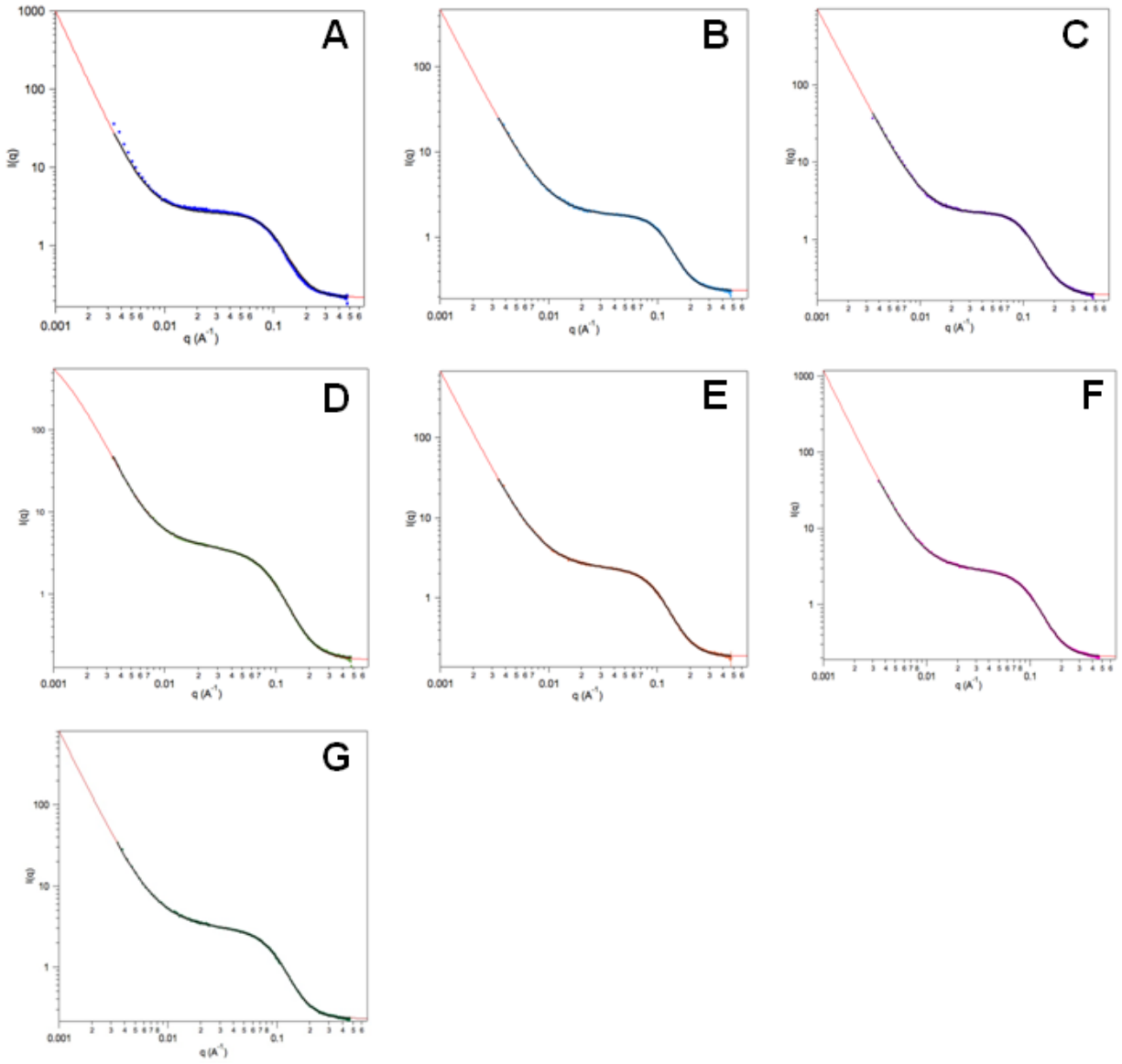

Figure S5.5: (B) Scattering intensities with fits using Porod model (in 10 mM D_2O PBS, 22˚C): **(A)** PO_{100} **(B)** PO_{100}-100/0 **(C)** PO_{100}-100/100 **(D)** PO_{100}-0/100 **(E)** PO_{100}-50/50 **(F)** PO_{100}-75/25 and **(G)** PO_{100}-25/75.

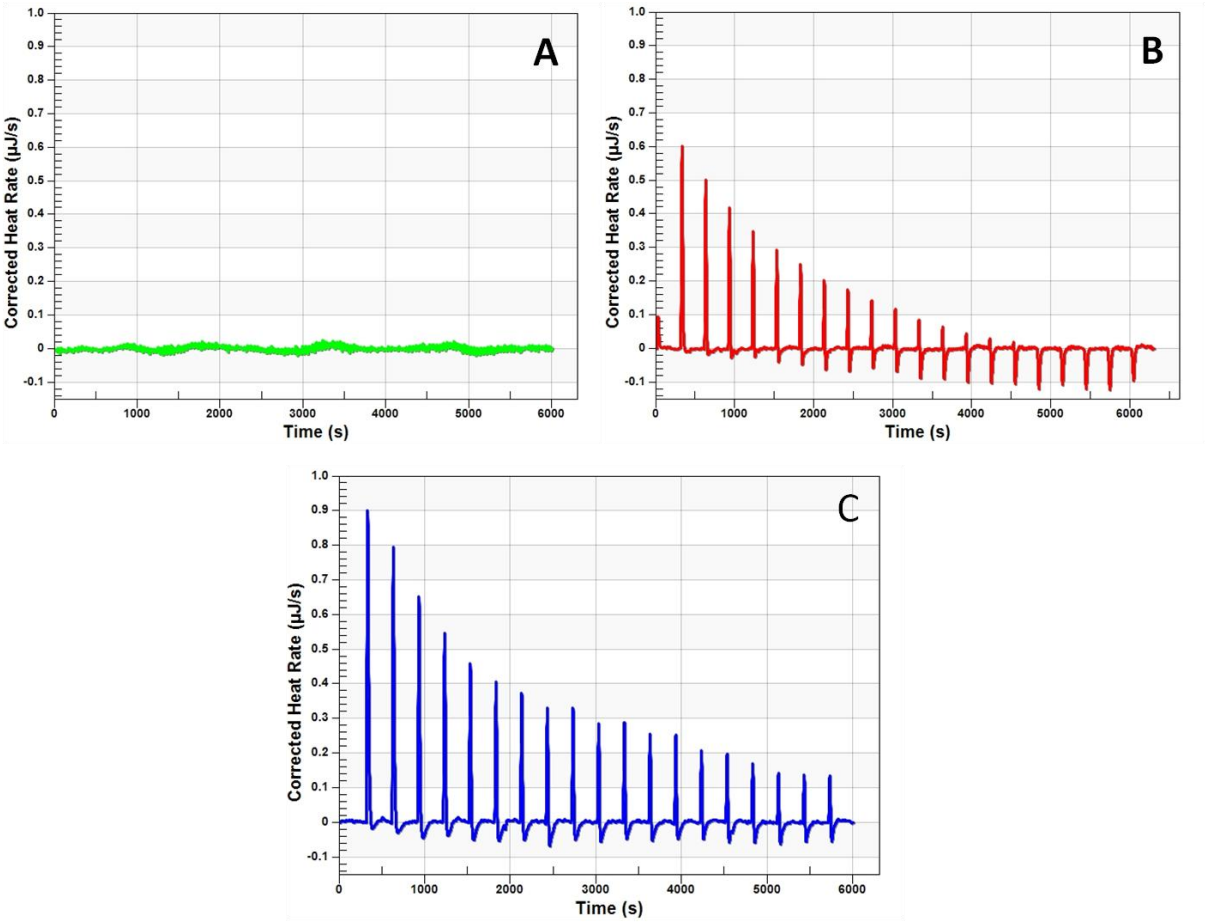

Figure S5.6 Corrected heat rates (calculated by subtracting the heat of dilution of 10 mM PBS) associated with mixing (A) POA + POH (uncharged but covalently crosslinkable), (B) POA(-) + POH (charged and covalently crosslinkable) and (C) POA(-) + unfunctionalized POEGMA (charged, not covalently crosslinkable).

Chapter 6: Injectable and Degradable Poly(Oligoethylene glycol methacrylate) Hydrogels With Tunable Charge Densities: Adhesive Peptide-Free Cell Scaffolds

Preface:

This chapter investigates the role of charge moieties within hydrogel networks and their interactions with biological proteins and cells. We have developed novel thermoresponsive charged POEGMA precursors that form injectable and degradable cationic, amphoteric, and anionic hydrogels through reactive hydrazone crosslinking. The physiochemical properties (gelation, swelling, degradation, mechanics) display defined properties of dual crosslinking networks (ionic and covalent crosslinking). Biological properties are further investigated to shown the positive support of 3T3 mouse fibroblast cells and ARPE-19 human retinal cells in 2D and 3D charged matrices respectively.

Emilia Bakaic[§], Niels M.B. Smeets[§], Maryam Badv[⊥], Megan Dodd[§], Owen Barrigar[§], Emily, Siebers[‖], Michael Lawlor[‖], Heather Sheardown[§] and Todd Hoare[§*]

[§]Department of Chemical Engineering, McMaster University, 1280 Main Street West, Hamilton, Ontario, Canada L8S 4L8.

[⊥]School of Biomedical Engineering, McMaster University, 1280 Main Street West, Hamilton, Ontario, Canada L8S 4L8.

[‖] Department of Pathology and Laboratory Medicine and Neuroscience Research Center, Medical College of Wisconsin, 8701 Watertown Plank Rd, Milwaukee, Wisconsin, USA, 53226.

Keywords

Hydrogels; pH-responsive materials; thermoresponsive materials; poly(oligoethylene glycol methacrylate); *in situ* gelling hydrogels; protein adsorption; cell encapsulation; charged hydrogels; retinal regeneration

Abstract

Injectable, dual-responsive, and degradable poly(oligo ethylene glycol methacrylate) (POEGMA) hydrogels are demonstrated to offer potential for cell delivery. Charged groups were incorporated into hydrazide and aldehyde-functionalized thermoresponsive POEGMA gel precursor polymers via the copolymerization of N,N'-dimethylaminoethyl methacrylate (DMAEMA) or acrylic acid (AA) to create dual temperature/pH responsive *in situ*-gelling hydrogels that can be injected via narrow gauge needles. The incorporation of charge significantly broadens the swelling, degradation, and rheological profiles achievable with injectable POEGMA hydrogels without significantly increasing non-specific protein adsorption or chronic inflammatory responses following *in vivo* subcutaneous injection. However, significantly different cell responses are observed upon charge incorporation, with charged gels significantly improving 3T3 mouse fibroblast cell adhesion in 2D and successfully delivering viable and proliferating ARPE-19 human retinal epithelial cells via an “all-synthetic” matrix that does not require the incorporation of cell-adhesive peptides.

6.1 Introduction

In situ-gelling injectable hydrogels have attracted wide-spread research attention given the practical limitations in using conventional bulk hydrogels *in vivo*.[1–3] Solutions of low-viscosity gel precursor polymers can be prepared *ex vivo* containing various drugs, therapeutics, growth factors or cells, and injected *in vivo* to rapidly form 3-dimentional water-swollen networks useful for filling tissue void defects, delivering drug reservoirs, or transplanting cells.[4,5] Various physical (e.g. temperature[6,7], ionic[8], light[9,10], pressure[11]) and chemical (e.g. *in situ* click chemistries,[2,12] enzyme mediated[13]) crosslinking approaches have been explored for the design of such materials. The most potentially translatable approaches allow facile chemical modification to tune the physicochemical gel properties, facilitate gelation and degradation *in vivo* over well-defined time scales, and are either thermodynamically or kinetically bio-orthogonal to avoid or minimize non-specific protein or tissue interactions and thus subsequent inflammation.

While several natural[14–16] and synthetic[17–19] polymers have been investigated in this context, stimuli-responsive polymers have demonstrated particular potential as biomedical materials based on their ability to specifically respond to varying physiological stimuli[6,20,21]. Temperature responsive hydrogels, typically formed by crosslinking polymers exhibiting a characteristic lower critical solution temperature (LCST), enable reversible swelling/shrinking phase transitions at tunable temperatures relative to physiological temperature. For example, the widely known thermoresponsive polymer poly(N-isopropylacrylamide) (PNIPAM) produces hydrogels with a volume phase transition temperature (VPTT) of 32˚C, switching from a swollen hydrophilic matrix at T<VPTT to a less hydrophilic and more collapsed structure at T>VPTT.[22] More recently, increasing interest in biomedical applications in particular has focused on poly(oligo ethylene glycol methacrylate) (POEGMA) due to the specific advantages of POEGMA relative to PNIPAM: (1) the VPTT can be tuned precisely from 22-90˚C by varying the length of ethylene oxide (EO) repeat units on the side chain[23]; and (2) the degradation products are all generally recognized as safe (GRAS) materials,[24] better facilitating potential clinical translation. The reversible thermoresponsive swelling properties of such materials have been widely applied in pulsatile or triggered drug delivery applications,[25] while the reversible hydrophilic-to-

(less hydrophilic) transition has been applied to design materials exhibiting reversible cell affinity or switchable cell sheet delamination.[26] In particular, the reversible control over the cell-gel interface provided by thermal switching offers potential benefits in the context of tissue engineering, in which reducing cell reliance on the synthetic matrix as a function of time (as cells make their own matrix) is generally desirable to promote functional tissue regeneration.[26,27] Our group has recently reported extensively on injectable, hydrazone-crosslinked POEGMA hydrogels prepared by co-extrusion of hydrazide and aldehyde-functionalized hydrogels that facilitate the minimally-invasive delivery of such gels *in vivo*[17,21,28], removing a key translational barrier to the use of such materials in the clinic.

pH-responsive hydrogels have also attracted considerable interest given their capacity to reversibly respond to changes in environmental pH, which naturally undergoes substantial variations both as part of normal function (e.g. within the gastrointestinal tract or vagina) or as a response to a diseased state (e.g. in tumors or wounds). pH-responsive hydrogels have been applied to site-specific drug delivery in the stomach[29,30] or the colon[31], microenvironment-specific delivery responsive to disease[30], and to promote tissue regeneration through the controlled release of growth factors during cell maturation.[32,33] Most work on the use of such gels in biomedical applications has focused on crosslinking pH-sensitive natural (chitosan[1,34], alginate[35]) and/or synthetic (poly(acrylic acid) (PAA)[36,37], polyethyleneimine (PEI) and poly (N,N'-dimethylaminoethyl methacrylate) (PDMAEMA))[38,39] polymers, all of which have different pK_a values, backbone hydrophobicities, and effective ionization ranges to enable tuning of the pH-driven response[40]. Amphoteric gels that contain both cationic and anionic charges have attracted particular attention both due to their demonstrated capacity to suppress non-specific protein adsorption (thought to be related to their protein-mimetic charge distributions)[41,42] as well as their ability to form ionic crosslinks under near-neutral pH conditions in which both the cationic and anionic functional groups are charged,[43] providing an additional crosslinking mechanism to enhance the mechanics of the resulting hydrogels.

Combining the advantageous properties of more than one of these "smart" responses into a single multi-responsive hydrogel can enable additional control over gel properties. For example, Khatoon et al. developed temperature and pH responsive PNIPAM-chitosan hydrogel

wound dressings for the release of gentamycin sulfate (GS) that trigger release of the antibiotic as both the temperature and pH of the wound environment was increased; alternately, we have designed dual-responsive microgels that utilize the thermal phase transition to instantaneously gel at an injection site followed by the pH-induced phase transition to de-aggregate and thus release the microgels at a controlled rate[44]. However, to our knowledge, there is no example of a dual thermoresponsive/pH responsive covalently *in situ*-gelling hydrogel that can exploit the benefits of these dual responses while also being capable of minimally invasive delivery *in vivo*.

Herein, we disclose the design of charged, thermoresponsive injectable and degradable POEGMA hydrogels prepared from precursor polymers exhibiting both thermal phase transitions as well as well-defined charge distributions (positive, negative, or amphoteric) that enable both pH-induced phase transitions and pH-tunable secondary (ionic) crosslinking. The dual responsiveness coupled with the switchable secondary crosslinking is demonstrated to result in hydrogels with substantially broadened swelling, degradation and mechanical profiles amenable to use in biomedical applications; at the same time, no significant increase in non-specific protein adsorption or chronic tissue responses following subcutaneous injection is observed as a result of charge incorporation, a result attributable to the brush copolymer structure of the POEGMA backbone polymer. We then apply these desirable physicochemical properties to demonstrate the potential of charged POEGMA injectable hydrogels for delivering retinal pigment epithelial (RPE) cells, a potential therapeutic strategy to arrest or reverse vision loss in patients with age-related macular degeneration (AMD) or retinitis pigmentosa (RP) by replacing and stimulating retinal epithelial growth once the native epithelium has been damaged or lost. Given the adhesion-dependent properties of RPE cells (which adhere to the basal membrane *in vivo* for support[45]), polymeric delivery vehicles that can support RPE adhesion while still enabling injection through narrow gauge needles into the back of the eye are essential to translate such therapies to the clinic. The combination of the thermoresponsive POEGMA backbone (facilitating cell interactions without compromising low non-specific protein adsorption) and charged functional groups (enabling electrostatic interactions between the matrix and the cells) within an injectable platform is demonstrated to

support high cell viability and, in some cases, proliferation without cell clumping over extended time periods, as desirable in such a vehicle.

6.2 Experimental

6.2.1 Materials: Oligo(ethylene glycol) methyl ether methacrylate with an average number-average molecular weight of 475 g/mol^{-1} ($OEGMA_{475}$, Sigma Aldrich, 95%) and di(ethylene glycol) methyl ether methacrylate ($M(EO)_2$ MA), Sigma Aldrich, 95%) were purified using an aluminum oxide packed column (Sigma Aldrich, type CG-20) to remove the methyl ether hydroquinone (MEHQ) and butylated hydroxytoluene (BHT) inhibitors. N-(2,2-dimethoxyethyl) methacrylamide (DMAEAm, Sigma Aldrich, 98%) was synthesized according to a previously reported procedure.[17] Acrylic acid (AA, Sigma Aldrich, 99%), N,N-dimethylaminoethyl methacrylate (DMAEMA, Sigma Aldrich 98%), adipic acid dihydrazyde (ADH, Alfa Aesar, 98%), N'-ethyl-N-(3-dimethylaminopropyl)-carbodiimide (EDC, Carbosynth, Compton CA, commercial grade), thioglycolic acid (TGA, Sigma Aldrich, 98%), bovine serum albumin (BSA, Sigma Aldrich, >96%), fluorescein isothiocyanate (FITC, Sigma Aldrich, 90%) and 2,2-azobisisobutryic acid dimethyl ester (AIBMe, Wako Chemicals, 98.5%) were used as received. For all experiments, Milli-Q grade distilled deionized water (DIW 18.2 MΩ cm resistivity) was used. Dimethyl sulfoxide (DMSO, reagent grade) was purchased from Caledon Laboratory Chemicals (Georgetown, ON). Hydrochloric acid (1 M) was received from LabChem Inc. (Pittsburgh, PA). Human retinal pigment epithelial cells (ARPE-19) were expanded in Dulbecco's Modified Growth Medium F12 (DMEM-F12, ThermoFisher Scientific) supplemented with 10% fetal bovine serum and 1% Penicillin Streptomycin (ThermoFisher Scientific), and cultured at 37°C with 5% CO_2 on tissue culture polystyrene (TCPS, Greiner).

6.2.2 Synthesis of neutral and charged hydrazide-functionalized POEGMA precursors (POH and POHC): Hydrazide functionalized POEGMA precursor polymers ($PO_{10}H_{30}$) were synthesized as described previously,[28] while cationic hydrazide-functionalized POEGMA precursor polymers ($PO_{10}H_{30}D_{20}$) were synthesized using a modification of that recipe. Briefly, AIBMe (37 mg), $M(EO)_2MA$ (3.9 g), $OEGMA_{475}$ (0.10 g), cationic functional monomer DMEAMA (0 µL for $PO_{10}H_{30}$,

1290 µL for $PO_{10}H_{30}D_{20}$), AA (523 µL for $PO_{10}H_{30}$, and 714 µL for $PO_{10}H_{30}D_{20}$), and TGA (7.5 µL) were dissolved in 1,4-dioxane (20 mL). Additional AA was added in the cationic precursor recipe to maintain an equivalence between the number of AA residues per chain (and thus degree of hydrazide functionalization) between neutral and cationic precursors, enabling matching of the reactive functional group contents and thus crosslinking potential in each precursor. After purging for 30 min, the flask was sealed and submerged in a pre-heated oil bath at 75°C for 4 hours under magnetic stirring. The solvent was removed, and the resulting dry polymer was dissolved in 100 mL DIW. Adipic acid dihydrazide (4.33 g for $PO_{10}H_{30}$, 6.85g for $PO_{10}H_{30}D_{20}$), was added, the pH was lowered to pH = 4.75 using 0.1 M HCl, and then EDC (1.93 g for $PO_{10}H_{30}$, 2.44g for $PO_{10}H_{30}D_{20}$) was added, with the pH maintained at pH = 4.75 by the dropwise addition of 0.1 M HCl over the subsequent 4 hours. The solution was left to stir overnight, dialyzed (MWCO= 3500 g mol^{-1}) against DIW for a minimum of 6 cycles, and lyophilized. The polymers were stored as 20 w/w% solutions in PBS at 4°C. The degree of functionalization was determined from conductometric base-into-acid titration (ManTech Associates), using a 0.1 wt% polymer solution in 1 mM NaCl as the sample and 0.1 M NaOH as the titrant. Hydrazide polymers are labeled using the convention $PO_xH_yC_z$, where x equals the mole fraction of $OEGMA_{475}$ among the PEG-based monomers added (the remainder of which is $M(EO)_2MA$), y equals the mol % of total monomer residues functionalized with hydrazide reactive groups, and z denotes the mol % of charged monomer incorporated into the polymer.

6.2.3 Synthesis of neutral and charged aldehyde-functionalized POEGMA precursors (POA and POAD): Aldehyde functionalized POEGMA precursor ($PO_{10}A_{30}$) was synthesized as described previously,[28] while anionic aldehyde functionalized POEGMA precursor ($PO_{10}A_{30}C_{20}$) was synthesized using a modification of that recipe. Briefly, AIBMe (50 mg), $M(EO)_2MA$ (3.9 g), $OEGMA_{475}$ (0.10 g), acetal functional monomer DMAEAm (1.30 g for $PO_{10}A_{30}$, 1.80 g for $PO_{10}A_{30}D_{20}$), anionic functional monomer AA (0 g for $PO_{10}A_{30}$, 0.52 g for $PO_{10}A_{30}C_{20}$), and TGA (7.5 µL) were dissolved in 1,4-dioxane (20 mL). Similar to the hydrazide polymer synthesis, the DMAEAm content was adjusted to ensure an equivalent number of aldehyde groups and thus crosslinking potential per polymer chain produced. After purging for at least 30 min, the flask

was sealed and submerged in a pre-heated oil bath at 75°C for 4 hours under magnetic stirring. The solvent was removed, and the polymer was subsequently dissolved in 100 mL of 0.5 M HCl. The solution was left to stir for 24 hours, dialyzed (MWCO= 3500 g mol^{-1}) against DIW for a minimum of 6 cycles, and lyophilized. The polymers were stored as 20 w/w% solutions in PBS at 4°C. The degree of functionalization was determined from ^{1}H-NMR analysis, comparing the integral values of the -OCH_3 signal (3H, δ = 3.35-3.45 ppm) and the –CHO signal (1H, δ = 9.50-9.58 ppm). Aldehyde polymers are labeled using the convention $PO_xA_yD_z$, where x equals the mole fraction of $OEGMA_{475}$ among the PEG-containing monomers (the remainder of which was $M(EO)_2MA$), y equals the mol % of total monomer residues functionalized with aldehyde reactive groups, and z denotes the mol % of charged monomer incorporated into the polymer.

6.2.4 Synthesis of fluorescein-isothiocyanate labelled proteins: Fluorescein-isothiocyanate (FITC)-labelled bovine serum albumin (BSA-FITC) and FITC labeled lysozyme (Lyz-FITC) were prepared by dissolving 50 mg of the protein in a 100 mL carbonate buffer at pH = 9.0. FITC (1 mg) was then added, and the solution was incubated at room temperature for at least 12 h under gentle mechanical agitation. The FITC-labelled proteins were subsequently dialyzed against deionized water for 6+ cycles and lyophilized. The isolated conjugated proteins were stored at -4°C in the dark.

6.2.5 Chemical Characterization: Size exclusion chromatography (SEC) was performed using a Waters 2695 separations module equipped with a Waters 2996 photodiode array detector, a Waters 2414 refractive index detector, a Waters 2475 multi λ fluorescence detector and four Polymer Labs PLgel individual pore size columns maintained at 40°C, with 5 μm bead size and pore sizes of 100, 500, 103 and 105Å. Tetrahydrofuran (THF) was used as the eluent at a flow rate of 1.0 mL/min, and polystyrene standards were used to calibrate the instrument. ^{1}H-NMR was performed using a Bruker AVANCE 600 MHz spectrometer and deuterated chloroform as the solvent. A Variant Cary Bio 100 UV-vis spectrophotometer was used to measure the LCST of the polymer precursor chains and the VPTT of the hydrogels. The polymers were dissolved at a concentration of 1 mg/mL in PBS (pH = 7.4), and the absorbance of the polymer solution was

recorded at 500 nm at every 0.5°C over a temperature range of 10°C to 80°C (temperature change of 1°C/min).

6.2.6 Hydrogel bulk gel formation and gelation kinetics: Both neutral and charged hydrogels were prepared via co-extrusion of hydrazide-functionalized (POH or POHC) and aldehyde-functionalized (POA or POAC) precursors dissolved at 75 mg/mL in 10 mM PBS using a double barrel syringe with a static mixer at the outlet to ensure intensive and complete mechanical mixing (Medmix L series, 2.5 mL volume capacity). The recipes for the hydrogels prepared in this study are shown in Table 2. Hydrogel disks for all bench-top testing (swelling, degradation and VPTT measurements) were prepared by extrusion of the reactive polymer precursors through the double barrel syringe directly into cylindrical silicone rubber molds (diameter = 7 mm, volume = 300 µL), with gels incubated at room temperature for at least 4 hours to ensure complete gelation prior to testing. Hydrogels for cell and protein adsorption studies were extruded directly into the wells of a multiwell plate (as described in sections 2.9-2.13), while hydrogels for *in vivo* experiments were injected directly into the subcutaneous space.

Gelation times were assessed by extruding 200 µL of the reactive precursor solutions at concentrations of 75 mg/mL in PBS into a 2 mL microcentrifuge tube that is rotated manually every 5 seconds. The gelation time is defined as the time point at which the hydrogel visually no longer flows on the time scale of the rotation (5 s).

6.2.7 Hydration and swelling: Hydrogel swelling was determined gravimetrically at 37°C in 10 mM citrate, phosphate and carbonate buffered solutions of pH 3, 7.4 and 10 respectively. Hydrogels were placed into cell culture inserts that were subsequently placed into a 12-well cell culture plate and completely submerged with PBS (4 mL/well). At predetermined time intervals, the cell culture inserts were removed from the well, the PBS was drained, and the hydrogel was gently dried to wick off non-absorbed PBS. The hydrogel disks were then weighed, after which the hydrogels were resubmerged into a fresh 4 mL of PBS solution and tested repeatedly until equilibrium swelling was reached (generally ~30 hours). Error bars represent the standard deviation of the replicate measurements (n = 4). The mass-based swelling ratio (Q_m) was

calculated by dividing the mass of the hydrogel at any given time point (m_h) by the dry mass of polymer in the hydrogel (m_p = initial hydrogel mass $\times$ (1 – water content)).

6.2.8 Hydrolytic degradation: Hydrogel degradation was determined gravimetrically in acid-accelerated conditions at 37°C in the presence of 100 mM HCl (pH = 1.0); these acid-catalyzed conditions were used to compare the degradation properties of the hydrogels on a more measurable time frame as well as assess specifically the role of hydrazone hydrolysis (catalyzed in acidic conditions)[44] on the relative degradation times of the gels. Hydrogels were placed into cell culture inserts that were subsequently placed in a 12-well cell culture plate and completely submerged in the HCl solution (4 mL per well). At predetermined time intervals, the cell culture inserts were removed from the well, excess solution was drained, and the hydrogel was gently wicked off to remove any non-absorbed solution prior to weighing the hydrogel. Hydrogels were then resubmerged in fresh HCl solution (4 mL/well) until the hydrogel was completely degraded (i.e. no separate phase was observed between the hydrogel and the HCl bath solution). Error bars represent the standard deviation of the replicate measurements (n = 4).

6.2.9 Rheology: The rheological properties of the hydrogels were measured using an ARES rheometer (TA Instruments) operating under parallel-plate geometry with a plate diameter of 7 mm and a plate spacing of 1 mm. Rheological properties were measured by first conducting a strain sweep from 0.1−100% strain at 1 Hz to identify the linear viscoelastic range of the hydrogels. A strain was then selected within this range and set as a constant to perform a frequency sweep from 1 to 100 rad/s to measure shear elastic (G') and loss (G") moduli. All measurements were conducted at 25 °C, with error bars representing the standard deviation of the replicate measurements (n = 3).

6.2.10 In vitro protein absorption: To assess whether protein uptake was occurring via adsorption or absorption, larger gel samples (for which absorption would be more prevalent) of cylindrical shape and volume 300 µL were formed in a 3.5 mm radius silicone mold and left to gel completely for 4 hours. Protein uptake into the hydrogel disks was measured by placing the

gels into cell culture inserts and subsequently in a 12-well cell culture plate, completely submerging the gel in a 5 mg/mL BSA-FITC solution (4 mL per well). After 2 hours, the cell culture inserts and gels were removed from the well, and a 300 µL sample of the residual BSA-FITC solution was transferred into a 48-well plate and quantified using fluorescence as previously described. Based on the initial weight of polymer present in each gel, a µg/mg BSA uptake of polymer was calculated. Each experiment (hydrogels as well as controls) was done in quadruplicate, with reported errors representing the standard deviation of the replicates.

6.2.11 In vitro protein adsorption: To differentiate between interfacial adsorption and bulk absorption, thin film hydrogel adsorption assays were conducted in 96 well plates. POH/POHC/POA/POAC polymer solutions (75 mg/mL) were first sterilized by passing the solutions through a 0.2 µm filter, after which 30 µL of each precursor solution was extruded into each well of the 96 well plate and left overnight to ensure complete gelation. Following, 180 µL of 10 mM PBS was added to each well, and hydrogels were allowed to swell to equilibrium prior to protein addition for 30 hours (a time confirmed to correspond to equilibrium swelling for all hydrogels tested, see Fig. 1B). Excess PBS was then removed, and 60 µL of either BSA-FITC or lysozyme-FITC solution at concentrations of 125, 250, 500 or 1000 µg/mL in PBS was added. The hydrogels were incubated for 2 hours at 37°C, after which the hydrogels were rinsed to remove unadsorbed protein and the fluorescence signal was measured using a VICTOR 3 multi-label microplate reader using an excitation wavelength of 495 nm and an emission wavelength of 535 nm; linear calibration curves (R^2 > 0.99) were observed in the concentration ranges of 1 to 10 µg/mL and 10 to 100 µg/mL for BSA-FITC and lysozyme-FITC respectively. Each experiment (hydrogels as well as controls) was done in quadruplicate, with reported errors representing the standard deviation of the replicates.

6.2.12 Precursor polymer cytotoxicity: Cell cytotoxicity of the charged POEGMA precursor polymers was evaluated using a rezasurin assay with varying exposure concentrations to 3T3 mouse fibroblasts. Briefly, 3T3 mouse fibroblasts were plated at a density of 10,000 cells/well in a 96 well polystyrene tissue culture plate. The 96 well plates were then incubated for 24 hr at

37˚C in DMEM supplemented with FBS (10%) and penicillin/streptomycin (1%). After incubation, cells were exposed to varying concentrations of charged hydrazide and aldehyde precursor polymer ranging from 100 to 1000 μg/mL. The plate was then incubated for another 24 hrs. Cytotoxicity was assessed through the addition of 10 μg/mL resazurin reagent. After 2 minutes of subsequent incubation at 37˚C, the fluorescence of each well was measured using a VICTOR 3 multi-label microplate reader using an excitation wavelength of 495 nm and an emission wavelength of 535 nm. Viabilities were determined by subtracting background fluorescence readings (blank well with no cells) from each well and then calculating the ratio of the signal intensity of polymer-exposed cells to untreated cell controls (no polymer exposure) (n=4).

6.2.13 Cell morphology on 2D hydrogels: The cell morphology of mouse 3T3 fibroblasts was assessed on the surface of the charged POEGMA hydrogels. Hydrogels were directly extruded into each well of a 48-well plate (100 μL of each sterilized polymer precursor solution prepared at 150 mg/mL in 10 mM PBS), leaving the gel overnight to ensure complete gelation. Gels were then incubated at 37˚C in 600 μL of sterilized 10 mM PBS and allowed to equilibrate for 24 hours prior to cell plating to ensure equilibrium swelling was achieved prior to cell plating. The PBS was then removed, and gels were washed with DMEM culture media prior to cell addition. Cells were plated on top of the hydrogels at a density of 1.0×10^4 cells per well together with 600 μL of DMEM and incubated for 48 hours at 37˚C. After the incubation period, a LIVE/DEAD assay was conducted to visualize cells using microscopy and quantify adhesion. Each well was washed three times with sterile 10 mM PBS to remove any non-adherent cells from the gels before staining. Once washed, fluorescent live cells were imaged for morphological characterization and counted using a Zeiss Axiovert 200M fluorescence/live cell imaging microscope, using ImageJ for image analysis. All experiments were conducted in quadruplicate, with multiple images (n=4) taken per well for analysis; error ranges report represent the standard deviation associated with the total cell counts (across the multiple images taken per replicate) in the replicate measurements (n=4 replicate samples).

6.2.14 In vivo subcutaneous injections: All animals received care that complied with protocols approved by the Animal Research Ethics Board at McMaster University and the guidelines of the Canadian Council on Animal Care. The *in vivo* response of the injectable charged hydrogels was assessed histopathologically following subcutaneous injection of the charged hydrogels using autoclaved double barrel syringes into male BALB/c mice (Charles River, Montreal; 22-24 g weight). Precursor polymer solutions (75 mg/mL) were filtered using a 0.2 mm syringe filter, loaded into an autoclaved double barrel syringe under aseptic conditions, and injected subcutaneously at a volume of 0.3 mL total gel volume/mouse in the scruff of the neck. Mice were anesthetized using isoflurane prior to injection to ensure reproducible injection sites and substantial gelation prior to mouse movement. Following visual tracking of mouse behavior and health during the experiment, animals were euthanized by carbon dioxide asphyxiation after acute (2 days) and chronic (30 days) time points. Tissue samples from around the injection site were recovered, fixed in formalin, and stained with eosin and hematoxylin. Inflammatory responses to the hydrogels were assessed using two methods. Leukocyte concentrations were determined through Image J analysis (n=4 for every material tested, 4 images were analyzed per mouse (n)). Additionally, gels were evaluated using a histological scoring system as established by the Medical College of Wisconsin: 0=Normal, 1= Noacute/chronic inflammation other than macrophages;prior to fat and other subcutaneous tissue, 2=inflammation without necrosis, 3=focal inflammation with some necrosis, 4= wide-spread inflammation with significant necrosis, 5= massive inflammation.

6.2.15 ARPE-19 3D cell encapsulation: Human retinal cells (ARPE-19) at passage 8 were rinsed with PBS, detached from the plate surface with TrypLE™ Express Enzyme (TypLE, ThermoFisher Scientific), resuspended in complete DMEMF12 media, and centrifuged to pelletize the cells. Supernatant media was carefully removed and pelleted cells were resuspended directly in the hydrazide-containing $PO_{10}H_{30}$ and $PO_{10}H_{30}D_{20}$ precursor polymers at a concentration of $2.5x10^6$ cells/mL. In advance, 15 µL of the appropriate aldehyde-containing $PO_{10}A_{30}$, and $PO_{10}A_{30}C_{20}$ precursor polymers was aliquoted to individual wells on coverslip bottom, 96-well plates. Aliquots (15 µL) of the hydrazide $PO_{10}H_{30}$ and $PO_{10}H_{30}D_{20}$ precursor suspensions containing

ARPE-19 cells were then added to the complementary aldehyde polymer-containing wells and rapidly mixed via pipette aspiration. ARPE-19 cells were identically resuspended in 15 µL of Geltrex® LDEV-Free Reduced Growth Factor Basement Membrane Matrix (Geltrex®, ThermoFisher Scientific) and aliquoted to wells containing 15 µL of Geltrex® to serve as a control with the same overall cell number and prepared using the same technique. Both the test and control gels were allowed to gel for 2 h at 37˚C. Following, 120 µL of DMEM containing 10% FBS and 1% penicillin streptomycin was placed on top of each gel, and the gels were incubated for up to two weeks to track cell viability, with media replaced every 2-3 days. Cell morphology, and viability was measured via confocal microscopy (Nikon Eclipse Ti), with image processing conducted using NIS Elements and ImageJ. A z-stack depth of 200 µm was scanned for each sample. Cells were fluorescently labeled using a live/dead assay by removing the media and adding 50 µL of live-dead solution consisting of 2 µM calcein AM (calcein, Sigma-Aldrich) and 4 µM Ethidium homodimer-1 (EthD-1, Sigma-Aldrich) in PBS. Cells were incubated for 30 minutes prior to imaging. Quantitative cell numbers were determined using a VICTOR 3 multi-label microplate reader and reading the fluorescence at an emission wavelength of 535 nm. Fluorescence intensities in relative fluorescence units were determined by subtracting background fluorescence readings (blank gel with no cells) from each well (n=6).

6.3 Results

6.3.1 Synthesis: Charged poly(oligoethylene glycol methacrylate) (POEGMA) hydrogel precursors were synthesized via chain transfer agent-mediated free radical copolymerization of oligoethylene glycol methacrylate monomers with varying ethylene glycol side chain lengths (n). Each multiresponsive pre-polymer was prepared by copolymerizing one functional monomer to allow covalent crosslinking via hydrazide/aldehyde chemistry and another functional monomer to impart charge into the polymer (AA for anionic precursor polymers or DMAEMA for cationic precursor polymers) (Scheme 1). The 90:10 monomer ratio between diethylene glycol methacrylate ($M(EO)_2MA$, n = 2) and oligoethylene glycol methacrylate ($OEGMA_{475}$ n = 8-9) used to prepare all precursor polymers was selected to produce (unfunctionalized) POEGMA polymers with a target LCST similar to PNIPAM (~32°C), providing

the desired thermosensitivity in the resulting copolymers. Each hydrazide $PO_xH_yC_z$ and $PO_xA_yD_z$ precursor reported in this paper was functionalized with a targeted y = 30 mol% functional hydrazide or aldehyde functional groups (such that the theoretical cross-link density in each hydrogel formed is equivalent regardless of how the different precursor polymers are mixed) and, where present, z = 20 mol% charged monomer. Conductometric titration confirms ~20 mol% charged monomer content in both $PO_{10}H_{30}C_{20}$ and $PO_{10}A_{30}D_{20}$ as well as ~30 mol% hydrazide functionalization in both $PO_{10}H_{30}$ and $PO_{10}H_{30}C_{20}$ (Table 6.1); however, the actual aldehyde incorporation into both $PO_{10}A_{30}$ and $PO_{10}A_{30}D_{20}$ was slightly lower than the stoichiometric expectation at ~22-24 mol%, a result we attribute to lower potential incorporation of acetal monomer during copolymerization. However, despite this lower aldehyde functionalization, the similar degree of functionalization of both aldehyde-functionalized precursors means that the potential for crosslink formation is the same between any pair of precursor polymers tested. As such, the hydrogels formed from these precursors polymers are expected to be chemically equivalent aside from the incorporation or exclusion of charged monomers. The number-average molecular weight (M_n) of the polymer precursors is also consistent between the different precursors and is controlled to be less than 20×10^3 g/mol (Table 6.1), well below the renal clearance limit of $40\text{-}50\times10^3$ g/mol to facilitate polymer elimination following gel degradation.

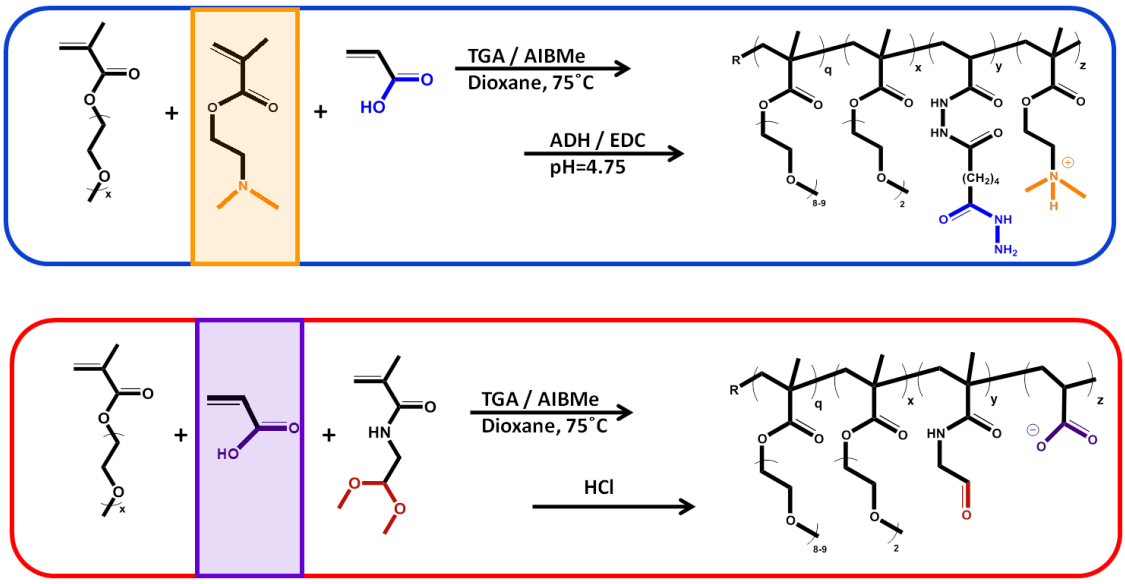

Scheme 6.1. Synthesis of charged POEGMA precursors.

Table 6.1. Chemical characterization of synthesized POEGMA polymer precursors.

	$M(EO)_2MA$ (mol%)	$OEGMA_{4}$ [a] (mol%)	Functional Reactive Group	Functional Reactive Monomer (mol%)	Charged Group	Functional Charged Monomer (+/-) (mol%)
$PO_{10}H_{30}$ (POH)	60.2	6.7	$NHNH_2$	33.1 [a]	N/A	-
$PO_{10}H_{30}C_{20}$ (POH-cat)	39.3	4.4	$NHNH_2$	33.1 [a]	DMAEMA	(+)18.4± 2.1 [a]
$PO_{10}A_{30}$ (POA)	70.6	7.8	CHO	21.6 [b]	N/A	-
$PO_{10}A_{30}D_{20}$ (POA-an)	53.5	4.1	CHO	23.9 [b]	AA	(-) 17.3±3.5 [a]

[a] Determined from conductometric titration, [b] Determined by ^{1}H-NMR

6.3.2 Physiochemical properties: Hydrogels were prepared by co-extruding binary combinations of hydrazide-functionalized (POH/POHC) and aldehyde-functionalized (POA/POAD) precursor polymers dissolved at 75 mg/mL in 10 mM PBS using a double barrel syringe to form neutral, cationic, amphoteric and anionically charged gels (Table 6.2). All binary combinations of precursor polymers gelled rapidly, between <5s to 45s (Table 6.2). The effect of charge was significantly different depending on the type and combination of charged precursor polymers used. Cationic hydrogels prepared with a cationic hydrazide precursor and a neutral aldehyde precursor exhibited slower gelation times than the neutral networks with

the same backbone composition, a result anticipated based on the electrostatic repulsion between the cationic DMAEMA residues of adjacent precursor polymers. On the other hand, amphoteric hydrogels consisting of a mixture of cationic hydrazide precursor polymer and anionic aldehyde precursor polymer gelled significantly faster than the neutral combination, a result expected based on the combination of both ionic attractions as well as covalent gelation driving interpolymer interactions in this system. Interestingly, hydrogels prepared with a neutral hydrazide precursor and an anionic aldehyde precursor gelled significantly faster than the neutral combination (indeed, on par with the amphoteric formulation that is aided by electrostatic interactions).

Table 6.2. Preparation of charged POEGMA hydrogels.

POEGMA Hydrogel			**Hydrazide Precursor**		**Aldehyde Precursor**	
Hydrogel	**Charge**	**Gelation Time (s)**	**Precursor**	**Concentration (mg/mL)**	**Precursor**	**Concentration (mg/mL)**
PO_{10}	Neutral	30	$PO_{10}H_{30}$	75	$PO_{10}A_{30}$	75
PO_{10}-cat	Cationic	45	$PO_{10}H_{30}D_{20}$	75	$PO_{10}A_{30}$	75
PO_{10}-amp	Amphoteric	<5	$PO_{10}H_{30}D_{20}$	75	$PO_{10}A_{30}C_{20}$	75
PO_{10}-an	Anionic	<5	$PO_{10}H_{30}$	75	$PO_{10}A_{30}C_{20}$	75

The effect of charge on hydrogel swelling was quantified at 37°C in buffers of 10 mM pH 3 (citrate), pH 7.4 (phosphate) and pH 10 (carbonate) over a time period of 30 hours; these pH values were chosen based on the pK_a values of both charged comonomers (AA pK_a = 4.25, DMAEMA pK_a = 8.5) such that only the cationic comonomer would be charged (pH 3), only the anionic monomer would be charged (pH 10), and both monomers would be charged (physiological pH 7.4). At pH=3 (Fig. 6.1a), the cationic and amphoteric gels swelling relative to their prepared state, the former due to ionization and the latter due to effective de-crosslinking of the ionic network as the AA residues are protonated; in contrast, the neutral gel deswells slightly (likely attributable to the slightly higher ionic strength) and the anionic gel collapses as –COOH groups are protonated and hydrogen bonding interactions with residual hydrazide groups are promoted. At pH 10, the anionic gel swells due to –COOH ionization while the

amphoteric gel also swells again due to disruption of the ionically crosslinked network (here, following DMAEMA deprotonation, leaving only anionic charged groups in the gel); the neutral gel remains near its initial volume while the cationic gel deswells slightly due to enhanced hydrogen bonding following functional group neutralization. Intermediate swelling behaviors were observed at pH 7.4, with the amphoteric gel shrinking the most over time consistent with the development of an ionically-crosslinked secondary network in the gel over time. Thus, the swelling profiles confirm the anticipated pH-responsive behavior of POEGMA hydrogels prepared with functionalized precursor polymers and our capacity to tune the charge type/content of the gels by simple mixing of functionalized precursor polymers.

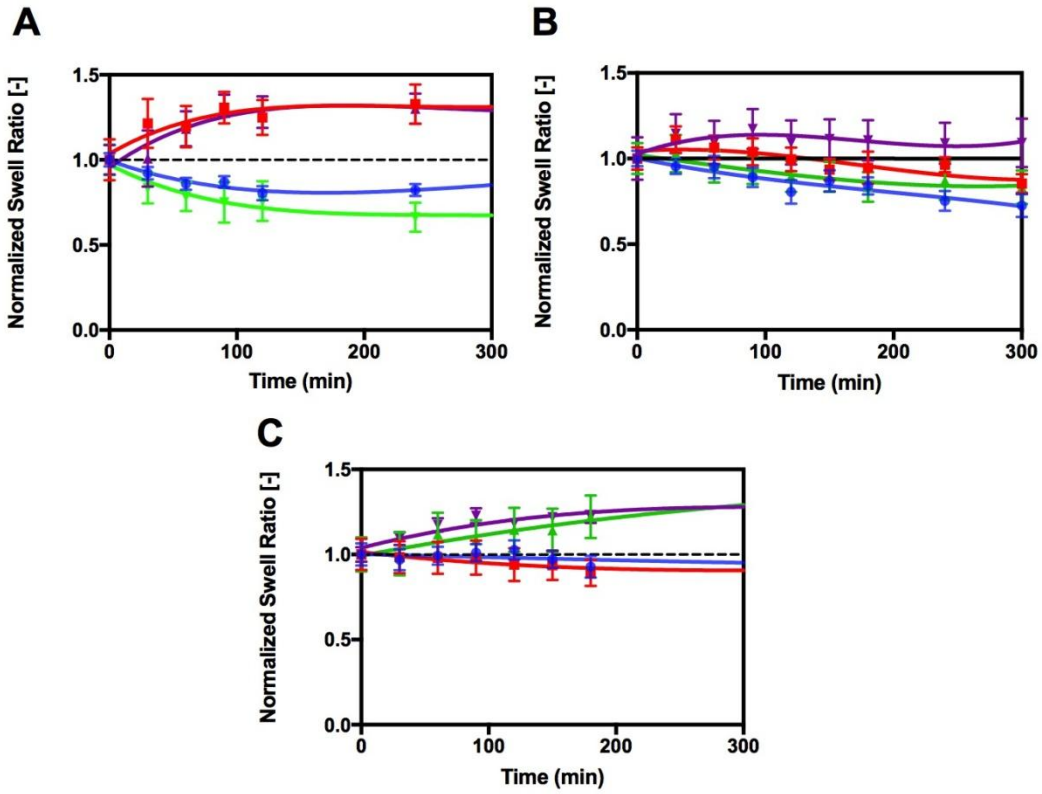

Figure 6.1. Swelling kinetics of POEGMA hydrogels in 10 mM (A) citrate buffer, pH 3; (B) phosphate buffer, pH 7.4; and (C) carbonate buffer, pH 10 at 37°C: (●, blue) PO_{10}; (●, red) PO_{10}-cat; (●, purple) PO_{10}-amp; (●, green) PO_{10}-an.

The effect of charge incorporation on temperature responsiveness was then quantified the same pH values tested for swelling by a step-wise temperature ramp from 20°C to 50°C at 5°C intervals, allowing 12 h between temperature steps to ensure that equilibrium conditions were reached for each temperature measurement. At pH = 7.4, the characteristic collapse profile of the neutral PO_{10} gel with a VPTT of ~32-33°C (similar to NIPAM) is observed; a similar phase transition is observed in the cationic PO_{10}-cat hydrogel, given that deprotonation of the cationic groups (pK_a ~ 8.5) is partially complete at physiological pH and the effective charge density on the gel is lower. However, the fully ionized anionic gel (ionic repulsion and higher bound water content) and the amphoteric gel (ionic crosslinking) both undergo much slower and less extreme phase transitions, consistent with observations on conventional charged hydrogels. At pH 3, the hydrazone bond is labile over ~96 hour course of the full temperature

ramp, leading to effective gel degradation in the cationic and amphoteric gels (both of which are more swollen and thus accessible to acid degradation at pH 3, Fig. 1a) as the temperature is ramped. This result is consistent with the accelerated 0.1 M HCl degradation results (Figure 6.3), indicating rapid swelling and subsequent degradation over time for the cationic and amphoteric gels but rapid collapse followed by extremely slow degradation of the collapsed network for the anionic and neutral gels. Alternately, at pH 10, the ester bond linking the ethylene oxide side chain to the methacrylate backbone in each gel tested is labile over the same time frame (Figure S3); consequently, the volume phase transition is suppressed in each gel tested due to the generation of ionized methacrylate residues on the backbone polymer as degradation occurs.

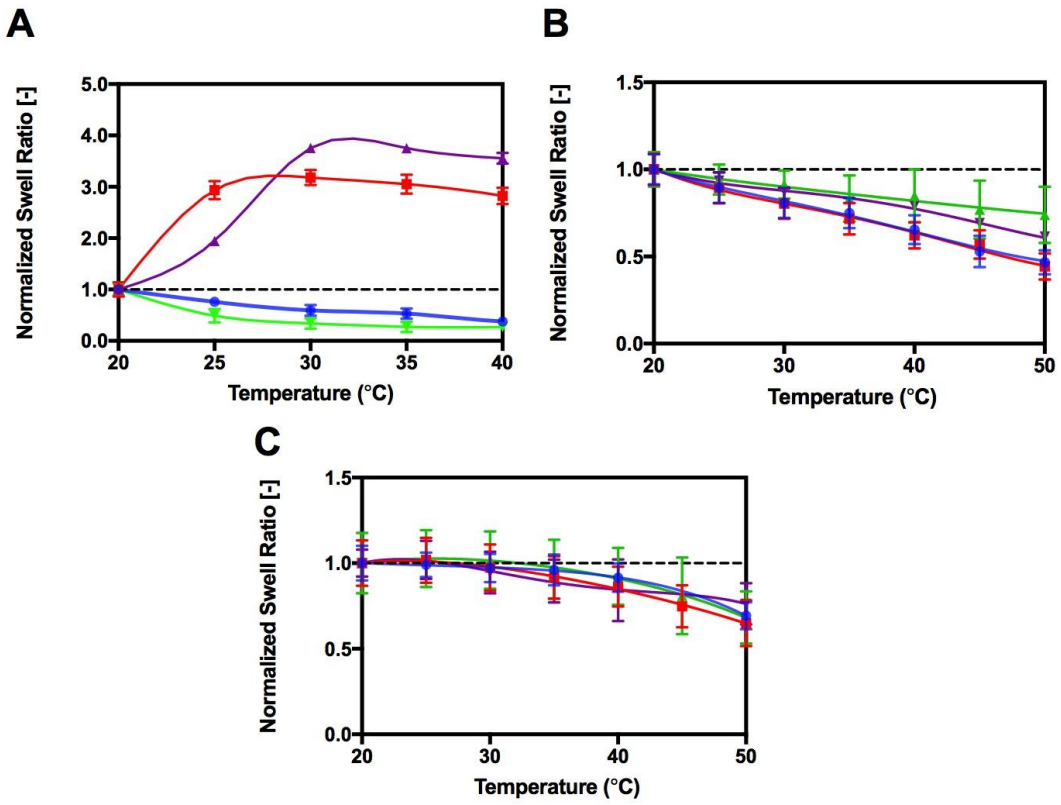

Figure 6.2. Swelling kinetics of POEGMA hydrogels in pH 3, 7.4 or 10 buffers as a function of temperature: (●, blue) PO_{10}; (●, red) PO_{10}-cat; (●, purple) PO_{10}-amp; (●, green) PO_{10}-an.

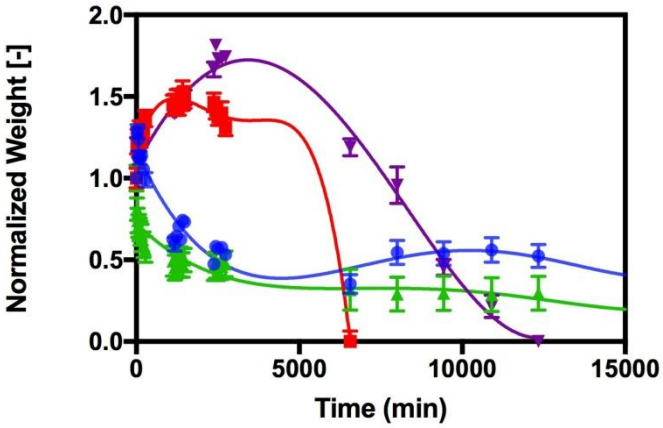

Figure 6.3. Degradation profiles of POEGMA hydrogels in 0.1 M HCl solution at 37°C: (●, blue) PO_{10}; (●, red) PO_{10}-cat; (●, purple) PO_{10}-amp; (●, green) PO_{10}-an.

The rheological properties of the charged POEGMA gels are shown in Figure 6.4. The plateau elastic storage modulus (G') increases with the incorporation of charge, with both cationic (~1160 ± 160 Pa) and anionic (~1650 ± 360 Pa) exhibiting higher elasticity relative to hydrogels prepared without charge (~820 ± 140). This result is consistent with an increase in bound water within the charged hydrogels, with the higher effective charge density in the anionic gel relative to the cationic gel at pH 7.4 resulting in a slightly higher enhancement of the anionic gel modulus. However, in the dual ionic-covalent crosslinked amphoteric gel, the contribution of the second electrostatic network results in a significant increase in the shear storage modulus (~2820 ± 370, a ~3.5-fold increase in G' compared to the neutral gel consistent with the presence of dual crosslinking.

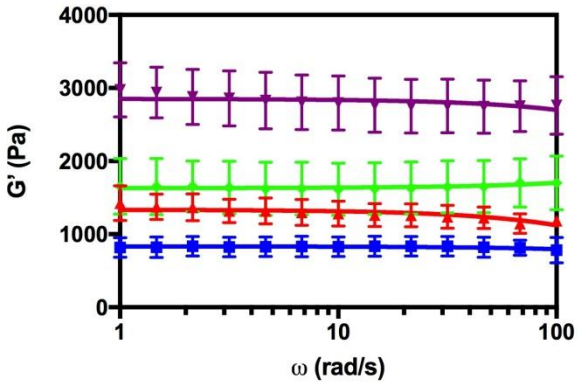

Figure 6.4. Average elastic storage moduli (*G'*) of the fully swollen mixed precursor POEGMA hydrogels in 10 mM PBS at 37°C: (●, blue) PO_{10}; (●, red) PO_{10}-cat; (●, purple) PO_{10}-amp; (●, green) PO_{10}-an.

6.3.3 In vitro cytocompatibility: To assess the biological potential of these hydrogels, the cytocompatibility of the charged polymer precursors was first assessed using a rezasurin cell viability reagent assay on 3T3 mouse fibroblasts to ensure the precursor polymers themselves did not negatively impact cells (Figure 6.5). Neither the cationic nor anionic precursor polymers (which also represent the degradation products post-hydrolysis) showed any cytotoxicity at concentrations up to 1000 μg/mL, analogous to the non-charged control precursor polymers. This result is important since cationic polymers in particular often exhibit cytotoxicity, particularly at the relatively high polymer concentrations tested in Fig. 6.5; this is not problematic in the cationic POEGMA polymers.

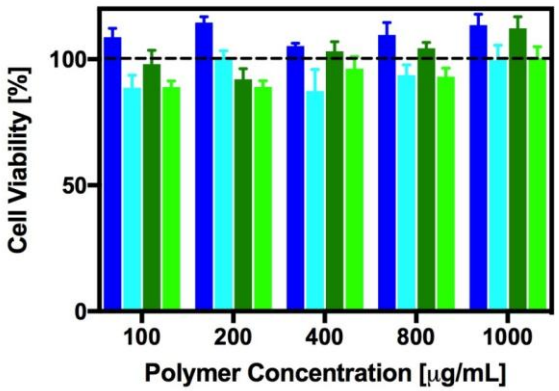

Figure 6.5. Resazurin cell viability assay of POEGMA precursor polymers after 24 hours incubation with 3T3 mouse fibroblasts at 37°C: $PO_{10}H_{30}$ (●, blue); $PO_{10}H_{30}C_{20}$ (●, light blue); $PO_{10}A_{30}$ (●, dark green); $PO_{10}A_{30}D_{20;}$ (●, green).

6.3.4 In vitro protein affinity: To assess the inflammatory potential of charged POEGMA hydrogels, the affinity between the charged hydrogels and proteins was assessed through two separate assays. First, protein *absorption* within the hydrogel was measured by fully immersing templated bulk cylindrical gels (surface area:volume ratio = 0.8:1) in a BSA solution and, without rinsing, removing the hydrogels and measuring the residual BSA content in solution (Table 6.3). In this case, protein uptake into the charged gels is uniformly higher than the corresponding neutral gel, with the cationic gel exhibiting higher uptake than the anionic gel (consistent with the net anionic charge of BSA at physiological pH) and the amphoteric gel

exhibiting highest uptake (consistent with the effective total charge density in the amphoteric gel being double the other two charged hydrogels, Table 6.2). Thus, from an absorption perspective, the charged POEGMA hydrogels behave similarly to previously reported charged gels in which the presence of more charge enhances protein uptake.

Table 6.3. BSA uptake into charged POEGMA hydrogels from 70 μg/mL BSA stock solution in 10 mM PBS (37°C).

Hydrogel	**[BSA] in stock solution after 48 hr (μg/mL)**	**μg BSA/mg polymer in gel**
PO_{10}	57 ± 9	0.3 ± 0.2
PO_{10}-cat	43 ± 5	0.6 ± 0.1
PO_{10}-amp	24 ± 4	1.3 ± 0.2
PO_{10}-an	29 ± 7	1.0 ± 0.2

Following, a protein *adsorption* experiment was performed on thin film hydrogels constrained within a 96-well plate (surface area:volume ratio 1.8:1) (Figure 6.6). Both lysozyme and BSA were tested at various concentrations, with 15 sequential PBS rinses performed to remove any absorbed or weakly bound protein prior to assaying the residual gel fluorescence. As such, this assay was designed to probe the interfacial interactions between the gels and proteins, which are more critical to predicting inflammatory potential.[48] Typically, introducing charge (and particularly cationic charge) significantly increases the amount of protein deposition on a biomaterial surface due to electrostatic interactions with either the net charge or local charged domains of proteins. For BSA (66 kDa, pI ~ 4.8), the cationic gel adsorbs slightly more protein than the neutral gels, consistent with expectations; however, both the anionic and amphoteric gels adsorb less protein than even the neutral POEGMA gel. For lysozyme, (14 kDa, pI ~ 11.3), protein adsorption is similar between all hydrogels tested irrespective of charge, despite net charge attraction between lysozyme and the anionic gel. Thus, very low protein *adsorption* is maintained irrespective of incorporation of even 10 mol% charge in the hydrogels. We hypothesize that the brush-like PEG side-chains tethered on the POEGMA backbone assist in masking the charges located closer to the backbone to maintain very low protein adsorption

in all cases. This is also consistent with the very low cytotoxicity of the cationic precursor polymer measured (Fig. 6.5) and represents a potential advantage of these injectable POEGMA materials in that a large fraction of charges can be introduced to affect other gel properties (e.g. swelling, thermoresponsivity, mechanics, etc.) without significantly affecting protein adsorption.

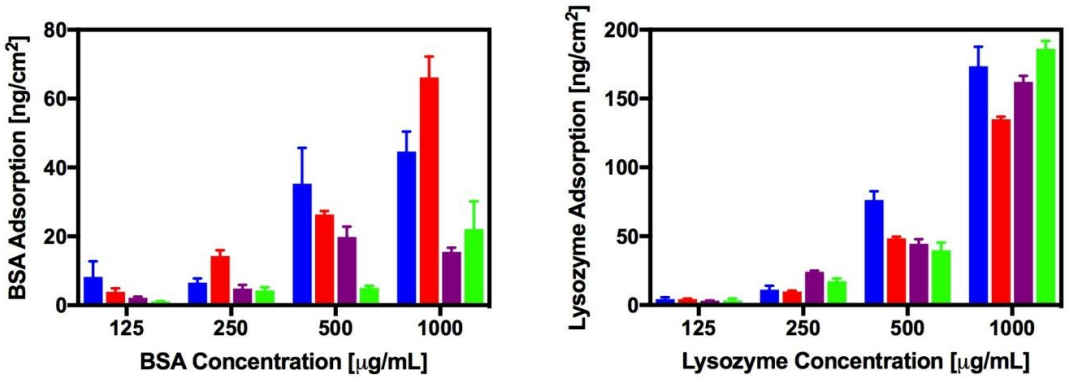

Figure 6.6. Protein adsorption to charged POEGMA hydrogels in 10 mM PBS at 37°C: (A) bovine serum albumin; (B) lysozyme: (●, blue) PO_{10}; (●, red) PO_{10}-cat; (●, purple) PO_{10}-amp; (●, green) PO_{10}-an.

6.3.5 In vitro cell adhesion: To assess the impact of introducing charge on the capacity of cells to adhere to the hydrogels, cell adhesion of 3T3 mouse fibroblasts was assessed following the plating of 10 000 cells/well on top of the same thin film hydrogel samples used for the interfacial protein binding tests (Figure 6.7). Significantly more cells adhered to all the charged hydrogels (Fig. 6.7B-D) relative to the neutral (uncharged) PO_{10} hydrogel (Fig. 6.7A). This result indicates that charge promotes cell adhesion to otherwise highly cell-repulsive POEGMA hydrogels without the need to incorporate additional bioadhesive functional groups. The PO_{10}-cat cationic hydrogel (Fig. 6.7B) shows particularly high cell adhesion consistent with the electrostatic attraction induced between the 3T3 cells and the hydrogel interface; indeed, the total fluorescence (related to number of live cells counted) on PO_{10}-cat is only ~20% of that of the tissue culture polystyrene control (Fig. 6.7E), albeit with significantly higher cell clumping observed indicative of weaker cell electrostatic interactions instead of stronger integrin bonding and promotion of focal adhesions with the gel interface.[45,46] Thus, the charged

POEGMA hydrogels can support the adhesion and proliferation of viable cells despite the low non-specific protein binding observed on these hydrogels (Fig. 6.6).

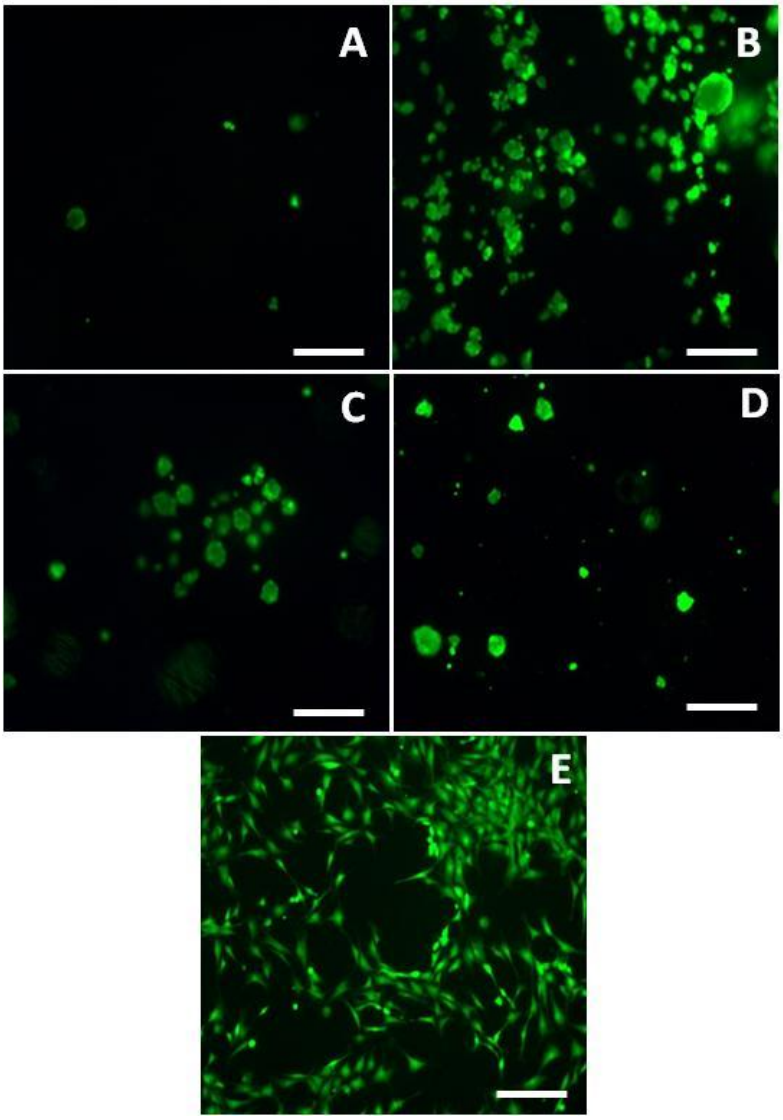

Figure 6.7. Adhesion of mouse 3T3 fibroblasts to charged POEGMA hydrogels following 48 hours of incubation: (A) PO_{10} (neutral); (B) PO_{10}-cat (cationic); (C) PO_{10}-amp (amphoteric); (D) PO_{10}-an (anionic) (E) tissue culture polystyrene control. Scale bar = 100 µm.

Significantly more cells adhered to all of the charged hydrogels (Fig. 6.7B-D) relative to the neutral (uncharged) PO_{10} hydrogel (Fig. 6.7A). This result indicates that charge promotes cell adhesion to otherwise highly cell-repellent POEGMA hydrogels without the need to incorporate additional bioadhesive functional groups. The PO_{10}-cat cationic hydrogel (Fig. 6.7B)

shows particularly high cell adhesion consistent with the electrostatic attraction induced between the 3T3 cells and the hydrogel interface; indeed, the total fluorescence (related to number of live cells counted) on PO_{10}-cat is only ~20% lower than that of the tissue culture polystyrene control (Fig. 6.7E), albeit with significantly higher cell clumping observed indicative of weaker cell electrostatic interactions instead of stronger binding interactions that can promote more focal adhesions with the gel interface.[49,50] Thus, charged POEGMA hydrogels can support the adhesion and proliferation of viable cells despite the low non-specific protein binding observed to these materials (Fig. 6.6).

6.3.6 Subcutaneous in vivo tissue compatibility: To assess the tissue compatibility of the charged POEGMA hydrogels *in vivo*, subcutaneous injections of the PO_{10}, PO_{10}-cat, PO_{10}-amp and PO_{10}-an hydrogels were performed using BALB/c mice (Figure 6.8). Each binary combination rapidly (<1 min) formed a hydrogel when injected, consistent with *in vitro* observations, and no obvious signs of skin irritation were noted in any of the mice injected. Injection of the PO_{10}, PO_{10}-amp, and PO_{10}-an hydrogels resulted in moderate infiltration of leukocytes to the hydrogel-tissue interface at the acute (2 day) time point, with both the anionic (490 ± 220 cells mm^{-2}) and in particular the amphoteric (450 ± 180 cells mm^{-2}) gels exhibiting comparable inflammatory responses to the neutral PO_{10} gel (~500 cells mm^{-2}). The cationic PO_{10}-cat gel showed a substantially higher presence of polymorphonuclear cells (1200 ± 180 cells mm^{-2}) then all other gels, indicating stronger acute inflammation consistent with the higher BSA adsorption observed (Fig. 6.6A). From histological scoring, all gels exhibited at least localized inflammatory responses inducing limited cell necrosis (Table 4; see scoring system in Experimental section). However, no significant difference in score was observed between $PO_{10\text{-}cat}$ and the other gels, indicating that the higher number of leukocytes present does not induce a significant difference in tissue morphology.

Table 6.4. Histological scores for determination of severity and reaction to the injection of charged POEGMA hydrogels into the subcutaneous space of BALB/c mice.

Hydrogel	**Histology Score**	
	Acute (2 days)	**Chronic (30 days)**
PO_{10}-cat	3.7 ± 1.2	1.0 ± 0.0
PO_{10}-amp	4.0 ± 1.1	2.0 ± 1.7
PO_{10}-an	3.5 ± 2.4	1.0 ± 0.0

At the chronic time point (30 days), all gels persisted in the subcutaneous space but showed evidence of at least some degradation, with cells penetrating between segments of gel in all cases. Only the neutral PO_{10} gel showed a considerable decrease in leukocytic concentration, with the polymorphonuclear cell density dropping to ~75 cells mm^{-2} compared to PO_{10}-amp (380 ± 170 cells mm^{-2}) and PO_{10}-an hydrogels (330 ± 100 cells mm^{-2}). We hypothesize that this result is attributable to the different degradation rates of these gels, leading to different concentrations of leukocytes over time. Of note, the cationic PO_{10}-cat gel shows a similar leukocyte density at the chronic time point relative to the other charged gels (360 ± 90 cells mm^{-2}), suggesting that the larger acute inflammation observed resolves at the chronic time point despite the continuing presence (and degradation) of the cationic hydrogel. Thus, while the cationic PO_{10}-cat gel induces higher acute inflammation, the chronic inflammatory response remains mild; this result is significant based on the large inflammatory responses often observed with cationic biomaterials.[51] This significant resolution of an inflammatory response is further confirmed through histological scoring, in which scores of 1 (PO_{10}, $PO_{10\text{-cat}}$, and $PO_{10\text{-an}}$, indicating no inflammation aside from a few macrophages due to ongoing gel degradation) or at most 2 ($PO_{10\text{-amp}}$, indicative of a macrophage response associated with gel degradation but no cell necrosis) were observed. It should also be emphasized that no clear evidence of fibrosis (or "walling off" of the gels) is observed for any of

the injected gels after 30 days, significant for the potential use of these materials for controlled release applications for either cells or therapeutics.

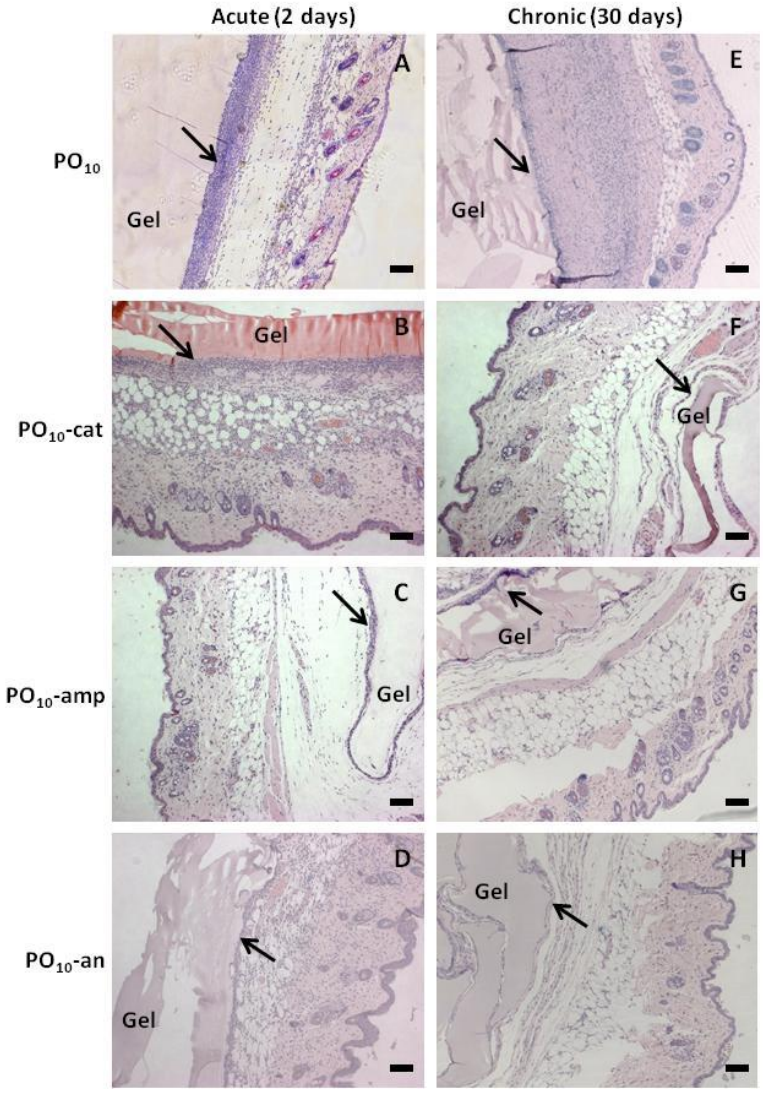

Figure 6.8. Histological sections of stained subcutaneous tissue samples following injection of PO_{10} (A,E), PO_{10}-cat (B,F), $PO\text{-}_{amp}$ (C,G) and $PO\text{-}_{an}$ (D,H) hydrogels following acute (A-D) and chronic (E-H) time points. Arrows indicate the presence of leukocytes. All hydrogels are still present at chronic time points. Scale bars = 100 µm.

6.3.7 3D cell encapsulation: Given the demonstrated potential of these charged POEGMA gels as injectable biomaterials, we next investigated the potential of leveraging both the thermoresponsivity and the charge of the hydrogels for creating delivery vehicles for human retinal pigment epithelial cells (ARPE-19) that are injectable, degradable, and do not require the

inclusion of bioadhesive biomolecules to support cell adhesion or proliferation. ARPE-19 cells were co-extruded with the charged and neutral POEGMA gel precursor polymers at a concentration of 2.5 x 10^6 cells/mL; cell viability and morphology was tracked over 15 days and compared to a commercially available Geltrex® hydrogel that consists of natural extracellular matrix components (laminin, collagen IV, entactin, and heparin sulfate) and has been previously used for retinal cell delivery to the back of the eye.[45] All of the POEGMA-based hydrogels tested could support and maintain cell viability over the full 15-day test period, with the cells remaining relatively isolated within the matrix; this is desirable for cell transplantation applications in the retina, as large aggregations of retinal cells during bolus injection lead to high cell death due to nutrient and oxygen suffocation and limited integration into native tissues.[52] In contrast, the Geltrex matrix induced significant clumping of ARPE-19 cells less desirable for cell delivery applications. Plate coverage measurements on live cell fluorescence indicated less proliferation inside the POEGMA gels relative to the Geltrex matrix (Fig. 6.9J); however, the Geltrex matrix fully degraded after 15 days whereas the POEGMA matrices can still support viable and largely isolated cells.

The benefits of charge incorporation are also observed by comparing the performance of the neutral PO_{10} hydrogel to the charged gels. PO_{10} gels (which show minimal 2D cell adhesion, Fig. 6.7) show a slight decrease in viable cell count between days 3 and 15 as well as more dead (red) cells in the matrix over time (Fig. 6.9B). In contrast, all the charged hydrogels support cell proliferation within the matrix over the same time period (Fig. 6.9J). While the number of cells supported is highest in the cationic $PO_{10\text{-}cat}$ gel at all time points (Figs. 6.9C and D), both the anionic $PO_{10\text{-}an}$ and, in particular, the amphoteric $PO_{10\text{-}amp}$ gels minimize the number of dead cells and cell clumping observed after 15 days (Figs. 6.9F and H). This trend is also reflected in fluorescence intensity measurements between days 1 and 3 (Figure 6.10), in which the anionic and amphoteric gels maintain highest cell viability immediately following the delivery process (i.e. at day 1) but support slower cell proliferation; the amphoteric gel in particular maintains highest cell viability at day 1 but supports only minimal cell expansion over following 14 days. We hypothesize this result is related to the crosslink density of the gels, as the amphoteric hydrogel has the highest internal crosslinking density due to the dual

covalent/ionic crosslinking present and thus likely provides the least space for cell proliferation. As such, while all charged POEGMA gels offer promise relative to existing (more expensive and more difficult to purify) options as injectable delivery matrices for retinal epithelial cells, the nature of the charge present can alter the cell response between maintenance and proliferation within the matrix.

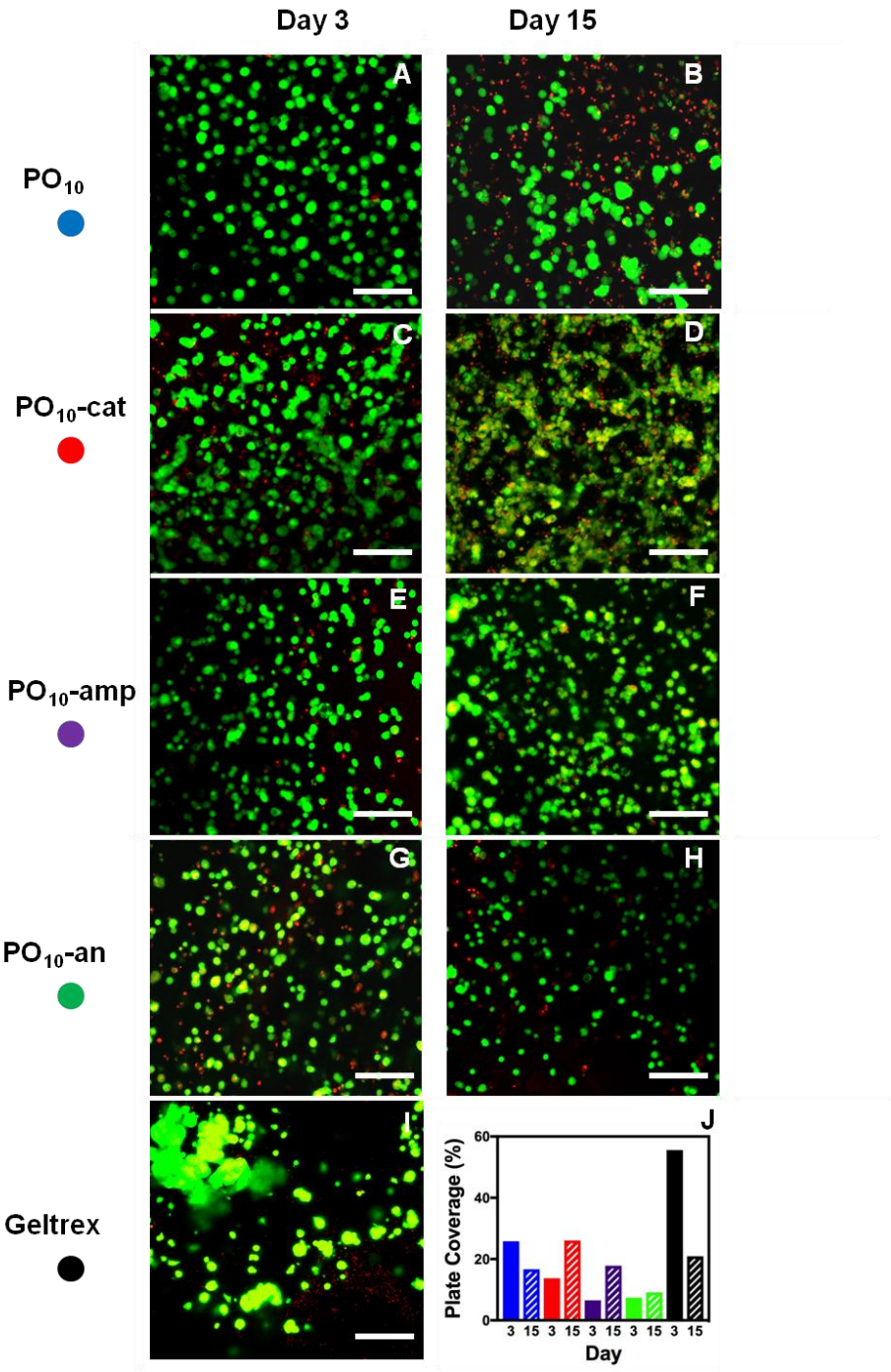

Figure 6.9. 3D encapsulation of ARPE-19 cells imaged using confocal microscopy (200 µm z-stack) after 3 days and 15 days in neutral and charged POEGMA hydrogels: (A,B) PO_{10} (neutral); (C,D) PO_{10}-cat (cationic); (E,F) PO_{10}-amp (amphoteric); (G,H) PO_{10}-an (anionic) (I) Geltrex matrix control. The percentage of fluorescence plate coverage of live cells for each gel and time point is shown as (J). Scale bar = 100 µm.

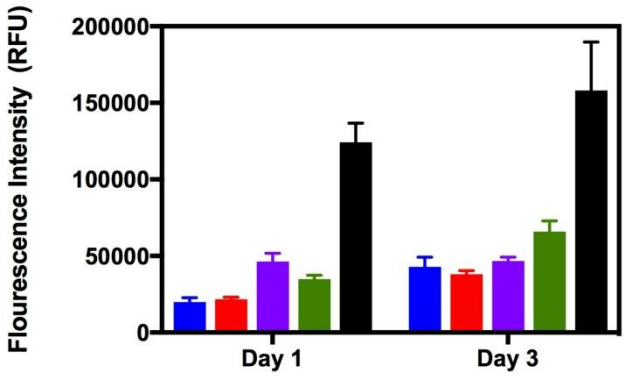

Figure 6.10. Average fluorescence reading taken using a VICTOR 3 multi-label microplate reader using calcein AM staining of -19 cells encapsulated within charged POEGMA hydrogels after Day 1 and Day 3 at 37°C: (●, blue) PO_{10}; (●, red) PO_{10}-cat; (●, purple) PO_{10}-amp; (●, green) PO_{10}-an; (●, back) Geltrex.

6.4 Discussion

The combination of a thermoresponsive polymer backbone with cationic and/or anionic groups that can be switched on or off as a function of pH leads to an injectable hydrogel formulation with a series of highly tunable properties under different environmental conditions. All formulations gelled in less than one minute following co-extrusion from a double barrel syringe and formed coherent gels that did not undergo syneresis as gelation proceeded. Uncharged PO_{10} hydrogels showed characteristic thermoresponsive swelling and interfacial responses, while the inclusion of a single type of ionizable functional groups shifts the hydrophilic/hydrophobic balance back to a more hydrophilic state, driving significant positive swelling effects in the case of single charge hydrogels that also facilitate accelerated degradation kinetics. Alternately, amphoteric hydrogels in which both anionic and cationic charges are present facilitate the creation of a secondary ionically-crosslinked network, resulting in an effectively dual-crosslinked hydrogel that swells less (Fig. 6.1) and has significantly higher modulus values (Fig. 6.4). Of note, anionically-functionalized hydrogels also exhibited somewhat faster gelation (Table 6.2), stronger mechanics (Fig. 6.4), and slower degradation (similar to the amphoteric hydrogels that have a well-defined secondary networking structure, Fig. 6.3) than the other tested hydrogels, suggesting the presence of an additional networking driving force in these materials. We hypothesize these results are related to hydrogen bonding between lone pair-donating ethers in the ethylene oxide repeat

units in the OEGMA side-chains and the lone pair accepting carboxylic acid groups of acrylic acid residues on the anionic POEGMA polymers, although elucidating the exact nature of this interaction would require further study.

The varying physicochemical and mechanical properties achieved via the incorporation of charge in thermoresponsive polymer precursors can subsequently be leveraged to engineer cell and tissue responses to these hydrogels. Inclusion of cationic, amphoteric and/or anionic charge within the POEGMA hydrogels significantly increases cell adhesion of 3T3 fibroblast cells to the matrix relative to neutral hydrogel controls (Fig. 6.7), facilitating cell adhesion without the need for using RGD or other adhesive peptides while still exhibiting low non-specific protein adsorption relative to other biomaterials or even neutral POEGMA gels (Fig. 6.6). The chronic inflammatory response of each of the hydrogels was mild, even though the gels were continuously degrading to release the functional polymer precursors at the one month chronic time point tested (Fig. 6.8). Furthermore, the successful encapsulation (and later proliferation) of ARPE-19 cells by injection within the charged POEGMA gels (Fig. 6.9) suggests the benefits of this combination of relatively low non-specific protein adsorption and charge in an injectable cell delivery vehicle, with the charged gels supporting higher cell viabilities and proliferation (albeit to different degrees based on the network structure) compared to neutral POEGMA gels and better suspension of the cells relative to the Geltrex control. Thus, manipulation of hydrogel charge to effect favorable application-based properties can be conducted without compromising the compatibility of the materials *in vivo.* Of note, given that these POEGMA hydrogels can be fabricated by simple mixing, the charge density of the hydrogels can be easily adjusted by mixing neutral and charged precursor polymers of the same functionality (i.e. hydrazide or aldehyde) in the appropriate barrel of the double barrel syringe, a modular design enabling rapid tuning of gel properties ideal for screening gel responses in specific applications.

6.5 Conclusions

Dual temperature and pH-responsive POEGMA hydrogels offer both physicochemical benefits in terms of highly tunable swelling, degradation, and rheological properties as well as biological benefits in terms of maintaining low non-specific protein adhesion and promoting

both cell adhesion and proliferation. In particular, manipulating the hydrogel charge can significantly improve both the 2D cell adhesive potential of 3T3 mouse fibroblasts and the 3D stabilization and proliferative potential of ARPE-19 human retinal epithelial cells without the need for cell adhesive ligands. Furthermore, the brush structure of POEGMA suppresses both non-specific protein adsorption and chronic inflammatory responses to the charged hydrogels relative to typical charged hydrogels (particularly for the cationic gels). On this basis, we suggest that these hydrogels offer significant potential as injectable and degradable matrices for in vivo cell delivery.

6.6 Acknowledgements

The Natural Sciences and Engineering Research Council of Canada (NSERC) is acknowledged for funding this work (Strategic Project Grant STPGP 447372 and Discovery Grant RGPIN 356609). This work utilized facilities supported in part by the National Science Foundation under Agreement No. DMR-1508249.

6.7 References

(1) Tan, H.; Chu, C. R.; Payne, K. A.; Marra, K. G. Injectable in Situ Forming Biodegradable Chitosan-Hyaluronic Acid Based Hydrogels for Cartilage Tissue Engineering. Biomaterials **2009**, 30, 2499–2506.

(2) Hudson, S. P.; Langer, R.; Fink, G. R.; Kohane, D. S. Injectable in Situ Cross-Linking Hydrogels for Local Antifungal Therapy. Biomaterials **2010**, 31, 1444–1452.

(3) Nguyen, M. K.; Lee, D. S. Injectable Biodegradable Hydrogels. Macromol. Biosci. **2010**, 10, 563–579.

(4) Wang, H.; Liu, Z.; Li, D.; Guo, X.; Kasper, F. K.; Duan, C.; Zhou, J.; Mikos, A. G.; Wang, C. Injectable Biodegradable Hydrogels for Embryonic Stem Cell Transplantation: Improved Cardiac Remodelling and Function of Myocardial Infarction. J. Cell. Mol. Med. **2012**, 16, 1310–1320.

(5) Ban, K.; Park, H.; Kim, S.; Andukuri, A.; Hwang, J.; Cho, K.; Cha, H.; YoonKim, S.; Woan-SangJun, H.; Yoon, Y. Cell Therapy with Embryonic Stem Encapsulated in Injectable Nanomatrix Gel Enhances Cell Engraftment. ACS Nano **2014**, 8, 10815–10825.

(6) Payyappilly, S.; Dhara, S.; Chattopadhyay, S. Thermoresponsive Biodegradable PEG-PCL-PEG Based Injectable Hydrogel for Pulsatile Insulin Delivery. J. Biomed. Mater. Res. A **2014**, 102, 1500–1509.

(7) Gong, C.; Qi, T.; Wei, X.; Qu, Y.; Wu, Q.; Luo, F.; Qian, Z. Thermosensitive Polymeric Hydrogels as Drug Delivery Systems. Curr. Med. Chem. **2013**, 20, 79–94.

(8) Van Tomme, S. R.; Van Steenbergen, M. J.; De Smedt, S. C.; Van Nostrum, C. F.; Hennink, W. E. Self-Gelling Hydrogels Based on Oppositely Charged Dextran Microspheres. Biomaterials **2005**, 26, 2129–2135.

(9) Hou, Y.; Schoener, C. A.; Regan, K. R.; Munoz-pinto, D.; Mariah, S.; Grunlan, M. A. Photo-Crosslinked PDMSstar-PEG Hydrogels: Synthesis, Characterization, and Potential Application for Tissue Engineering Scaffolds. Biomacromolecules **2010**, 11, 648–656.

(10) Jiang, Y.; Chen, J.; Deng, C.; Suuronen, E. J.; Zhong, Z. Click Hydrogels, Microgels and Nanogels: Emerging Platforms for Drug Delivery and Tissue Engineering. Biomaterials **2014**, 35, 4969–4985.

(11) Annabi, N.; Mithieux, S. M.; Weiss, A. S.; Dehghani, F. Cross-Linked Open-Pore Elastic Hydrogels Based on Tropoelastin, Elastin and High Pressure CO2. Biomaterials **2010**, 31, 1655–1665.

(12) Patenaude, M.; Hoare, T. Injectable, Mixed Natural-Synthetic Polymer Hydrogels with Modular Properties. Biomacromolecules **2012**, 13, 369–378.

(13) Moreira Teixeira, L. S.; Leijten, J. C. H.; Wennink, J. W. H.; Chatterjea, A. G.; Feijen, J.; van Blitterswijk, C. A; Dijkstra, P. J.; Karperien, M. The Effect of Platelet Lysate Supplementation of a Dextran-Based Hydrogel on Cartilage Formation. Biomaterials **2012**, 33, 3651–3661.

(14) Matsuno, T. Design of Injectable Bone Tissue Engineering Scaffold Consists of SS-Tricalcium Phosphate Beads and Alginate. Tissue Engineering **2005**, 297–307.

(15) Frey, N.; Linke, A.; Süselbeck, T.; Müller-Ehmsen, J.; Vermeersch, P.; Schoors, D.; Rosenberg, M.; Bea, F.; Tuvia, S.; Leor, J. Intracoronary Delivery of Injectable Bioabsorbable Scaffold (IK-5001) to Treat Left Ventricular Remodeling After ST-Elevation Myocardial Infarction: A First-in-Man Study. Circ. Cardiovasc. Interv. **2014**, 1–7.

(16) Hori, Y.; Winans, A. M.; Huang, C. C.; Horrigan, E. M.; Irvine, D. J. Injectable Dendritic Cell-Carrying Alginate Gels for Immunization and Immunotherapy. Biomaterials **2008**, 29, 3671–3682.

(17) Smeets, N. M. B.; Bakaic, E.; Patenaude, M.; Hoare, T. Injectable and Tunable Poly(ethylene Glycol) Analogue Hydrogels Based on Poly(oligoethylene Glycol Methacrylate). Chem. Commun. **2014**, 50, 3306–3309.

(18) Tai, H.; Howard, D.; Takae, S.; Wang, W.; Vermonden, T.; Hennink, W. E.; Stayton, P. S.; Hoffman, A. S.; Endruweit, A.; Alexander, C.; et al. Photo-Cross-Linked Hydrogels from Thermoresponsive PEGMEMA-PPGMA-EGDMA Copolymers Containing Multiple Methacrylate Groups: Mechanical Property, Swelling, Protein Release, and Cytotoxicity. Biomacromolecules **2009**, 10, 2895–2903.

(19) García, A. J. PEG-Maleimide Hydrogels for Protein and Cell Delivery in Regenerative Medicine. Ann. Biomed. Eng. **2014**, 42, 312–322.

(20) Sá-Lima, H.; Tuzlakoglu, K.; Mano, J. F.; Reis, R. L. Thermoresponsive poly(N-

Isopropylacrylamide)-G-Methylcellulose Hydrogel as a Three-Dimensional Extracellular Matrix for Cartilage-Engineered Applications. J. Biomed. Mater. Res. A **2011**, 98, 596–603.

(21) Bakaic, E.; Smeets, N. M. B.; Dorrington, H.; Hoare, T. "Off-the-Shelf" thermoresponsive Hydrogel Design: Tuning Hydrogel Properties by Mixing Precursor Polymers with Different Lower-Critical Solution Temperatures. RSC Adv. **2015**, 5, 33364–33376.

(22) Patenaude, M.; Hoare, T. Injectable, Degradable Thermoresponsive Poly(N -Isopropylacrylamide) Hydrogels. ACS Macro Lett. **2012**, 1, 409–413.

(23) Lutz, J.-F. Thermo-Switchable Materials Prepared Using the OEGMA-Platform. Adv. Mater. **2011**, 23, 2237–2243.

(24) Working, P. K., Newman, M.S.; Johnson, J.; Cornacoff, J. B. Safety of Poly(ethylene Glycol) and Poly(ethylene Glycol) Derivatives. Poly(ethylene glycol) **1997**, 45–57.

(25) Hu, Z.; Cai, T.; Chi, C. Thermoresponsive Oligo(ethylene Glycol)-Methacrylate- Based Polymers and Microgels. Soft Matter **2010**, 6, 2115.

(26) Haraguchi, Y.; Shimizu, T.; Yamato, M.; Okano, T. Regenerative Therapies Using Cell Sheet-Based Tissue Engineering for Cardiac Disease. Cardiol. Res. Pract. **2011**, 2011, 845170.

(27) Cooperstein, M. A; Canavan, H. E. Biological Cell Detachment from poly(N-Isopropyl Acrylamide) and Its Applications. Langmuir **2010**, 26, 7695–7707.

(28) Smeets, N. M. B.; Bakaic, E.; Patenaude, M.; Hoare, T. Injectable Poly(oligoethylene Glycol Methacrylate)-Based Hydrogels with Tunable Phase Transition Behaviours: Physicochemical and Biological Responses. Acta Biomater. **2014**, 10, 4143–4155.

(29) Guo, B.; Finne-Wistrand, A.; Albertsson, A.-C. Facile Synthesis of Degradable and Electrically Conductive Polysaccharide Hydrogels. Biomacromolecules **2011**, 12, 2601–2609.

(30) Khutoryanskiy, V. V. Advances in Mucoadhesion and Mucoadhesive Polymers. Macromol. Biosci. **2011**, 11, 748–764.

(31) Kakoulides, E. P.; Smart, J. D.; Tsibouklis, J. Azocrosslinked Poly(acrylic Acid) for Colonic Delivery and Adhesion Specificity: In Vitro Degradation and Preliminary Ex Vivo

Bioadhesion Studies. J. Control. Release **1998**, 54, 95–109.

(32) Matsusaki, M.; Akashi, M. Novel Functional Biodegradable Polymer IV: pH-Sensitive Controlled Release of Fibroblast Growth Factor-2 from a Poly(gamma-Glutamic Acid)-Sulfonate Matrix for Tissue Engineering. Biomacromolecules **2005**, 6, 3351–3356.

(33) Wu, D. Q.; Sun, Y. X.; Xu, X. D.; Cheng, S. X.; Zhang, X. Z.; Zhuo, R. X. Biodegradable and pH-Sensitive Hydrogels for Cell Encapsulation and Controlled Drug Release. Biomacromolecules **2008**, 9, 1155–1162.

(34) Hoemann, C. D.; Sun, J.; Légaré, a; McKee, M. D.; Buschmann, M. D. Tissue Engineering of Cartilage Using an Injectable and Adhesive Chitosan-Based Cell-Delivery Vehicle. Osteoarthritis Cartilage **2005**, 13, 318–329.

(35) D'Arrigo, G.; Di Meo, C.; Pescosolido, L.; Coviello, T.; Alhaique, F.; Matricardi, P. Calcium Alginate/dextran Methacrylate IPN Beads as Protecting Carriers for Protein Delivery. J. Mater. Sci. Mater. Med. **2012**, 23, 1715–1722.

(36) Bocourt, M. Interpenetrated Chitosan-Poly(Acrylic Acid-Co-Acrylamide) Hydrogels. Synthesis, Characterization and Sustained Protein Release Studies. Mater. Sci. Appl. **2011**, 2, 509–520.

(37) Elliott, J. E.; Macdonald, M.; Nie, J.; Bowman, C. N. Structure and Swelling of Poly (Acrylic Acid) Hydrogels : Effect of pH , Ionic Strength , and Dilution on the Crosslinked Polymer Structure. **2004**, 45, 1503–1510.

(38) van de Wetering, P.; Zuidam, N. J.; van Steenbergen, M. J.; van der Houwen, O. A. G. J.; Underberg, W. J. M.; Hennink, W. E. A Mechanistic Study of the Hydrolytic Stability of Poly (2-(Dimethylamino) Ethyl Methacrylate). Macromolecules **1998**, 31, 8063–8068.

(39) Zhai, M.; Chen, Y.; Yi, M.; Ha, H. Swelling Behaviour of a New Kind of Polyampholyte Hydrogel Composed of Dimethylaminoethyl Methacrylate and Acrylic Acid. Polym. Int. **2004**, 53, 33–36.

(40) Yan, H.; Jin, B. Influence of Environmental Solution pH and Microstructural Parameters on Mechanical Behavior of Amphoteric pH-Sensitive Hydrogels. Eur. Phys. J. E. Soft Matter **2012**, 35, 36.

(41) Feng, Z.; Shao, Z.; Yao, J.; Chen, X. Protein Adsorption and Separation on Amphoteric

Chitosan/ Carboxymethylcellulose Membranes. JBRM **2008**, 86, 694–700.

(42) Damodaran, V. B.; Murthy, N. S. Bio-Inspired Strategies for Designing Antifouling Biomaterials. Biomater. Res. **2016**, 20, 18.

(43) Sun, T. L.; Kurokawa, T.; Kuroda, S.; Ihsan, A. Bin; Akasaki, T.; Sato, K.; Haque, M. A.; Nakajima, T.; Gong, J. P. Physical Hydrogels Composed of Polyampholytes Demonstrate High Toughness and Viscoelasticity. Nat. Mater. **2013**, 12, 932–937.

(44) Hoare, T.; Young, S.; Lawlor, M. W.; Kohane, D. S. Thermoresponsive Nanogels for Prolonged Duration Local Anesthesia. Acta Biomater. **2012**, 8, 3596–3605.

(45) Parker, J.; Mitrousis, N.; Shoichet, M. S. Hydrogel for Simultaneous Tunable Growth Factor Delivery and Enhanced Viability of Encapsulated Cells in Vitro. Biomacromolecules **2016**, 17, 476–484.

(46) McKinnon, D. D.; Domaille, D. W.; Cha, J. N.; Anseth, K. S. Bis-Aliphatic Hydrazone-Linked Hydrogels Form Most Rapidly at Physiological pH: Identifying the Origin of Hydrogel Properties with Small Molecule Kinetic Studies. Chem. Mater. **2014**, 26, 2282–2387.

(47) Adroher-Benítez, I.; Martin-Molina, A.; Ahualli, S.; Quesada-Perez, M.; Odriozola, G.; Moncho Jorda, A. Competition between Excluded-Volume and Electrostatic Interactions in Nanogels Swelling: Effect of the Counterion Valence and Nanogel Charge. Phys. Chem. Chem. Phys. **2017**, 9–11.

(48) Su, J.; Hu, B.-H.; Lowe, W. L.; Kaufman, D. B.; Messersmith, P. B. Anti-Inflammatory Peptide-Functionalized Hydrogels for Insulin-Secreting Cell Encapsulation. Biomaterials **2010**, 31, 308–314.

(49) Nicodemus, G. D.; Bryant, S. J. Cell Encapsulation in Biodegradable Hydrogels for Tissue Engineering Applications. Tissue Eng. Part B. Rev. **2008**, 14, 149–165.

(50) O'Cearbhail, E.; Ng, K.; Karp, J. Emerging medical devices for inimally invasive cell therapy. Mayo Clinic Preceedings **2011,** 2, 259-273.

(51) Samal, S. K.; Dash, M.; Van Vlierberghe, S.; Kaplan, D. L.; Chiellini, E.; van Blitterswijk, C.; Moroni, L.; Dubruel, P. Cationic Polymers and Their Therapeutic Potential. Chem. Soc. Rev. **2012**, 41, 7147–7194.

(52) Lavik, E. B.; Klassen, H.; Warfvinge, K.; Langer, R.; Young, M. J. Fabrication of Degradable

Polymer Scaffolds to Direct the Integration and Differentiation of Retinal Progenitors. Biomaterials **2005**, 26, 3187–3196.

6.8 TOC Graphic

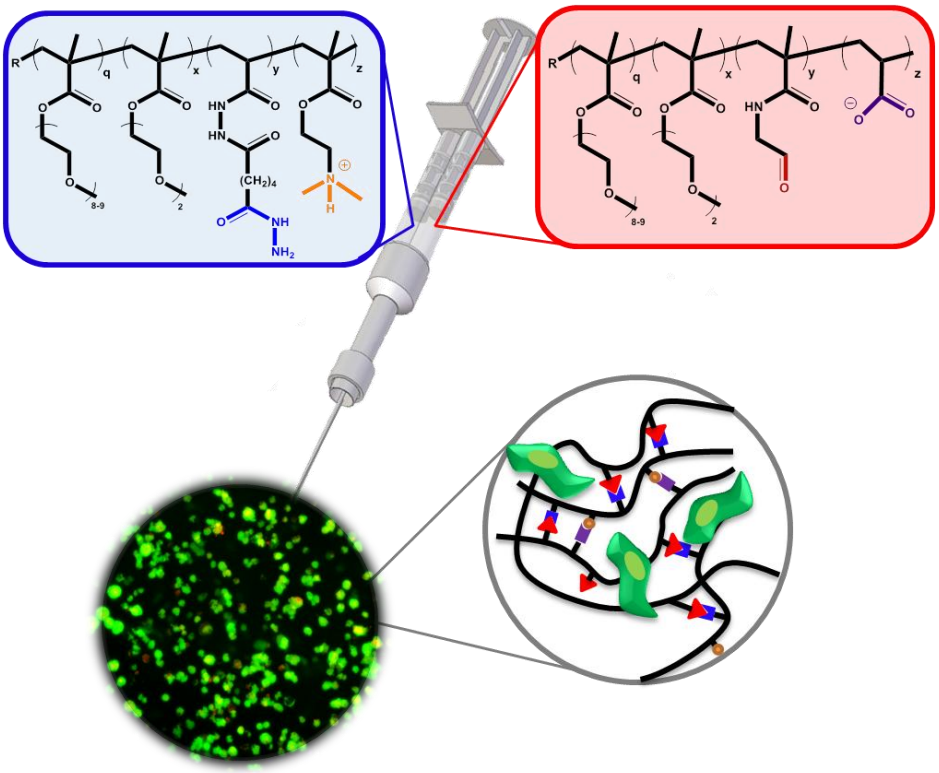

6.9 Supporting Information

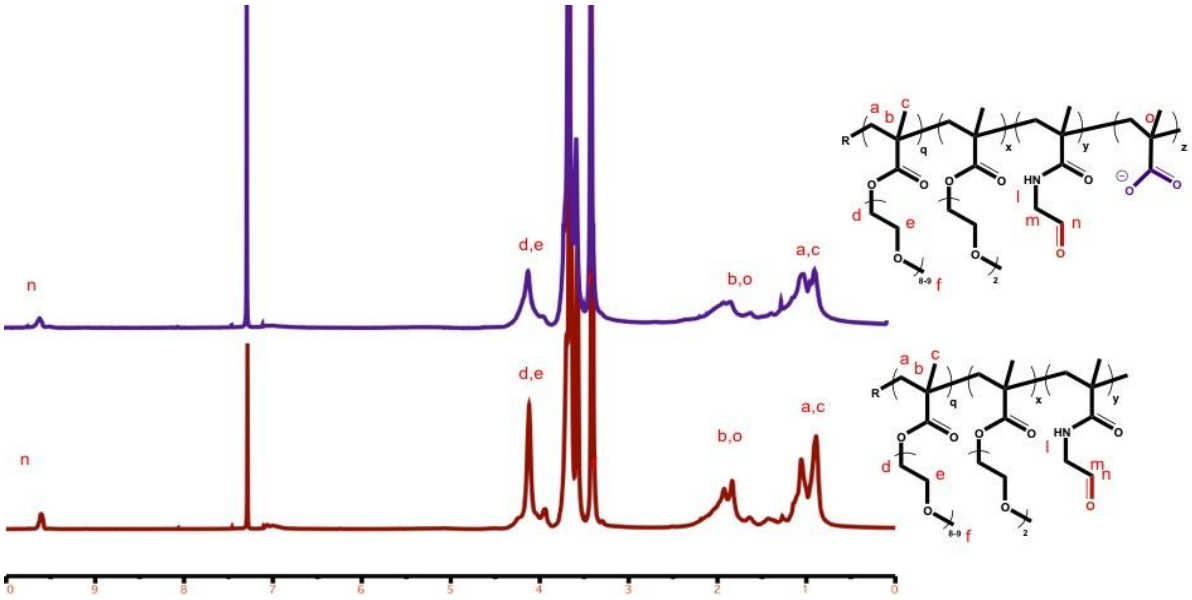

Figure S6.1. ^{1}H-NMR spectra for $PO_{10}A_{30}$ (red) and $PO_{10}H_{30}D_{20}$ (purple).

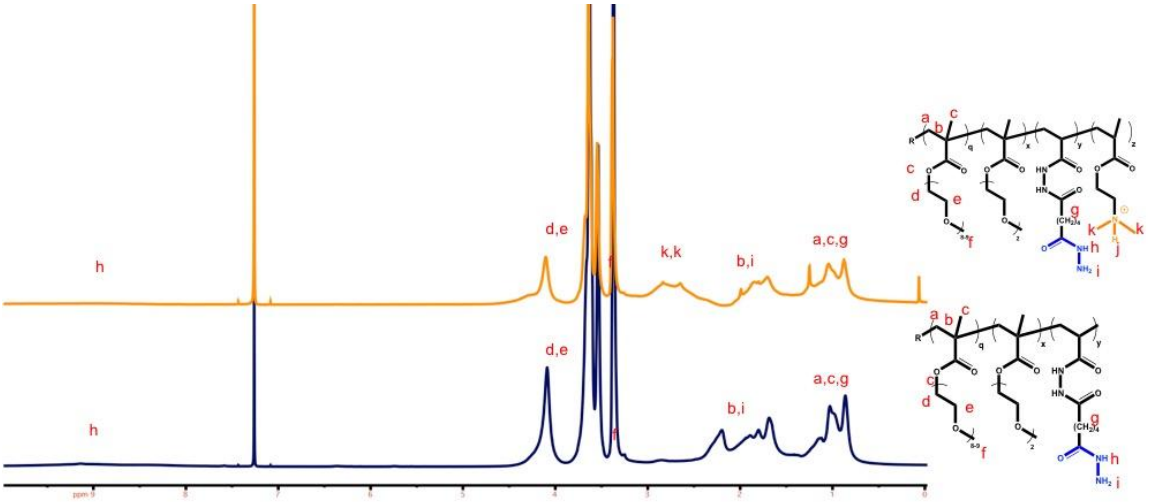

Figure S6.2. ^{1}H-NMR spectra for $PO_{10}H_{30}$ (blue) and $PO_{10}H_{30}C_{30}$ (orange).

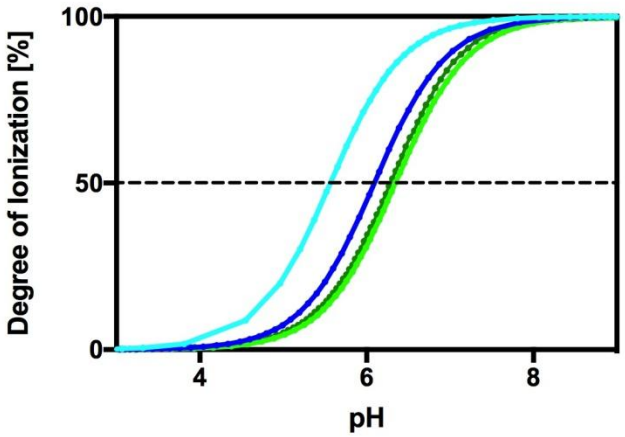

Figure S6.3. $PO_{10}H_{30}$ precursor polymer after being in pH=11 environment for; 0 hrs (●, blue); 24 hrs (●, light blue); 48 hrs (●, dark green); 96 hrs (●, green).

Chapter 7: Poly(oligoethylene glycol methacrylate)-Dextran In situ Gelling Hydrogels with Defined Biological Properties for Extracellular Matrix Design

Preface:

This chapter describes the development of the first POEGMA hydrogel platform system to incorporate a natural polymer to exploit the native biological responses to natural polymers in biomedical applications. Using reactive hydrazone chemistry, we created an injectable and degradable hydrogel with tunable physiochemical and biological properties based on the ability to easily change the LCST of the polymer precursors as well as the functional group density of the hydrazide POEGMA polymer precursor. We also show that the inclusion of the natural polymer dextran has the potential to change the response of our materials in both *in vitro* and *in vivo* environments with 3T3 mouse fibroblasts and BALB/c mice respectively. This research greatly widens the ultimate potential application of the POEGMA-based hydrogels to fabricate bioactive materials.

Emilia Bakaic‡, Niels M.B. Smeets‡, Mathew Patenaude and Todd Hoare

Department of Chemical Engineering, McMaster University, 1280 Main St. W, Hamilton, Ontario, Canada L8S 4L7

‡ These authors contributed equally

Keywords: Hydrogels, hydrazone, *in situ* gelling, dextran, poly(oligoethylene glycol methacrylate), cell adhesion

Abstract

The design of injectable modular hydrogels based on the simple mixing of hydrazide or aldehyde-functionalized synthetic poly(oligoethylene glycol methacrylate) (POEGMA) and natural dextran (DEX) polymers is presented. The synthetic POEGMA component imparts the hydrogel with the "stealth" properties of poly(ethylene glycol) and thermoresponsive properties, whereas the natural DEX components significantly enhances cell adhesion to the matrices (as is generally desirable for adhesion-dependent mammalian cells). Hydrogel properties such as swelling, degradation, and mechanics can be controlled by systematically varying the lower critical solution temperature and functional group density of the POH precursor. Relative to POEGMA hydrogels alone, POEGMA-DEX hydrogels facilitate improved potential for cell adhesion, significantly increasing the adhesion of 3T3 mouse fibroblasts *in vitro*; relative to dextran hydrogels alone, non-specific protein adsorption is significantly lower and chronic inflammation following subcutaneous injection into BALB/c mice is significantly suppressed. Furthermore, by changing which polymer is functionalized with hydrazide or aldehyde groups, substantial differences in biointerfacial properties are observed between gels containing the same mass fractions of POEGMA and DEX, an effect we hypothesize to be related to the higher interfacial affinity of the POEGMA polymers in an aqueous environment.

7.1 Introduction

Hydrogels have been widely applied as promising materials for mimicking native extracellular matrices (ECM) to facilitate cell proliferation, growth, and migration, leveraging the potential of hydrogels to create and maintain a dynamic three-dimensional space for tissue formation and present cell-specific environmental and metabolic cues.[1–3] Hydrogels used to encapsulate cells must enable both cell adhesion as well as migration through the hydrogel, behaviour that is related both to the mechanical and physiochemical properties of the hydrogel as well as functional moieties within the hydrogel network[4–7]. Besides promoting favorable cell responses, hydrogels designed for *in vivo* applications must also be non-inflammatory and fully degradable into non-toxic fragments that can be cleared or metabolized. Finally, for the majority of controlled release or tissue engineering applications, it is desirable that the hydrogel can be introduced *in vivo* through a minimally invasive procedure such as injection.[8–10]

We have previously reported injectable and degradable hydrogels based on poly(oligoethylene glycol methacrylate (POEGMA), an material that exhibits similar non-immunogenic, non-cytotoxic, and protein and cell repellent properties to poly(ethylene glycol) (PEG)[11,12]. These hydrogels are synthesized by co-extruding hydrazide and aldehyde functionalized POEGMA precursors that quickly cross-link through hydrazone chemistry. The composition[13], morphology,[14,15] and type/degree of functionalization[16] of the POEGMA precursors can be modified to control the physiochemical and biological properties of the resulting hydrogel. The use of covalent dynamic hydrazone chemistry allows cleaving and reforming of cross-links in response to cell-induced stress and/or as a function of time[17]. We have shown that *in situ*-gelling POEGMA hydrogels can mimic the mechanical properties of biological tissues and the degradation products were well tolerated *in vivo*,[18,19] making them of significant interest for potential tissue engineering applications. However, while the low protein adsorption and minimal chronic inflammation observed with POEGMA hydrogels was favourable in a tissue engineering context, cell adhesion to such hydrogels was minimal unless the only short-chain OEGMA comonomers are used to prepare the gel[18], in which case the ease of handling and low non-specific protein adsorption benefits of POEGMA are at least somewhat

compromised.[18] Incorporating tethered cell adhesive peptide RGD does significantly improve cell adhesion, but at a cost of synthetic simplicity and overall material cost.

Improving the cell adhesive properties of POEGMA-based injectable hydrogels via an inexpensive and biomimetic pathway would thus be highly beneficial to stimulate and regulate cell signalling, activation, maturation, and communication[20–22]. For example, many cell types rely on adhesion to proteins or other specific matrix components within their extracellular space as well as matrix degradation cues in order to stimulate migrate through the three-dimensional microenvironment[21–24]. On this basis, the incorporation of natural polymeric materials with defined cell interactions as well as the potential for enzymatic degradation (enabling improved remodeling by native cell processes) thus offers an attractive approach to advance extracellular matrix design.

To explore the potential of this concept of mixing natural polymers with POEGMA to develop new functional biomaterials with the benefits of each, we are employing dextran as our model natural polymer. Dextran is a polysaccharide consisting of 1,6-linked D-glucopyranose residues and is commonly used as an anti-thrombotic given its demonstrated ability to promote angiogenesis and fibrinolysis[25,26]. Dextran hydrogels have been previously investigated as drug delivery vehicles [27,28] and more recently in tissue engineering applications because of the inherent resistance of dextran to protein adsorption[29,30]. The hydroxyl groups along the dextran backbone render it particularly suitable for chemical modification to introduce reactive groups for cross-linking into a hydrogel, and the *cis*-hydroxyl groups present on the chain facilitate easy conversion of the (2,3) hydroxyl groups to aldehydes via periodate treatment[31]. Such functionalization enables facile crosslinking of dextran with nucleophiles (such as the hydrazide groups used to produce *in situ*-gelling POEGMA hydrogels) and/or conjugation of bioactive agents through either non-degradable or degradable linkages for tunable release[32]. Furthermore, dextran can be degraded *in vivo* by naturally occurring enzymes[33] such as dextranases and/or oxidizing agents[33] in various organs in the human body. In addition to itself being of interest as a functional material, dextran also serves as an effective and much less expensive analogue of extracellular matrix glycosoaminoglycans such as heparin sulfate (HS) or hyaluronic acid (HA), both of which could be incorporated into POEGMA hydrogels using

a similar approach. Coupling these advantages with the recently reported use of dextran for fabricating artificial wound sealants[34,35] suggests potential benefits of combining POEGMA and dextran in a single hydrogel that maintains the highly protein-repellent and potentially thermoresponsive properties of POEGMA with the cell adhesion/spreading properties and enzymatic degradability offered by dextran.

In this paper, we report on the synthesis and both physical and biological characterization of injectable hydrazone-cross-linked hydrogels based on rapid mixing of hydrazide-functionalized POEGMA (POH) and aldehyde-functionalized dextran (DEXA). We postulate that the incorporation of dextran into POEGMA hydrogels can promote cell interactions with our otherwise bio-inert POEGMA hydrogels, opening up the potential use of these (relatively inexpensive) soft materials in cell encapsulation applications. The results show that these POEGMA-Dextran (POEGMA-DEX) hydrogels provide cells with sufficient adhesive support to stick to the gels while preserving most of the bioinert and smart characteristics of the synthetic POEGMA polymer. Furthermore, both the POEGMA-DEX hydrogels and polymer precursors (and degradation products) are demonstrated to be non-cytotoxic and well-tolerated *in vivo* provided that excess aldehyde:hydrazide ratios are kept reasonably low. Taken together, we believe that by combining POEGMA and dextran in a single injectable hydrogel formulation provides a promising route for designing biologically-translatable thermoresponsive injectable hydrogels applicable to the challenge of ECM design.

7.2 Experimental

7.2.1 Materials: Di(ethylene glycol) methyl ether methacrylate ($M(EO)_2MA$, Sigma Aldrich, 95%) and oligo(ethylene glycol) methyl ether methacrylate with a number-average molecular weight of 475 Da ($OEGMA_{475}$, Sigma Aldrich) were purified by passing each monomer through a column of basic aluminum oxide (Sigma Aldrich, type CG-20) to remove the methyl ether hydroquinone (MEHQ) and butylated hydroxytoluene (BHT) inhibitors. 2,2-azobisisobutryic acid dimethyl ester (AIBMe, Wako Chemicals, 98.5%), acrylic acid (AA, Sigma Aldrich, 99%), adipic acid dihydrazide (ADH, Alfa Aesar, 98%), dextran from Leuconstroc spp. M_r = 500,000 (Sigma Aldrich), sodium periodate (Sigma Aldrich, ≥99.8%), glacial acetic acid (Sigma Aldrich, ≥99%), chloroacetic acid

(Sigma Aldrich, ≥%99), ethylene glycol (Sigma Aldrich, 99.8%), N'-ethyl-N-(3-dimethylaminopropyl)-carbodiimide (EDC, Sigma Aldrich, commercial grade) and thioglycolic acid (TGA, Sigma Aldrich, ≥99.8%) were used as received. N-(2,2-dimethoxyethyl) methacrylamide (DMAEAm, 98%) was synthesized as previously reported.[19] For all experiments Milli-Q grade distilled deionized water (DIW) was used. Dimethyl sulfoxide (DMSO, reagent grade) and methanol (grade) was purchased from Caledon Laboratory Chemicals (Georgetown, ON). Hydrochloric acid (1M) was received from LabChem Inc. (Pittsburgh, PA). 3T3 Mus musculus mouse cells were obtained from ATCC: Cedarlane Laboratories (Burlington, ON). Cell proliferation media, recovery media, and trypsin-EDTA were obtained from Invitrogen (Burlington, ON). Thiazolyl blue tetrazolium bromide (MTT) was purchased from Sigma Aldrich (Oakville, ON). LIVE/DEAD assay were purchased from Invitrogen Canada (Burlington).

7.2.2 Synthesis of hydrazide-functionalized POEGMA (POH): In a typical experiment (Table 1 entry PO_5H_{30}), AIBMe (37 mg, 0.14 mmol), $M(EO)_2MA$ (3.5 g, 18.6 mmol), $OEGMA_{475}$ (0.50 g, 1.1 mmol), AA (0.60 g, 8.3 mmol), and TGA (8 µL, 0.12 mmol) were added to a 100 mL three-necked round-bottom flask. 20 mL dioxane was added, and the solution was purged with nitrogen for at least 30 minutes. Subsequently, the flask was submerged in a pre-heated oil bath at 75°C for 4 hours under magnetic stirring. After the solvent was removed, the resulting poly(ethylene glycol methacrylate-co-acrylic acid) polymer was rotovaped to remove any remaining solvent, purified by dialysis against DIW for a minimum of 6 (6+ hour) cycles and lyophilized to dryness. The carboxylic acid groups on the AA residues were subsequently converted to hydrazide groups via carbodiimide coupling of a large excess of adipic acid dihydrazide. PO_5H_{30} (3.0 g) was dissolved in 150 mL DIW and added to a 500 mL round-bottom flask. ADH (3.6 g, 20.5 mmol) was added, and the pH of the solution adjusted to pH = 4.75 using 0.1 M HCl. Subsequently, EDC (1.6 g, 10.2 mmol) was added, and the pH was maintained at pH = 4.75 by the dropwise addition of 0.1 M HCl for 4 hours. The solution was left to stir overnight, dialyzed against DIW for a minimum of 6 cycles, and lyophilized. The polymers were stored as 20 w/w% solutions in 10 mM PBS at 4°C.

7.2.3 Synthesis of aldehyde-functionalized POEGMA (POA): Briefly, In a typical experiment AIBMe (50 mg), $M(EO)_2MA$ (3.9 g), $OEGMA_{475}$ (0.10 g), acetal functional monomer DMAEAm, as described previously[16], (1.30 g)and TGA (7.5 µL) were dissolved in 1,4-dioxane (20 mL) into a 100 mL round bottom flask. After purging for at least 30 min, the flask was sealed and submerged in a pre-heated oil bath at 75°C for 4 hours under magnetic stirring. After the reaction was completed, the solvent was removed, and the polymer was subsequently dissolved in 100 mL of 0.5 M HCl. The solution was left to stir for 24 hours, dialyzed (MWCO= 3500 g mol^{-1}) against DIW for a minimum of 6 cycles, and lyophilized. The polymers were stored as 20 w/w% solutions in 10 mM PBS at 4°C.

7.2.4 Synthesis of hydrazide-functionalized dextran (DEXH): 3.0 g of dextran (M_w ~ 500 kDa) was dissolved in 42 mL of 3.0 M NaOH solution. Upon dissolution, chloroacetic acid (7.29 g, 77 mmol) was added and the solution was stirred for 90 min at 70°C. The solution was cooled to room temperature and neutralized using glacial acetic acid. The resulting carboxymethylated polymer was precipitated in methanol and subsequently purified by stirring in acetone and drying under vacuum. To convert carboxyl groups to hydrazide groups, 1.5 g of carboxymethylated dextran was dissolved in 150 mL DIW and ADH (3.5 g, 20.5 mmol) was added, after which the pH of the solution adjusted to pH = 4.75 using 0.1 M HCl. EDC (1.6g, 10.2 mmol) was then added and the pH was maintained at pH = 4.75 by the dropwise addition of 0.1 M HCl for 4 hours. The product was left to stir overnight, dialyzed against DIW for a minimum of 6 cycles, and lyophilized.

7.2.5 Synthesis of aldehyde-functionalized dextran (DEXA): 3.0 g of dextran (M_w = 500 kDa) was dissolved in 300 mL of DIW in a 500 mL round bottom flask. 1.6 g of sodium periodate was dissolved in 10 mL of DIW and added to the dextran solution dropwise under magnetic stirring. After two hours, 0.8 mL of ethylene glycol was added to the solution and the solution was stirred for one more hour to quench the oxidation. The product was subjected to 6 x 6+ hour cycles of dialysis for purification and lyophilized for storage.

7.2.6 Analysis of functionalized polymers: Polymer molecular weight was measured by gel permeation chromatography (GPC) using a Waters 2695 separations module equipped with a Waters 2996 photodiode array detector, a Waters 2414 refractive index detector, a Waters 2475 multi λ fluorescence detector and four Polymer Labs PLgel individual pore size columns, with 5 µm bead size and pore sizes of 100, 500, 103 and 105Å, maintained at 40°C. Tetrahydrofuran (THF) was used as the eluent at a flow rate of 1.0 mL min^{-1}, and polystyrene standards were used to calibrate the instrument. ^{1}H-NMR was performed on a Bruker AVANCE 600 MHz Spectrometer using deuterated chloroform as the solvent. The mole fraction of $M(EO)_2MA$ (n) and $OEGMA_{475}$ (m) incorporated into each polymer was calculated based on the NMR results using the methodology reported by the Wang group.[36] The acrylic acid content of the polymers was determined using base-into-acid conductometric titration (ManTech Associates), using 50 mg of polymer dissolved in 50 mL of 1 mM NaCl as the analysis sample and 0.1 M NaOH as the titrant. The degree of aldehyde functionalization of dextran was determined by selectively oxidizing aldehyde groups to carboxylic acid groups using silver (I) oxide and quantifying the resulting acid groups using conductometric titration. Briefly, DEXA (0.1 g, 0.0002 mmol) was dissolved in 10 mL of DIW with sodium hydroxide (0.248 g, 6.2 mmol). Subsequently, silver (I) oxide (0.386 g, 1.6 mmol) was added to the solution and the solution was allowed to stir overnight. Following, 5 mL of the reaction solution was added to 45 mL of deionized water and the solution was titrated using 0.1M NaOH. The degree of POEGMA aldehyde functionalization was determined from ^{1}H-NMR analysis, comparing the integral values of the $-OCH_3$ signal (3H, δ = 3.35-3.45 ppm), and –CHO signal (1H, δ = 9.50-9.58 ppm). The cloud point temperature of the POEGMA polymers was measured using a Variant Cary Bio 100 UV-Vis spectrophotometer. The polymers were dissolved at a concentration of 1 mg/mL in either PBS (pH = 7.4) or a KCl/HCl (pH = 2.0), and the absorbance was recorded at 500 nm at every 0.5°C over a temperature range of 10°C to 80°C, ramped at a rate of 1°C/min.

7.2.7 Preparation of injectable hydrogels: The composite hydrogels were fabricated via co-extrusion of hydrazide-functionalized and aldehyde-functionalized copolymers dissolved in 10 mM PBS. Typical concentrations used for all hydrogels reported are 60 mg/mL for POH and

POA, 60 mg/mL of DEXH and 60 mg/mL for DEXA, with specific recipes used defined in the results. Intensive mechanical mixing of both polymer precursor solutions was achieved through the use of a double barrel syringe fitted with a static mixer at the outlet (Medmix L series). Hydrogel disks were prepared by extrusion of the reactive polymer precursors through the double barrel syringe into cylindrical silicone rubber molds (volume = 300 µL) and allowed to gel for a minimum of 30 minutes prior to testing.

7.2.8 Hydrogel morphology: The morphology of the gels was analyzed via scanning electron microscopy (SEM) using a Hitachi S-2150 instrument. Following gelation as described in section 7.2.7, hydrogels were placed into scintillation vials and rapidly frozen in liquid nitrogen. The frozen samples were then freeze fractured overnight to create a dried porous scaffold. Each sample was prepared in triplicate. Samples were sputter coated with platinum before analysis to minimize charging.

7.2.9 Phase transition of POEGMA-DEXA hydrogels: The volume phase transition temperature of the hydrogel disks was determined gravimetrically. Hydrogels were placed inside scintillation vials filled with 10 mM PBS and submerged into a thermostatted water bath. After a 12-hour incubation period, the hydrogels were gently dried using a Kimwipe to remove non-absorbed PBS and weighed. The PBS was replenished after every incubation cycle, and the temperature of the water bath increased by 5°C. The mass loss of the hydrogels was calculated by comparing the mass of the hydrogel at any given temperature to the initial mass of the same hydrogel measured at 22.5°C (room temperature). All experiments were performed in triplicate, with reported error bars representing the standard error of the repeat measurements.

7.2.10 Reversible swelling of POEGMA-DEXA hydrogels: The capacity of the hydrogels to undergo reversible swelling responses with temperature was determined gravimetrically using cell culture inserts (10.5 cm, 8 µm pore size). Hydrogel disks were individually placed into cell culture inserts, which were subsequently placed into a 12-well cell culture plate, submerged in 4 mL of 10 mM PBS, and allowed to equilibrate for 12 hours at room temperature (22.5°C) or

physiological temperature (37°C). After the equilibration period, the hydrogels were gently dried with a Kimwipe to wick off non-absorbed PBS and weighed. Eight complete thermal cycles were conducted in triplicate, with error bars representing the standard error of the repeat measurements.

7.2.11 Hydrogel degradation: Hydrogel degradation via hydrazone bond hydrolysis was assayed in both PBS as well as accelerated acid-catalyzed conditions, the latter of which is useful to more directly compare the effects of different gel compositions on degradation via hydrazone hydrolysis. Hydrogel disks were placed inside the same cell culture inserts used for the reversible swelling assay and submerged in 4.0 mL of 0.1 M HCl, 1.0 M HCl, or 10 mM PBS. Degradation was quantified gravimetrically at pre-determined time intervals until the hydrogel had completely degraded (i.e. no separate hydrogel phase could be identified). All experiments were repeated in triplicate, with error bars representing the standard deviation of the measurement.

7.2.12 Hydrogel rheology: The rheological properties of the hydrogels were measured using an ARES rheometer (TA Instruments) operating under parallel-plate geometry with a plate diameter of 7 mm and a plate spacing of 1 mm. Rheological properties were measured by first conducting a strain sweep from 0.1−100% strain at 1 Hz to identify the linear viscoelastic range of the hydrogels. A strain was then selected from within this linear range and set as a constant to perform a frequency sweep from 0.1 to 100 rad/s to measure shear elastic (G') and loss (G") moduli. All measurements were conducted in triplicate at room temperature.

7.2.13 Cytotoxicity assay: The cytocompatibility of polymer precursors and hydrogels was quantified using a MTT assay using NIH 3T3 fibroblasts. Cells were plated at density of 1.0×10^4 cells per well in a 24-well plate and maintained in DMEM media supplemented with 10% FBS and 1% penicillin. After one day of incubation, polymer concentrations ranging from 200 to 2000 μg/mL were added into wells with cultured cells and incubated for an additional 24 hours. Cell viability was then characterized by removing the polymer solution, adding the MTT reagent

solution, and incubating over four hours. The resultant formazin precipitate was solubilised with DMSO and the absorbance was read using a Biorad microplate reader (model 550) at 570 nm. Each sample was tested four times, with error bars representing the standard error of the cell viability percentages measured. Viability results were compared to controls of media-only (no cells, to correct for media absorbance) and cells-only (no materials added).

7.2.14 Protein adsorption: Protein adsorption of fluorescently-labeled bovine serum albumin (BSA, prepared as previously described)[15,16] was assessed by directly extruding the hydrogels into the wells of a 96 well plate, allowing gelation to complete (4 hours), and then fully swelling the hydrogels in 10 mM PBS (30 hours). Following incubation, the PBS was removed and BSA stock solutions of 125, 250, 500 and 1000 μg/mL prepared in 10 mM PBS were added and incubated at 37°C for 2 hours. Each sample was tested six times, with error bars representing the standard deviation of the adsorption measured.

7.2.15 In vitro cell adhesion assay: Cell adhesion was assayed in 48-well plates using 3T3 fibroblasts as a model cell. Hydrogels were extruded directly into the wells, left overnight to ensure complete gelation, and then washed with culture media prior to cell addition. Cells were then plated on top of the hydrogel at a density of 1.0×10^4 cells per well together with 400 μL of DMEM media and incubated for 24 hours at 37°C. After incubation, cell viability on the hydrogels was visualized using a LIVE/DEAD assay performed according to the manufacturer's protocol. Post staining, each well was washed three times with sterile 10 mM PBS to remove any non-adherent cells from the gels. Stained gels in the 48-plate wells were visualized under fluorescence using an OLUMPUS light microscope. All experiments were conducted in quadruplicate.

7.2.16 In vivo tolerability assay: The in vivo toxicity of the hydrogels was assessed using a mouse subcutaneous injection model. BALB/c mice (22-24 g, Charles River Laboratories) were injected with 0.35 mL samples of $PO_{10}H_{30}$-DEXA and DEXH-DEXA hydrogels subcutaneously in the scruff of the neck using a double-barrel syringe pre-loaded with gel precursor polymers

corresponding to the specific gel type. Each precursor polymer was dissolved in 10mM PBS at a concentration of 60mg/mL, and sterilized through a 0.2µm cellulose acetate syringe filter. Animals were visually observed to identify any systemic toxic response until the pre-determined end points of 2days (acute response) and 1 month (chronic response), at which point animals were sacrificed. A tissue sample that includes skin, underlying tissue, and residual material was recovered from the animals and subjected to histological analysis using hematoxylin and eosin staining. Tissue responses to the materials were assessed relative to control animal injections of only 10 Mm PBS. Animals were cared for in compliance with protocols approved by the Animal Research Ethics Board at McMaster University and regulations of the Animals for Research Act of the Province of Ontario and the guidelines of the Canadian Council on Animal Care.

7.3 Results

7.3.1 Synthesis of hydrazide and aldehyde functionalized polymer precursors: The synthetic schemes used to prepare each functional precursor polymer are shown in Scheme 7.1.

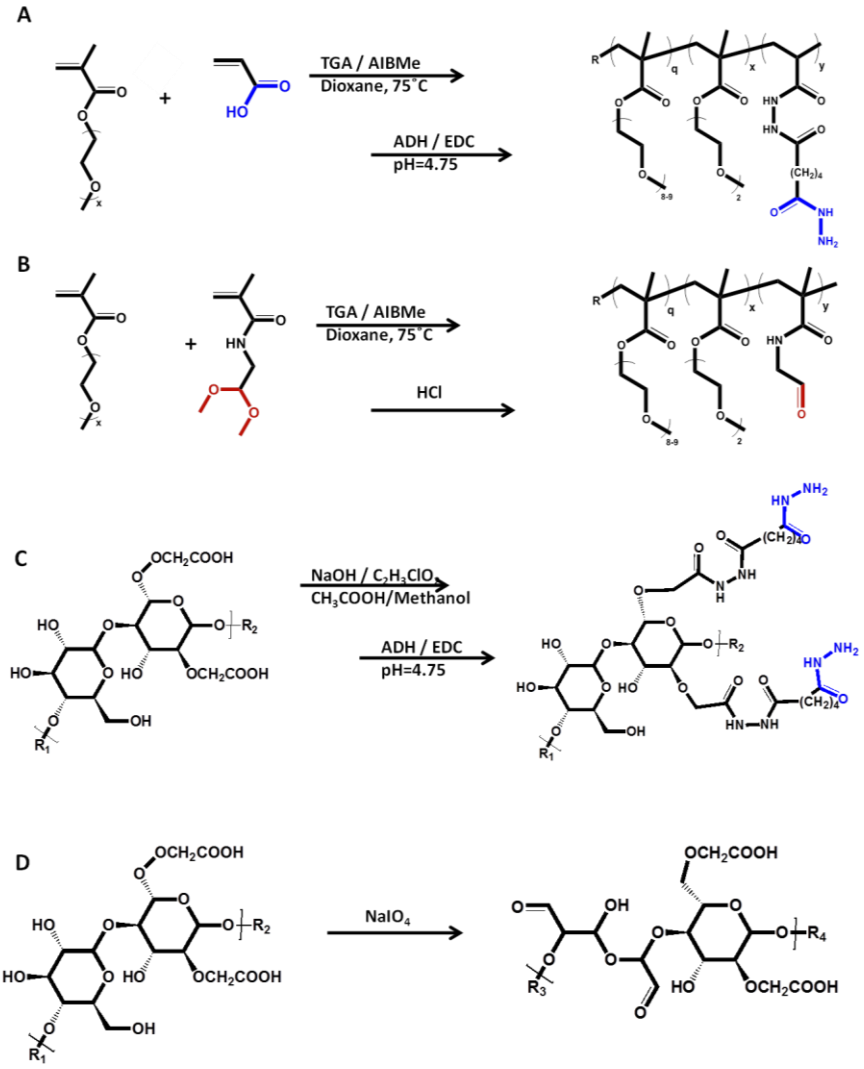

Scheme 7.1. Synthesis of (A) hydrazide (POH) and (B) aldehyde (POA)-functionalized poly(oligoethylene glycol methacrylate) and (C) hydrazide (DEXH) and (D) aldehyde-functionalized dextran (DEXA).

Dextran-aldehyde (DEXA) was synthesized by oxidizing the vicinal diols on the glucose repeat unit dextran (DEX) by sodium periodate (Scheme 7.1). Silver ion titration indicated that ~43% of the vicinal diol groups were oxidized to aldehyde groups, resulting in an aldehyde

content of $8.6x10^{-7}$ mol aldehyde groups/g polymer. Hydrazide-functionalized dextran (DEXH) was prepared via carboxylation of the vicinal diols using chloroacetic acid followed by carbodiimide coupling of adipic acid dihydrazide (ADH), yielding a polymer containing $6.0x10^{-7}$ mol hydrazide groups/g polymer as per conductometric titration analysis. Hydrazide-functionalized poly(oligoethylene glycol methacrylate) (PO_xH_y, where x represents the mole fraction of $OEGMA_{475}$ and y represents the mole fraction of total monomer residues bearing a hydrazide group) was produced via free radical copolymerization of OEGMA monomers and acrylic acid and subsequent carbodiimide coupling of adipic acid dihydrazide. The amount of acrylic acid, and thus the number of hydrazide groups per polymer chain, was systematically varied from ~10 for $PO_{10}H_{15}$ ($1.0x10^{-5}$ mol hydrazide/g polymer) to ~20 for $PO_{10}H_{30}$ ($1.3x10^{-5}$ mol hydrazide/g polymer) to ~50 for $PO_{10}H_{50}$ ($2.4x10^{-5}$ mol hydrazide/g polymer) (entries 2, 5, and 6, Table 7.1). Hydrazide-functionalized polymers were also prepared with different phase transition temperatures by varying the $M(EO)_2MA$: $OEGMA_{475}$ mol fraction from 95:5 to 80:20 (entries 1-4, Table 7.1); good agreement was observed between the theoretical and experimental compositions of the copolymers by ^{1}H-NMR analysis. Finally, aldehyde-functionalized poly(oligoethylene glycol methacrylate) ($PO_{10}A_{30}$, corresponding to 90% $M(EO)_2MA$:10% $OEGMA_{475}$ and 30 mol% of monomer residues bearing an aldehyde group) was prepared via free radical copolymerization of OEGMA monomers with the acetal-containing monomer DMAEAm followed by hydrolysis of the acetal in acid. ^{1}H NMR again confirms near-stoichiometric incorporation of the OEGMA monomers and 23.9 mol% of monomer residues bearing an aldehyde group ($1.2x10^{-5}$ mol aldehyde/g polymer).

Table 7.1. Chemical characterization of synthesized POH polymer precursors

	$M(EO)_2MA$ [mol%]	$OEGMA_{475}$ [mol%]	AA[a] [mol%]	% $M(EO_2)MA$[b]	M_n [kDa]	*Đ*	Funct. groups [#/chain]	CP_{95}[c] [°C]	CP_{50}[d] [°C]
PO_5H_{30}	0.75	0.02	0.23	0.97	19.3	1.77	26	61.9	65.8
$PO_{10}H_{30}$	0.73	0.05	0.22	0.93	17.0	1.59	21	64.1	67.2
$PO_{15}H_{30}$	0.72	0.09	0.19	0.89	17.3	1.40	18	67.7	70.8
$PO_{20}H_{30}$	0.66	0.14	0.20	0.82	20.9	1.44	21	75.9	80.0
$PO_{10}H_{50}$	0.56	0.04	0.40	0.93	17.1	1.91	47	N/A[e]	N/A[e]
$PO_{10}H_{15}$	0.79	0.06	0.15	0.93	14.4	1.70	11	54.7	56.8

[a] Determined from conductometric titration; [b] Percentage of total OEGMA monomers incorporated that are $M(EO)_2MA$ (remainder $OEGMA_{475}$) as determined by ^{1}H-NMR; [c] Determined at 95% transmittance at 1 mg/mL in 10 Mm PBS; [d] Determined at 50% transmittance at 1 mg/mL in PBS [e] No LCST was observed up to 80°C.

In order to limit the molecular weight of the synthetic, non-degradable POH polymers to facilitate clearance of these backbone non-degradable polymers via renal filtration, the free-radical copolymerization was performed in the presence of thioglycolic acid (TGA). The chain transfer constant (C_s) of TGA was determined experimentally to be 0.95. According to the Mayo Equation, the [TGA] / [monomer] was kept constant at 4.1×10^{-3} to synthesize functional POEGMA polymers with a similar number-average molecular weight (M_n) below the renal clearance limit of 40×10^3 g·mol^{-1}.[37–39] All polymers produced here had a $M_n \leq 20 \times 10^3$ g·mol^{-1} and a dispersity (*Đ*) of < 2.0 (Table 7.1). The relatively low values for *Đ* compared to other chain transfer-controlled polymerizations may be in part attributable to the branched nature of POEGMA polymers, leading to different elution behaviour when compared to the linear poly(styrene) (PS) calibration standards used to reference the molecular weight.

The cloud point of the hydrazide-functionalized POEGMA polymers as a function of the polymer composition is shown in Figure 7.1. UV-vis turbidimetric experiments were performed on polymer solutions (concentration 1 mg/mL) in either KCl/HCl aqueous solution (10 mM, pH = 2, all AA residues protonated) or PBS (10 mM PBS, pH = 7.4, most AA residues ionized). The cloud point values shown in Fig. 7.1 correspond to the temperatures at 50% (CP_{50}) and 95% (CP_{95}) transmittance; complete turbidimetric data is available in Supporting Information Figures S7.1 and S7.2. In 10 Mm PBS, POEGMA polymers prior to hydrazide functionalization contain

high fractions of ionized acrylic acid groups and are thus completely water-soluble, with no LCST observed up to at least 75°C. The LCST of the non-functionalized polymers was therefore measured in KCl/HCl to prevent ionization of the carboxylic acid groups (Fig. 7.1, black symbols) to facilitate comparisons between the precursor polymers.

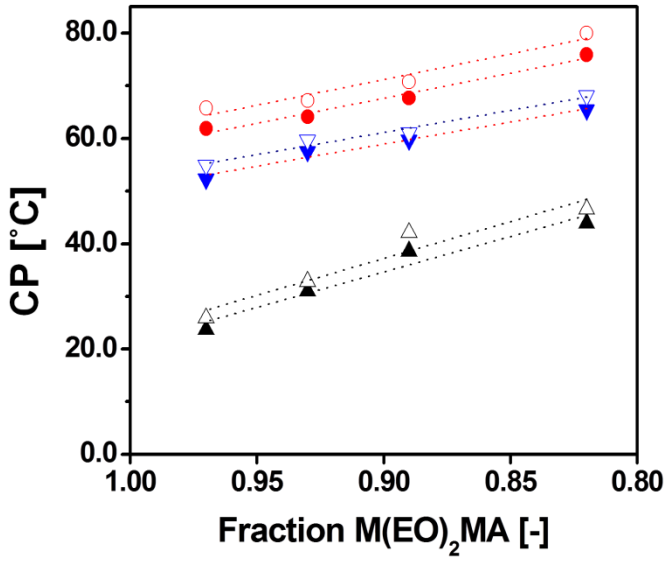

Figure 7.1. Cloud points (CP) of POEGMA polymers as a function of composition. The CP is determined from UV-vis turbidimetric experiments at either 95% transmittance (CP_{95}, open symbols) or 50% transmittance (CP_{50}, closed symbols): (▲, black) POEGMA-co-AA measured in KCl/HCl at pH = 2; (●, red) hydrazide functionalized POEGMA measured in PBS at pH = 7.4; (▼, blue) hydrazone functionalized POEGMA following reaction of hydrazide groups with acrolein measured in PBS at pH = 7.4. The dotted-lines are best linear fits.

The CP increases linearly with the mole fraction of OEGMA (f_{OEGMA}) from 25.9°C for PO_5H_{30} (3 mol% $OEGMA_{475}$) to 46.6°C for $PO_{20}H_{30}$ (18 mol% $OEGMA_{475}$), according to relationship CP = 23.2(±3.1) + 140.0(±27.4)·f_{OEGMA} (R^2 = 0.929). The linear correlation between the $OEGMA_{475}$ mole fraction and the cloud point of the polymer is in agreement with observations of other groups on the synthesis of statistical POEGMA copolymers[40–42], a result that holds here even in the presence of other functional monomers. The CP can consequently be tuned anywhere between the CP of $PM(EO)_2MA$ (LCST ~ 24°C) and $POEGMA_{475}$ (LCST ~ 90°C) by controlling the copolymer composition. The facile tunability and large LCST range that can be achieved using OEGMA monomers while still preserving sharp, discontinuous phase

transitions[41] (Fig. 7.1 and Supporting Information, Figure S1) provides a significant advantage over the use of N-isopropylacrylamide-based polymers, which typically exhibit broader and lower magnitude phase transitions in copolymers with higher CP values due to the required presence of more hydrophilic comonomers.

Functionalization of the POEGMA polymers with adipic acid dihydrazide significantly affects the cloud point of the POEGMA polymer (Fig. 7.1, Table 7.1; see also Supporting Information, Fig. S7.2). Whereas the POEGMA-co-AA polymers had no CP in 10 Mm PBS, the POH polymers (Fig. 7.1, circles) display a CP ranging from 61.9°C for PO_5H_{30} to 75.9°C for $PO_{20}H_{30}$. Of note, the linear dependency of the CP on the copolymer composition is preserved upon hydrazide functionalization (LCST = 61.5(±1.8) + 97.4(±15.7)·f_{OEGMA}; R^2 = 0.950). The hydrazide functional group of POH has a pK_a of approximately 3.4,[43] such that all hydrazide groups conjugated to the polymers are uncharged at pH = 7.4. Furthermore, titrimetric analysis showed that the EDC conjugation was highly efficient (> 95%), suggesting the presence of only a small number of residual AA groups in each polymer. As such, the polarity of hydrazide group is the primary driver of the increased LCST values in 10 mM PBS. This result is helpful in the ultimate clearance of these precursor polymers as degradation products, since the polymers will be freely soluble (not aggregated) at normal body temperature following gel degradation.

To estimate the effect of gelation on the phase transition behavior of the precursor polymers (and thus predict the volume phase transition temperature (VPTT) of *in situ*-gelled hydrogels, the POH precursors were reacted with a molar excess of acrolein (CH_2=CHO) to form a hydrazone bond, after which cloud points were re-measured (Fig. 7.1. Hydrazone bond formation significantly lowered the cloud points of the polymers relative to the hydrazide-functionalized polymer, although the trend in the cloud point as a function of f_{OEGMA} was preserved (CP = 61.6(±1.6) + 97.9(±14.4)·f_{OEGMA}; R^2 = 0.959).

7.3.2 Preparation of POEGMA-DEXA hydrogels: POEGMA-DEXA hydrogels were prepared by co-extruding 60 mg/mL solutions of the two reactive polymer precursors into a silicone mold using a double-barrel syringe. Gelation occurs quickly upon mixing, with elastic hydrogels formed with all combinations tested in <2 minutes at room temperature. Macroscopically, the

hydrogels vary significantly with the degree of cross-linking (see Fig. 7.2). Hydrogels prepared from $PO_{10}H_{15}$ (low hydrazide content) are mechanically weak and are unable to maintain the shape of the mold; conversely, hydrogels prepared from $PO_{10}H_{30}$ and $PO_{10}H_{50}$ (higher hydrazide contents) maintain the shape of the mold and cannot be deformed without physically breaking the hydrogel. Scanning electron microscopy (SEM) images of frozen, lyophilized and fractured hydrogels reveals that the hydrogels are homogeneous and do not contain micron-sized pores, with no systematic differences observed between the morphologies of hydrogels prepared using POH polymers with different hydrazide contents (Figure 7.2). This observation is in-line with previous studies that concluded that micron-sized pores are likely due to artefacts occurring during freezing of the hydrated samples.[44–46]

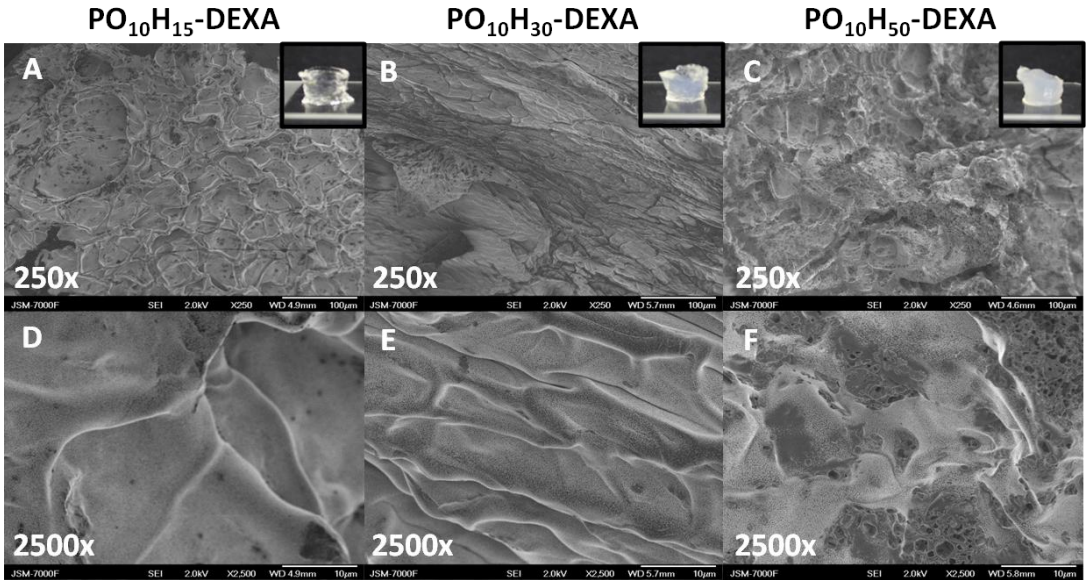

Figure 7.2. Scanning electron microscopy images of the lyophilized fractured POEGMA-DEX hydrogels at 250x and 2500x magnification. $PO_{10}H_{15}$-DEXA (A, D); $PO_{10}H_{30}$-DEXA (B, E) and $PO_{10}H_{50}$-DEXA (C, F). Insets show the macroscopic appearance of the different hydrogels.

7.3.3 Thermoresponsive swelling: To assess the thermoresponsive properties of the resulting synthetic-natural polymer hydrogels (and specifically how the DEX component affects the thermoresponsivity of the POEGMA component, the POEGMA-DEXA hydrogels were slowly heated (12 hour equilibration intervals) from 20°C to 50°C in 5°C increments. The resulting

thermal phase transitions of the hydrogels (measured via gravimetry) are shown in Figure 7.3. The VPTT curves of a DEXA-DEXB hydrogel and a $PO_{10}H_{30}$ hydrogel (based on $PO_{10}H_{30}$ and $PO_{10}A_{30}$) were also included for comparison.

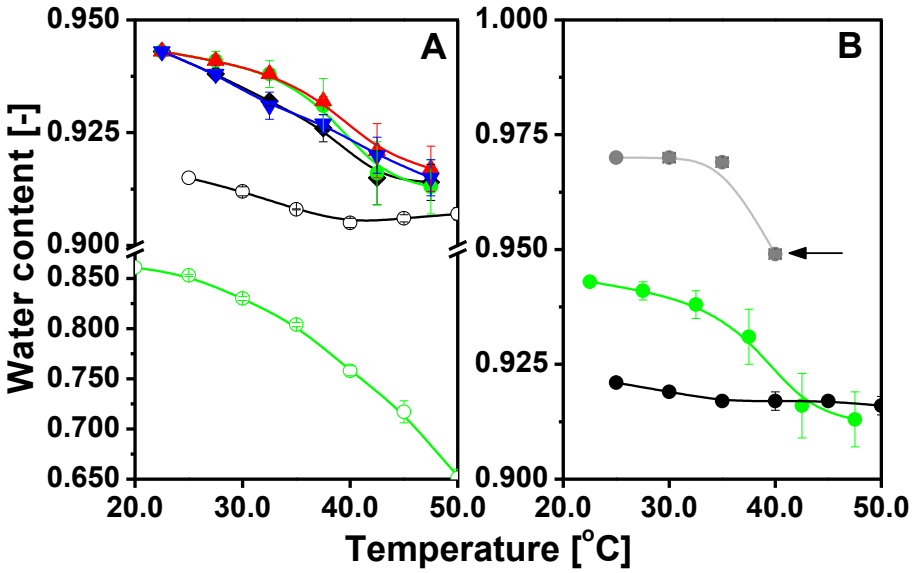

Figure 7.3. Deswelling of POEGMA-DEXA hydrogels as a function of the temperature: A) Effect of the $M(EO)_2MA$: $OEGMA_{475}$ composition: (◆, black) PO_5H_{30}; (●, green) $PO_{10}H_{30}$; (▲, red) $PO_{15}H_{30}$; (▼, blue) $PO_{20}H_{30}$. A DEXH-DEXA hydrogel (○, black) and a POEGMA hydrogel based on $PO_{10}H_{30}$ and $PO_{10}A_{30}$ (○, green) were added for comparison. B) Effect of the average number of functional groups per polymer chain: (●, grey) $PO_{10}H_{15}$ = 10; (●, green) $PO_{10}H_{30}$ = 20; (●, black) $PO_{10}H_{50}$ = 50. The arrow indicates the point of complete degradation of $PO_{10}H_{15}$. Lines are guides to the eye.

All POEGMA-DEXA hydrogels tested displayed a clear volume phase temperature transition (VPTT), with water continuously expelled from the hydrogel matrix as the gel was heated. The water content of all hydrogels prepared with hydrazide functionalized POEGMA (POH) and aldehyde functionalized dextran (DEXA) decreases from 0.940 to 0.915±0.002. As a comparison, the all-POEGMA hydrogels prepared by mixing $PO_{10}H_{30}$ and $PO_{10}A_{30}$ at 60 mg/mL show a decrease in water content from 0.861 to 0.555 over this same temperature range, corresponding to a weight loss of almost 50%; conversely, the DEX hydrogel, prepared by mixing DEXA and DEXH at 60 mg/mL showed no significant temperature response. These results show that the thermoresponsive behaviour of the POEGMA hydrogels is preserved but is significantly suppressed by the presence of the non-thermosensitive dextran component.

Analogous to the results reported on injectable POEGMA hydrogels,[47] the measured volume phase transition temperatures of the POEGMA-DEXA hydrogels (Fig. 7.3A) are significantly lower than the measured cloud points of the hydrazide-functionalized precursors (Table 7.1 and Fig. 7.1). However, the clear correlation between the POH composition and the cloud point observed in Fig. 7.1 is not maintained within the composite hydrogels, with broader and clustered volume phase transitions observed irrespective of the POH cloud point. Thus, the ~13°C difference between the cloud points observed between the different POH precursors (ΔT = 13°C, $f_{M(EO)2MA}$ = 0.97 – 0.82) is suppressed by the effects of cross-linking (known to broaden phase transition responses)[48] and the presence of the hydrophilic (non-responsive) DEX component of the hydrogel.

The cross-link density of the hydrogel has a significant effect on the thermoresponsive behavior of POEGMA-DEXA hydrogels, as shown in Fig. 7.3B. All three hydrogels were initially prepared at 60 mg/mL (corresponding to a water content of 0.940). In 10 Mm PBS at room temperature, POEGMA-DEXA hydrogels based on $PO_{10}H_{15}$ swelled to a water content of 0.970, hydrogels based on $PO_{10}H_{30}$ exhibited almost no swelling response, and hydrogels based on $PO_{10}H_{50}$ de-swelled to a water content of 0.921. Upon heating from 22.5°C to 50°C, hydrogels prepared from $PO_{10}H_{15}$ (~10 functional groups/chain) initially swell with water and then exhibit rapid mass loss followed by complete dissolution of the hydrogel after 48 hours (Fig. 7.3B). As such, no thermoresponsive behaviour analogous to that observed with other POEGMA-DEXA hydrogels was observed since degradation occurs at a more rapid time scale. Conversely, POEGMA-DEXA hydrogels prepared from $PO_{10}H_{30}$ and $PO_{10}H_{50}$ (~20 and ~50 functional groups/chain, respectively) display a continuous decrease in water content as a function of the increasing temperature and remained macroscopically stable for at least 3 weeks. However, the 2-fold higher number of average functional groups per chain for $PO_{10}H_{50}$ relative to $PO_{10}H_{30}$ results in an increased cross-link density which significantly restricts the magnitude of the phase transition observed; the water content for $PO_{10}H_{30}$-DEXA decreases from 0.941 to 0.913 (weight loss of 40%) compared to a water content reduction from 0.921 to 0.916 (weight loss of 6%) for $PO_{10}H_{50}$-DEXA over the same temperature range. Thus, the phase transition behavior of

the hydrogels can be tuned based on the number of cross-linkable functional groups available in the pre-polymers.

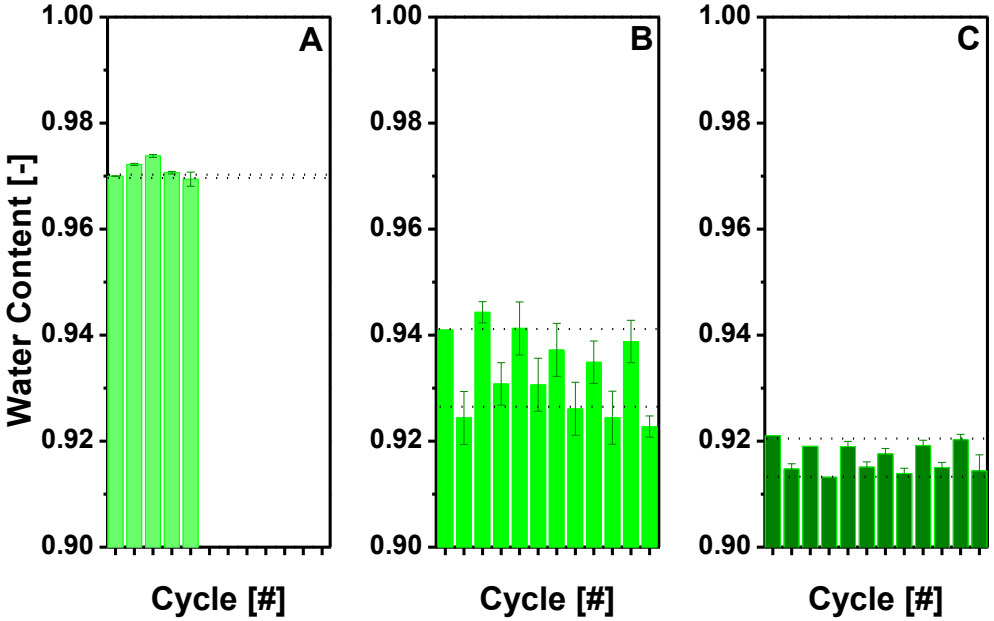

Figure 7.4. Reversibility of the thermal phase transition of POEGMA-DEXA hydrogels in 10 Mm PBS: A) $PO_{10}H_{15}$-DEXA; B) $PO_{10}H_{30}$-DEXA; C) $PO_{10}H_{50}$-DEXA.

The thermal phase transition of all the prepared POEGMA-DEX hydrogels is completely reversible and shows little hysteresis (Figure 7.4 and Supporting Information, Fig. S7.3). For POEGMA-DEXA hydrogels based on PO_5H_{30}, $PO_{10}H_{30}$, $PO_{15}H_{30}$, or $PO_{20}H_{30}$ (i.e. same crosslinking potential but different cloud point temperature), the water content of each of the hydrogels switches reversibly from 0.940±0.003 to 0.927±0.003 (corresponding to a weight change of 15 ± 3%) with little to no hysteresis over multiple cycles nor any significant effect of the composition of the POH precursor observed ($p < 0.05$ for any pair-wise comparison via t-test. This result corresponds with the very similar VPTT results among this series (Fig. 7.3A). In contrast, for POEGMA-DEXA hydrogels based on $PO_{10}H_{15}$, $PO_{10}H_{30}$, or $PO_{10}H_{50}$ (same cloud point but different numbers of hydrazide groups and thus crosslinking potential per chain, Fig. 7.4A-C), the magnitude and reversibility of the phase transition is significantly different as a function of the hydrazide content. The $PO_{10}H_{15}$-DEXA hydrogel (Fig. 7.4A) is loosely cross-linked such that hydrogel degradation competes with thermoresponsive de-swelling, resulting in no significant

thermoresponsive behaviour observed in the thermal cycling experiment followed by degradation after 48-60 hours, (consistent with Fig. 7.3B). Swelling/de-swelling of the $PO_{10}H_{30}$-DEXA and $PO_{10}H_{50}$-DEXA hydrogels showed the expected reversible behaviour without significant hysteresis, but the extent of de-swelling is governed by the degree of cross-linking; the water content for more highly cross-linked $PO_{10}H_{50}$-DEXA hydrogel decreases reversibly from 0.920±0.001 to 0.915±0.001 (corresponding to a weight loss of 5 ± 1%), less than one third the volume change observed with the less cross-linked $PO_{10}H_{30}$-DEXA hydrogel.

7.3.4 Rheology: The rheological properties of POEGMA-DEXA hydrogels are reported in Figure 7.5, with Fig. 7.5A showing the storage modulus (*G'*) versus frequency results for hydrogels prepared with the same number of hydrazide groups but different ratios of OEGMA monomers (i.e. cloud point temperatures, PO_5H_{30}-DEXA – $PO_{20}H_{30}$-DEXA) while Fig. 7.5B shows the storage modulus (*G'*) versus frequency for hydrogels prepared with the same ratio of OEGMA monomers but different numbers of hydrazide groups ($PO_{10}H_{15}$ – $PO_{10}H_{50}$).

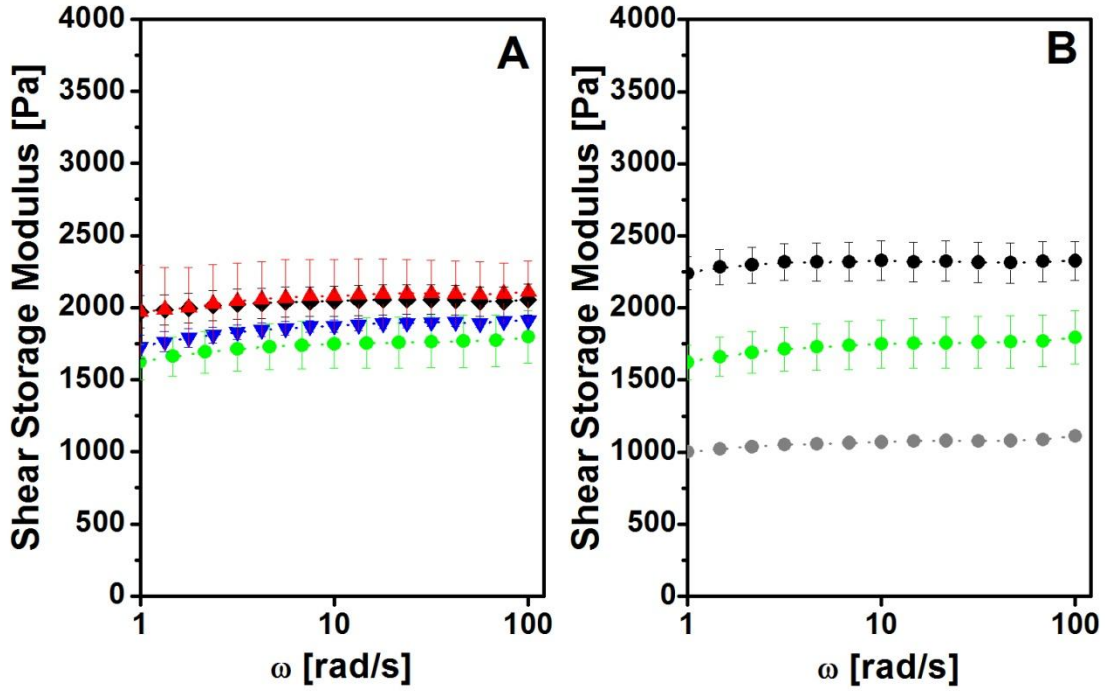

Figure 7.5. Storage (G') moduli of POEGMA-DEXA hydrogels: A) Effect of the $M(EO)_2MA$: $OEGMA_{475}$ composition: (◆, black) PO_5H_{30}-DEXA; (●, green) $PO_{10}H_{30}$-DEXA; (▲, red) $PO_{15}H_{30}$-DEXA; (▼, blue) $PO_{20}H_{30}$-DEXA. B) Effect of the average number of functional groups per polymer chain: (●, grey) $PO_{10}H_{15}$-DEXA (~10 hydrazides/chain); (●, green) $PO_{10}H_{30}$-DEXA (~20 hydrazides/chain); (●, black) $PO_{10}H_{50}$-DEXA (~50 hydrazides/chain).

No significant difference in elastic modulus was observed between hydrogels prepared with the same hydrazide functionalization but different OEGMA monomer ratios, with all hydrogels exhibiting plateau *G'* values of 1.5-2.0 kPa at high frequency. It should be noted that this elastic modulus matches that of neural and adipose tissue within the body, relevant for the successful use of such materials as cell scaffolds *in vivo*. Conversely, when the number of functional groups per chain was varied (Fig. 7.5B), the mechanical properties of the hydrogels were significantly different. Hydrogels based on $PO_{10}H_{15}$ (~10 functional groups/chain) had a lower plateau *G'* of approximately 1.0 kPa, compared to 1.6 kPa for $PO_{10}H_{30}$ and 2.3 kPa for $PO_{10}H_{50}$. This increase in mechanical rigidity can be directly attributed to the increase in the cross-link density between the different hydrogels, illustrating the potential for modulus matching by tuning the precursor polymer properties of the injectable hydrogels to match the mechanics of native tissue.

Based on the results of the thermoresponsivity, mechanical and degradation experiments, we chose to continue our biological investigation of the POEGMA-DEXA hydrogels using $PO_{10}H_{30}$-DEXA as the key gel of interest among all dual natural-synthetic hydrogels tested. This gel was chosen given that its properties are most favourable to application as a physiological injectable hydrogel, with a VPTT of ~37°C, a shear storage modulus of 1.6kPa mimicking neural/adipose tissue, and rapid (<1 minute) gelation kinetics.

7.3.5 Cytotoxicity: Figure 7.6 shows the *in vitro* cytotoxicity of hydrogel precursors (which are also the degradation products, Fig. 7.6A) as screened using an MTT assay with 3T3 fibroblasts. In all experiments, the precursors induce no significant decrease in cell viability when added at concentrations from 200 to 2000 µg/mL relative to the cell control (i.e. cells seeded in the multiwell plate but not exposed to the materials).

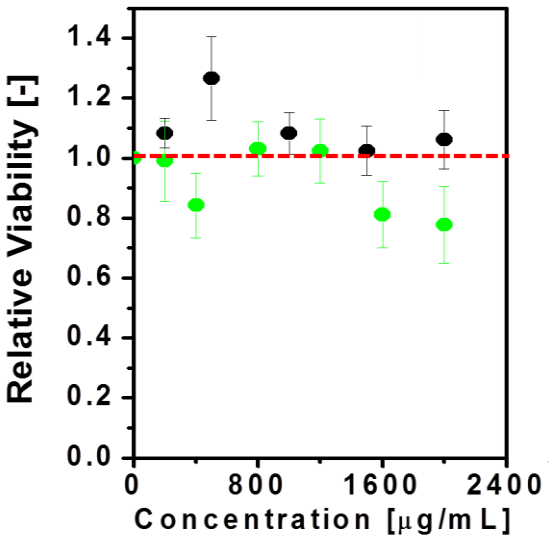

Figure 7.6 Cell viability of 3T3 fibroblasts for the polymer precursors. A) Linear precursor polymers: (●, green) $PO_{10}H_{30}$; (●, black) DEXA.

After establishing that the precursors were non-cytotoxic, cell adhesion was tested by plating NIH 3T3 mouse fibroblasts on to DEXH-DEXA, $PO_{10}H_{30}$-DEXA, and $PO_{10}H_{30}$-$PO_{10}A_{30}$ hydrogels (Figure 7.7). The all-POEGMA hydrogels display little to no cell adhesion (Figs. 7.7D and E), consistent with our earlier reports on the bio-inert (or "stealth") characteristics of POEGMA-based injectable hydrogel materials[18]. Incorporation of dextran within POEGMA hydrogels increased cell adhesion of 3T3 fibroblasts to 28 ± 2% of the total added cells (Figs. 7.7B and E), although cells exhibit a round morphology suggesting relatively weak adhesion to the gels without focal adhesion development. By comparison, the all-dextran DEXH-DEXA gel can adhere 77 ± 2% of added cells (Figs. 7.7C and E), although the cells appear more aggregated than in the polystyrene control (Figs. 7.7A and E). Thus, by incorporating dextran into the gels, significant increases in cell adhesion can be achieved that can be controlled by the amount of dextran incorporated.

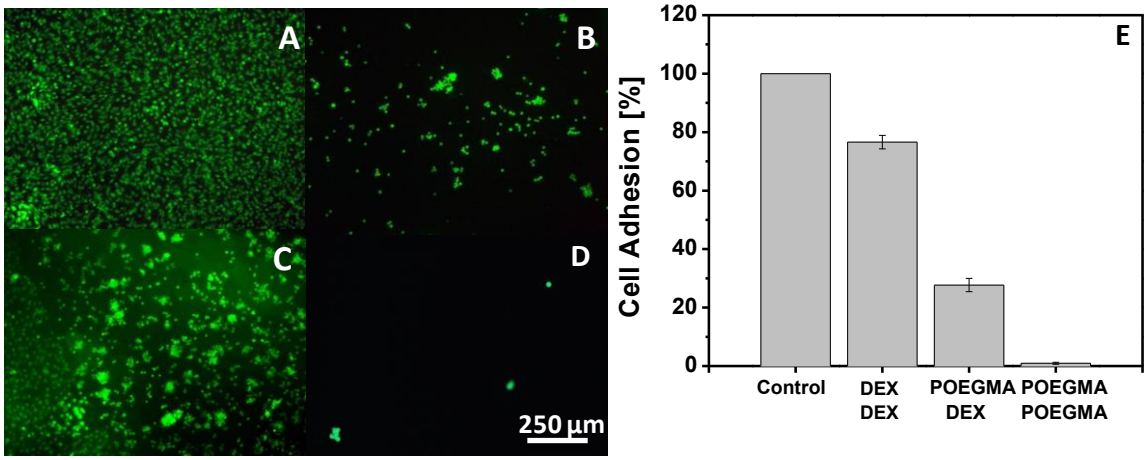

Figure 7.7. Cell adhesion of 3T3 fibroblasts on (A) polystyrene control, (B) $PO_{10}H_{30}$-DEXB hydrogel, (C) DEXH-DEXA hydrogel and (D) $PO_{10}H_{30}$-$PO_{10}A_{30}$ hydrogel. Relative cell adhesion compared to the control (as determined by fluorescence analysis) is shown in (E). Note that the percentage cell adhesion for the $PO_{10}H_{30}$-$PO_{10}A_{30}$ hydrogel equals 0.9 ± 0.3% and is therefore barely visible on the chosen scale.

7.3.6 Protein adsorption: Protein adsorption of bovine serum albumin (BSA) to the DEXH-$PO_{10}A_{30}$, $PO_{10}H_{30}$-DEXA, DEXH-DEXA and $PO_{10}H_{30}$-$PO_{10}A_{30}$ hydrogels was assessed to determine the effect of the dextran component on the protein affinity of the hydrogels (Figure 7.8). Over the full range of BSA concentrations tested, lowest protein adsorption was observed to the all-

POEGMA $PO_{10}H_{30}$-$PO_{10}A_{30}$ hydrogel (122 ± 12 ng/cm^2 at 1 mg/mL BSA). DEXH-$PO_{10}A_{30}$ and DEXH-DEXA hydrogels (160 ± 8 ng/cm^2 and 201 ± 8 ng/cm^2 at 1 mg/mL BSA respectively) absobserd more protein then the all POEGMA gel, but less then the $PO_{10}H_{30}$-DEXA (210 ± 13 ng/cm^2 at 1 mg/mL BSA) hydrogel. The substantial difference in protein adsorption between the DEXH-$PO_{10}A_{30}$ and $PO_{10}H_{30}$-DEXA hydrogels was surprising given that both these hydrogels have the same mass ratio of POEGMA to dextran. The key difference between these gels is the number of theoretical free aldehydes present based on the stoichiometry between the hydrazide and aldehyde polymers used, with the hydrazide:aldehyde ratio in the starting materials; residual aldehydes may form Schiff bases with amines on proteins to drive protein uptake via a chemical mechanism. However, DEXH-$PO_{10}A_{30}$ hydrogels (hydrazide:aldehyde ratio = 2:3, close to the 1:1 ratio observed in the very low protein binding all-POEGMA $PO_{10}H_{30}$-PO_{10}-A_{30} hydrogel), contain substantially fewer free aldehyde groups than $PO_{10}H_{30}$-DEXA hydrogels (hydrazide:aldehyde ratio = 1:4, close to the 1:5 ratio observed in the more highly protein binding all-dextran DEXH-DEXA hydrogel). As such, the differences in protein adsorption between DEXH-$PO_{10}A_{30}$ and $PO_{10}H_{30}$-DEXA can be driven by the residual aldehyde content in the gels. This result was further supported by an additional experiment we conducted by varying the relative reactive precursor concentrations to fabricate an all-POEGMA hydrogel with the same 1:4 hydrazide:aldehyde ratio to match that of $PO_{10}H_{30}$-DEXA to match that of the POEGMA-DEX gels, the amount of BSA adsorbed increases from 122 ± 12 ng/cm^2 (1:1 hydrazide:aldehyde ratio) to 369± 43 ng/cm^2 (1:4 hydrazide:aldehyde ratio). As such, while this result proves that increasing residual aldehyde content can substantially influence protein adsorption as anticipated, the combination of $PO_{10}H_{30}$ and DEXB appears to suppress this effect as compared to the all-POEGMA gels at the same hydrazide:aldehyde ratio. Given that protein adsorption is governed primarily by the interfacial properties of the gel, we hypothesize that POEGMA has higher surface affinity than DEX in an aqueous environment. As such, when aldehyde groups are tethered on the POEGMA component, the higher surface affinity of POEGMA results in more aldehyde groups at the interface and thus higher protein adsorption; conversely, when aldehyde groups are tethered on the DEX component, the surface becomes

enriched in the POEGMA-bound hydrazide groups which do not significantly influence protein adsorption.

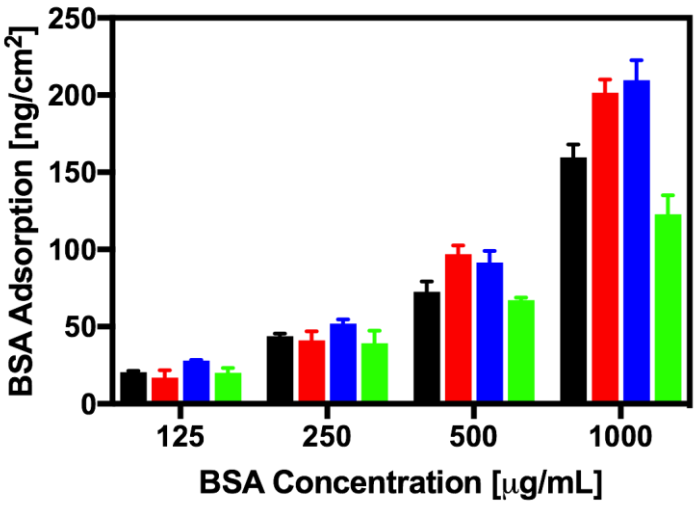

Figure 7.8. BSA protein adsorption to DEXH-$PO_{10}A_{30}$ (●, black), DEXH-DEXA (●, red), $PO_{10}H_{30}$-DEXA (●, blue) and $PO_{10}H_{30}$-$PO_{10}A_{30}$ (●, green) hydrogels at varying BSA protein concentrations.

7.3.7 In vivo studies: Histopathological analysis of subcutaneous sections recovered following both acute and chronic time points for both gel types are shown in Figure 7.9. After two days of *in vivo* incubation, an initial leukocyte infiltration composed of neutrophils and monocytic cells was found primarily at the tissue-hydrogel interface (approximately 500 mm^{-1}) for both $PO_{10}H_{30}$-DEXA (Fig. 7.9A) and DEXH-DEXA gels (Fig. 7.9C). This higher response to the all-dextran gel is consistent with the significantly higher protein adsorption (Fig. 7.8) and cell adhesion (Fig. 7.7) observed to this hydrogel, and again occurs independently of the net aldehyde content of the two gels (which is roughly equivalent). Interestingly, substantial infiltration of inflammatory cells is observed into the $PO_{10}H_{30}$-DEXA gel (Fig. 7.9A) that is not seen in the case of DEXH-DEXA gels (Fig. 7.9C), suggesting that gel degradation is initiated relatively early in the $PO_{10}H_{30}$ gel that is not observed in either the DEXH-DEXA nor $PO_{10}H_{30}$-$PO_{10}A_{30}$ control gels. This suggests a significant potential benefit of using this combination of POEGMA (facilitating high water accessibility) and dextran (exhibiting enzymatic or oxidative degradation) to accelerate the

degradation of injectable hydrogels without substantially increasing the intensity of the acute inflammatory response.

At the chronic time point (1 month), the hydrogel was degraded and removed from the site of application in case of $PO_{10}H_{30}$-DEXA (Fig. 7.9B), with no morphological difference observed between these samples and the PBS-only injection control (Fig. 7.9E). In contrast, the DEXH-DEXA gels persist at the injection site and show evidence of chronic inflammation, including adhesion toward the material, the formation of granulation tissue in the areas surrounding the gel, and the presence of macrophages at the gel interface (Fig. 7.9D inset). Thus, incorporating POEGMA substantially accelerates degradation *in vivo* but also substantially suppresses Based on the differences in host response toward the injected biomaterials, the $PO_{10}H_{30}$-DEXA gels appear to be better tolerated within the sub-cutaneous environment relative to dextran-only hydrogels.

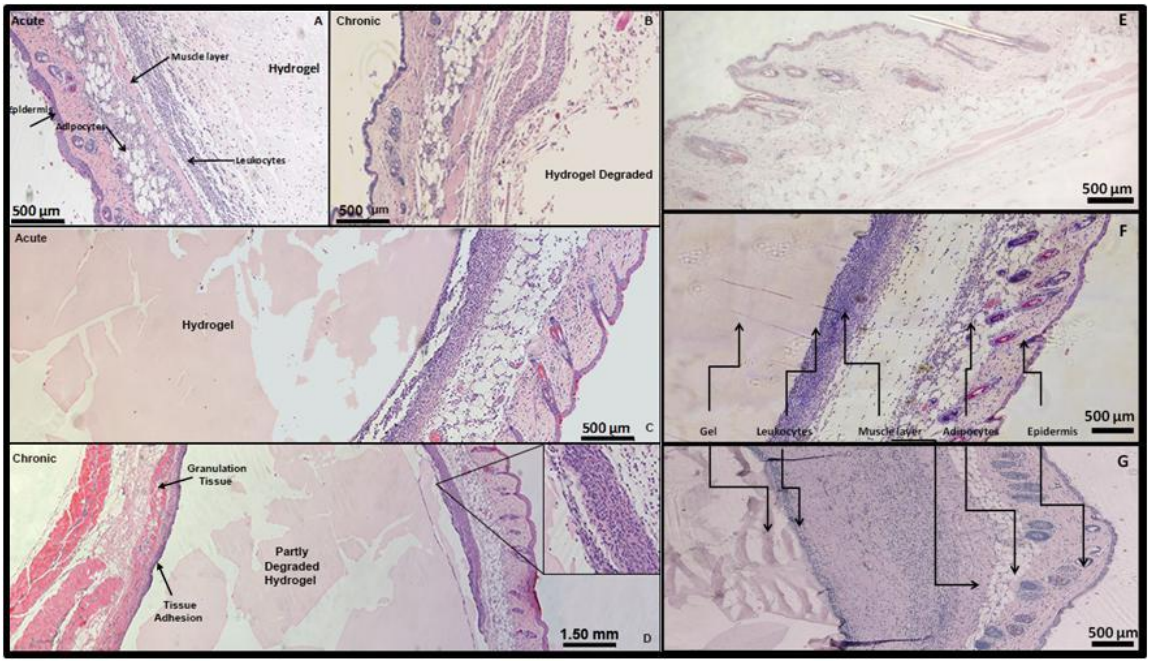

Figure 7.9. Host response toward 6 w/w% $PO_{10}H_{30}$-DEXA and DEXH-DEXA hydrogels following subcutaneous injection in BALB/c mice. A) 2 day acute time point following injection of $PO_{10}H_{30}$-DEXA; B) One month chronic time point following injection of $PO_{10}H_{30}$-DEXA; C) 2 day acute time point following injection of DEXH-DEXA; D) One month chronic time point following injection of DEXH-DEXA. E) 10 mM PBS injection control.

7.4 Discussion

The results of this study demonstrate that the physiochemical properties of injectable hydrogels based on combinations of POEGMA and dextran can be tuned in two ways: altering the chemistry of the precursor polymers themselves as well as altering which precursor is functionalized with which functional group. By changing the degree of hydrazide functionalization of the POH precursors, the thermoresponsive (Fig. 7.3B and Fig. 7.4) and mechanical (Fig. 7.5B) properties of the POEGMA-DEX hydrogels can be adjusted consistent with the different cross-link density of the hydrogels; increased cross-link density (achieved with precursor polymers containing more hydrazide groups) inhibits swelling/deswelling responses and results in stiffer hydrogel networks. In comparison, adjusting the $M(EO)_2MA$: $OEGMA_{475}$ ratio (and thus the cloud point of the synthetic precursors, with all ratios chosen to keep the transition temperatures within the range of physiological temperature) proved to have little to no influence on any physicochemical properties of the hydrogels. This result is likely attributable to the significant averaging effect we observed on the phase transition temperature when POEGMA precursor polymers were crosslinked with dextran, which does not have a phase transition temperature; the dual impacts of crosslinking and increasing the overall hydrophilic:hydrophobic balance of the gels at the test temperatures used resulted in similar thermal responses between different gels even though the precursors themselves had cloud points spanning a ~14°C range.

While the thermal phase transition is significantly suppressed due to this averaging effect, the residual transition was highly reversible (Fig. 7.4). Unlike poly(N-isopropylacrylamide) (PNIPAM, the most popular among thermoresponsive polymers), the POEGMA collapsed state is stabilized by relatively weak van der Waals interactions.[41] This weak interaction provides POEGMA polymers with a phase transition characterized by excellent reversibility and little hysteresis, consistent with the results presented in Fig. 7.4B for POEGMA-DEX hydrogels. In comparison, PNIPAM hydrogels display some degree of hysteresis, attributable to the much stronger hydrogen bonds formed between the amide and carbonyl.[47]

While the effect of which functional group was attached to which polymer was somewhat minor in the physicochemical property analysis, substantial differences were

observed in the interfacial biological responses depending on whether the POEGMA or DEX polymer was functionalized with hydrazide or aldehyde groups. By mixing POEGMA and dextran at the same ratio but putting the reactive functional groups on different components, our results indicate that we can engineer the interfacial properties of the hydrogels dramatically; more specifically, the functional group tethered to POEGMA appears to be more enriched at the interface, such that gels prepared with aldehyde-POEGMA adsorb ~7-fold more protein than gels prepared with hydrazide-POEGMA despite the net (bulk) excess of aldehydes being substantially higher in the latter gel (Fig. 7.8). Thus, by judiciously selecting the correct precursor polymer to functionalize, the benefits of incorporating an enzymatically degradable natural polymer (dextran) into the hydrogel can minimally affect the desirable interfacial properties of POEGMA.

Biologically, neither the reactive polymer precursors nor the hydrogels (over a range of different concentrations or hydrogel compositions) induced a significant cytotoxic response *in vitro* to 3T3 mouse fibroblasts (Fig. 7.6). Cells could also grow and remain viable on hydrogels containing at least some dextran component, although the POEGMA-DEXA hydrogels supported only relatively weak cell adsorption (Fig. 7.7). Furthermore, *in vivo* subcutaneous injections into BALB/c mice indicated only minor acute inflammation and no significant chronic inflammation for POEGMA-DEXA similar to that observed for an all-POEGMA hydrogel (Fig. 7.9), suggesting that the POEGMA-DEXA hydrogels are well tolerated *in vivo*. In contrast, the all-dextran DEXH-DEXA hydrogels induced both acute and chronic inflammation, demonstrating the benefits of introducing the POEGMA component. Note that, although limited specific cell adhesive properties of dextran hydrogels have been shown previously (often, but not exclusively, in conjunction with cell adhesive peptides[49]), the higher aldehyde content of DEXA compared to the $PO_{10}A_{30}$-containing gels cannot be definitively ruled out as a contributing factor to this higher adhesive potential; indeed, dextran-aldehyde/tissue-derived amine chemistry (promoted by the higher aldehyde content of DEXA) has been successfully exploited in the design of dextran hydrogels as wound sealants[35,50]. High molecular weight aldehyde functionalized dextran polymers have also been shown to allow viscoelastic adhesive soft tissue crosslinking, contrasting the effect of small aldehyde-based fixatives, such as formaldehyde and

glutaraldehyde, which tightly crosslink tissues and radically alter physical and mechanical properties. This property is extremely relevant for the practical use of hydrogels in as large molecular weight natural polymers can afford free reactive groups without causing cell toxicity (Fig. 7.6); glutaraldehyde or formaldehyde full kill cells at much lower functional aldehyde concentrations.[51]

These results show that the POEGMA-DEXA hydrogel platform is both cytocompatible and appropriate for studying cellular responses to tissue mimicking environments. The molecular composition of the functional POEGMA precursor polymers can be designed such that the resulting hydrogel matches the mechanical properties of the target tissue, consistent with our previous observations; correspondingly, DEX incorporation offers favourable support for 3T3 fibroblast weak adhesion as well as enhanced degradation rates *in vivo*. Furthermore, the decoupling of biological responses to physicochemical properties observed for many of the tested compositions facilitate the design of optimized biomaterials with favorable physical, mechanical, and biological properties for specific end applications, such as synthetic-natural drug discovery platforms, injectable tissue scaffolds and drug release matrices.

7.5 Conclusions

Synthetic-natural poly(oligoethylene glycol methacrylate) (POEGMA)-dextran (DEX) injectable hydrogels based on hydrazone chemistry offer significant benefits in terms of combining the favorable thermoresponsive and non-specific adsorption suppressing properties of POEGMA with the more cell adhesive and enzymatic/oxidative degradation potential of dextran. The physiochemical properties of the injectable hydrogels (mechanical and thermoresponsive swelling) can be tuned by changing the density of reactive functional groups on the synthetic POEGMA precursor (easy to do via facile copolymerization), although changing the cloud point temperature of the POEGMA precursors had no significant effect on the gel properties; alternately, the biointerfacial properties of the hydrogels could be tuned by incorporating dextran and changing which precursor polymer was grafted with which functional group, utilizing apparent differences in interfacial partitioning in water between POEGMA and dextran to alter the interfacial chemistry. POEGMA-DEX hydrogels and precursors are non-

cytotoxic, support weak cell adhesion, and are well-tolerated *in vivo*, facilitating faster degradation than either all-POEGMA or all-dextran materials while maintaining the very mild inflammatory responses of the all-POEGMA hydrogels. The modular design and tunable mechanical and biological properties of these injectable hydrogels makes then ideal candidates for cell encapsulation and scaffolding applications.

7.6 Acknowledgements

Funding for this work was provided by the NSERC 20/20 Ophthalmic Materials Research Network. EB acknowledges funding from the NSERC CREATE-IDEM (Integrated Design of Extracellular Matrices) training program. NMBS gratefully acknowledges a postdoctoral fellowship sponsored by the Ontario Ministry of Research and Innovation.

7.7 References

(1) Liu, Z. C.; Ming, T.; Chang, S. Cells in Regenerative Medicine , Tissue Engineering and Cell Therapy. *Chapter 7: Therapeutic Applications of Cell Microencapsulation*. **2010**, 7, 68-79.

(2) Nicodemus, G. D.; Bryant, S. J. Cell Encapsulation in Biodegradable Hydrogels for Tissue Engineering Applications. *Tissue Eng. Part B. Rev.* **2008**, *14*, 149–165.

(3) Seal, B. L.; Otero, T. C.; Panitch, A. Polymeric Biomaterials for Tissue and Organ Regeneration. *Materials Science and Engineering.* **2001**, *34*, 147–230.

(4) Guarnieri, D.; Capua, A.; Ventre, M.; Borzacchiello, A.; Pedone, C.; Marasco, D.; Ruvo, M.; Netti, P. A. Covalently Immobilized RGD Gradient on PEG Hydrogel Scaffold Influences Cell Migration Parameters. *Acta Biomater.* **2010**, *6*, 2532–2539.

(5) McKinnon, D. D.; Domaille, D. W.; Cha, J. N.; Anseth, K. S. Biophysically Defined and Cytocompatible Covalently Adaptable Networks as Viscoelastic 3D Cell Culture Systems. *Adv. Mater.* **2014**, *26*, 865–872.

(6) Chan, V.; Zorlutuna, P.; Jeong, J. H.; Kong, H.; Bashir, R. Three-Dimensional Photopatterning of Hydrogels Using Stereolithography for Long-Term Cell Encapsulation. *Lab Chip* **2010**, *10*, 2062–2070.

(7) Chatterjee, K.; Young, M. F.; Simon, C. G. Fabricating Gradient Hydrogel Scaffolds for 3D Cell Culture. *Comb. Chem. High Throughput Screen.* **2011**, *14*, 227–236.

(8) Nicodemus, G. D.; Bryant, S. J. Cell Encapsulation in Biodegradable Hydrogels for Tissue Engineering Applications. *Tissue Eng. Part B. Rev.* **2008**, *14*, 149–165.

(9) Temenoff, J. S.; Mikos, A. G. Injectable Biodegradable Materials for Orthopedic Tissue Engineering. *Biomaterials* **2000**, *21*, 2405–2412.

(10) Anseth, K. S.; Metters, A. T.; Bryant, S. J.; Martens, P. J.; Elisseeff, J. H.; Bowman, C. N. In Situ Forming Degradable Networks and Their Application in Tissue Engineering and Drug Delivery. *J. Control. Release* **2002**, *78*, 199–209.

(11) Lutz, J. F. Thermo-Switchable Materials Prepared Using the OEGMA-Platform. *Adv. Mater.* **2011**, *23*, 2237–2243.

(12) Lutz, J. F.; Akdemir, O.; Hoth, A. Point by Point Comparison of Two Thermosensitive

Polymers Exhibiting a Similar LCST: Is the Age of poly(NIPAM) Over? *J. Am. Chem. Soc.* **2006**, *128*, 13046–13047.

(13) Urosev, I.; Bakaic, E.; Alsop, R. J.; Rheinstädter, M. C.; Hoare, T. Tuning the Properties of Injectable Poly(oligoethylene Glycol Methacrylate) Hydrogels by Controlling Precursor Polymer Molecular Weight. *J. Mater. Chem. B* **2016**, *4*, 6541–6551.

(14) Smeets, N. M. B.; Bakaic, E.; Yavitt, F. M.; Yang, F.; Rheinstädter, M. C.; Hoare, T. Probing the Internal Morphology of Injectable Poly(oligoethylene Glycol Methacrylate) Hydrogels by Light and Small-Angle Neutron Scattering. *Macromolecules* **2014**, *47*, 6017–6027.

(15) Bakaic, E.; Smeets, N. M. B.; Dorrington, H.; Hoare, T. "Off-the-Shelf" thermoresponsive Hydrogel Design: Tuning Hydrogel Properties by Mixing Precursor Polymers with Different Lower-Critical Solution Temperatures. *RSC Adv.* **2015**, *5*, 33364–33376.

(16) Smeets, N. M. B.; Bakaic, E.; Patenaude, M.; Hoare, T. Injectable and Tunable Poly(ethylene Glycol) Analogue Hydrogels Based on Poly(oligoethylene Glycol Methacrylate). *Chem. Commun.* **2014**, *50*, 3306–3309.

(17) Bakaic, E.; Smeets, N. M. B.; Hoare, T. Injectable Hydrogels Based on Poly(ethylene Glycol) and Derivatives as Functional Biomaterials. *RSC Adv.* **2015**, *5*, 35469–35486.

(18) Smeets, N. M. B.; Bakaic, E.; Patenaude, M.; Hoare, T. Injectable Poly(oligoethylene Glycol Methacrylate)-Based Hydrogels with Tunable Phase Transition Behaviours: Physicochemical and Biological Responses. *Acta Biomater.* **2014**, *10*, 4143–4155.

(19) Smeets, N. M. B.; Bakaic, E.; Patenaude, M.; Hoare, T. Injectable and Tunable Poly(ethylene Glycol) Analogue Hydrogels Based on Poly(oligoethylene Glycol Methacrylate). *Chem. Commun.* **2014**, *50*, 3306–3309.

(20) Lin, C. C.; Anseth, K. S. Cell-Cell Communication Mimicry with Poly(ethylene Glycol) Hydrogels for Enhancing Beta-Cell Function. *Proc. Natl. Acad. Sci. U. S. A.* **2011**, *108*, 6380–6385.

(21) Watt, F. M.; Huck, W. T. S. Role of the Extracellular Matrix in Regulating Stem Cell Fate. *Nat. Rev. Mol. Cell Biol.* **2013**, *14*, 467–473.

(22) Kaji, H.; Camci-Unal, G.; Langer, R.; Khademhosseini, A. Engineering Systems for the Generation of Patterned Co-Cultures for Controlling Cell-Cell Interactions. *Biochim.*

Biophys. Acta **2011**, *1810*, 239–250.

(23) Santos, E.; Hernández, R. M.; Pedraz, J. L.; Orive, G. Novel Advances in the Design of Three-Dimensional Bio-Scaffolds to Control Cell Fate: Translation from 2D to 3D. *Trends Biotechnol.* **2012**, *30*, 331–341.

(24) Lee, J.; Cuddihy, M. J.; Kotov, N. A. Three-Dimensional Cell Culture Matrices : State of the Art. *Tissue Engineering B.* **2008**, *14*, 61-80.

(25) Sun, G.; Zhang, X.; Shen, Y. I.; Sebastian, R.; Dickinson, L. E.; Fox-Talbot, K.; Reinblatt, M.; Steenbergen, C.; Harmon, J. W.; Gerecht, S. Dextran Hydrogel Scaffolds Enhance Angiogenic Responses and Promote Complete Skin Regeneration during Burn Wound Healing. *Proc. Natl. Acad. Sci. U. S. A.* **2011**, *108*, 20976–20981.

(26) Sun, G.; Shen, Y. I.; Kusuma, S.; Fox-Talbot, K.; Steenbergen, C. J.; Gerecht, S. Functional Neovascularization of Biodegradable Dextran Hydrogels with Multiple Angiogenic Growth Factors. *Biomaterials* **2011**, *32*, 95–106.

(27) D'Arrigo, G.; Di Meo, C.; Pescosolido, L.; Coviello, T.; Alhaique, F.; Matricardi, P. Calcium Alginate/dextran Methacrylate IPN Beads as Protecting Carriers for Protein Delivery. *J. Mater. Sci. Mater. Med.* **2012**, *23*, 1715–1722.

(28) Hwang, M. R.; Kim, J. O.; Lee, J. H.; Kim, Y. Il; Kim, J. H.; Chang, S. W.; Jin, S. G.; Kim, J. A.; Lyoo, W. S.; Han, S. S.; *et al.* Gentamicin-Loaded Wound Dressing with Polyvinyl Alcohol/dextran Hydrogel: Gel Characterization and in Vivo Healing Evaluation. *AAPS PharmSciTech* **2010**, *11*, 1092–1103.

(29) Geng, X.; Mo, X.; Fan, L.; Yin, A.; Fang, J. Hierarchically Designed Injectable Hydrogel from Oxidized Dextran, Amino Gelatin and 4-Arm Poly(ethylene Glycol)-Acrylate for Tissue Engineering Application. *J. Mater. Chem.* **2012**, *22*, 25130.

(30) Liu, Y.; Chan-Park, M. B. Hydrogel Based on Interpenetrating Polymer Networks of Dextran and Gelatin for Vascular Tissue Engineering. *Biomaterials* **2009**, *30*, 196–207.

(31) Patenaude, M.; Hoare, T. Injectable, Mixed Natural-Synthetic Polymer Hydrogels with Modular Properties. *Biomacromolecules* **2012**, *13*, 369–378.

(32) Hudson, S. P.; Langer, R.; Fink, G. R.; Kohane, D. S. Injectable in Situ Cross-Linking Hydrogels for Local Antifungal Therapy. *Biomaterials* **2010**, *31*, 1444–1452.

(33) Mehvar, R. Dextrans for Targeted and Sustained Delivery of Therapeutic and Imaging Agents. *J. Control. Release* **2000**, *69*, 1–25.

(34) Shazly, T. M.; Artzi, N.; Boehning, F.; Edelman, E. R. Viscoelastic Adhesive Mechanics of Aldehyde-Mediated Soft Tissue Sealants. *Biomaterials* **2008**, *29*, 4584–4591.

(35) Artzi, N.; Shazly, T.; Crespo, C.; Ramos, A. B.; Chenault, H. K.; Edelman, E. R. Characterization of Star Adhesive Sealants Based on PEG/dextran Hydrogels. *Macromol. Biosci.* **2009**, *9*, 754–765.

(36) Dong, Y.; Saeed, A. O.; Hassan, W.; Keigher, C.; Zheng, Y.; Tai, H.; Pandit, A.; Wang, W. "One-Step" Preparation of Thiol-Ene Clickable PEG-Based Thermoresponsive Hyperbranched Copolymer for In Situ Crosslinking Hybrid Hydrogel. *Macromol. Rapid Commun.* **2011**, *33*, 120–126.

(37) Rippe, C.; Rippe, A.; Torffvit, O.; Rippe, B. Size and Charge Selectivity of the Glomerular Filter in Early Experimental Diabetes in Rats. *Am. J. Physiol. Renal Physiol.* **2007**, *293*, F1533-8.

(38) Asgeirsson, D.; Venturoli, D.; Rippe, B.; Rippe, C. Increased Glomerular Permeability to Negatively Charged Ficoll Relative to Neutral Ficoll in Rats. *Am. J. Physiol. Renal Physiol.* **2006**, *291*, F1083-9.

(39) Salmon, A. H. J.; Toma, I.; Sipos, A.; Muston, P. R.; Harper, S. J.; Bates, D. O.; Neal, C. R.; Peti-Peterdi, J. Evidence for Restriction of Fluid and Solute Movement across the Glomerular Capillary Wall by the Subpodocyte Space. *Am. J. Physiol. Renal Physiol.* **2007**, *293*, F1777-86.

(40) Dong, H.; Matyjaszewski, K. Thermally Responsive P(M(EO) 2 MA- Co -OEOMA) Copolymers via AGET ATRP in Miniemulsion. *Macromolecules* **2010**, *43*, 4623–4628.

(41) Sun, S.; Wu, P. On the Thermally Reversible Dynamic Hydration Behavior of Oligo(ethylene Glycol) Methacrylate-Based Polymers in Water. *Macromolecules* **2013**, *46*, 236–246.

(42) Lutz, J. F. Polymerization of Oligo(ethylene Glycol) (Meth)acrylates: Toward New Generations of Smart Biocompatible Materials. *J. Polym. Sci. Part A Polym. Chem.* **2008**, *46*, 3459–3470.

(43) Sivakumaran, D. N.; Maitland, D.; Hoare, T. R. Injectable In Situ Gellable Hydrogel-Microgel Composites For Prolongued Drug Delivery. *Biomacromolecules.* **2011**, *12,* 4112-4120.

(44) Ooi, H. W.; Jack, K. S.; Peng, H.; Whittaker, A. K. "Click" PNIPAAm Hydrogels – a Comprehensive Study of Structure and Properties. *Polym. Chem.* **2013**, *4,* 4788-4800.

(45) Apkarian, R. P.; Wright, E. R. Cryo and Cryo-Etch Methods for Quality Preservation of Hydrogels Imaged at High Magnification by Low Temperature SEM. *Microsc. Microanal.* **2005**, *11*, 1088–1089.

(46) Fujikawa, S. Artificial Biological Membrane Ultrastructural Changes Caused by Freezing. *Electron Microsc. Rev.* **1988**, *1*, 113–140.

(47) Patenaude, M.; Hoare, T. Injectable, Degradable Thermoresponsive Poly(N -Isopropylacrylamide) Hydrogels. *ACS Macro Lett.* **2012**, *1*, 409–413.

(48) Ohya, S.; Matsuda, T. Poly(N-Isopropylacrylamide) (PNIPAM)-Grafted Gelatin as Thermoresponsive Three-Dimensional Artificial Extracellular Matrix: Molecular and Formulation Parameters vs. Cell Proliferation Potential. *J. Biomater. Sci. Polym. Ed.* **2005**, *16*, 809–827.

(49) Lévesque, S. G.; Shoichet, M. S. Synthesis of Cell-Adhesive Dextran Hydrogels and Macroporous Scaffolds. *Biomaterials* **2006**, *27*, 5277–5285.

(50) Wang, T.; Nie, J.; Yang, D. Dextran and Gelatin Based Photocrosslinkable Tissue Adhesive. *Carbohydr. Polym.* **2012**, *90*, 1428–1436.

(51) Huang Lee, L. L. H.; Cheung, D. T.; Nimni, M. E. Biochemical Changes and Cytotoxicity Associated with the Degradation of Polymeric Glutaraldehyde Derived Crosslinks. *J. Biomed. Mater. Res.* **1990**, *24*, 1185–1201.

7.8 Supporting Information

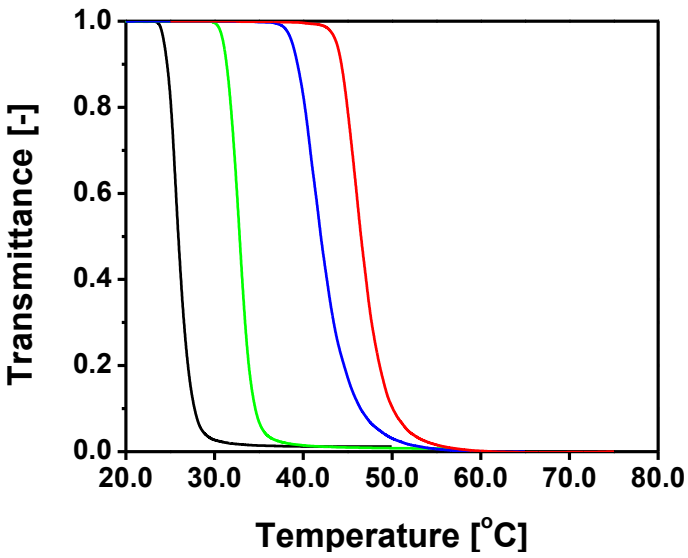

Figure S7.1 Cloud point temperature measurements of PO_5H_{30}-$PO_{20}H_{30}$ prior to hydrazide functionalization as measured in HCl/KCl buffer at pH = 2 (ensuring protonation of the -COOH groups). PO_5H_{30}-DEXA (●, black), $PO_{10}H_{30}$-DEXA (●, green), $PO_{25}H_{30}$-DEXA (●, blue) and $PO_{20}H_{30}$-DEXA (●, red).

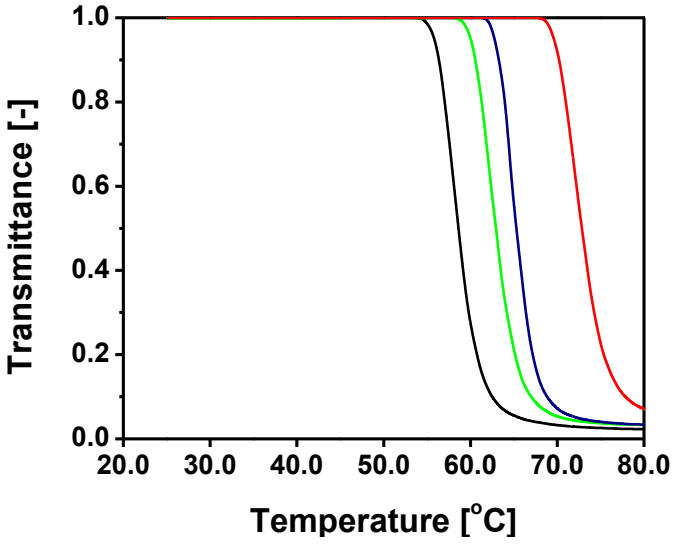

Figure S7.2 Cloud point temperature measurements of PO_5H_{30}-$PO_{20}H_{30}$ after to hydrazide functionalization as measured in PBS buffer at pH = 7.4. PO_5H_{30}-DEXA (black), $PO_{10}H_{30}$-DEXA (green), $PO_{15}H_{30}$-DEXA (blue) and $PO_{20}H_{30}$-DEXA (red).

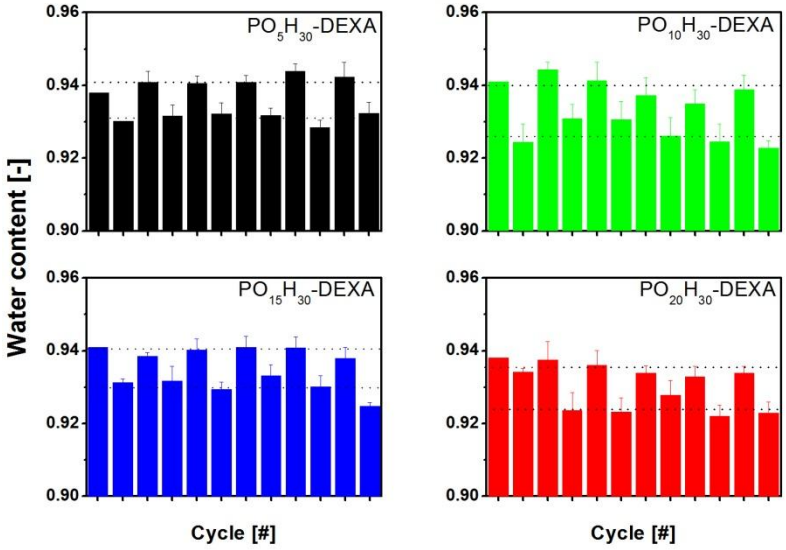

Figure S7.3. Reversibility of the thermal phase transition of POEGMA-DEXA hydrogels in PBS.

Chapter 8: Conclusions and future perspectives

8.1 Conclusions and summary

Overall, this thesis makes seminal contributions on understanding how to fabricate *in situ*-gelling synthetic hydrogels with favourable biological properties in a variety of applications. In particular, I have leveraged the relatively recent development of poly(oligoethylene glycol methacrylate) (POEGMA) hydrogels to design new functional biomaterials that exhibit the extremely low protein adsorption, tunable cell interfacial properties, and favourable tissue responses desired while being amenable to minimally invasive injection-based delivery. Such a development is expected to significantly aid in the potential translation of these materials to the clinic, an activity in which we are already actively engaged following filing of U.S. patent application on these materials.

Chapter 1 of this thesis gives an overview of injectable PEG-based hydrogels and provides insight as to the design requirements for covalently crosslinked injectable hydrogels. A particular focus is paid to the properties of the precursor polymers that make the formation of injectable hydrogels a possibility and the types of degradation products that are formed once the hydrogels are hydrolytically degraded *in vivo,* the key factors motivating the basic polymer design in this thesis. This chapter also discusses at great length the chemistries which make injectable hydrogel systems possible, such as azide-alkyne cycloadditions, disulfide formation, Diels-Alder cycloadditions, Schiff base formation and oxime chemistry. The end of this chapter focuses more specifically on the development of poly (oligoethylene glycol methacrylate) (POEGMA)-based hydrogels and their advantageous use as PEG hydrogel mimics, the background work on which the work described in this thesis was built.

Chapter 2 discusses the development of novel POEGMA injectable hydrogels formed by copolymerizing functional monomers acrylic acid (AA) and N-(2,2-dimethoxyethyl)methacrylamide (DMEMAm) with monomer oligothylene glycol methacrylate using free radical polymerization. These incorporated functional monomers are then post functionalized (via grafting and hydrolysis respectively) to introduce hydrazide and aldehyde reactive groups to form two complementary polymers. Mixing of these

reactive polymers using a double barrel syringe results in rapid gelation is acheived to produce bulk hydrogels. As the first embodiment of injectable POEGMA hydrogels, we focus on the tunable physiochemical properties (swelling, degradation and mechanics) of the hydrogels achievable through varying the functional group content or concentration of the reactive precursor polymers. The resulting PEG-analogue hydrogels exhibit all of the desirable protein and cell-repellent properties of conventional PEG hydrogels while also being injectable, degradable, and highly chemically and mechanically tunable, enabling facile preparation of *in situ*-gelling hydrogels with potential uses in tissue engineering and drug delivery (both of which we explore later in the thesis), among other potential applications.

Chapter 3 describes the design of POEGMA polymers with lower critical solution temperatures (LCSTs) achievable through the copolymerization of OEGMA monomers of varying ethylene oxide chain lengths. In this chapter, we discuss the creation of three distinctly different hydrogel systems: one of which was fully collapsed at room temperature (PO_0, all n=2 OEGMA monomer), one of which mimics poly(N-isopropylacrylamide) by collapsing at ~32°C (PO_{10}, 90% n=2 and 10% n=8-9 OEGMA monomer), and one of which has no functional phase transition temperature (PO_{100}, 100% n=8-9 OEGMA, as described in Chapter 2). The physiochemical properties (e.g. gelation, mechanics, degradation) were demonstrated to vary systematically with the phase transition temperature when gels were prepared using the same mol % of functional monomer and polymer concentration. The biological properties are also quite different according to the interfacial hydrophobicity of the gels. The PO_0 system adsorbs a large amount of protein and induces moderate inflammation when injected subcutaneously into BALB-C mice, while incorporating only 10 mol% of the long-chain POEGMA monomer results in significantly reduced protein affinity, cell adhesion, and both acute and chronic inflammatory responses. On this basis, the concepts in this chapter have the potential to significantly improve the translatability of temperature-responsive hydrogels to the clinic, as the materials are both injectable and degradable.

Chapter 4 describes the concept of modular, mix-and-match mixing of hydrogel

precursors with different properties (here, thermoresponsive PO_{10} and non-responsive PO_{100} precursor polymers) to enable systematic control of both physical and biological properties via simple mixing. This work was very exciting in the sense that we could obtain bulk hydrogels with properties that were systematically tunable without having to constantly synthesize new precursor polymers; we also demonstrated that we could *a priori* predict the composition of a single precursor polymer that would yield a hydrogel with a specific property based on the mixture of polymers that yield that same property. A number of hydrogel properties were investigated, including mechanics, swelling, degradation and gelation times; many of these were nearly additive based on the properties of the precursor polymers. This chapter also discusses the development of hetergeneous versus homogeneous hydrogels, in which mixing of polymers with different transition temperatures led to nano and microscale phase separation to form internal domains inside the gels that have substantial impacts on both the optical properties of the gels as well as the release kinetics of proteins from the gels, a result we are interested in pursuing to leverage these gels for long-term macromolecule delivery.

Chapter 5 of this thesis describes the incorporation of two charged monomers into the PO_{100} hydrogel system via copolymerization of N,N-dimethylaminoethylmethacrylate (cationic) and/or acrylic acid (anionic) with long-chain OEGMA (n=8-9) and functional monomer acrylic acid (leading to hydrazide groups) or N-(2,2-dimethoxyethyl)methacrylamide (DMEMAm, leading to aldehyde groups). Subsequently, bulk hydrogels were formed through the reactive mixing of hydrazide cationic or uncharged polymers with reactive aldehyde anionic charged or uncharged polymers. In addition to introducing pH-responsive properties into the gels, significantly broadened mechanical and swelling properties are achievable through the inclusion of charge. In paticular, a surprising enhancement in the mechanics of anionically-charged POEGMA hydrogels was thoroughly investigated using isothermal titration calorimetry and small angle neutron scattering (SANS), providing insight into a new way of mechanically reinforcing POEGMA hydrogels. SANS also provides significant insight into the effects of charge on gel morphology, including how the inclusion of anionic charge within the POEGMA hydrogels can create

"zippered" or ordered microscopic morphologies within the gel networks due to hydrogen bonding or dipole-dipole interactions. Additionally, cationic monomer incorporation can create repulsive polymer chain behaviours leading to larger swelling profiles, increased degradation kinetics and weaker mechanical properties. The structure-property correlations developed through this work give significant insight to facilitate the rational design of charged POEGMA hydrogels for targeted applications.

Chapter 6 builds on the idea of charge inclusion into the POEGMA platform hydrogels by using a similar chemistry to incorporate cationic and anionic charges into the thermoresponsive POEGMA hydrogel platform developed in Chapter 3. In this embodiment, we create five different temperature responsive, charged materials; neutral, cationic, amphoteric and anionic gels. Interestingly, the effects of charge on hydrogel mechanics were substantially different then observed in Chapter 5, with significantly less mechanical enhancement observed in the anionic gels prepared with shorter chain (thermoresponsive) OEGMA residues but significantly more effect of ionic self-crosslinking within the amphoteric gels. Cell adhesion of 3T3 mouse fibroblasts and cell viability/proliferative ability of ARPE-19 human retinal epithelial cells were both found to be enhanced in the charged hydrogels, with different charges influencing cell viability, clumping, and proliferation in subtly different ways over the 15 day time course observed. Additionally, the *in vivo* chronic tissue response following subcutaneous injection into BALB/c mice was mild for gels prepared with all charge types. The results of this chapter confirm the potential translatability of these POEGMA hydrogels for practical *in vivo* applications.

Chapter 7 describes the effects of incorporating a natural polymer (dextran) into the POEGMA gels by oxidizing dextran to expose aldehyde groups and forming gels using the same hydrazone chemistry. Our interest in such modification is to introduce native biological activity (e.g. enzymatic degradation) into such hydrogels while still maintaining the benefits of POEGMA hydrogels. Dextran is shown to enhance cell adhesion to the gels while maintaining the thermoresponsive properties and low non-specific protein adsorption of POEGMA, at least when the residual aldehyde content of the gel is kept low. This chapter thus outlines the effect of including a natural polymer into the POEGMA gel system and the

subsequent impacts of that natural polymer on the both the physiochemical and biological properties, offering the potential to better mimic cell extracellular matrices to control cell responses.

8.2 Future work

This thesis has outlined the systemically ability to tune various properties of POEGMA-based hydrogels by controlling the ratio of short to long side chain OEGMA monomers, the polymer concentration, the functional group density of the precursor polymers, and the inclusion of charged moieties and natural polymers. I am extremely proud of the work done to develop this patented platform, as it has represented the groundwork for the development of various systems developed by other colleagues in the lab including electrospun POEGMA hydrogels that enable the maintenance of high cell viability during the electrospinning process, cellulose nanocrystal-POEGMA nanocomposite gels with significantly enhanced moduli, degradable self-assembled POEGMA microgels with potential for targeted drug delivery, and highly protein-repellent coatings for biosensor applications.

Moving forward, I believe the following research avenues would be worth pursuing to further leverage the beneficial properties of POEGMA (*in situ*-gelling, protein-repellent, and tunable chemistries and cell interfaces) in applications.

(1) I have developed a method to perform POEGMA hydrazone chemistry inside an inverse emulsion, ideal for the encapsulation of cells in micron sized beads. I am currently working on the further development of these POEGMA microbeads for the encapsulation of human retinal epithelial (ARPE-19) and mouse mesenchymal stem cells (MSCs) cells for cell therapy *in vivo*. Coupling this assembly approach with our RGD-functionalized POEGMA precursors is expected to lead to the fabrication of cell-loaded microbeads with much more controllable stabilities and cell-matrix interactions than possible with calcium-alginate microbeads that are typically used for such applications. This encapsulation method enables the fabrication of microbeads with tunable synthetic composition, typically challenging to acheive without an alginate templating system for crosslinking and bead formation. Our

library of POEGMA-based precursor polymers described in this thesis, can now be used to pinpoint application specific formulations. With the addition of gel morphology manipulation to create matrices not only in an injectable bulk gel embodiment, the scope of potential use of our POEGMA technology for cell delivery applications is greatly widened.

(2) Addditionally, in collaboration with Dr. Ben Muirhead, from the Department of Biomedical Engineering at McMaster University, the further investigation of encapsulated ARPE-19 cells in the injectable charged POEGMA hydrogels developed in Chapter 6 of this thesis, can be investigated. Specifically, using a microfluidic microinjecter developed previously in our lab, we can successfully inject micronsized amounts of hydrogel into the back of rat eyes. Building on the successfull delivery of our neutral, transparent, zero-swelling POEGMA hydrogels to the subretinal space of rats, we can now use this technique to develop a specific back of the eye ARPE-19 cell delivery system for retinal regeneration. Our thermorepsonsive, charged POEGMA hydrogels are conducive to extrusion through a 33G needle, a limitation seen by many other hydrogel systems that are too viscous to extrude this way, and can enable the effective distribution of ARPE-19 cells needed for integaration in the subretinal space. This atributes make this charged POEGMA system an ideal candidate for in vivo translation.

(3) Our characterized library of POEGMA precursor polymers described in this thesis has spawned a successful and innovative collaboration with a 3D printing company. The systematically tunable bulk properties of our hydrogel system, make our hydrogels conducive to various printing processes and facilitate rapid gelation, without using UV, heat, or catalysts typically needed for gel crosslinking in other hydrogels. Our POEGMA hydrogel platform can offer printing companies, with a novel, simple to use synthetic system to work with and has many advantages of use over natural alginate-based gelling systems used in 3D printing spaces currently. The 3D printing process is currently being used to print various artificial tissues and we are looking forward to working with them in the near future to further develop application-specific

POEGMA hydrogel technologies. The RGD-functionalized precursor polymers we have synthesized previously, will also offer a highly cell-adhesive support component to our gels and further aid in the successful translation of our POEGMA materials as tissue engineering scaffolds.